Master Thesis, Department of Geosciences

Petrology of akerite (quartz monzonite) in the Oslo Rift, SE Norway

Gustav Borg

UNIVERSITY OF OSLO

FACULTY OF MATHEMATICS AND NATURAL SCIENCES

Petrology of akerite (quartz monzonite) in the Oslo Rift, SE Norway

Gustav Borg

Master Thesis in Geosciences

Discipline: Geology

Department of Geosciences

Faculty of Mathematics and Natural Sciences

University of Oslo

2011.06.22

Acknowledgements

More than being a test of what I have learned so far, writing this thesis has been a process of learning. Learning how to find and use information, learning the methods of laboratory work, and how to interpret the data I retrieve from my analyses, learning scientific writing, and presentation of data. In lack of relevant courses, I have searched through several dozens of books, articles and web pages, and, not least, I have fully exploited the enormous reservoir of knowledge of my supervisor, Professor Tom Andersen. Therefore, I would like to thank Tom for always giving me the help I have needed to push through the barriers. Even when tired and overworked, Tom has been there to answer my numerous questions, and to give me guidance in how to produce high-standard scientific material.

I will also like to thank Siri Simonsen, who, although I tend to scare her, has helped me with all aspects of isotope analysis, from sample preparation to treatment of data.

Further, I will like to thank Professor Marlina Elburg at the University of Ghent, for doing chemical analyses, and for constructive discussions on data interpretation.

I will like to thank Gunnborg Bye Fjeld for help with stone crushing, Berit Løken Berg for assistance with the SEM analysis and Muriel Erambert for help with the EMP.

Warm hugs and thanks are also sent to all my fellow students at the institute of geosciences, who have filled my last five years with warmth and humor.

More than anyone else, I would like to thank my fantastic wife Karianne and our two daughters Marte and Maja, who have showed me patience and unreserved support from start to end of this process.

Finally, I would like to thank all those who, despite unfavorable economic priorities, spend their careers seeking and spreading knowledge about the mysteries of magmatic petrology. Keep up the good work!

Abstract

The Permian Oslo Rift contains a large number of intermediate igneous rocks, including a quartz monzonitic variety known as akerite. Several minor bodies of akerite are found within the Nordmarka-Hurdal Batholith north of Oslo. The Sognsvann-Holmenkollen akerite is situated at the southern rim of the batholith, at the contact between the large syenitic plutons to the north and the Cambro-Silurian metasediments to the south. Previous studies are few, and have all concluded that the akerite is a product of contamination of nordmarkitic magma with material from the shaly limestones of the Cambro-Silurian succession. In this study, LAM-ICPMS Hf and U-Pb isotopic analysis of zircon, have been applied to investigate the age and magma source of the akerite. U-Pb dating has given an emplacement age of 279Ma for the akerite. A granitic dike cutting the akerite body has been dated at 275Ma. Calculated ε_{Hf} values of -3 to +5 strongly indicate a lithospheric mantle source of the akerite magma. MELTS modeling of fractional crystallization have proved it possible to generate a magma of akeritic composition by fractionating a magma similar to the early B_1 basalts to approximately 1070°C. The Lu-Hf data and the MELTS modeling, combined with geochemical characteristics, points to the conclusion that the Sognsvann-Holmenkollen akerite has a petrogenetic history similar to larvikites of the 10-20 million years older Larvik Plutonic complex, and that crustal contamination have played only a minor role in generating the akerite composition.

Table of Contents

Acknowledgements 3

Abstract 4

1 Introduction 8

1.1 Intermediate igneous rocks of the Oslo Rift 8

1.2 Earlier work 8

1.3 Purpose of study 9

2 Regional geology 10

2.1 Introduction 10

2.2 Pre-rift geology 10

2.3 Geometry of the Oslo Rift 11

2.4 Tectonic development 13

2.4.1 Large-scale tectonic systems 13

2.4.2 Rift initiation 13

2.4.3 Mantle plume 16

2.4.4 Magmatic underplating 16

2.4.5 Rock volume 17

2.5 Temporal development 17

2.5.1 *1*. The pre-rift stage 19

2.5.2 2. The initial rifting stage 19

2.5.3 3. The main rifting stage 21

2.5.4 4. The central volcano stage 21

2.5.5 5. The batholith stage: 21

2.6 Petrogenetic processes 23

2.6.1 Source and evolution of the magma 23

2.6.2 Cause of partial melting 24

3 Methods 26

3.1 Field work 26

3.2 Sample collecting and preparation 26

3.3 Petrographic microscopy 28

3.4 Scanning electron microscopy 28

3.5 Electron microprobe analysis 28
3.6 Whole-rock analysis 28
3.7 Zircon U-Pb and Lu-Hf isotope analysis 29
3.7.1 Zircon 29
3.7.2 The U-Th-Pb isotopic system 30
3.7.3 The Lu-Hf isotopic system 31
3.7.4 Inductively coupled plasma mass spectrometry (ICP-MS) 33
3.8 Fractional crystallization modeling 34
4 Results 35
4.1 Field observations 35
4.2 Petrography 36
4.3 Zircon petrography 40
4.4 Major elements 41
4.5 Trace elements 45
Electron microprobe analysis 48
4.5.1 Sample description 48
4.5.2 Amphibole 48
4.5.3 Clinopyroxene 53
4.5.4 Orthopyroxene 54
4.5.5 Biotite 54
4.6 Zircon U-Pb and Lu-Hf isotope analysis 56
4.6.1 U-Pb geochronology 56
4.6.2 Lu-Hf isotope geochemistry 56
4.7 Fractional crystallization modeling 67
5 Discussion 71
5.1 Field observations 71
5.2 Major and trace element chemistry 71
5.3 Mineral chemistry 72
5.4 Alteration 73
5.5 U-Pb dating 74
5.6 Lu-Hf isotope geochemistry 75
5.7 Fractional crystallization modeling 75
5.8 Magma source 77

6 Conclusions 79
7 References 80
8 Appendix 91
8.1 Petrographic microscopy 91
8.2 ICP-OES bulk chemical analysis 107
8.3 U-Pb isotope analysis 108
8.4 Lu-Hf isotope analysis 118
8.5 Mineral analyses 128

1 Introduction

1.1 Intermediate igneous rocks of the Oslo Rift

Rift-related magmatism (and intracontinental magmatism as a whole) makes up a very small volume fraction of the earths igneous rocks, but accounts for a large number of all described igneous rock types (Le Maitre et al. 2004). No other magmatic regime shows a greater diversity of rocks than does the continental rifts, including the Permian Oslo Rift. The Oslo Rift contains such different magmatic suites as the strongly undersaturated, alkaline Skien basalt and the peralumineous, highly silisic Drammen granite. However, in terms of rock volume, the rift is dominated by slightly oversaturated to undersaturated alkaline intermediate rocks, including both intrusive and extrusive varieties. A large number of now obsolete rock names have been suggested for felsic-intermediate rock types (Brøgger 1890, Barth 1945) of the Oslo Rift, illustrating the great diversity of the region: akerite, bjørnsjøite, hedrumite, heumite, hurumite, husebyite, katnosite, kjelsåsite, lardalite, larvikite, mænaite, nordmarkite, sølvsbergite, sørkedalite, tønsbergite, østern porphyry among others. The petrogenesis of the main intermediate to felsic intrusive rock types is well understood (Neumann 1980, Rasmussen et al. 1988, Trønnes and Brandon 1992), but most minor rock types are poorly covered by data, and their petrology has not been subject to modern studies.

1.2 Earlier work

The quartz monzonite variety known as akerite (Brøgger 1890, Oftedahl 1946) is the most widespread and potentially most important for the Oslo Rift petrology among the minor felsic-intermediate rock types. It mainly occurs as a minor component in the felsic-intermediate Nordmarka-Hurdal plutonic complex north of Oslo. Akerite has long been considered a contamination product (Oftedahl 1946, Neumann 1976), and has largely been excluded from recent studies. Petrographic descriptions and bulk geochemical data are presented by Brøgger (1890) and Oftedahl (1946). Neumann (1976) presented a few chemical analyses of akerite, but the further discussion were limited to the conclusion that akerite is a product of extensive crustal contamination. No previous isotopic studies of akerite are known.

Due to this lack of good analytical material, the claims of most earlier workers that akerite is a product of crustal contamination has, before this study, not been tested by modern

analytical methods, and thus seems to be more of an assumption, than a well-based conclusion.

1.3 Purpose of study

The aim of this study is to investigate the source, evolution and crustal contamination of the akerite magma by applying modern methods of geochemical, mineralogical, petrographic and isotopic analysis. The eastern part of the Sognsvann-Holmenkollen akerite body has been mapped, and the relation to adjacent rock units has been examined by structural investigations of the contact zones. Zircon U-Pb ages have been attained. Lu-Hf isotopic data are used as a tracer to put constraints on the origin and contamination of the magma. Geochemical analyses have been compared with other intermediate rocks of the Oslo Rift, to reveal petrogenetic links.

2 Regional geology

2.1 Introduction

The Oslo rift, located around the City of Oslo at N 59° 54.7', E 10° 44.0' comprises a series of linked-up graben segments, stretching approximately 500 km in NNE-SSW direction from around lake Mjøsa to south of the city of Larvik, with further continuation into the Skagerrak graben to the south. The Oslo Rift is the northernmost of several rift zones related to the northern-European post-Variscan extensional system in late Carboniferous-early Permian. In a ~40 million year period, through most of the Permian, the area was subject to extensive magmatism, with emplacement of large volumes of both extrusive and intrusive rocks (Fig. 5).

2.2 Pre-rift geology

The basement rocks in the Oslo region consist of 1800-1550 Ma amphibolite to granulite facies gneisses, metagabbros, metasediments, granites and migmatites (Neumann et al. 1992), metamorphosed during the Sveconorwegian orogeny 1130-900Ma (Nordgulen and Andresen 2006). In addition, ~920Ma post-orogenic Sveconorwegian granites are found in southern Østfold and the Swedish west coast (the Iddefjord-Bohus granite) SE of the rift, and in the Valdres-Hallingdalen area (the Flå granite) to the NW (Eliasson and Schöberg 1991, Nordgulen 1999). The Precambrian basement rocks are presently exposed along both rims of the rift, and in some places also within the rift (Larsen et al. 2008) (Fig. 1). Overlying the basement rocks is a <2000 meter thick succession of Cambro-Silurian limestones, shales and sandstones (Nakrem and Worsley 2006). During the Caledonian orogeny, this succession was folded and transported in a south-easterly direction, corresponding to the direction of the Laurentia-Baltica collision (Heeremans et al. 1996). The Cambro-Silurian rocks are now found along the length of the rift, exposed in between the igneous units. Unconformably overlying the folded Cambro-Silurian sediments is a 15-90m succession of continental to shallow marine sediments called the Asker Group (Sundvoll and Larsen 1994, Kristoffersen 2011).

2.3 Geometry of the Oslo Rift

The part of the Oslo rift exposed on land, makes up a ~300km long en-echelon array of three linked-up graben segments (Fig. 2) (Larsen et al. 2008). Starting from the north, the *Rendalen graben*, is a half graben downfaulted along the west-dipping Rendalen Fault (Larsen et al. 2008). The existence of the Rendalen Graben north of lake Mjøsa was mentioned by Neumann et al. (1992) and Neumann (1994) without further evidence. Larsen et al (2006) and (2008) concludes that the Rendalen Graben makes up the northernmost part of the rift, adding approximately 100km to the total length of the rift zone.

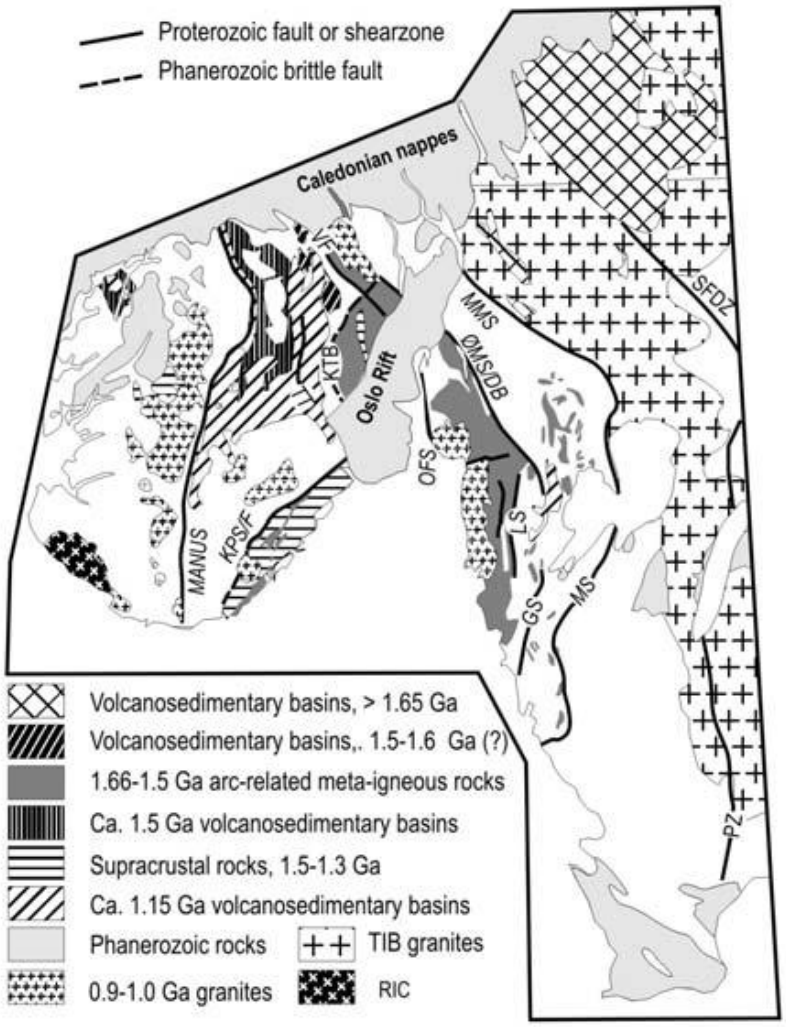

Figure 1. Simplified geologic map of southern Norway and Sweden, showing the different units of the Precambrian basement surrounding the Oslo Rift. The major shear zones are given the following abbreviations: MANUS: Mandal-Ustaoset lineament, KPS/F: Kristiansand-Porsgrunn shear zone and brittle fault, KTB: "Kongsberg-Telemark boundary", VF: Vardefjell shear zone, OFS: Oslo Fjord shear zone LS: Lerdal shear zone, ØMS/DB: Ørje mylonite zone / Dalsland boundary fault, GS: Göta Älv shear zone: MS: Mylonite zone, PZ: Protogine zone. SFDZ: Sveconorwegian frontal deformation zone. TIB: Paleoproterozoic Transscandinavian Igneous Belt (granites), RIC: Rogaland Intrusive Complex (ca. 930 Ma anorthosite and associated rocks). Modified after (Andersen et al. 2007).

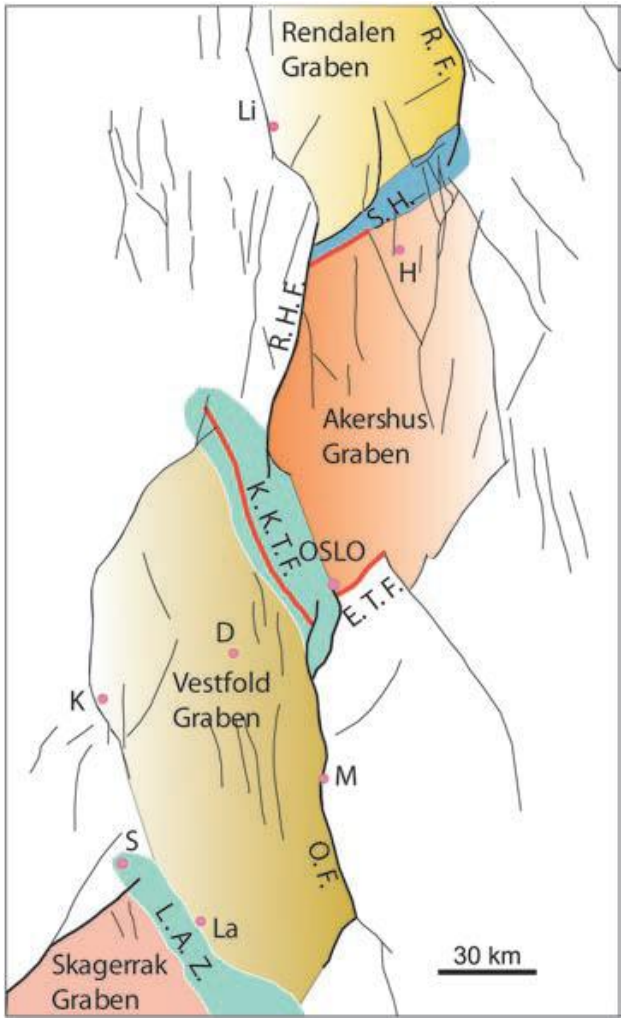

Figure 2. Map showing the four graben segments with their respective master faults and the accomodation zones. The following abbreviations are used: *R.F. = Rendalen fault, S.H. = Solberg Horst, R.H.F = Randsfjorden-Hunnselv Fault, K.K.T.F. = Krokkleiva-Kjaglidalen Transfer Fault, E.T.F. = Ekeberg. Transfer Fault. O.F. = Oslofjord Fault, L.A.Z. = Langesund Accommodation Zone. Li = Lillehammer, H = Hamar, D = Drammen, K =* Kongsberg, M = Moss, S = Skien, La = Larvik. After Larsen et al. (2008)

South of this, from lake Mjøsa to Oslo, separated from the Rendalen Graben by the Solberg Horst, is the *Akershus Graben*, which is a half-graben downfaulted along the east-dipping Randsfjorden-Hunnselv Fault (Larsen et al. 2008). The Akershus Graben terminates to the south in the dextral NW-SE trending Krokkleiva-Kjaglidalen Transfer Fault, separating it from the *Vestfold Graben*, a half-graben downfaulted along the west-dipping Oslofjord Fault (Larsen et al. 2008). To the south, separated from the Vestfold Graben by the Langesund Accommodation Zone, is the offshore *Skagerrak Graben*, a 180 km long zone of several linked-up graben segments, terminating perpendicularly into the NW-SE trending Sorgenfrei-Tornquist line, a suture zone separating the old Fennoscandian craton in NE from the younger assembly of accreted terranes to the SW (Larsen et al. 2008). The Akershus graben and the Vestfold graben combined are often referred to as the Oslo graben.

In addition, it has been suggested that the Särna Alkaline Complex in Sweden may be connected to the Oslo rift (Bylund and Patchett 1977). The Särna Alkaline Complex is situated ~150km NE of the Oslo Rift, in the line of continuation of the rift trend, and consist of alkaline syenites of an age (287±14Ma, Rb-Sr age of Bylund & Patchett (1977)) within the period of magmatism in the Oslo Rift (Sundvoll et al. 1990). The total length of the Oslo Rift, with the three on-shore graben segments, and the off-shore Skagerrak Graben is ~500km, trending NNE-SSW (Larsen et al. 2008). The width is 35-65km in the Oslo graben (Neumann 1994) and somewhat more in the Skagerrak

Graben (Larsen et al. 2008). The area of rift-related faults and dikes are, however, considerably larger than the rift, and appears to widen southwards, following a decrease in crustal thickness (Neumann 1994). Seismic investigations presented by Kinck et al (1991) reveals a moho depth of ~28km beneath Denmark and the southern Skagerrak Graben, increasing to ~35km at the northern termination of the Oslo graben. A moderate increase was found to the NW, with depths of 36-40km in south-central Norway, while crustal thicknesses up to 52km were found in southern Sweden (Kinck et al. 1991) (Fig. 3).

2.4 Tectonic development

2.4.1 Large-scale tectonic systems

The opening of the Oslo rift is believed to be related to a larger system of north-south compression generated through the assemblage of Pangaea and the subsequent Variscan orogeny in mid-late Carboniferous (Heeremans et al. 1996, Larsen et al. 2008, Sippel et al. 2010). The subsequent anticlockwise rotation of Pangaea caused Late Carboniferous-early Permian transtensional movements along the NW-SE trending Sorgenfrei-Tornquist Zone, generating a system of extension in the Skagerrak-North Sea area (Fig. 4) (Heeremans et al. 1996, Larsen et al. 2008). Ziegler (1982) describes the Oslo Rift as a pull apart-basin generated by dextral movements along the Sorgenfrei-Tornquist Zone. During the period of extension in the Permian, several rifts formed in northern Europe, both within the Variscan domain, and in the northern foreland. The Oslo Rift is the largest and the northernmost of these rifts, being situated entirely within the Fennoscandian craton (Larsen et al. 2008).

2.4.2 Rift initiation

According to Sundvoll and Larsen (1994), deposition of the Asker group sediments within the period of 315-300Ma indicates that the Oslo Rift started as a crustal sag before developing into a series of grabens. The subsequent emplacement of a complex of syenitic (mænaitic) to basaltic (camptonitic) sills within the lower part of the Cambro-Silurian sediments, found at locations from Langesund in the south to Lake Mjøsa in the north, is indicative of compressional stress fields, at least locally, during the proto-rift stage (Sundvoll and Larsen 1994).

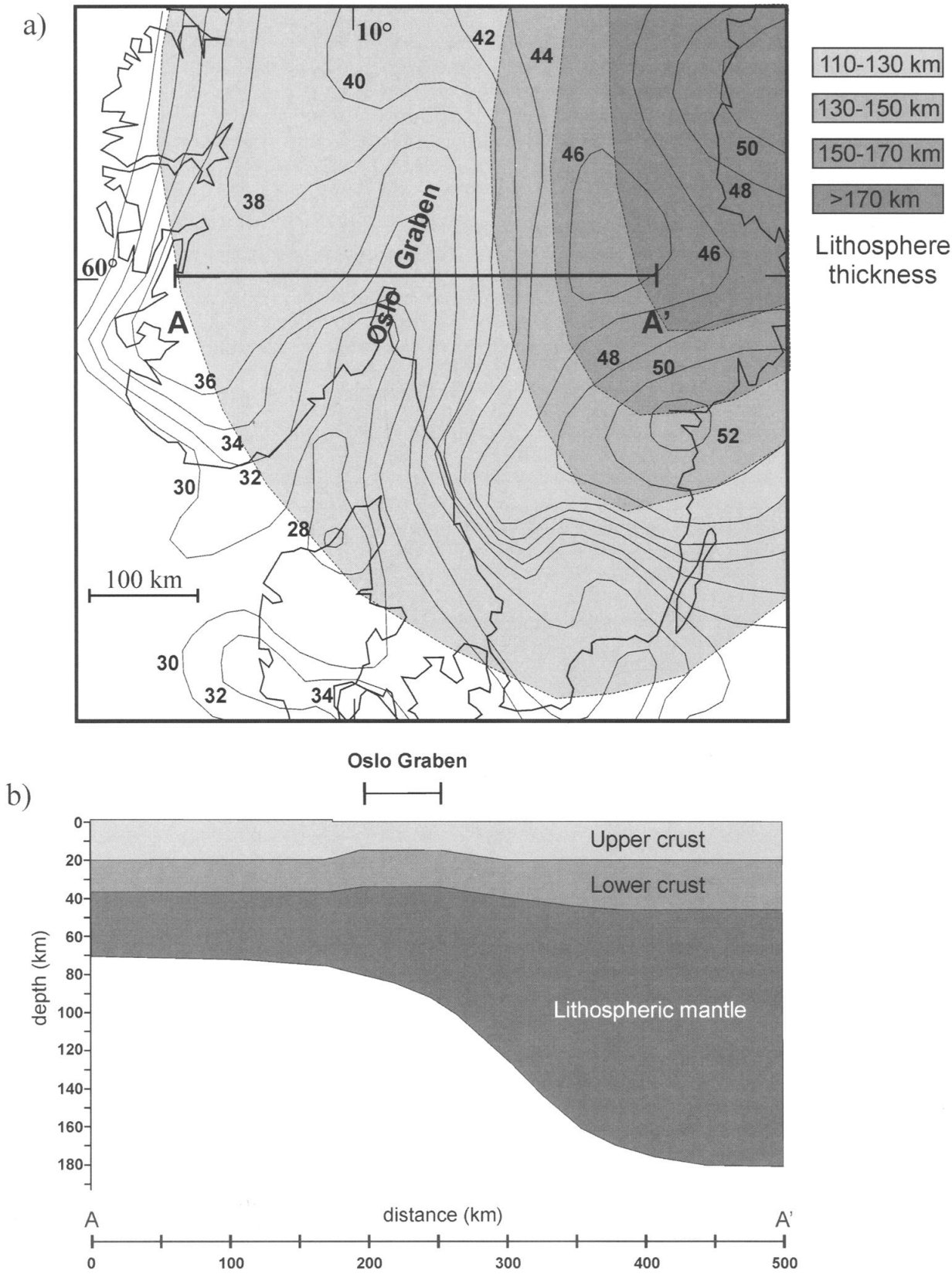

Figure 3. (a) Present-day moho depth (km) and lithospheric thickness in southern Scandinavia. (b) Lithospheric structure along the section A-A' in figure (b). From Pascal et al. (2004), based on data from Kinck et al. (1993), Calcagnile (1982), Kanestrøm (1971), Tryti and Sellevoll (1977), Cassel et al. (1983), Lie et al. (1990), Guggisberg et al. (1991), Plomerova et al. (2001).

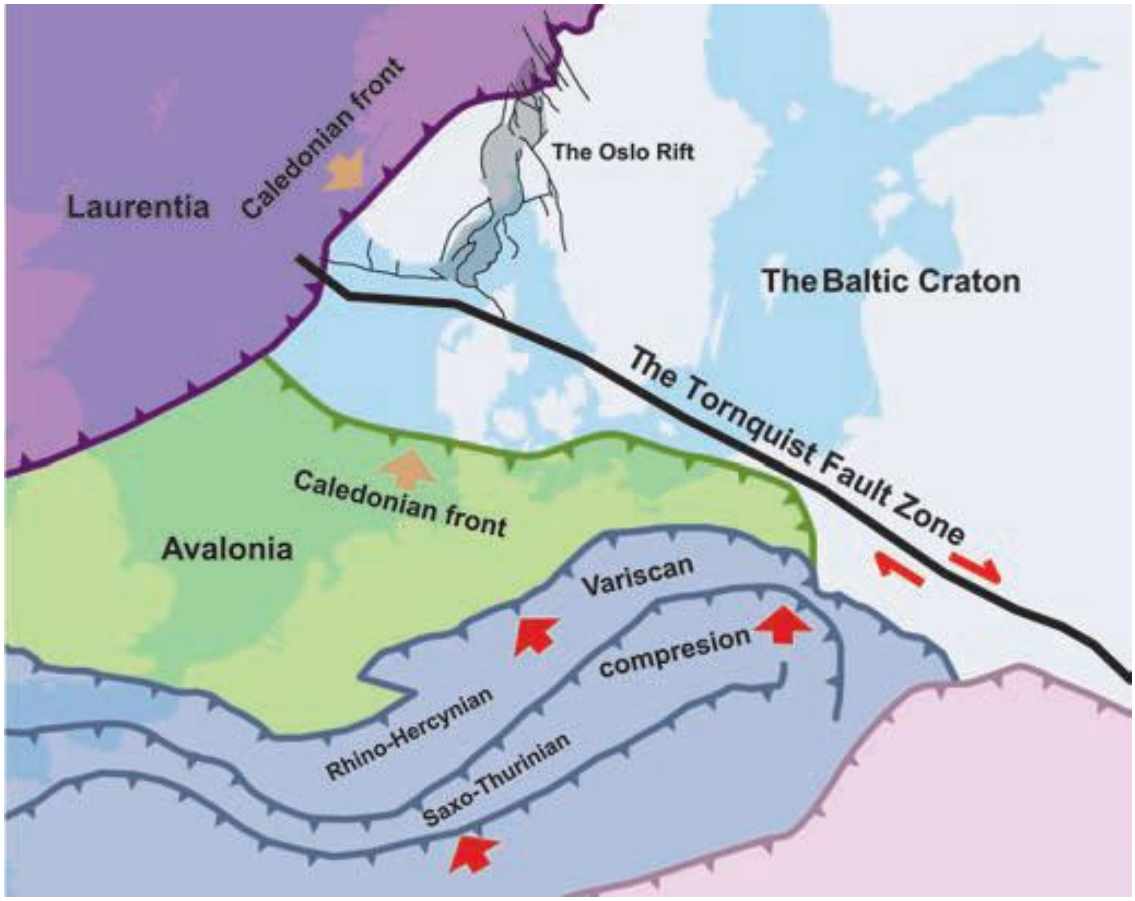

Figure 4. Main tectonic units of northern Europe, and direction of movement of the major fault zones. The Oslo Rift and the Variscan terranes are shown together with the older Caledonian nappes and the Baltic craton. The Tornquist zone is seen striking NW-SE. From Larsen et al. (2008).

Reactivation of older faults and faulting along pre-existing zones of weakness are generally believed to be important causal elements in the rifting process, generating the different graben segments of the Oslo Rift (Sundvoll et al. 1990, Neumann et al. 1992, Sundvoll and Larsen 1994, Heeremans et al. 1996, Ebbing et al. 2005). Slagstad (2006) does, however, point out that the Oslo Rift crosscut, rather than follow, the major Precambrian shear zones of the area (Fig. 1), placing doubt on the importance of fault reactivation. He suggests thermal weakening caused by high heat-producing Sveconorwegian granites as the main causal mechanism, allowing opening of the Oslo rift within the strong Fennoscandian shield. The Oslo Rift has been found to coincide with a rapid >55km eastward increase in lithosphere thickness, believed to be older than the formation of the rift (Pascal et al. 2004). Modeling by Pascal et al (2004) indicates that this thickness contrast played a major role in rift initiation, and in causing decompression melting at the lithosphere-asthenosphere boundary.

2.4.3 Mantle plume

The question of whether a mantle plume has contributed to rifting and magmatism in the Oslo Rift is an ongoing debate. Most authors support a model of passive rift initiation, without the involvement of a plume rising from the core-mantle boundary (Heeremans et al. 1996, Pascal et al. 2004, Kirstein et al. 2006, Sippel et al. 2010, Heeremans 2011). However, Wessel and Husebye (1987), Heeremans et al (1996) and Sippel et al (2010) among others, consider it likely that a certain degree of mantle upwelling have occurred after passive initiation of the rift. This is supported by an early Permian change in the stress-regime, from pure extension to radial extension, as described by Heeremans et al (1996). The arguments against a mantle plume most commonly agreed upon, are listed in Heeremans (2011):

1. The lack of an age-progressive volcanic track.
2. Pre-magmatic subsidence instead of uplift.
3. Low to moderate $^{3}He/^{4}He$ values.
4. The absence of a large igneous province.
5. Normal or only slightly elevated mantle temperature.

Torsvik et al (2008) refer to the large volume of volcanic rocks emplaced in the Skagerrak-North Sea area at 297±4Ma, and introduces the term the Skagerrak-Centered Large Igneous Province. They disapprove of the arguments of Heeremans (2011), and claim that the combination of large volumes of volcanic rocks, short interval of eruption and the presence of convergent dike swarms, indicate the existence of a plume rising from the core-mantle boundary beneath the Skagerrak area in late Carboniferous-early Permian. According to Torsvik et al (2008), only the early magmatic rocks of the Oslo Rift, with ages corresponding to the period of volcanism further south in the Skagerrak-North sea area are plume-related, the later batholiths and dikes are believed to be unrelated to the Skagerrak-Centered Large Igneous Province and thus, the assumed mantle plume.

2.4.4 Magmatic underplating

Several investigations have revealed a marked positive gravity anomaly below the Oslo Rift (Ramberg and Smithson 1971, Ramberg 1976, Ebbing et al. 2005). According to Ramberg (1976), Neumann et al (1986), (1992), (2004) and Neumann (1994), this anomaly is caused by a dense body of fractional crystallization cumulates located within the lower half of the crust, combined with the thinned crust of the rift zone. Based on measured S- and P-wave

velocities, Stratford and Thybo (2011) concludes that a body of mixed intermediate, mafic and ultramafic rocks is situated at depths of 21-34km beneath the central rift axis.
The presence of a cumulate body is supported by findings of pyroxenite xenoliths, with cumulate textures, in an alkaline basalt at Krokskogen NW of Oslo, and within the Larvik plutonic complex in Vestfold (Neumann et al. 1988a, Andersen and Seiersten 1994).

Ebbing et al (2005) and (2007) present a different interpretation of the gravity anomaly, and suggest that the positive anomaly is caused by dense Precambrian basement rocks combined with thinned crust. They claim that the gravity anomaly is highly asymmetric, increasing westwards from the Oslo Rift, and interpret this as a steeply eastwards dipping body of high-grade metamorphic rocks. They further claim that the crust beneath the Oslo Rift shows the same structure as the adjacent Precambrian craton, and argues that the rate and volumes of magmatism in the Oslo Rift does not require a magmatic underplated body. As an alternative to the generally accepted model involving fractionation of mantle melts, they propose mafic and intermediate rocks in the middle to upper crust as sources for the now-exposed magmatic rocks of the Oslo Rift. This is contradicted by the radiogenic isotope signature generally taken to indicate a mainly mantle source for the bulk of the Oslo Rift igneous rocks (Jacobsen and Wasserburg 1978, Neumann. 1980, Neumann et al. 1988b, Rasmussen et al. 1988, Sundvoll et al. 1990, Neumann et al. 1992, Neumann et al. 2004, Larsen et al. 2008).

2.4.5 Rock volume

Neumann et al (2004) suggests that the volume of intrusive and extrusive rocks emplaced in the shallow crust, including the part that has been removed by the estimated 3-4 km of surface erosion, is in the order of 60000km^3, the bulk of these being felsic-intermediate rocks. In addition to this comes the presumably large amounts of magma emplaced at deeper levels in the crust (Neumann et al. 2004). Based on 50-90% fractionation for intermediate-felsic magmas, Neumann et al (2004) estimated the volume of mafic-ultramafic cumulates beneath the Oslo Rift to be at least 65000km^3. This gives a total rock volume of the Oslo Rift of more than 120000 km^3. Disapproving the existence of a magmatic underplated body, Ebbing (2007) suggests a lower total volume of ~63000 km^3.

2.5 **Temporal development**

The upper age of the Asker Group sediments is constrained by ID-TIMS U-Pb dating of detrical zircons at 319±5Ma (Dahlgren and Corfu 2001), while the lower age is constrained

by the oldest dated basalt flow at Brunlanes in the southern Vestfold graben, yielding an U-Pb age of 300.4±0.7Ma (Corfu and Dahlgren 2008b). ID-TIMS U-Pb zircon dating of a mænaite sill at Høgenheia in the southern Vestfold graben has given an age of 300,1±0.5 Ma, which is contemporaneously with the first basaltic volcanism (Corfu and Dahlgren 2008b). The age of the last magmatic activity, and thus, the total time span of the Oslo Rift magmatism, is still uncertain. An alkali feldspar granite from the Tryvann Granite Complex has revealed a Rb-Sr age of 241±3Ma, and the syenitic ring dike of the adjacent Bærum Cauldron has yielded a Rb-Sr age of 243±3Ma (Sundvoll and Larsen 1990). Corfu and Dahlgren (2008b) present a zircon U-Pb age of 259±1Ma from the Tryvann Granite Complex, also this for an alkali feldspar granite, proposing this unit as the youngest voluminous igneous activity in the Oslo Rift. The Tryvann granite complex is, however, cut by some basaltic dikes, indicating, at least minor, later magmatism (Nilsen 1992). Late dike emplacement is supported by ^{40}Ar-^{39}Ar dating of intermediate to mafic dikes in the central-northern parts of the rift, revealing ages as low as 243±5Ma (Torsvik et al. 1998) and 246±3Ma (Timmerman et al. 2009).

Several authors place doubt on the validity of the Rb-Sr dating, proposing possible reset due to post-magmatic hydrothermal activity in the area, and thus, claim that the generally higher U-Pb ages are more reliable (Pedersen et al. 1995, Neumann et al. 2004, Corfu and Dahlgren 2008b). Thus, according to Corfu and Dahlgren (2008b), the main magmatic phase in the Oslo rift lasted approximately 40 million years, from 300Ma to 259Ma, only succeeded by minor dike emplacement. This is some 20 million years less than what was indicated by the Rb-Sr dating of Sundvoll and Larsen (1990) and Sundvoll et al (1992), namely 304Ma-241Ma.

Generation of the Oslo rift has in several later articles been presented as a five or six stage development (Ramberg and Larsen 1978, Olaussen et al. 1994, Neumann et al. 2004, Larsen et al. 2006, Larsen et al. 2008). Although it appears constructed, with partly overlapping stages, the model provides a convenient framework for describing the development of the rift, and is thus applied in this text. The general outline of the stages is displayed below (Table 1).

Tectonomagmatic stages of the Oslo Rift			
Rift stage	Products	Stratigraphic or Rb-Sr age ranges (Ma)	U-Pb age ranges (Ma)
1: Pre-rift stage	The Asker Group sediments, mænaite sills	Upper Westphalian ~300-312 (Asker gr.), 304 (sills)	<319 - >300 (Asker gr.) 300 (sills)
2: Initial rifting stage	Basaltic volcanism	>294-291	300-299
3: Main rifting stage	Romb porphyry, basalt, larvikite	294-276	298-292
4: Central volcano stage	Calderas, diverse volcanic rocks, ring dikes	280-243	No available data
5: Batholith stage (6: Terminal stage)	Larvikites, syenites, granites, dikes	273-241	286-259

Table 1. Tectonomagmatic stages of the Oslo Rift. Data from: Sundvoll and Larsen (1990), Sundvoll et al (1992), Sundvoll and Larsen (1994), Olaussen et al (1994), Dahlgren and Corfu (2001), Haug (2007), Corfu and Dahlgren (2008a), Corfu and Dahlgren (2008b).

No known U-Pb ages exist for the central volcano stage. However, Timmerman et al (2009) have dated the syenitic ring dike of the Øyangen caldera by the ^{40}Ar-^{39}Ar method, yielding an age of 273±2.8Ma.

2.5.1 *1*. The pre-rift stage

Characterized by the deposition of the Asker group sediments plus mænaite and camptonite sills (Larsen et al. 2008).

2.5.2 2. The initial rifting stage

The first major magmatic suite of the Oslo Rift, overlying the Asker group sediments is the B_1 basalts (Olaussen et al. 1994). The B_1 lavas show a northwards decrease in thickness and flow intensity. Segalstad (1979) reports a minimum thickness of 1500m for the Skien basaltic sequence in the southern Vestfold Graben, while the northernmost B_1 basalts at Krokskogen in the southern end of the Akershus Graben constitutes only one 30m thick flow (Ramberg and Larsen 1978). There are indications that the B_1 basalts show a northwards decrease in age (Neumann et al. 2002). Rb-Sr dating by Sundvoll and Larsen (1990) revealed an age of 294±6Ma for the overlying RP in Vestfold, being a minimum age for the B_1 basalt, while an age of 291±8Ma was found for the B_1 unit at Krokskogen. The assumed decrease in age from south to north of the B_1 lavas corresponds to a northwards increase in the degree of silicity. The Brunlanes and Skien lavas are highly silica-undersaturated, the basalts of the central Vestfold graben are mildly undersaturated to saturated, while the Krokskogen B_1 unit is quartz tholeiitic (Neumann et al. 2002, Larsen et al. 2006).

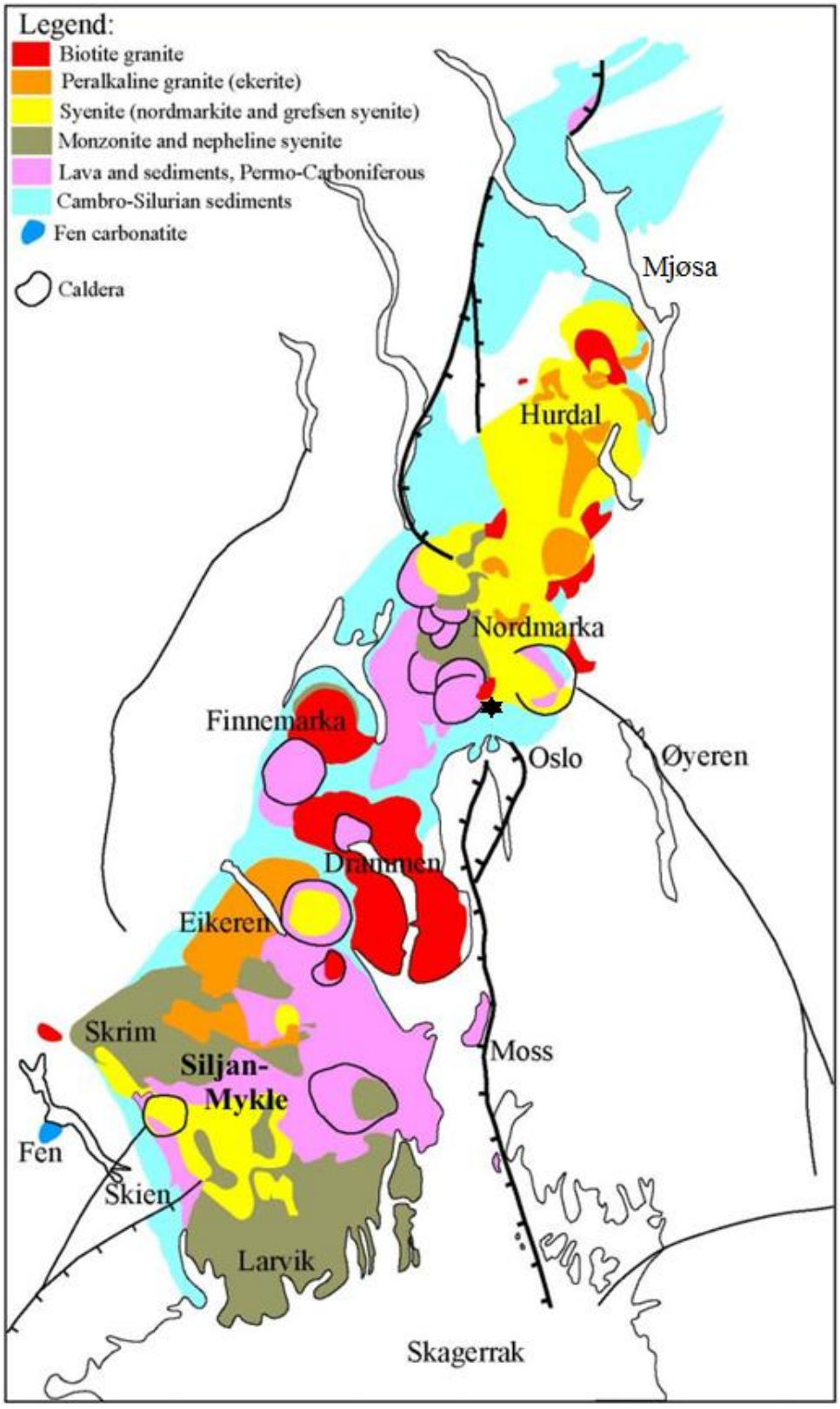

Figure 5. Simplified geologic map of the on-shore Oslo Rift, showing the locations of the major magmatic units and the pre-rift sediments. The black star just north of the City of Oslo shows the location of the Sognsvann-Holmenkollen akerite at the triple-contact between the southernmost Nordmarka syenites (yellow), the lavas of the Bærum cauldron (pink) and Cambro-Silurian metasediments (light blue).

2.5.3 3. The main rifting stage

Overlying the B_1 basalts is an extensive succession of Romb Porphyry (RP) lavas interspersed with minor basaltic units. Romb porphyry is a volcanic rock of latitic composition, characterized by ternary feldspar phenocrysts of varying shape, size and numerosity (Neumann et al. 1992, Larsen et al. 2006). The succession reaches ~3km thickness in Vestfold, decreasing northwards to approximately 900m at Krokskogen (Larsen et al. 2008). The RP lavas erupted along large N-S trending fissure vents corresponding to the E-W oriented extensional stress regime that dominated this period (Ramberg and Larsen 1978, Larsen et al. 2006). Contemporaneously with the RP eruptions, the Larvik Plutonic Complex was emplaced in the southern Vestfold Graben. The Larvik Plutonic Complex is built up of nearly circular bodies of hypersolvus monzonites (Larvikite) and nepheline syenites (Petersen 1978, Andersen et al. 2010), and has revealed zircon U-Pb ages of 298Ma to 290Ma (Corfu and Dahlgren 2008a). RP lavas and Larvikites have been found to show great chemical, isotopic and age similarities, leading to the conclusion that they are products of the same magma suite (Rasmussen et al. 1988, Pedersen et al. 1995).

2.5.4 4. The central volcano stage

This period is characterized by strings of large central volcanoes, stretching from the southern Vestfold Graben to the Northern Akershus Graben, possibly emplaced from south to north (Larsen et al. 2006, Larsen et al. 2008). Calderas containing basaltic, trachytic and rhyolitic extrusives along with syenitic to granitic ring dikes, indicate a gradual evolvement of the lavas terminating in caldera collapse (Nilsen 1992, Neumann et al. 2004).

2.5.5 5. The batholith stage:

Large composite batholiths of monzonitic to granitic composition, make up approximately 50 percent of the presently exposed igneous rocks, and constitutes the youngest period of major magmatic activity in the Oslo Graben (Neumann et al. 2004). This period is dominated by three areas of batholitic complexes, the neighboring Skrim-Mykle and Siljan-Hvarnes complexes in the southwestern Vestfold Graben, the Drammen and Finnemarka batholiths in the northeastern Vestfold Graben, and the Nordmarka-Hurdalen batholith in the southern-central Akershus Graben (Ramberg and Larsen 1978, Trønnes and Brandon 1992, Pedersen et al. 1995). The Siljan-Mykle area is dominated by monzonites, syenites and peralkaline granites (ekerite) of ages 281.2±0.6Ma-277.3±0.8Ma (zircon U-Pb ages of Pedersen et al (1995)). A more homogeneous pluton, composed of peralkaline granite, the Eikeren ekerite, is situated between the Skrim-Mykle and Drammen complexes, with contacts to the Skrim

larvikite (Pedersen et al. 1995). The Drammen and Finnemarka batholiths, NE of the Eikeren area, are built up of different units of biotite granites (Trønnes and Brandon 1992), of ages 287±2Ma to 273±1Ma (zircon U-Pb ages of Haug (2007)). In terms of magma source and evolution, the Drammen and Finnemarka granites are believed to be unrelated to the other major batholiths of the Oslo Rift (Neumann 1978, Trønnes and Brandon 1992), and has by many authors been ascribed to an earlier phase in the tectonomagmatic development of the rift (Ramberg and Larsen 1978, Sundvoll 1978, Larsen et al. 2006, Larsen et al. 2008). The Drammen and Finnemarka Batholiths are, however, according to Rb-Sr dating (Sundvoll et al. 1990) and U-Pb dating (Pedersen et al. 1995, Haug 2007) contemporaneous with granites and syenites of the Eikeren and Siljan-Skrim area.

The largest and youngest plutonic complex in the Oslo rift is the Nordmarka-Hurdal Batholith, covering approximately half of the Akershus graben. Unlike the older Drammen Batholith, no major faults are found in the Nordmarka-Hurdal Batholith, indicating rift termination during the period between emplacement of the two plutonic complexes (Ramberg and Larsen 1978). Rocks of this complex include quartz-bearing alkali feldspar syenites (nordmarkite), syenites (Grefsen syenite), alkali feldspar granites (ekerite), biotite granites, fine-grained quartz monzonites (akerite) and monzonites-monzodiorites (larvikite, kjelsåsite, sørkedalitt) (Sæther 1962, Holtedahl and Dons 1966, Nilsen 1992, Gjelle and Sigmond 1994, Le Maitre et al. 2004). In addition, calderas with syenitic-granitic ring dikes, and extrusive rocks of basaltic to rhyolitic composition are found at several locations within the plutonic complex (Nilsen 1992, Larsen et al. 2008).

2.5.5.1 Akerite

The name akerite was first defined by Brøgger (1890) and has since then been applied for a number of different monzonitic to syenitic rocks in the Oslo Rift (Oftedahl 1946, Holtedahl and Dons 1966, Gjelle and Sigmond 1994). Oftedahl (1946) separates them from the other intermediate rock types by the following definition:

"The akerite is a fine-grained monzonitic rock, plagioclase< >alkali feldspar, but with considerable amounts of both, color index <30, and usually <10% quartz; the texture is more or less marked by the rectangular plagioclase individuals which are often selvaged by alkali feldspar."

Bodies of akerite are found at several locations in the complex, mainly concentrated at the surroundings and interior of the Bærum Cauldron, showing a varying degree of phorphyritic texture and variations in grain size between the different units (Oftedahl 1946, Holtedahl and Dons 1966). The Sognsvann-Holmenkollen akerite is a 4km long and up to 1km wide body separating the Nordmarkite bodies to the north from the Cambro-Silurian metasediments to the south (Holtedahl and Dons 1966). Based on the dominating mafic mineral, Brøgger (1890) described the different varieties of this Akerite body as *hypersthene-akerite*, *pyroxene-quartz-akerite* and *hornblende-akerite*. Akerite has generally been considered a highly contaminated border-facies between intrusive bodies and Cambro-Silurian metasediments, or situated within plutonic rocks with a high content of sedimentary xenoliths (Oftedahl 1946, Neumann 1980). However, at the present level of erosion, only the Sognsvann-Holmenkollen akerite body appears to be located in such a setting.

2.6 Petrogenetic processes

2.6.1 Source and evolution of the magma

The earliest B_1 basalts in the southern Vestfold Graben are believed to be the most primitive of the Oslo Rift rocks (Neumann et al. 2002). These basalts are enriched in Ti, P and high field strength elements (HFSE) and show a steep REE pattern, as well as HIMU-like (Zindler and Hart 1986) isotopic depletion (Anthony et al. 1989, Neumann et al. 2002). Combined with a high CaO/Al_2O_3 ratio, this is indicative of a non-peridotitic magma source, and thus, a veined phlogopite-bearing garnet clinopyroxenite at the base of the lithosphere is suggested as the source of these early basalts (Neumann et al. 2002). The enrichment in incompatible elements is believed to be caused by an earlier event of metasomatism of asthenospheric fluids, possibly associated with the near-lying 580Ma Fen carbonatites (Anthony et al. 1989, Meert et al. 1998, Neumann et al. 2004). Further partial melting, and mixing with magmas of at least two other mantle sources produced the later low-Ti basalts which show a higher, PREMA-type (Stein and Hofmann 1994), isotopic enrichment, and a flatter REE pattern (Neumann et al. 2002). Further fractionation of clinopyroxene and olivine in large lower crustal magma chambers led to generation of the more evolved RP lavas and larvikite batholiths, still without major crustal contamination (Neumann 1980, Neumann et al. 1988b, Rasmussen et al. 1988, Larsen et al. 2008). According to Neumann (1980), generation of the

later syenites and alkali granites dominating the Nordmarka-Hurdal Batholith is compatible with further fractionation of the magma that produced the RP lavas and the larvikites. It has, however, been pointed out that a longer crustal residence time would lead to greater heating of the wall rock causing increased crustal contamination (Neumann et al. 2002). This is supported by later major- and trace element analyses as well as isotope studies of these rock suites (Neumann et al. 1988b, Rasmussen et al. 1988, Andersen and Knudsen 2000, Neumann et al. 2002). Neumann et al (1988b) suggest as much as 60% contamination for the most highly contaminated felsic rocks, as well as the Krokskogen tholeiite, and up to 40% for the Vestfold basalts.

The peraluminous, high-silica biotite granite of the Drammen and Finnemarka Batholiths differs from the other plutonic suites of the rift, and have been proposed to be a product of partial melting of Precambrian crust (Neumann et al. 1977 and references therein). However, Based on the negative ε_{Sr} and positive ε_{Nd} values found in the Finnemarka- and northernmost Drammen granites, Trønnes and Brandon (1992) concluded that these rocks are derived from a mantle source, with minimal crustal contamination. The southernmost Drammen granites shows higher ε_{Sr} values of +35 to +67, which is interpreted as a result of either crustal contamination or metasomatic enrichment of Rb from the wall rocks (Trønnes and Brandon 1992). The silicic nature of the rocks is ascribed to a highly efficient density filtering, as a result of earlier intracrustal differentiation of Sveconorwegian granites (Trønnes and Brandon 1992). Andersen and Knudsen (2000) suggest a low-Sr crust with characteristics similar to what is found in the Rjukan group rhyolites, metasediments and low-Sr granitic gneisses from the Telemark and Bamble sectors and lower Paleozoic, western provenance, Oslo Rift sediments as a possible contaminant for the Drammen granite. This is supported by U-Pb and Lu-Hf isotopic data of Haug (2007).

2.6.2 Cause of partial melting

Neumann (1994) proposed that the partial melting of mantle rocks, initiating the Oslo Rift magmatism, was caused by a combination of extensional decompression, a weak positive thermal anomaly and possibly a fluid-induced reduction in solidus temperature. Pascal et al (2004) does not rule out a minor positive thermal anomaly nor a slight increase in water content, but claims that high stretching velocities in the initial stage of rifting alone could have been sufficient to cause partial melting. This is compatible with the assumption that the highest rates of partial melting occurred in the early phase of rifting (Sundvoll et al. 1990,

Neumann et al. 2004, Pascal et al. 2004, Larsen et al. 2008). According to Neumann et al (2004), the involvement of a plume in melt initiation, as proposed by Torsvik et al (2008), is supported by the PREMA-type nature of the magmas, an affinity usually associated with OIB lavas.

3 Methods

3.1 Field work

The area examined in the field covers about 2km^2 west of lake Sognsvann in Oslo. The entire field area is forested, except for a minor park area at the southern end of lake Sognsvann. The geological map of Holtedahl & Dons (1966) plus a 1:10000 topographic orienteering map was used for navigation in the field. A sketch after the map of Holtedahl & Dons (1966) is shown, covering the area (Fig. 6). To avoid intruding private properties, the area examined was limited to cover the akerite exposed west of Vettaliveien. Below approximately 215 m.a.s.l, Holocene marine and glacial sediments cover most of the rocks. Above this altitude, sediment cover is thinner and less continuous. This zone is, however, extensively covered by moss, which, to some extent, has been removed by hand in search of good exposures. Due to the discontinuous nature of the outcrops along the contact zones, the mapping is based on interpolation between approximately 90 points. A Garmin GPSmap 60CSx were used to acquire UTM coordinates. Due to easy logistics, field work was almost exclusively done in good weather.

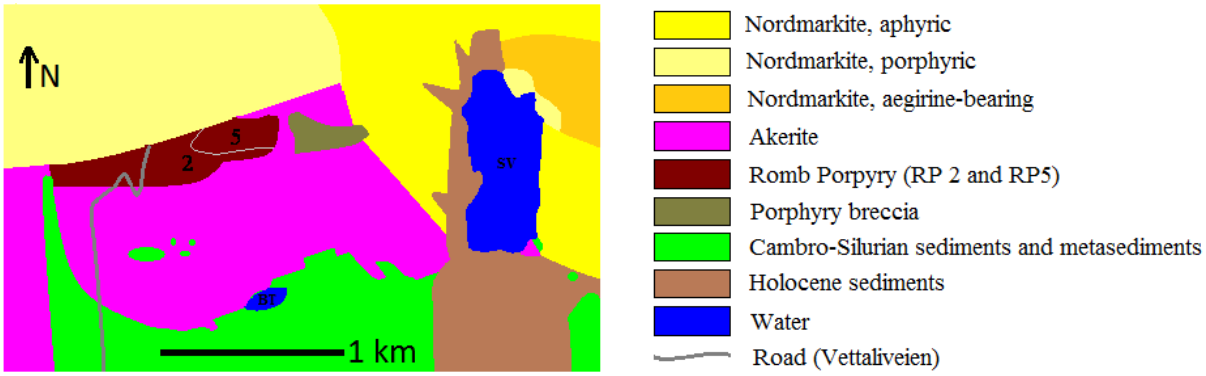

Figure 6. Simplified geologic map of the Sognsvann-Holmenkollen area. After Holtedahl and Dons (1966). This map was used for navigation, and shows the different rock units of the field area. The term porphyric nordmarkite used by Holtedahl and Dons (1966) are outdated. It was called Grefsen syenite as early as 1948 by Oftedahl (1948), a name commonly used today. A new map has been constructed, based on mapping of the akerite body, where minor corrections are suggested (Fig. 10). SV=Sognsvann, BT=Bånntjern.

3.2 Sample collecting and preparation

During field work, approximately 90 samples were collected. Of these, eight samples (GB-A,B,C,D,E,F,G and H) were used for bulk chemistry and trace element analysis, and for collecting zircons for isotope analyses. These eight samples were collected along a line

crossing the akerite body from east to west (Fig. 10). Another eight samples (GB-18,19,20,21,22,23,24 and 25) were collected along a 30m long traverse across the contact between the neighboring nordmarkite into the akerite (Fig. 10). Polished thin sections were made of each of these two series of samples. The thin sections were produced by Dr. Ulrich Schüssler at the university of Würzburg, Germany.

The 2-4 kg rock pieces used for chemical analysis were cut by a hydraulic cutter and a hammer before crushing. The material used for crushing was fragments of unweathered rock taken from the interior of the samples, avoiding weathered and fractured areas. Due to the homogeneity of the sample material and the fine crystalline texture of the rock, this was considered representative, and thus, a splitter was not used. The rock fragments were crushed to powder with a steel sling mill. 30-50g of powder was attained from each of the eight samples. The mill was washed with water and detergent, plus alcohol, and dried, between each run.

The material used for collecting zircons for isotope analyses was crushed with a jaw crusher and a Retch percussion mill. Between each use, the jaw crusher was disassembled and cleaned with a steel brush, alcohol, water and plastic brush, ultrasonic bath and compressed air, and then dried in an oven. The Retch percussion mill was given the same treatment, except for the steel brush.

Mineral separation was done with a plastic gold pan under running water. Between every use, the pan was cleaned with water and soap, ultrasonic bath, and compressed air. After drying, it was examined under microscope to ensure no mineral grains were left to contaminate the next sample. Zircons were picked from a Petri-dish with alcohol. This was done under a binocular microscope, using a pair of steel tweezers. 30 grains were picked from each sample. The zircons were placed on a piece of plastic tape, and casted in epoxy. The mount was abraded down to gain a larger surface for laser ablation, and then polished. Casting and abrading/polishing was done by Siri L Simonsen at the department of geosciences, University of Oslo.

3.3 Petrographic microscopy

Thin sections of samples GB-A,B,C,D,E,F,G,H and GB-18,19,20,21,22,23,24,25 have been examined by petrographic microscope. All minerals identified in each of the 16 thin sections are listed and characterized in Appendix, Tables 7-22.

3.4 Scanning electron microscopy

All zircons mouthed for ICP-MS analysis have been examined using a JEOL-JSM-6460LV scanning electron microscope (SEM). Prior to analysis, the epoxy mount containing the zircons was coated with carbon to prevent charging of the sample. Cathodoluminescence (CL) images were made for each of the zircons. By acquiring spectra, a minor number of the 120 grains picked was found to be apatite or titanite, and thus not suitable for the ICP-MS analysis. SEM analysis was performed at the department of geosciences, University of Oslo, under assistance of Berit Løken Berg.

3.5 Electron microprobe analysis

Electron microprobe (EMP) analysis was performed using a Cameca SX100 instrument fitted with 5 wavelength-dispersive spectrometers. An accelerating voltage of 15 kV, a beam current of 15 nA and a focused beam were applied. Counting time was 10 s on peak (and 5 s on each background positions). Na, and K were analyzed first. Calibration standards and X-ray lines used were wollastonite (Si Kα, Ca Kα), Al_2O_3 (Al Kα), Cr_2O_3 (Cr K α), pyrophanite (Ti Kα, Mn Kα), Fe metal (Fe Kα), MgO (Mg Kα), orthoclase (K Kα), and albite (Na Kα). Matrix corrections were done according to the PAP procedure (Pouchou and Pichoir 1984) Backscattered electron (BSE) images were attained before each analysis to ensure chemical homogeneity at the points of analysis. The analysis was performed at the department of geosciences, University of Oslo, under assistance of Muriel Erambert. The following samples were analyzed by EMP: GB-A and BG-C (akerite), GB-B (granite) and GB-18 (nordmarkite).

3.6 Whole-rock analysis

The chemical analysis was performed using an *inductively coupled plasma optical emission spectrometer* (ICP-OES) by Professor Marlina Elburg at the university of Ghent, Belgium. Standards used are *BCR-2* (http://minerals.cr.usgs.gov/geo_chem_stand/basaltbcr2.html) (*U.S. Geological Survey* 2011), *JB-2* (http://riodb02.ibase.aist.go.jp/geostand/igneous.html)

(*Geological Survey of Japan* 2011). The following eight samples were analyzed: GB-A, GB-C, GB-D, GB-E, GB-F, GB-G, GB-H (akerite) and GB-B (granitic dike). Weight percent values were obtained for the following major element oxides: SiO_2, TiO_2, Al_2O_3, Fe_2O_3, MnO, MgO, CaO, Na_2O, K_2O and P_2O_5. In addition, parts pr million (ppm) values were obtained for the trace elements Cr, Ni, Zn, V, Sc, Co, Ba, Sr, Zr, Hf, La, Ce, Nd, Dy, Yb, Y, Th, Be.

TAS diagram, CIPW norm and ternary plots were made using the computer program *GCDkit for Windows* (Janousek et al. 2008).

3.7 Zircon U-Pb and Lu-Hf isotope analysis

3.7.1 Zircon

Zircon ($ZrSiO_4$) is a common accessory mineral in a wide variety of igneous, metamorphic and sedimentary rocks. Due to its abundance, resistance to alteration, and the tendency of Zr to be substituted by elements such as U, Th and Hf, zircon is commonly used for isotope studies of rocks. Because of the high blocking temperature of >900°C (Ireland and Williams 2003), very high-temperature metamorphism is needed to reset the U-Pb isotopic system of zircons.

Due to the almost identical ionic radius of Hf^{4+} (0.83Å) and Zr^{4+} (0.84Å), zircons normally contain considerable amounts of Hf (Finch and Hanchar 2003). Lu^{3+} does not shear the same charge, and has a higher ionic radius (0.98Å) , and thus, appears in distinctively lower concentrations (Hoskin and Schaltegger 2003). The average Hf concentration of zircon is ~15000 ppm, with an average Lu/Hf ratio of ~0.0016 (Faure and Mensing 2005). The high concentrations of Hf, and the correspondingly low concentrations of Lu make zircons highly suitable for Lu-Hf isotopic studies.

U^{4+} (1.00Å) and Th^{4+} (1.05Å) are commonly found in zircons, in concentrations typically ranging from tens to some thousands of ppm (Hoskin and Schaltegger 2003). Although Pb generally is excluded from entering the crystal structure of zircon, lower values of common-lead (typically ~0.01 ppm, but in some cases distinctively higher) frequently occur (Watson et al. 1997). The high initial U/Pb ratio, in combination with abundance and resistance to alteration, makes zircon a highly suitable mineral for U-Pb dating.

3.7.2 The U-Th-Pb isotopic system

Uranium is an actinide series metal with three naturally occurring isotopes, ^{238}U, ^{235}U and ^{234}U, all of which are radioactive.

Thorium is another actinide series metal, with one naturally occurring non-radiogenic isotope, ^{232}Th, plus several short lived radiogenic isotopes which occur as intermediate steps in the decay series of ^{238}U, ^{235}U and ^{232}Th.

The following half-lives and decay constants are generally accepted for ^{234}U, ^{238}U, ^{235}U and ^{232}Th (data from Steiger and Jäger (1977) and Faure and Mensing (2005) (Table 2):

Isotope	Abundance (%)	Half-life (years)	Decay constant (y^{-1})
^{238}U	99.2743	4.468×10^{9}	1.55125×10^{-10}
^{235}U	0.7200	0.7038×10^{9}	9.8485×10^{-10}
^{234}U	0.0055	2.45×10^{5}	2.829×10^{-6}
^{232}Th	100.00	14.010×10^{9}	4.9475×10^{-11}

Table 2. Abundances, half-lives, and decay constants for ^{238}U, ^{235}U ^{234}U and ^{232}Th.

Lead is a main-group metal with three naturally occurring stable isotopes, ^{208}Pb, ^{207}Pb and ^{206}Pb which all are radiogenic, and one non-radiogenic radioactive isotope, ^{204}Pb, with a half-life in excess of 1.4×10^{17} years. Because this is more than 30 million times the age of the earth, ^{204}Pb is treated as a stable isotope in U-Pb dating.

^{238}U, ^{235}U and ^{232}Th undergo the following decay to ^{206}Pb, ^{207}Pb and ^{208}Pb respectively:

$$^{238}_{92}U \rightarrow {}^{206}_{82}Pb + 8\alpha + 6\beta^{-} + q, \quad (1)$$

$$^{235}_{92}U \rightarrow {}^{207}_{82}Pb + 7\alpha + 4\beta^{-} + q, \quad (2)$$

$$^{232}_{90}Th \rightarrow {}^{208}_{82}Pb + 6\alpha + 4\beta^{-} + q, \quad (3)$$

Where α is an alpha particle ($^{4}_{2}He$), β^{-} is a negative beta particle and q is the decay energy.

All three decay series show several intermediate steps, none of which are shared between two or more series.

The decay of ^{238}U to ^{206}Pb as a function of time is expressed by equation 4:

$$^{238}U_t = {}^{206}Pb_{initial} + {}^{238}U\,(e^{\lambda t}-1), \quad (4)$$

where *e* is the base-number of the natural logarithm (2,718281828), *t* is years elapsed since the initial value was attained and λ is the decay constant of ^{238}U. Similar equations are used for ^{235}U and ^{232}Th.

To get a reference, and allow for common-lead corrections, it is common to divide each term of equation (4) by the pseudostable non-radiogenic isotope ^{204}Pb, giving equation 5:

$$\left(\frac{^{206}Pb}{^{204}Pb}\right)_t = \left(\frac{^{206}Pb}{^{204}Pb}\right)_{initial} + \left(\frac{^{238}U}{^{204}Pb}\right)_t \left(e^{\lambda t} - 1\right) \quad (5)$$

Which is used for calculating isochron ages, where the slope of the isochron $(e^{\lambda t} - 1)$ gives the age of the sample. The weakness of isochron dating is that it requires no gain or loss of U, Pb or intermediate daughters after the time of crystallization, a criteria that in most cases are not fulfilled. Both U and Pb are commonly lost due to weathering or metamictization of the host crystal.

This problem is partly overcome by use of the concordia diagrams of Wetherill (1956), where $^{206}Pb/^{238}U$ is plotted against $^{207}Pb/^{235}U$, and Tera and Wasserburg (1972) where $^{207}Pb/^{206}Pb$ is plotted against $^{238}U/^{206}Pb$. Using concordia diagrams, good intercept ages could in many cases be calculated based on discordant data. The Tera-Wasserburg diagram is especially useful when high levels of common-lead is causing discordance. In such cases, the plotted data will form an array where the upper intercept is corresponding to the $^{207}Pb/^{206}Pb$ ratio of the common-lead, and the lower intercept to the $^{238}U/^{206}Pb$ ratio (Parrish and Noble 2003).

3.7.3 The Lu-Hf isotopic system

Lutetium is the heaviest of the rare earth elements. It has two naturally occurring isotopes, ^{175}Lu which is stable, and ^{176}Lu which is unstable. Both are non-radiogenic.

Hafnium is a transition metal, with 6 naturally occurring isotopes, including the stable radiogenic ^{176}Hf.

^{176}Lu undergoes the following decay to ^{176}Hf:

$$^{176}_{71}Lu \rightarrow {}^{176}_{72}Hf + \beta^- + \nu^- + q, \quad (6)$$

where ν^- is an anti-neutrino.

The decay of ^{176}Lu to ^{176}Hf as a function of time is expressed by equation 7:

$$^{176}Hf_t = {}^{176}Hf_{initial} + {}^{176}Lu_t\,(e^{\lambda t}\text{-}1), \quad (7)$$

where λ is the decay constant of ^{176}Lu.

To get a reference, it is common to divide each term of the equation by the stable nonradiogenic isotope ^{177}Hf. Applying this on equation 7, and solving for the initial ratio, gives equation 8, which is used to calculate the initial value of ^{176}Hf/^{177}Hf from the measured values of ^{176}Hf/^{177}Hf and ^{176}Lu/^{177}Hf:

$$\left(\frac{^{176}Hf}{^{177}Hf}\right)_{initial} = \left(\frac{^{176}Hf}{^{177}Hf}\right)_{present} - \left(\frac{^{176}Lu}{^{177}Hf}\right)_{present}\left(e^{\lambda t} - 1\right) \quad (8)$$

Where *t* is the age given by U-Pb dating of the same zircon grain.

Hf initial values is commonly expressed as ε_{Hf}, which is the parts pr 10000 deviation from the chondritic undifferentiated reservoir (CHUR) Hf value at any given time. This is expressed by equation 9:

$$\varepsilon_{Hf}(t) = \left[\left(\frac{\left(\frac{^{176}Hf}{^{177}Hf}\right)_{sample}}{\left(\frac{^{176}Hf}{^{177}Hf}\right)_{CHUR}}\right)_t - 1\right] x\ 10^4 \quad (9)$$

The ε_{Hf} notation is used to compare the ^{176}Hf/^{177}Hf ratio of the analyzed sample at the time of crystallization with the ^{176}Hf/^{177}Hf ratio of CHUR at the same age, and thus, makes up an effective tool for investigating magma origin and contamination. In the mantle, Hf is more incompatible than Lu, and therefore more readily mobilized during partial melting. During repeated events of anatexis, the upper mantle has suffered Hf depletion through time, while the crust has become enriched by rising Hf-rich mantle magmas. The increased Lu/Hf values of the upper mantle gives elevated ^{176}Hf/^{177}Hf ratios (more radiogenic Hf), while the opposite is found in most crustal rocks. As a consequence of this, high ε_{Hf} values plotting near the Depleted Mantle (DM) line, indicate a mainly mantle magma origin, while lower ε_{Hf} values indicate magmas originated from, or contaminated by, crustal rocks.

As a petrogenetic tracer, the Lu-Hf system behaves similarly to the Sm-Nd system (Faure and Mensing 2005).

3.7.4 Inductively coupled plasma mass spectrometry (ICP-MS)

U-Pb and Lu-Hf isotope analyses of zircons were performed using a Nu Plasma HR multicollector ICP-MS system with a U-Pb collector block and a New Wave/Merchantek LUV-213 Nd:YAG laser microprobe. All analyses were performed with static ablation, in a helium atmosphere. The following 8 samples were analyzed for U-Pb and Lu-Hf isotopes: GB-A,C,D,E,F,G,H (akerites) and GB-B (granite), approximately 25 zircons from each sample. SEM cathodoluminescence images were used during analysis, for navigation, and to ensure laser ablation being done at the most homogeneous areas in the zircons, avoiding inclusions and fractures. A 30 s on-mass background measurement was done immediately before each run. NU Plasma time-resolved analysis software was applied for isotope ratio calculations. The raw data were corrected for mass discrimination using an exponential law. The analysis was performed at the department of geosciences, University of Oslo, under assistance of Siri L. Simonsen.

3.7.4.1 U-Pb analysis

U-Pb was analyzed using a beam diameter of 40µm and a pulse frequency of 10Hz. The standards applied for U-Pb analysis were the reference zircons Temora 2 (Woodhead and Hergt 2005) and 91500 (Wiedenbeck et al. 1995), while Mud Tank reference zircon (Black and Gulson 1978) was run as unknown. An ablation time of 30s were used for all samples. Data reduction and calibration follows the protocol of Rosa et al (2009), using the in-house Excel spread sheet NuAge.xlt. All U-Pb data plots have been made using the computer software *Isoplot 4.0* (Ludwig K. 2008)

3.7.4.2 Lu-Hf analysis

For Lu-Hf analyses, a beam diameter of 55µm and a pulse frequency of 5Hz were applied. Reference zircons Mud Tank and Temora were used as standards. An ablation time of approximately 150s were used for Lu-Hf analysis, ensuring $^{176}Hf/^{177}Hf$ internal precision of ≤0.000020 (1SE). Analyses with poorer internal precision were generally rejected. The mass discriminating factor for Hf was determined assuming a $^{179}Hf/^{177}Hf$ ratio of 0.7325. Correction for ^{176}Yb interference on ^{176}Hf was done by the procedure described by Heinonen et al. (2010), based on multiple analyses of the reference zircons Temora-2 ($^{176}Yb/^{177}Hf$ = 0.01-0.11) and LV-11 ($^{176}Yb/^{177}Hf$ = 0. 1-0.3), both of which are homogeneous in terms of initial $^{176}Hf/^{177}Hf$. All calculations was performed using a ^{176}Lu decay constant of 1.867 x 10^{-11} y^{-1} (Soderlund et al. 2004). ε_{Hf} was calculated using a present-day chondritic $^{176}Hf/^{177}Hf$ ratio of 0.282785 and a $^{176}Lu/^{177}Hf$ ratio of 0.0336 (Bouvier et al. 2008). The DM model of

Griffin et al. (2000) have been modified to the chondritic $^{176}Hf/^{177}Hf$ and $^{176}Lu/^{177}Hf$ ratios applied.

3.8 Fractional crystallization modeling

Fractional crystallization was modeled using the computer software MELTS (Ghiorso and Sack 1995) with the text driven interface ADIABAT (Antoshechkina and Asimow 2008). The aim of the modeling was to test the hypothesis that the Akerite could have evolved through fractional crystallization of a basaltic parent magma. The input data applied for the modeling was bulk chemical major element values of high-Ti- as well as low-Ti B_1 basalts from Holmestrand, taken from Neumann et al (2002). For both sets of input data, the temperature interval of 1400°C - 900°C was modeled at pressures of 3-10 kilobars. Log fO_2 paths at the fayalite-magnetite-quartz buffer (FMQ) as well as FMQ+1 and FMQ+2 were applied.

4 Results

4.1 Field observations

The akerite body examined is situated at the southern rim of the Nordmarka-Hurdal batholith, bordered by nordmarkite to the northeast and Cambro-Silurian metasediments to the south (Fig. 5 and 10). A small (~0.1km^2) body of intrusive breccia borders the akerite to the north, while a somewhat larger body of RP makes up the northwestern border (Fig. 10). The contact between nordmarkite and akerite is generally sharp. Abundant nordmarkitic veins and apophyses cut the akerite (Fig. 8). Several exposures show akerite xenoliths in nordmarkite (Figs. 7). Some nordmarkite exposures show a reduction in grain size towards the akerite. Where profiles have been made across the contact, the akerite shows an increasingly red color towards the nordmarkite. This color has also been found in samples taken from the interior of the akerite body (see appendix: petrographic microscopy, sample GB-D). The akerite body is cut by granitic and RP dykes of up to 10-15m width. The intrusive breccia body contains several romb-porphyry units plus an aphyric basalt. The contact to akerite is gradual. Syenitic/granitic veins are found cutting across the contact. At the contact to the nordmarkite, apophyses of nordmarkite are seen in the intrusive breccia. The ~1km long romb-porphyry body in the north-west contains several RP-units. At the contact to the akerite, abundant akerite veins and dikes cut the RP. The contact is generally gradual.

At the contact between akerite and the Cambro-Silurian metasediments in the south-east, abundant akerite veins cut the metasediments. The contact is generally sharp, with a marked change in color on the akerite towards the metasediments (Fig. 9). Cambro-Silurian xenoliths of up to ~40m in size are found in the akerite.

At the contact between akerite and the Cambro-Silurian metasediments in the south-east, abundant akerite veins cut the metasediments. The contact is generally sharp, with a marked change in color on the akerite towards the metasediments (Fig. 9). Cambro-Silurian xenoliths of up to ~40m in size are found in the akerite.

Based on field observations and measured UTM coordinates, a map has been made, showing the field area (Fig. 10). The map differs from the map of Holtedahl and Dons (1966) on several points, including:

-A contact between the intrusive breccia and the RP body.

-A greater complexity in the RP body, with several RP units found repeatedly along the RP-akerite contact.
-Several akerite exposures found at or near the southern shore of lake Sognsvann.

4.2 Petrography

The Sognsvann-Holmenkollen akerite is a dark grey quartz-bearing micromonzonite with <10mm black subhedral plagioclase phenocrysts in a fine grained inequigranular matrix. Quartz makes up roughly 5-10% of the rock, and is found interstitially between plagioclase and alkali feldspar matrix grains in all akerite samples except for sample GB-D which is quartz-free. <2.5mm sized amphiboles are the dominating dark mineral, showing light yellow to dark olive green pleochroism. Biotite is found in lower abundance. Clino- and orthopyroxene are found as cores in amphiboles. <1.5mm sized anhedral magnetite is abundant, showing exsolution lamellae of ilmenite, and commonly biotite overgrowths. Needle-shaped euhedral apatite is common.

Altered samples show a light red matrix color. Plagioclase phenocrysts are less altered than matrix feldspars, and generally show grey to black color. Chloritization of biotite, pyroxene and amphibole is common. Orthopyroxene is absent at a relatively moderate level of alteration, where relict clinopyroxene still is seen. The most highly altered samples contain no pyroxene. Epidote is found in veins.

The granitic dike, sample GB-B, consist of light red alkali feldspar, approximately 20% quartz and minor amphibole and biotite. The feldspar is highly sericitized. Amphibole and biotite are strongly chloritized.

See Appendix, Tables 7-22 for individual discriptions on all analysed samples.

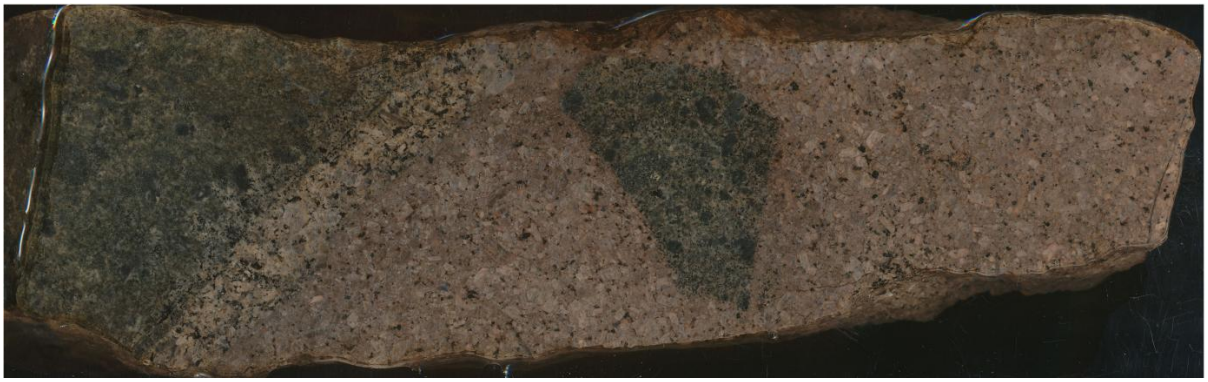

Figure 7. Photo of a sample taken from the contact between akerite (dark grey) and nordmarkite (light reddish). A ~5 cm akeritic xenolith is clearly seen in the nordmarkite. Xenoliths of this size were found at several outcrops. Field of view is 23cm.

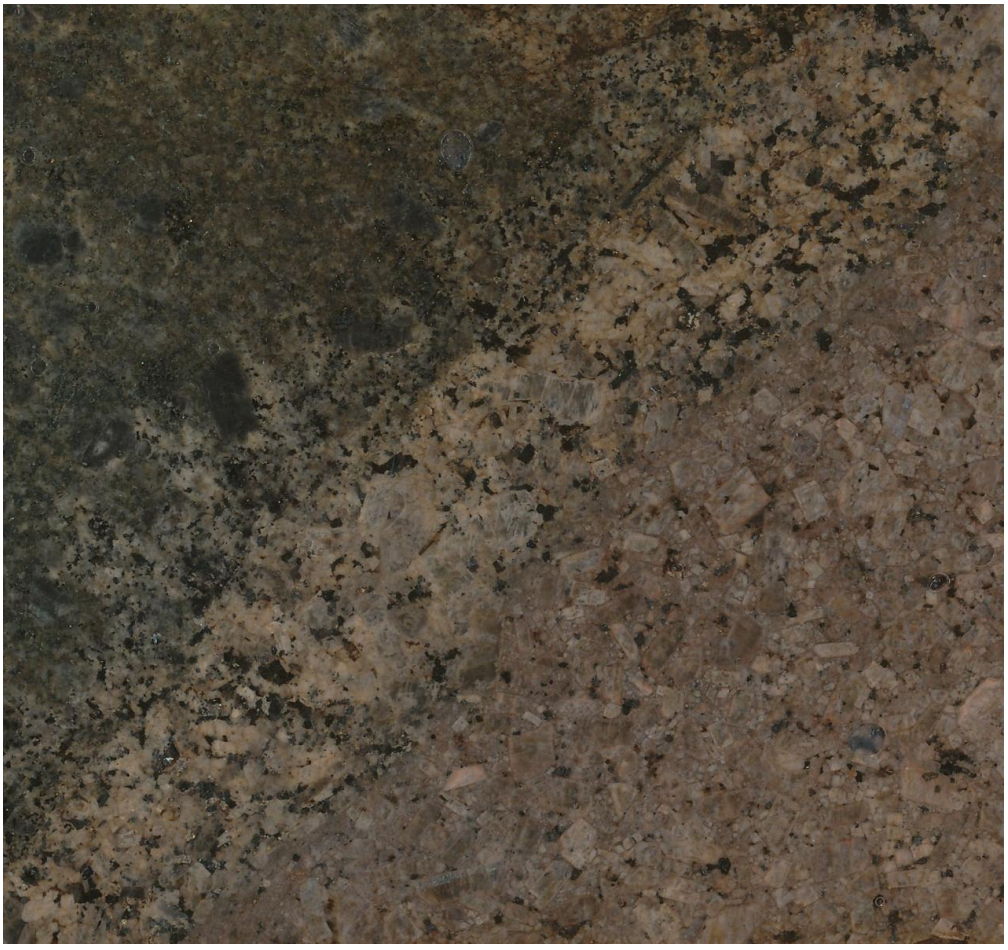

Figure 8. Close-up photo of the contact zone seen in figure 8. The ~1.5cm wide zone of white grayish rock at the contact may have been generated through partial melting of the akerite, causing contamination of the nordmarkite, and possibly also rapid crystallization of the nordmarkitic magma due to the cooling effect of the akerite. Note the many small apophyses intruding the akerite. Field of view is 6cm.

Figure 9. Two samples found at the contact between akerite and Cambro-Silurian metasediments. Akerite is down to the right in both samples. Both samples show changes in texture and color towards the metasediments, indicating contamination from this. Field of view is 12cm for the upper sample and 7cm for the lower.

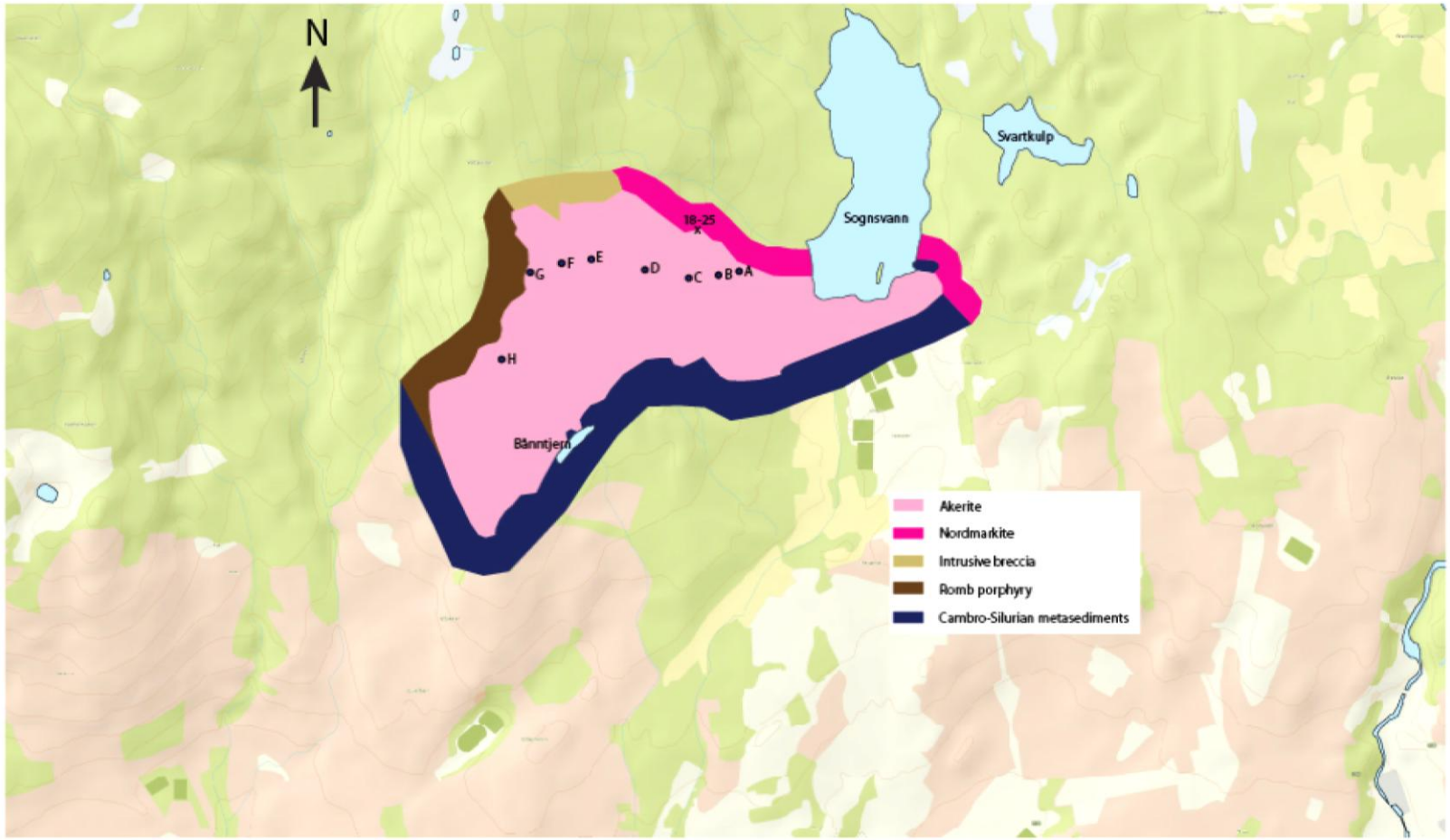

Figure 10. Map of the field area, showing the akerite body with neighboring units. Locations of samples A-H and 18-25 are marked. Background colors: light green: forest, greyish pink: the rural area of Oslo. Light blue: lakes.

4.3 Zircon petrography

Zircon is an abundant accessory mineral in all studied samples. SEM-CL images have been used to study the morphology of zircons in polished epoxy mounts. Zircons of sample GB-B (granitic dike) differs greatly from the akerite zircons in their textural appearance on CL images. In GB-B, ~70% of the zircons show distinct concentric zoning, while this is found in only ~10% of the zircons from the 7 akerite samples (GB-A,C,D,E,F,G and H). In akerite, ~50% of the Zircons show no zoning, while ~35% show various degrees of irregular zoning/inhomogeneity. Inclusions were found in ~40% of the zircons, consisting of the minerals apatite, plagioclase, alkali feldspar, ilmenite, quartz and titanite. CL images of a selection of zircons are presented (Fig. 11).

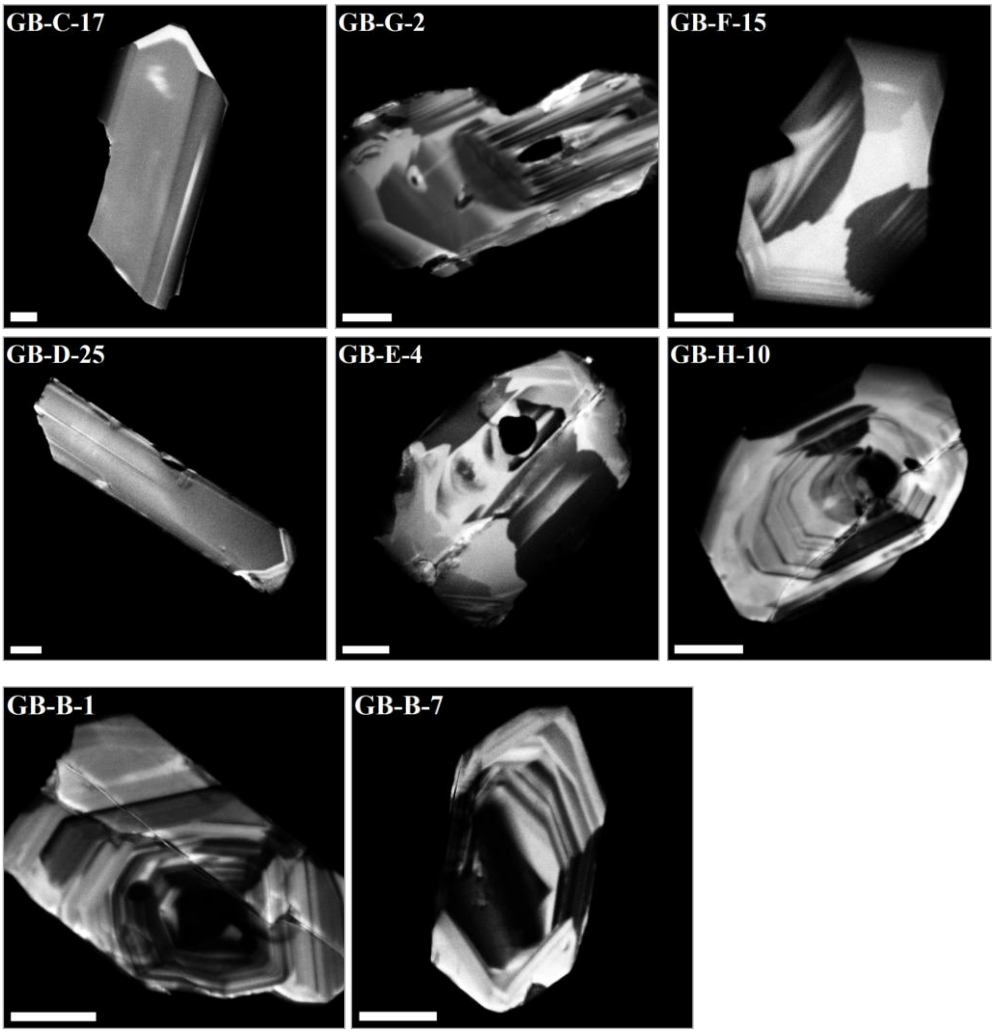

Figure 11. CL images of a selection of zircons from akerite (upper six images) and granite (lower two images). ~50% of the zircons in the akerite show a more or less homogeneous texture, exemplified by zircons GB-C-17 and GB-D-25. ~35% show different irregular zonation patterns, as seen in zircons GB-G-2 and GB-E-4. Well-developed radial zoning was found only in ~10% of the zircons, here represented by zircons GB-F-15 and GB-H-10. The white line is 20µm. The majority of the zircons in the granite (GB-B) show well developed concentric zoning, represented by zircons GB-B-1 and GB-B-7.

4.4 Major elements

All major element values are presented in Appendix, Table 23. With the exception of sample GB-D, the akerite analyses generally show low variations in major element weight percent values, with SiO_2=59.5-58.1, Al_2O_3=16.6-16.5, Fe_2O_3 (representing total Fe)=6.7-7.5, MgO=2.0-2.2, CaO=4.2-5.0, Na_2O=4.2-4.6 and K_2O=3.2-3.7. Sample GB-D differs from the other akerite analyses in having lower SiO_2 (57.2%), CaO (4.0%), K_2O (2.5%), and higher Na_2O (6.5%). For the other oxides, values are near the akerite average. A total alkalis vs silica (TAS) diagram is calculated after Middlemost (1994) (Fig 12). With one exception, all akerite samples plot in the quartz monzonite field. Being lower in silica and higher in alkalis, sample GB-D plots at the low-silica end of the syenite field. Sample GB-B plots at the division line between granite and alkali feldspar granite.

CIPW norms are calculated for akerite plus the granitic dike (Table 3). An Fe_2O_3/FeO ratio of 0.4 as recommended by Middlemost (1989) have been used in the calculations. Excluding sample GB-D, from the akerite analyses, quartz varies from 6.5% to 7.8%, orthoclase from 19.0% to 22.1%, albite from 35.8% to 39.0%, while anorthite is at 13.0 to 16.0. All akerites have normative diopside (2.7%-4.8%), and hypersthene (8.2% to 9.3%). GB-D differs from the other akerite samples in being olivine normative (5.2%), and thus, show no normative quartz. Further, it has higher normative albite (55.3%) and diopside (6.4%), and lower normative orthoclase (15.0%), anorthite (9,0%) and hypersthene (0.8%). The granitic dike (sample GB-B) is hypersthene normative (2.9%), shows distinctively higher normative quartz (17.6%) and orthoclase (29.4%), and lower anorthite (4.0%) than the akerite. In normative albite (42.4%), it is slightly higher than the bulk of the akerite analyses, but markedly lower than the anomalous akerite GB-D. All samples have normative magnetite, ilmenite and apatite.

Neumann (1980) used plots of agpaitic index ((Na+K)/Al) vs MgO/(Fe_2O_3+FeO+MgO) and different major elements vs D.I. (normative quartz + orthoclase + albite + nepheline) to illustrate internal variations in the Larvik ring complex. Two plots are presented, where the akerite is superimposed on Neumann's (1980) diagrams (Figs. 13-14).

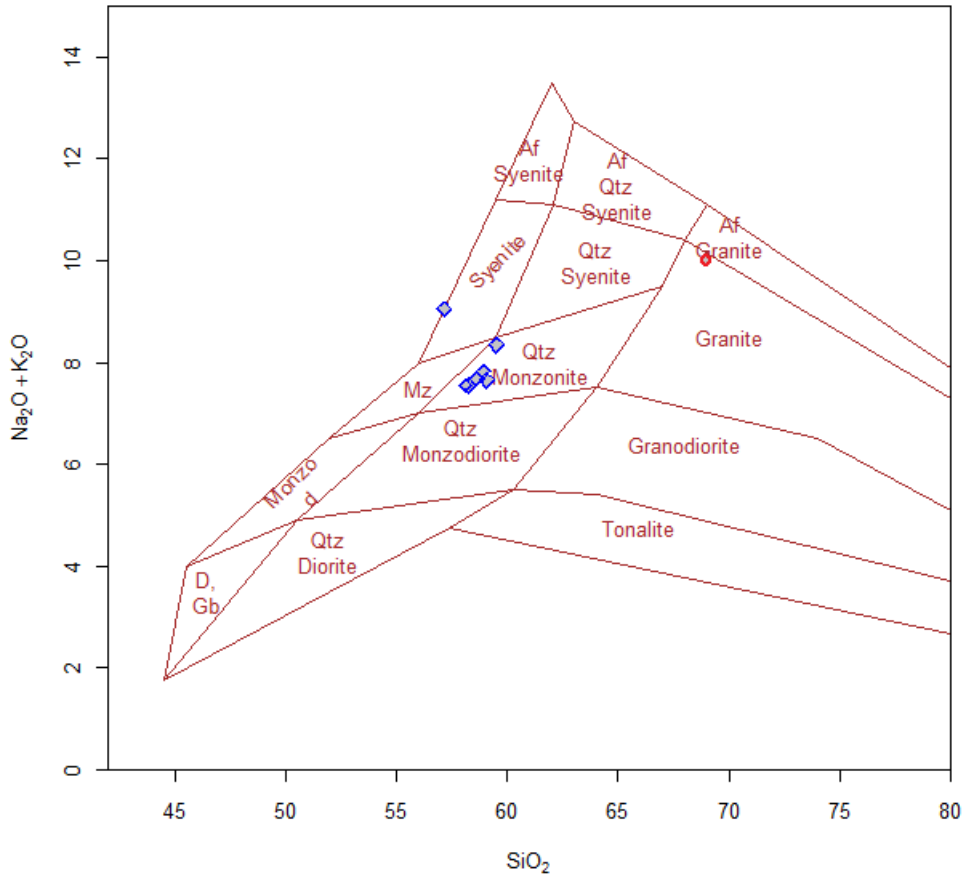

Figure 12. TAS diagram calculated after Middlemost (1994). Akerite is shown as blue diamonds, granite as a red circle. All but one of the akerite samples plot as quartz monzonite. Sample GB-D is quartz-free and slightly higher in alkalis, and plot as syenite. The one granite sample analyzed, taken from a dike intruding the akerite, plots at the border between granite and alkali feldspar granite.

CIPW Norm

				Akerite				Granite
Mineral	**GB-A**	**GB-C**	**GB-D**	**GB-E**	**GB-F**	**GB-G**	**GB-H**	**GB-B**
Quartz	7.84	7.40	0.00	6.87	6.88	7.71	6.51	17.55
Corundum	0.00	0.00	0.00	0.00	0.00	0.00	0.00	0.15
Orthoclase	19.68	20.33	14.95	19.38	19.03	20.92	22.10	29.43
Albite	36.64	35.79	55.26	36.05	36.72	36.22	39.01	42.39
Anorthite	15.56	15.27	9.03	15.50	15.98	14.95	12.98	4.01
Diopside	4.09	4.22	6.41	4.75	4.30	2.67	3.81	0.00
Hypersthene	8.51	8.92	0.81	9.02	8.84	9.34	8.18	2.88
Olivine	0.00	0.00	5.23	0.00	0.00	0.00	0.00	0.00
Magnetite	2.93	3.03	3.15	3.10	3.00	2.91	2.77	1.28
Ilmenite	2.76	2.89	2.79	2.95	2.89	2.76	2.62	0.93
Apatite	1.21	1.23	1.11	1.18	1.23	1.18	1.18	0.17
Sum	99.20	99.08	98.73	98.81	98.86	98.66	99.16	98.78

Table 3. CIPW norm calculated for seven akerite samples and one granite sample. Note that sample GB-B is olivine normative, while the other akerite samples contain 6.5-7.8 % normative quartz. The amphibole granite GB-B, is hypersthene normative because water is excluded from the norm calculations.

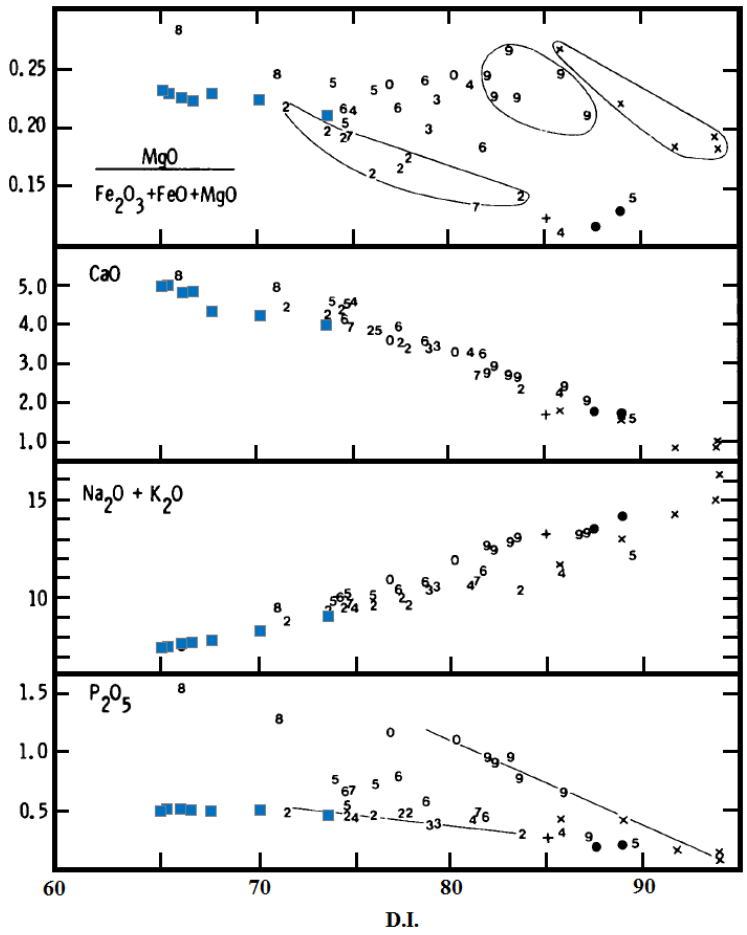

Figure 13. Selected major element parameters plotted against differentiation index (DI). Blue squares show akerite analyses superimposed on a diagram from Neumann (1980). The numbers 2-8 denote larvikites from ring-sections 2-8. 9 and 0 are lardalites from ring-sections 9 and 10 respectively. x and + are foyaite/hedrumites inside and outside ring-section 10 respectively. Filled circles are ditroites. D.I. is based on cation norm calculations for both akerite and the Larvik complex rocks. The akerite show a clear correlation with the larvikites in all diagrams, plotting at the least evolved end of the trend lines for the quartz normative ring-section 2.

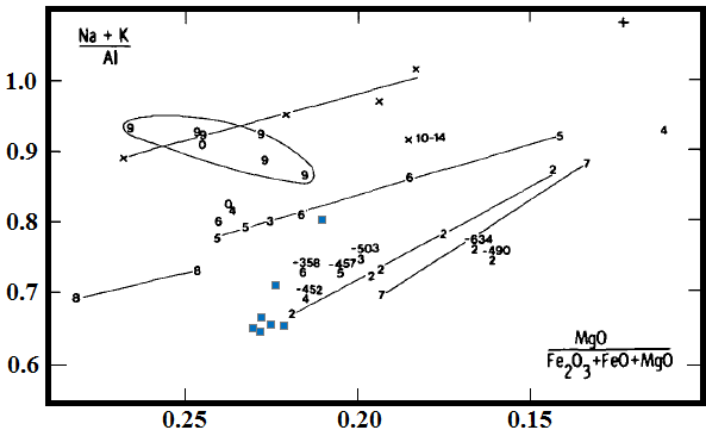

Figure 14. Agpaitic index ((Na+k)/Al) plotted against MgO/(Fe_2O_3+FeO+MgO). Blue squares show akerite analyses superimposed on a diagram from Neumann (1980). Symbols as in figure 13. Samples deviating significantly from their ring-section trend are marked with complete sample numbers. As in figure 13, it can be seen that the akerite plots in the least evolved end of the trend line for the quartz-bearing ring-section 2. The sample deviating in showing significantly higher agpaitic index is GB-D.

The plots show that the akerite generally follows the same trends as the Larvikites, plotting at the least evolved end of the trend line for the quartz-normative larvikite of ring section 2 (Neumann 1980). Due to its higher Na level, sample GB-D plots somewhat away from the other analyses, in a more evolved direction. Except for sample GB-D, the akerite generally show lower agpaitic index than the larvikites.

By the definition of Frost et al (2001), based on aluminum saturation index (ASI = Al/(Ca-1.67P+Na+K)) and agpaitic index, the akerite classifies as *Metaluminous*, while ASI is somewhat higher in the granitic dike, placing it at the boarder between metaluminous and *Peraluminous*. A diagram is shown, where FeO/(FeO+MgO) and Na_2O+K_2O-CaO, respectively, are plotted against SiO_2 (after Frost et al (2001)) (Fig.15). In the FeO/(FeO+MgO) plot, all akerite analyses, plus the granitic dike, plot at the division line between *Magnesian* and *Ferroan*. The deviating sample, GB-D, plots somewhat higher in the Ferroan field. In the Na_2O+K_2O-CaO plot, the bulk of the akerite samples plot within the *Alkali-calcic* field, near the division line between the Alkali-calcic and the *Alkalic* field. Sample GB-D and the granite sample (GB-B) plots well within the Alkalic field.

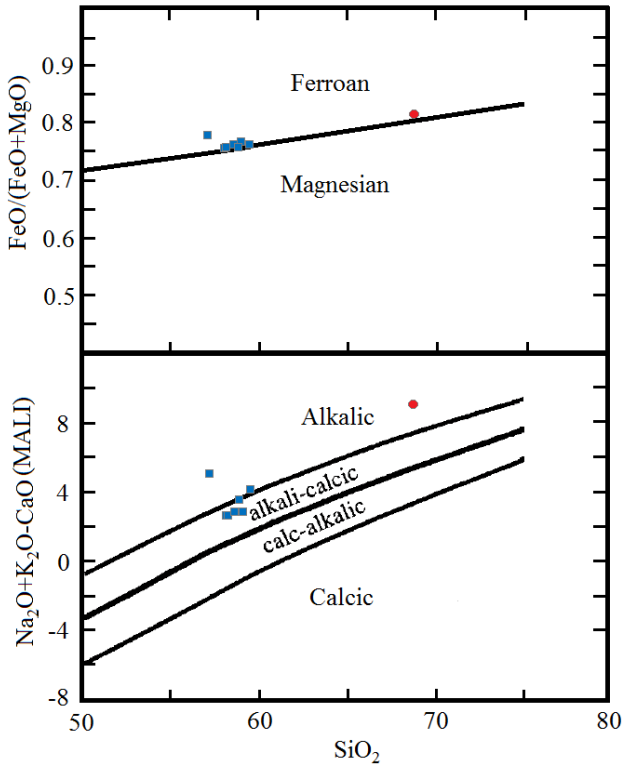

Figure 15. Bulk rock classification diagram of Frost et al. (2001). In the upper diagram, of FeO/(FeO+MgO) vs SiO_2, akerite and granite plots at the lowermost ferroan field, near the division line between ferroan and magnesian. In the lower diagram, of Na_2O+K_2O-CaO vs SiO_2, most akerite analyses plot as alkali-calcic, near the division line between alkali-calcic and alkalic. Sample GB-D and the Granite (GB-B) plots in the alkalic field.

4.5 Trace elements

All trace element analyses are presented in Appendix, Table 24. The unexpectedly high levels of Cr are most likely caused by contamination from the mill used to crush the rock samples. Sample GB-D shows a lower value of Ba (1570 ppm) than the other akerite samples (1810-2262 ppm).

The early B_1 basalts from Vestfold are considered amongst the most primitive and uncontamined basalts of the Oslo Rift (Neumann et al. 2002), and are thus used as a reference to test the hypothesis that akerite is a more or less uncontaminated derivate of a primary basaltic magma. A plot of both B_1 suites and akerite normalized to primitive mantle (PM) of Sun and McDonough (1989) are shown (Fig. 16). Trace elements values for the 7 akerite samples (GB-A,C,D,E,F,G and H) plus the granitic dike (GB-B) are plotted, normalized to average values for high-Ti and low-Ti B_1 basalts from Holmestrand, Vestfold (samples F6, F8b, F11, F12 and F15 (high-Ti) and PP4, PP5, P7, P8, P8b, OB59, P9a, P9b, P9c, P9d, P13, P14, P16 and B3V1X (low-Ti) of Neumann et al (2002)) (Figs. 17-18). Plotted against the high-Ti basalt, the akerite shows 1.1-3.5 times enrichment in Ba, K, La, Ce, and Zr, while Sr, P, Ti, Ce, Co and Ni are depleted. Relative to the low-Ti basalt, the akerite shows 1.1-3.5 times enrichment in the elements Ba, K, La, Ce, P, Zr and Yb, while Sr, Ti, Co and Ni are depleted. The granite sample shows stronger enrichment than the akerite in K, La, Ce and Yb and stronger depletion in Sr, P, Ti, Co and Ni in both plots. The seven akerite analyses (GB-A,C,D,E,F,G,H) and the granitic dike (GB-B), are plotted with 17 analyses of RP_1 from Andresen (1985), all normalized to an average of B_1samples F6, F8b, F11, F12 and F15 (high-Ti) of Neumann et al (2002) (Fig. 19) The akerite shows Sr values 2-4 orders of magnitude lower than RP_1. K, P and Ti generally plot within or close to the RP_1 field, while Zr is somewhat lower in the akerite.

Figure 16. Average values of Low-Ti B1 basalt, High-Ti B1 basalt (both from Neumann et al. (2002)), akerite and the granitic dike, normalized to Primitive Mantle values of Sun and McDonough (1989).

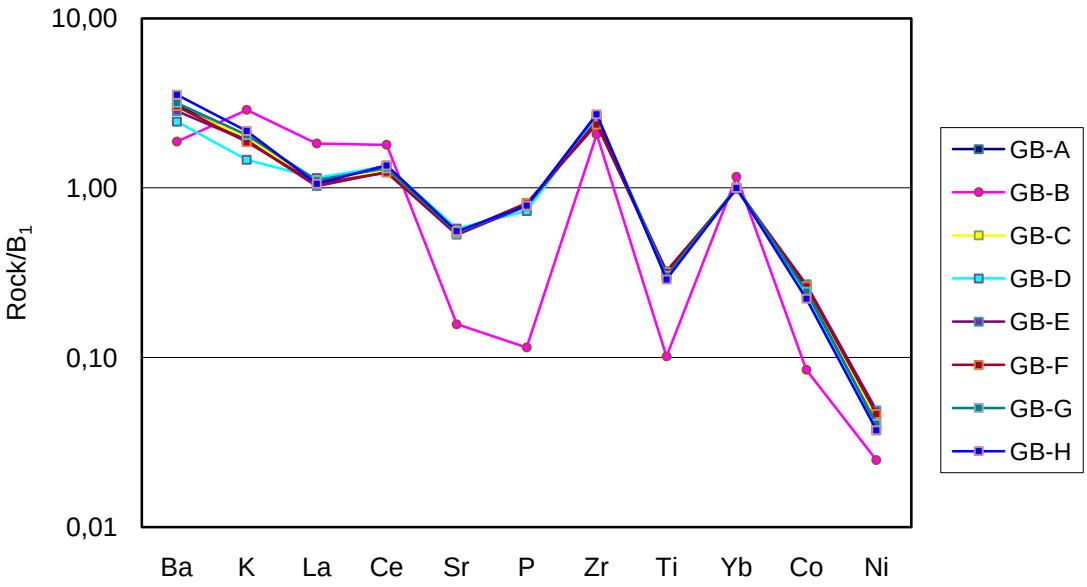

Figure 17. Trace element values of all analyzed samples normalized to values for high-Ti B_1 basalt from Holmestrand. Data from Neumann et al. (2002). The akerite is enriched in Ba, K, La, Ce, and Zr and depleted in Sr, P, Ti, Ce, Co and Ni relative to the basalt. Yb shows similar values. The granite shows more developed values, following the trend of the akerite.

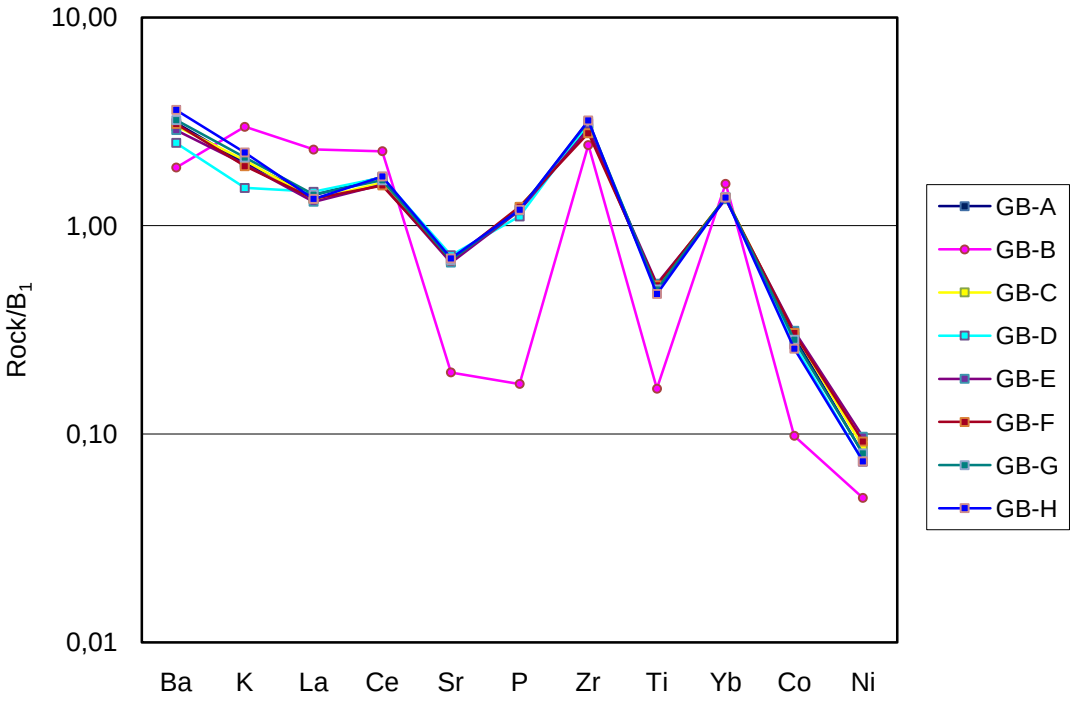

Figure 18. Trace element values of all analyzed samples normalized to values for low-Ti B_1 basalt from Holmestrand. Data from Neumann et al. (2002). The akerite is enriched in Ba, K, La, Ce, P Zr and Yb and depleted in Sr, Ti, Co and Ni relative to the basalt. The granite shows more developed values, following the trend of the akerite. It deviates, however, in its marked depletion in P.

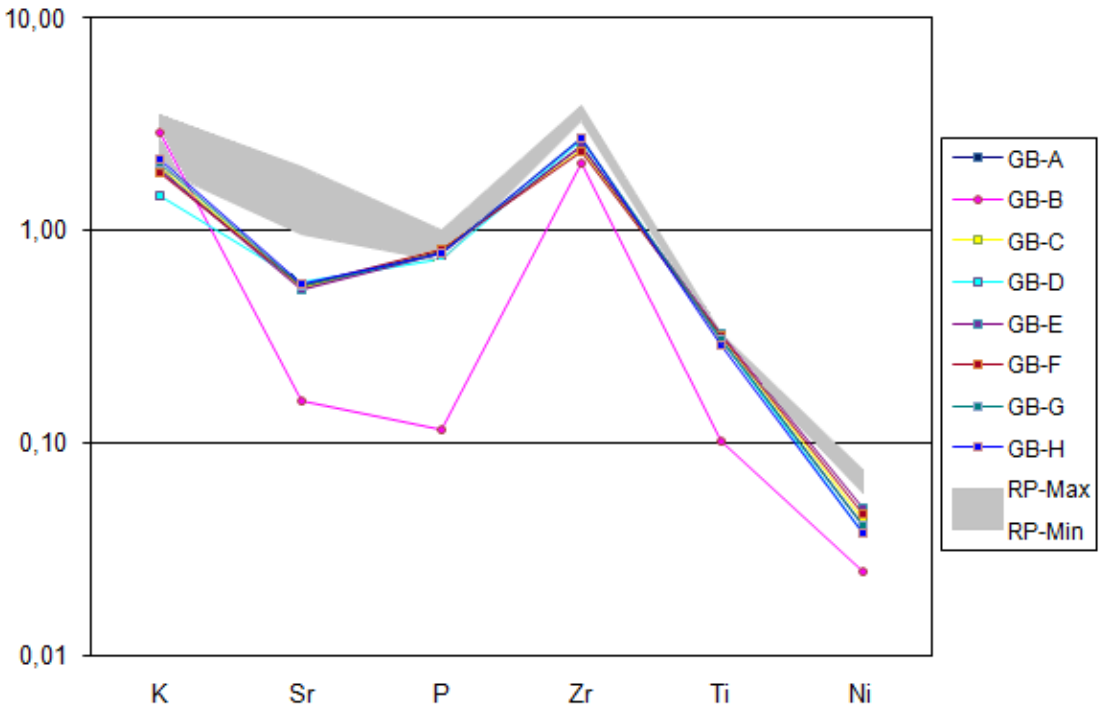

Figure 19. Trace element values plotted against values for RP_1, both normalized to high-Ti B_1 basalt from Holmestrand. Data from Andresen (1985) and Neumann et al. (2002). Although not showing perfect fit, the akerite show a trend similar to RP_1. Sr is markedly lower in akerite.

Electron microprobe analysis

4.5.1 Sample description

4.5.1.1 GB-A and GB-C (akerite)

By petrographic microscope examination, GB-A and GB-C was found to be the akerite samples with the lowest degree of low-temperature alteration. Some chloritization is found on biotites and clinopyroxenes, orthopyroxenes are cut by veins of alteration minerals, amphiboles are generally unaltered. In addition to EMP analysis, both samples have been subject to major- and trace element bulk chemical analysis, plus ICP-MS U-Pb and Lu-Hf isotope analyses of zircons. The following minerals were analyzed: amphibole, clinopyroxene, orthopyroxene and biotite.

4.5.1.2 GB-B

The sample is taken from a granitic dike cutting the interior of the akerite body. Through petrographic microscope examination, clear indications of low-temperature alteration were found. Feldspars are strongly sericitized, and some chloritization is found on the amphiboles. This has been avoided when selecting points of analysis. The sample has been subject to major- and trace elements bulk chemical analysis, plus ICP-MS U-Pb and Lu-Hf isotope analyses of zircons. Analysis was done on amphiboles only.

4.5.1.3 GB-18

Taken from within the nordmarkite body, 0.5m from the contact between nordmarkite and akerite. Through petrographic microscope examination, clear indications of low-temperature alteration were found. Feldspars are strongly sericitized and amphiboles show distinct alteration zoning. Analysis was done on amphiboles only.

For a visual description of each sample, see Appendix, Tables 7-9 and 15. Measured oxide values and structure formulas are presented in Appendix, Tables 45-49. Calculated distribution of cations in sites T_1+T_2, M_1+M_2+M_3, M_4 and A respectively (Table 4).

4.5.2 Amphibole

Measured oxide values plus structure formulas are presented in Appendix, Tables 45-46. All amphiboles in the two akerite samples and in the granitic dike (GB-A+GB-C and GB-B respectively) have $Ca_B > 1.5$ and $(Na+K)_A > 0.5$. All but one has Mg/(Mg+Fe) ratios > 0.5 and thus classify as the calcic amphibole edenite (Leake et al. 1997). One amphibole grain analyzed in the granite shows an Mg/(Mg+Fe) ratio of 0.49 and thus plots just within the ferro-edenite field (Leake et al. 1997). Both the akerite and the granite show high degree of

chemical homogeneity between the different analyses. Some variations are, however, found in the Mg/(Mg+Fe) ratios, ranging from 0.49 to 0.54 for the granite and 0.55 to 0.62 for the akerite. Amphiboles in the akerite show higher values of Ti, Al, Mg, Ca and K than what is found in the granite, while the latter show higher values of Si, Fe, Mn and Na. The akerite amphiboles have $(Al+Mg+Fe+Ti)_{M1-3} = 5$, with excess Fe placing in M_4. In the granite, $(Al+Mg+Fe+Ti)_{M1-3} < 5$, with Mn filling up the M_{1-3} position. Cr is below detection limits in most analyses.

		T1+T2		M1+M2+M3					M4				A		
Rock type	**Analysis**	**Si**	**Al**	**Al**	**Mg**	**Fe**	**Ti**	**Mn**	**Fe**	**Mn**	**Ca**	**Na**	**Na**	**K**	**Name**
Granitic dike	**27.1**	7.03	0.97	0.05	2.56	2.20	0.14	0.05	0.00	0.18	1.73	0.08	0.57	0.15	Edenite
	28.1	7.01	0.99	0.04	2.53	2.25	0.15	0.03	0.00	0.20	1.72	0.08	0.59	0.16	Edenite
	29.1	7.05	0.95	0.05	2.46	2.25	0.14	0.09	0.00	0.17	1.73	0.10	0.57	0.15	Edenite
	30.1	7.05	0.95	0.06	2.34	2.36	0.15	0.08	0.00	0.17	1.74	0.10	0.53	0.16	Edenite
	31.1	7.01	0.99	0.06	2.47	2.28	0.14	0.04	0.00	0.20	1.72	0.08	0.57	0.16	Ferroedenite
Nordmarkite	**32.1**	7.68	0.32	0.11	2.28	2.37	0.09	0.15	0.00	0.21	0.79	1.01	0.78	0.25	Ferrorichterite
	33.1	7.81	0.19	0.16	2.66	2.08	0.06	0.05	0.00	0.29	0.69	1.02	0.78	0.15	Richterite
	34.1	8.04	-0.04	0.24	1.79	2.83	0.08	0.05	0.00	0.30	0.34	1.36	0.68	0.24	Ferrorichterite
	35.1	7.95	0.05	0.15	1.62	2.96	0.09	0.17	0.00	0.21	0.51	1.28	0.76	0.24	Ferrorichterite
	36.1	7.91	0.09	0.12	1.77	2.84	0.08	0.19	0.00	0.21	0.64	1.16	0.74	0.22	Ferrorichterite
	1.2	7.76	0.24	0.03	3.04	1.57	0.07	0.28	0.00	0.06	1.11	0.83	0.73	0.17	Richterite
	2.2	7.98	0.02	0.19	2.22	2.39	0.07	0.13	0.00	0.22	0.44	1.35	0.80	0.24	Ferrorichterite
	3.2	7.98	0.02	0.18	1.64	3.00	0.08	0.10	0.00	0.28	0.57	1.15	0.60	0.23	Ferrorichterite
	4.2	7.36	0.64	-0.02	3.32	1.36	0.15	0.19	0.00	0.04	1.39	0.57	0.74	0.19	Richterite
	5.2	8.02	-0.02	0.22	1.66	3.00	0.09	0.04	0.00	0.30	0.40	1.30	0.63	0.25	Ferrorichterite
	6.2	7.79	0.21	0.02	1.64	3.08	0.03	0.22	0.00	0.08	1.81	0.12	0.18	0.06	Ferrowinchite
	7.2	7.46	0.54	0.00	3.32	1.36	0.12	0.20	0.00	0.05	1.35	0.60	0.72	0.17	Richterite
	8.2	8.03	-0.03	0.23	1.56	3.03	0.08	0.10	0.00	0.28	0.33	1.39	0.73	0.24	Ferrorichterite
Akerite	**1.1**	6.93	1.07	0.09	2.74	1.99	0.18	0.00	0.11	0.06	1.81	0.02	0.45	0.19	Edenite
	2.1	6.90	1.10	0.06	2.77	1.98	0.19	0.00	0.10	0.07	1.81	0.03	0.48	0.19	Edenite
	4.1	6.91	1.09	0.07	2.75	1.98	0.20	0.00	0.10	0.05	1.81	0.04	0.46	0.21	Edenite
	13.1	6.90	1.10	0.05	2.83	1.92	0.20	0.00	0.12	0.06	1.78	0.04	0.48	0.21	Edenite
	16.1	6.87	1.13	0.07	2.90	1.83	0.20	0.00	0.13	0.06	1.77	0.03	0.48	0.21	Edenite
	18.1	6.96	1.04	0.06	2.83	1.93	0.18	0.00	0.11	0.06	1.79	0.04	0.46	0.19	Edenite
	10.2	6.92	1.08	0.07	2.98	1.75	0.20	0.00	0.11	0.06	1.78	0.06	0.45	0.21	Edenite
	17.2	6.92	1.08	0.10	2.65	2.05	0.20	0.00	0.13	0.06	1.76	0.05	0.42	0.19	Edenite
	18.2	6.95	1.05	0.10	2.81	1.91	0.19	0.00	0.12	0.06	1.79	0.04	0.45	0.17	Edenite
	26.2	6.90	1.10	0.07	2.89	1.84	0.21	0.00	0.14	0.05	1.76	0.05	0.46	0.21	Edenite
	29.2	6.91	1.09	0.07	2.67	2.05	0.20	0.00	0.10	0.07	1.80	0.03	0.44	0.19	Edenite
	31.2	6.89	1.11	0.06	2.85	1.89	0.21	0.00	0.13	0.06	1.78	0.03	0.47	0.20	Edenite

Table 4. Distribution of cations within structural sites (T1,T2), (M1,M2,M3), M4 and A for amphibole analyses of akerite, nordmarkite and granite. Following numbers marked with the same gray tone denotes analyses done at the same grain. Note the large chemical variations within each grain of the nordmarkite.

With one exception, the amphiboles of the nordmarkite sample (GB-18) gave $(Na+K)_A$ > 0.5, $(Ca+Na_B)$ >1,5, and Na_B between 0.5 and 1,5. They further have $Mg/(Mg+Fe^{2+})$ ratios of between 0.34 and 0.71, and thus plot on both side of the division line between richterite and ferrorichterite (Leake et al. 1997). One analysis gave a $(Na+K)_A$ value as low as 0.24, and a $Mg/(Mg+Fe^{2+})$ ratio of 0.35, and thus plot as ferrowinchite (Leake et al. 1997). The Nordmarkite amphiboles generally show less chemical homogeneity than the granite and akerite samples, with especially large variations in Na, Fe, Mg and Ca within each grain. Backscattered electron image and element maps for Na, Fe, Mg and Ca for the amphibole grain of analyses 7.2 and 8.2 (nordmarkite)are presented (Fig. 20). The maps show large zonal variations in all four elements. Fe and Mg show opposite trends, with highest Mg values in central parts of the grain, and highest Fe at the edges. The same is found with Na and Ca. The center shows the highest Ca values, while Na is highest at the edges. The red zones on the Ca map, showing the highest concentrations, are inclusions of titanite. A plot of Na+K against Ca has been made (Fig 21). The nordmarkite amphiboles plot along the red line showing the one to one substitution of Na and K for Ca. Ternary plots of Na+K/Fe+Mn/Mg are shown comparing amphibole analyses from nordmarkite, akerite and granite with nordmarkite and larvikite analyses of Andersen (1984a), from the Sande cauldron (Fig. 22). The plot shows a close correlation between the GB-18 nordmarkite and Sande nordmarkite/alkali syenite, as well as between the GB-A/GB-C akerite and the Sande larvikite.

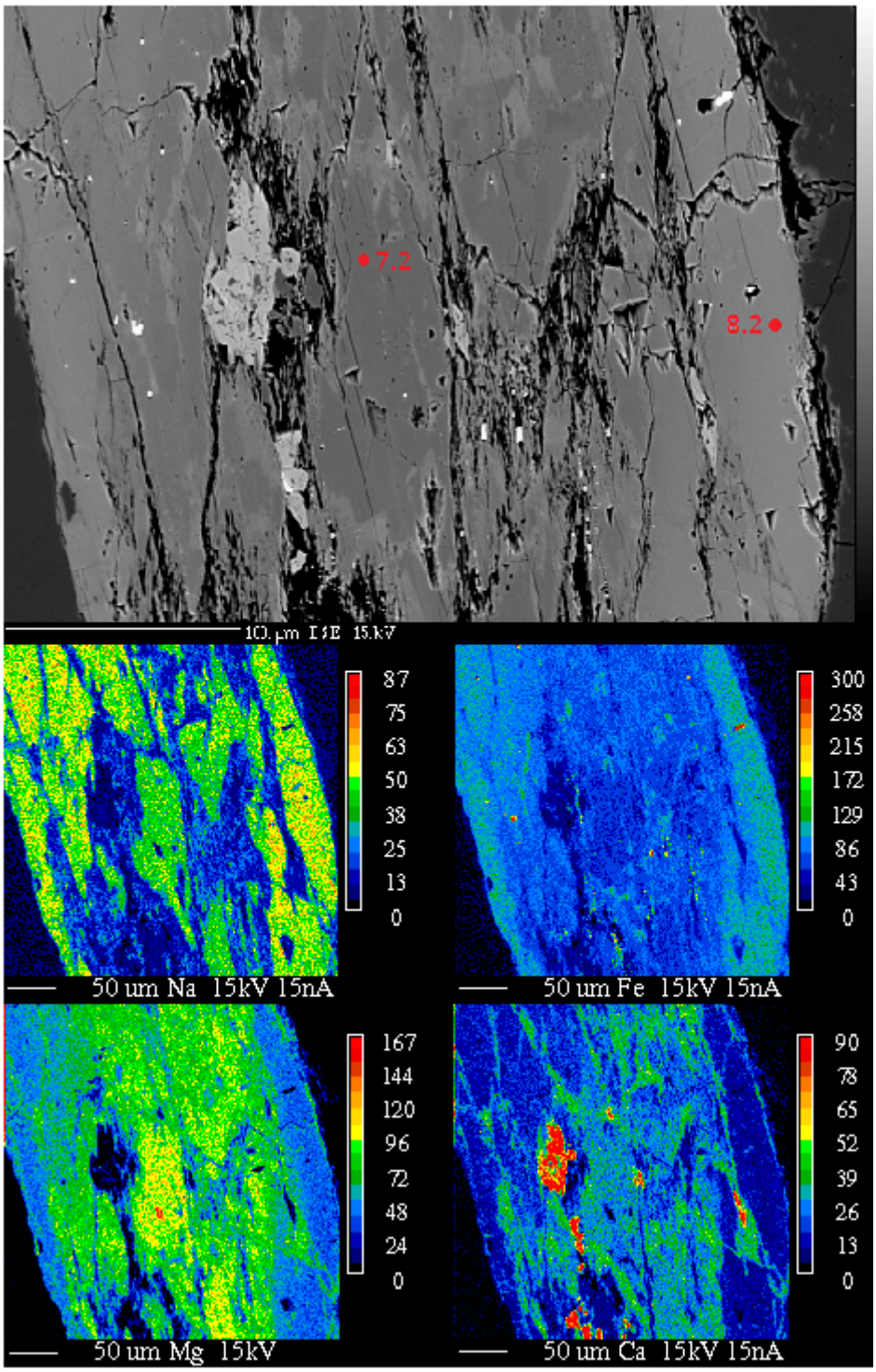

Figure 20. BSE image plus EMP element maps of Na, Fe, Mg and Ca respectively, for a representative amphibole grain of the nordmarkite (sample GB-18). Note that the concentration of Na and Fe is increasing towards the edges, while Mg and Ca show the opposite trend. This is reflected in the structural formulas of analyses 7.2 and 8.2 (Table 4). The inclusions seen as light grey zones on the CL image and red spots on the Ca map are titanite.

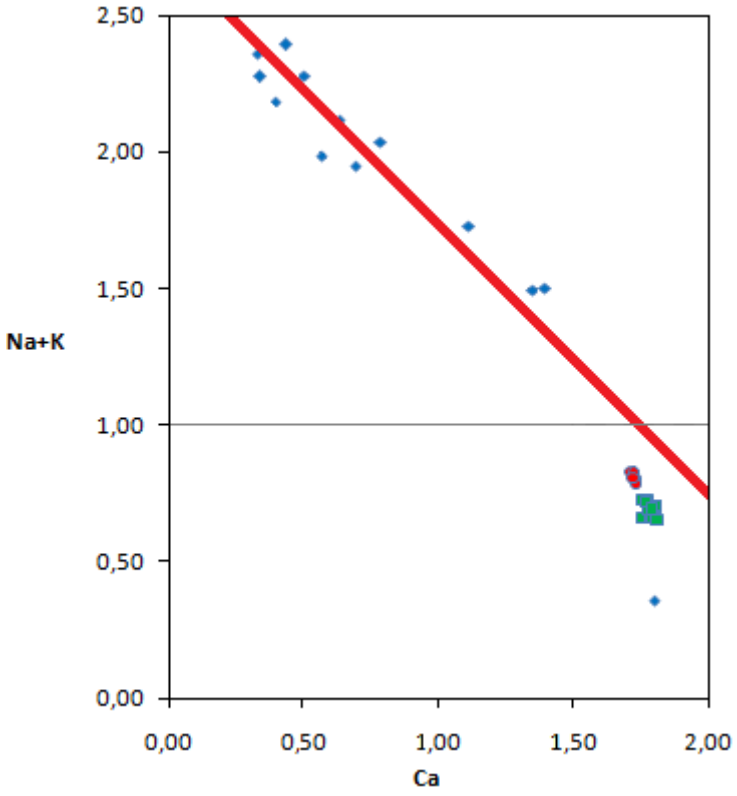

Figure 21. Na+K vs Ca plot of all the analyzed amphiboles. Red circles: granite, green squares: akerite, blue diamonds: nordmarkite. Note that the nordmarkite amphiboles plot along a one to one substitution line of Na+K for Ca. Note that amphiboles of the granite and akerite samples show significantly greater homogeneity.

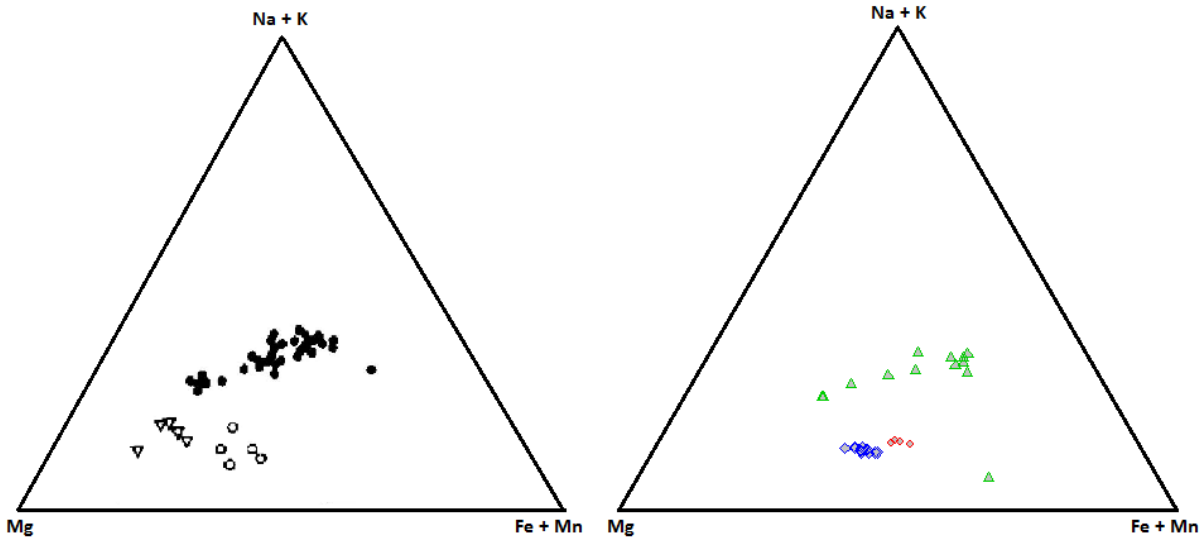

Figure 22. Ternary plots of Na+K, Fe+Mn and Mg. Left triangle shows plots of amphiboles from larvikite, nordmarkite and alkali syenite of the Sande Cauldron (Andersen 1984b). Open circles: larvikite, closed circles and black triangles: different suites of nordmarkite and alkali syenite. Right triangle show all analyzed amphiboles (Table 4). Blue diamonds: akerite, red circles: granite: green triangles: nordmarkite. Note the close correlation between amphiboles of the two different complexes.

4.5.3 Clinopyroxene

Structure formulas are calculated, based on 6.00 oxygens, and then normalized to 4.00 cations. Based on the excess cations in the structure formula prior to normalization, Fe^{3+} and Fe^{2+} values were calculated. Measured oxide values, plus structure formulas, are presented in Appendix, Table 47. Chemical variations between samples are generally low. Some scatter can, however, be seen in the classification diagram after Morimoto (1989) (Fig. 23). All analyses plot near the division line between augite and diopside, with the majority within the augite field. The $Fe^{3+}/(Fe^{3+}+Fe^{2+})$ ratio varies from 0.05 to 0.17. Cr shows values close to or below detection limits. All clinopyroxenes examined showed parallel exsolution lamellas of orthopyroxene (Fig 24).

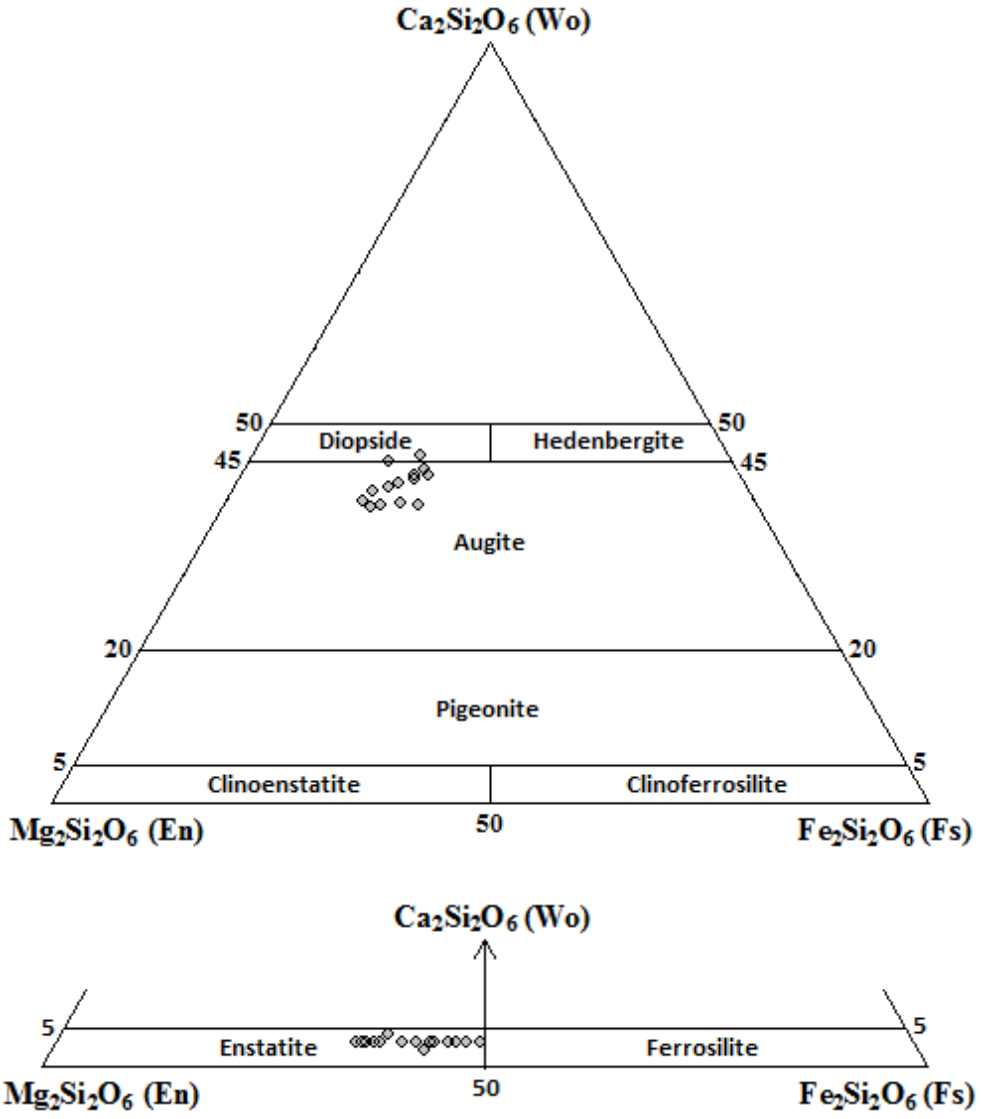

Figure 23. Classification diagrams for clinopyroxenes (upper diagram) and orthopyroxenes (lower diagram). After Morimoto (1989). All analyses are from akerite samples GB-A and GB-C. The clinopyroxenes show little scatter, and plot near the division line between diopside and augite, mainly at the augite side. Orthopyroxenes vary from En_{51} to En_{65}. This does to a large degree reflect zonal variations within each grain, showing increasing Fe content towards the edges.

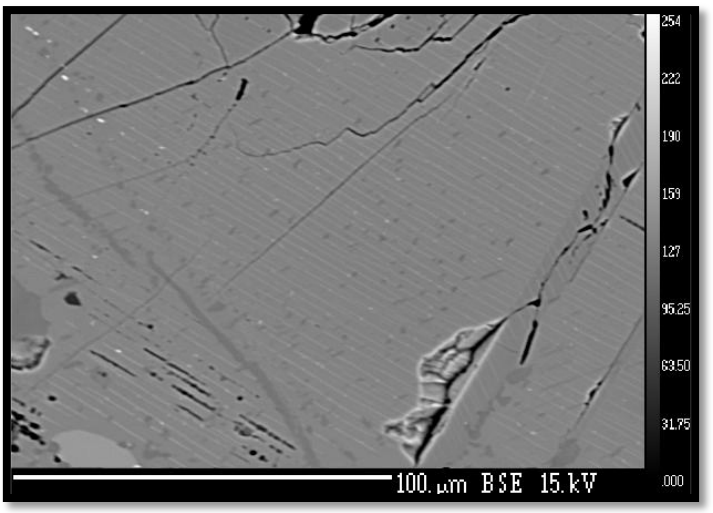

Figure 24. BSE image of a section from a clinopyroxene grain of akerite sampleGB-A. The white lines are exsolution lamellae of orthopyroxene.

4.5.4 Orthopyroxene

Measured oxide values plus structure formulas are presented in Appendix, Table 48. Compositions vary from En_{51} to En_{65}, with values of (Ti+Al+Mn+Ca) between 0.6 and 0.9 a.p.f.u. Cr is below detection limits in most analyses. Orthopyroxenes show zonal variations in Fe and Mg content, with Fe increasing towards the edges of the grains. All analyses are plotted in a classification diagram (Morimoto 1989) (Fig. 23). BSE images are shown, displaying orthopyroxenes cross-cut by veins of alteration minerals (Fig 26). The two images are representative for all orthopyroxenes in samples GB-A and GB-C. Analyses were done in the interior of the unaltered segments.

4.5.5 Biotite

Measured oxide values plus structure formulas are presented in Appendix, Table 49. The Fe-Mg-Al-2 plot (Fig. 25) shows that chemical variations between samples are low. All analyses plot near the centre of the biotite field, between the Fe endmember annite, and the Mg endmember phlogopite.The Fe/(Fe+Mg) ratio varies between 0.45 and 0.52.

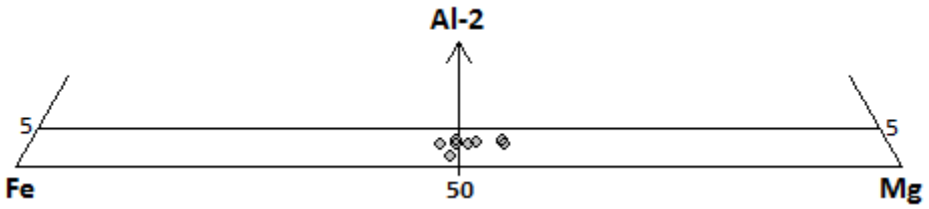

Figure 25. Classification diagram for biotite. All analyses plot near the center between the Fe end member annite and the Mg endmember phlogopite.

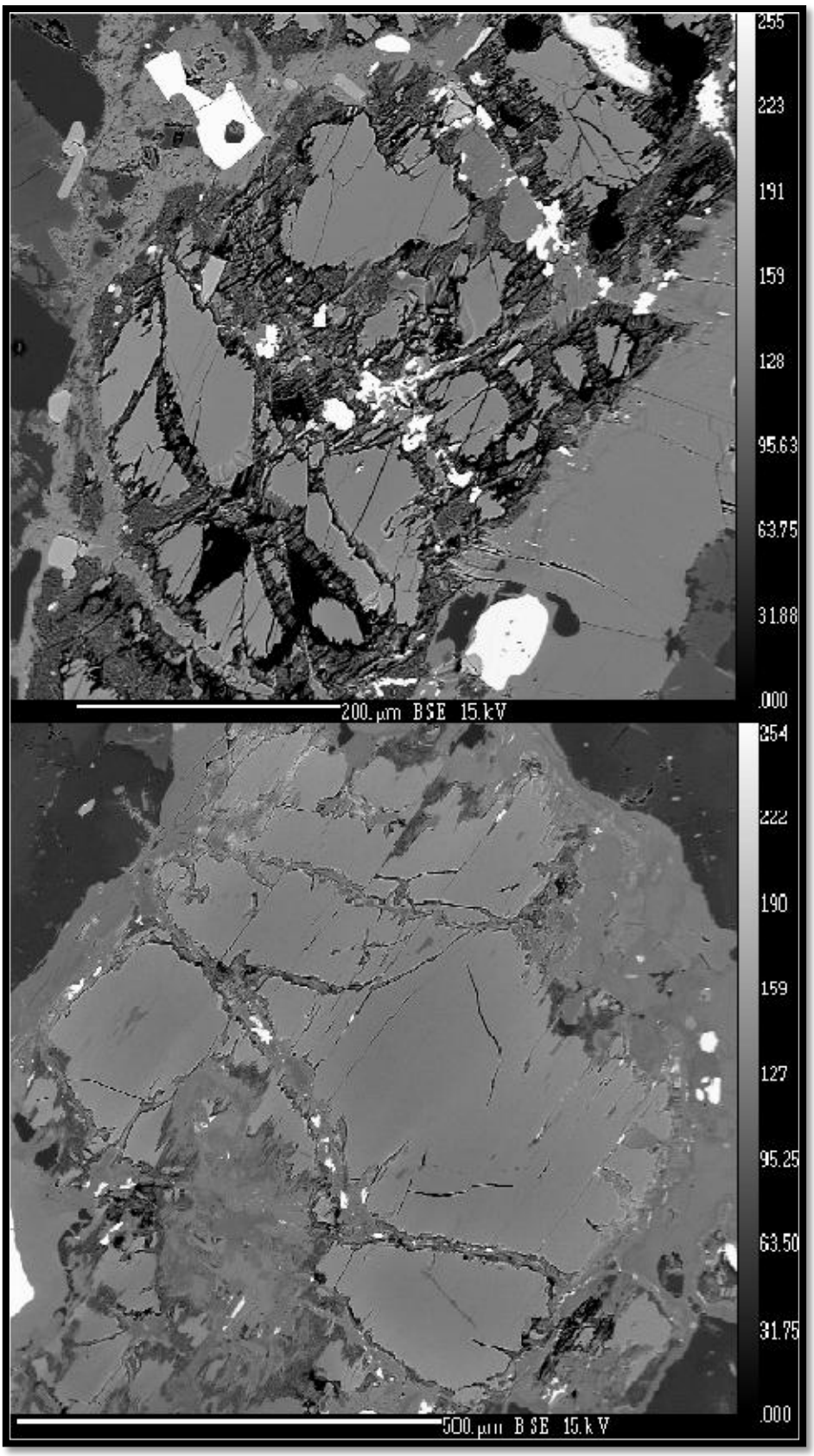

Figure 26. BSE images of two orthopyroxenes from akerite samples GB-C (upper image) and GB-A (lower image). Note the extensive alteration of the pyroxenes along cross-cutting fractures. GB-A and GB-C are among the least altered of the akerite samples. In the most altered samples, orthopyroxene is totally replaced.

4.6 Zircon U-Pb and Lu-Hf isotope analysis

4.6.1 U-Pb geochronology

Concordia diagrams, plus $^{206}Pb/^{238}U$ weighted average and relative probability charts are plotted for all analyzed samples (Figs. 27-34). All ages are calculated with errors at $\pm 2\sigma$ confidence level. U content are generally low, ranging from 33 to71ppm. Highly discordant data (~40% discordance) are omitted from the weighted average age calculations. The concordia diagrams generally show low probabilities of concordance, reflecting high $^{207}Pb/^{206}Pb$ ratios. Analyses showing high levels of common-lead have tentatively been corrected, giving poor results. These analyses were therefore excluded from the concordia and weighted average calculations. Sample GB-B showed only one concordant analysis. A concordia age could therefore not be calculated for this sample, and an intercept age is instead given. Four of the seven akerite samples gave the same $^{206}Pb/^{238}U$ weighted average age of 279Ma, with only minor differences in uncertainties. The last three differs somewhat in age, but are all within uncertainties of the 279Ma samples. The mean age of the akerite, calculated from $^{206}Pb/^{238}U$ weighted average ages of the seven analyzed samples, is 279Ma which is thought to represent the age of emplacement of the intrusion. The granitic dike (GB-B) yields a slightly lower weighted average age at 275±2Ma.

4.6.2 Lu-Hf isotope geochemistry

Measured Hf signal strengths of the eight analyzed samples are generally low relative to the applied standards Temora-2 and Mud Tank. This may result in poor precision in the $^{176}Hf/^{177}Hf$ ratios. The uncertainties obtained were, however, generally within the level considered acceptable (1SE <0.000020), and thus, few analyses were rejected due to poor internal precision. The $^{178}Hf/^{177}Hf$ ratio is monitored as a measure of analytical quality. Analyses deviating more than ±0.00010 from the average measured value of 1.46727 (lab average through several years) have been rejected. All analyses of Temora-2 reference zircon were within the long-time measured mean $^{176}Yb/^{177}Hf$ ratio of 0.01-0.11. Temora-2 gave a $^{176}Hf/^{177}Hf$ ratio of 0.282666 ±76 which is comparable to the value of Woodhead and Hergt (2005) of 0.282680 ± 22. Mud-Tank gave a $^{176}Hf/^{177}Hf$ ratio of 0.282504±49 which is nearly identical to the values of Woodhead and Hergt (2005) of 0.282504±44.

ε_{Hf} values are calculated for all analyses, and plotted with values of CHUR and DM (Fig. 35). The akerite analyses show ε_{Hf} values of -3 to +5, while the granite plots at -1 to +2. ε_{Hf} values of akerite and granite samples are compared with values for larvikites from the Larvik and

Sande complexes, plus granites from the Drammen complex (Haug 2007, Andersen et al. 2009b) (Fig. 36). The plot shows a clear correlation between the different units.
Söderlund et al. (2005) presented Lu-Hf, Sm-Nd and U-Pb isotopic data for a large number of mafic dikes in southern Sweden. The ε_{Hf} values of 0 to +6, and ε_{Nd} values of -1 to +4 found for these rocks, corresponds to a mildly depleted mantle. The bulk of these dikes are taken to represent lithospheric mantle melts, and are by Andersen et al. (2009a) referred to as sub-Fennoscandian lithospheric mantle (SFLM). Andersen et al. (2009a) presented Lu-Hf data on 1.88-1.68Ga granites from the Trans Scandinavian Igneous Belt (TIB) in Sweden, and concluded that these granites represent a long-lived, relatively homogeneous crustal magma source, interpreted to be representative of Paleoproterozoic Svecofennian crust (SC). ε_{Hf} development lines of SC and SFLM are presented together with ε_{Hf} data for the analyzed akerite and the granitic dike (Fig. 37). The bulk of the akerites (average $\varepsilon_{Hf} = 0.9$) plots in the lower half of the SFLM field, and significantly above the predicted range for SC at 279Ma.

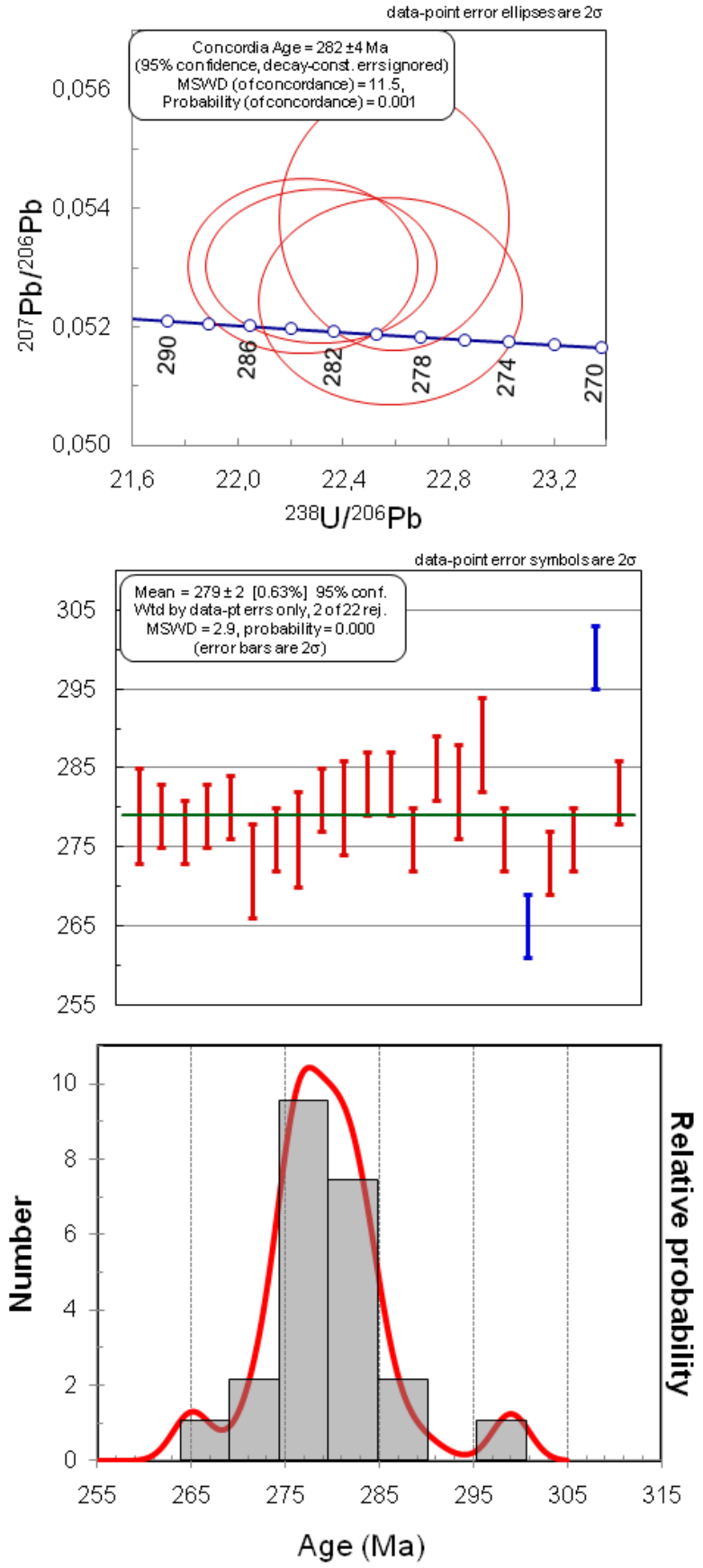

Figure 27. Concordia diagram, weighted average plot and relative probability chart for sample GB-A

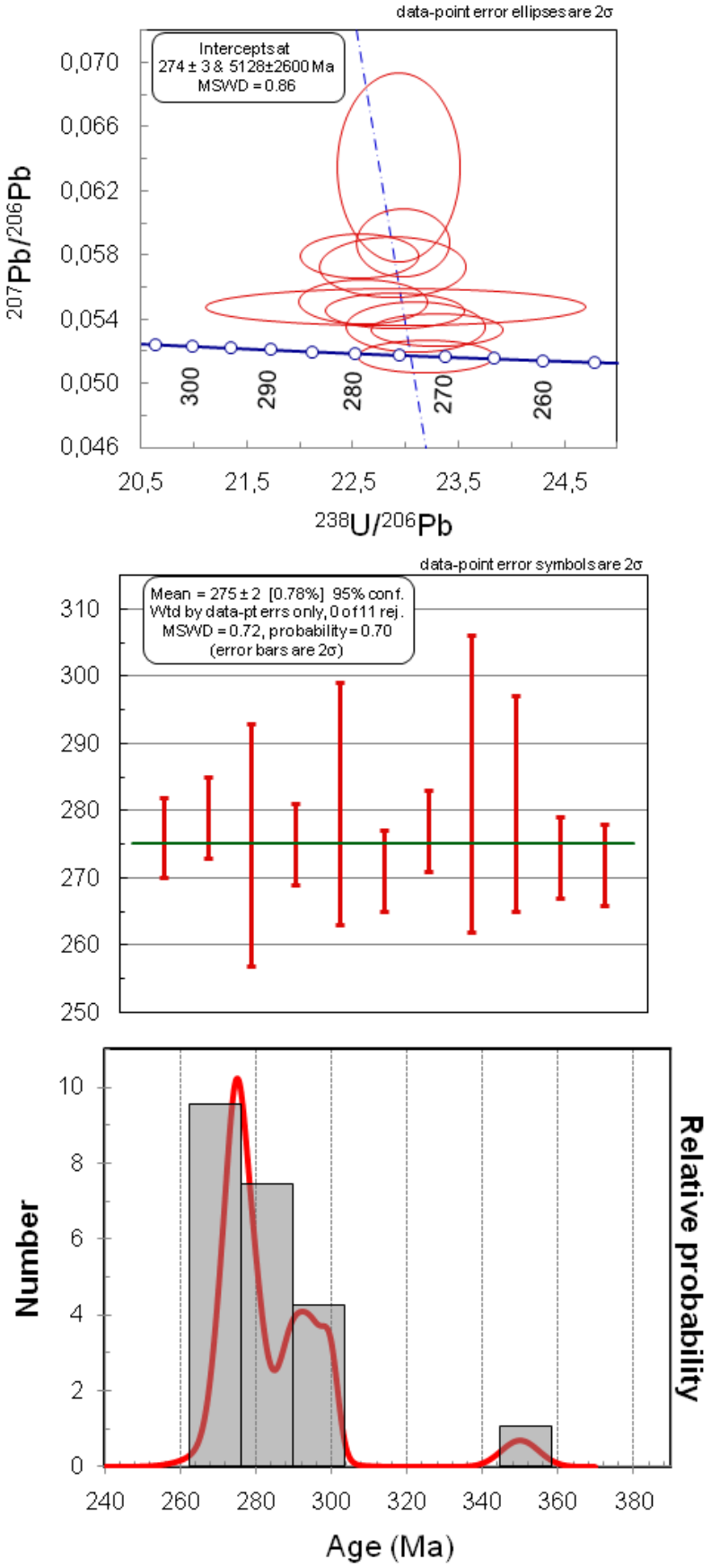

Figure 28. Concordia diagram, weighted average plot and relative probability chart for sample GB-B

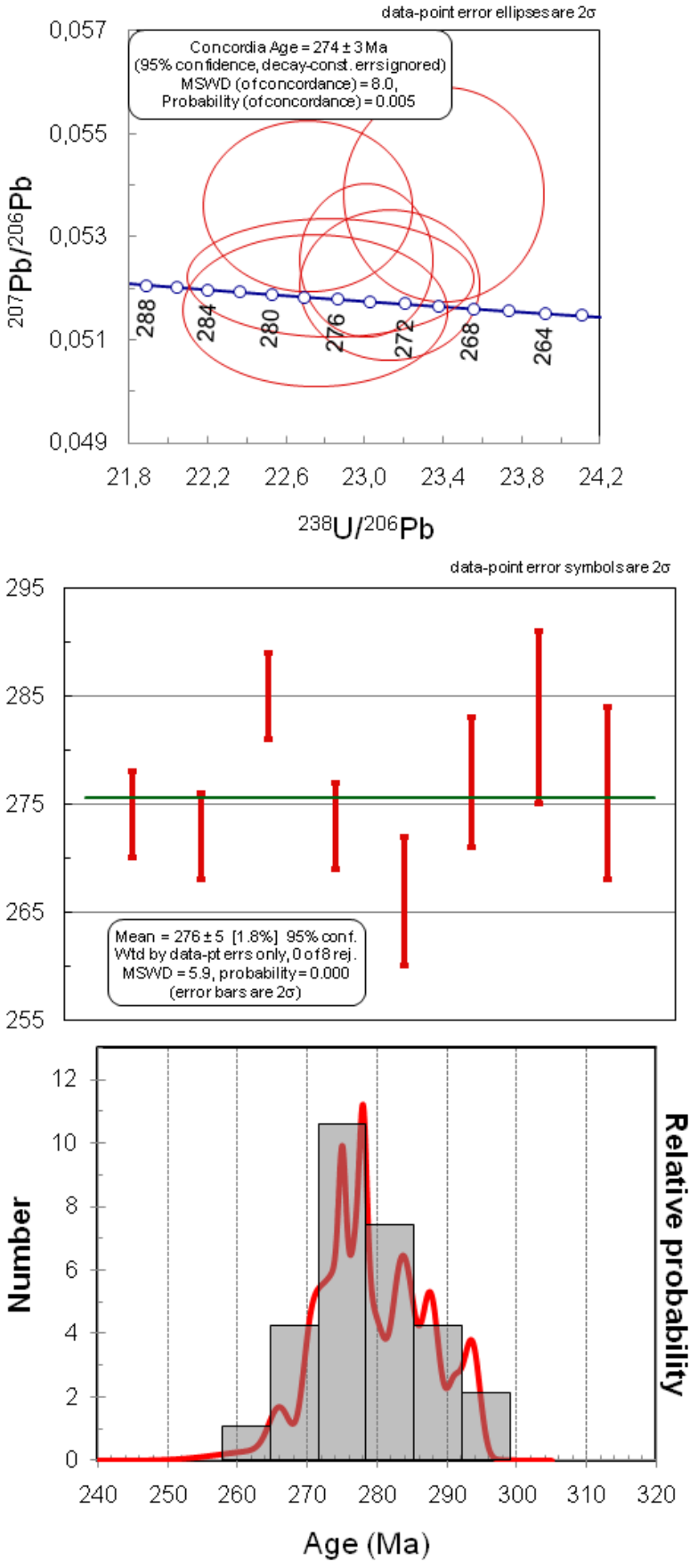

Figure 29. Concordia diagram, weighted average plot and relative probability chart for sample GB-C

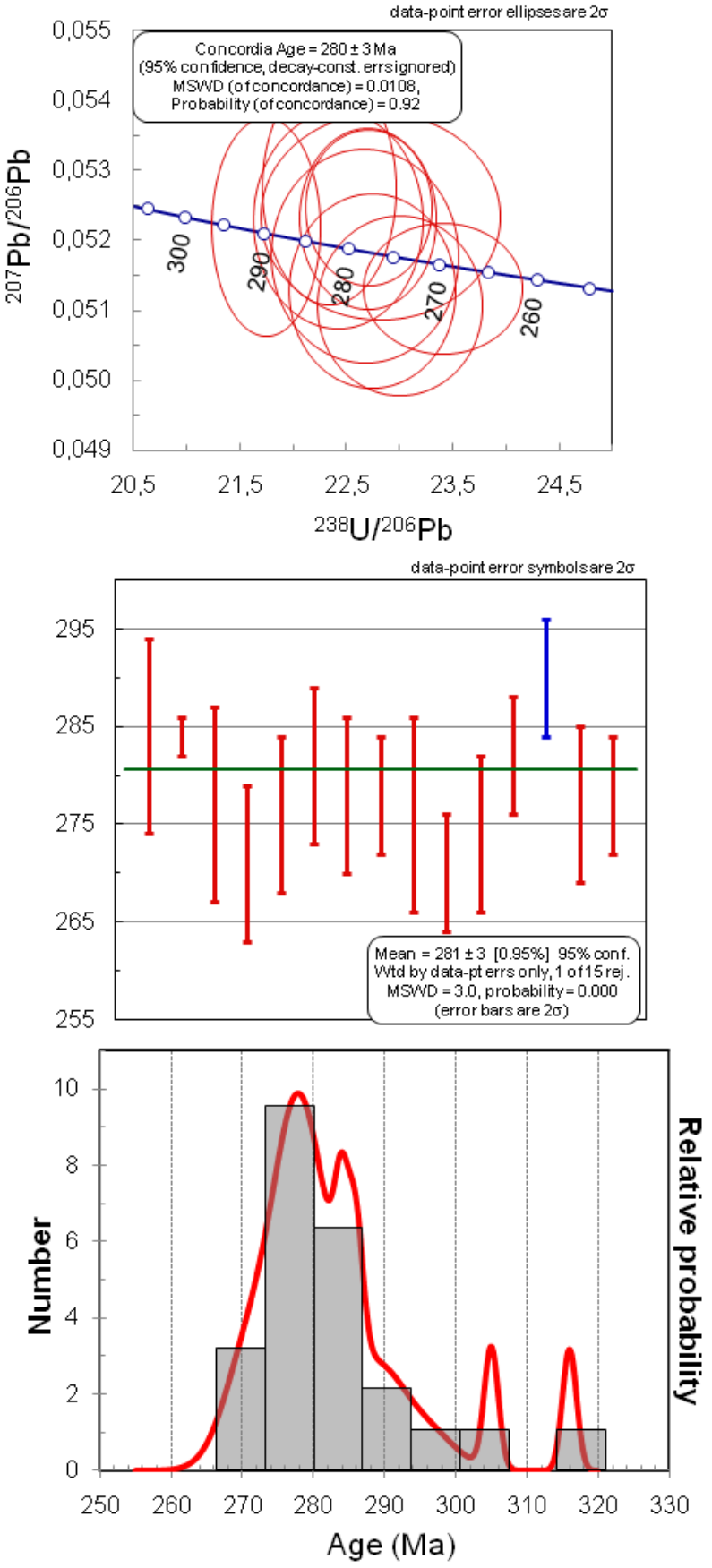

Figure 30. Concordia diagram, weighted average plot and relative probability chart for sample GB-D

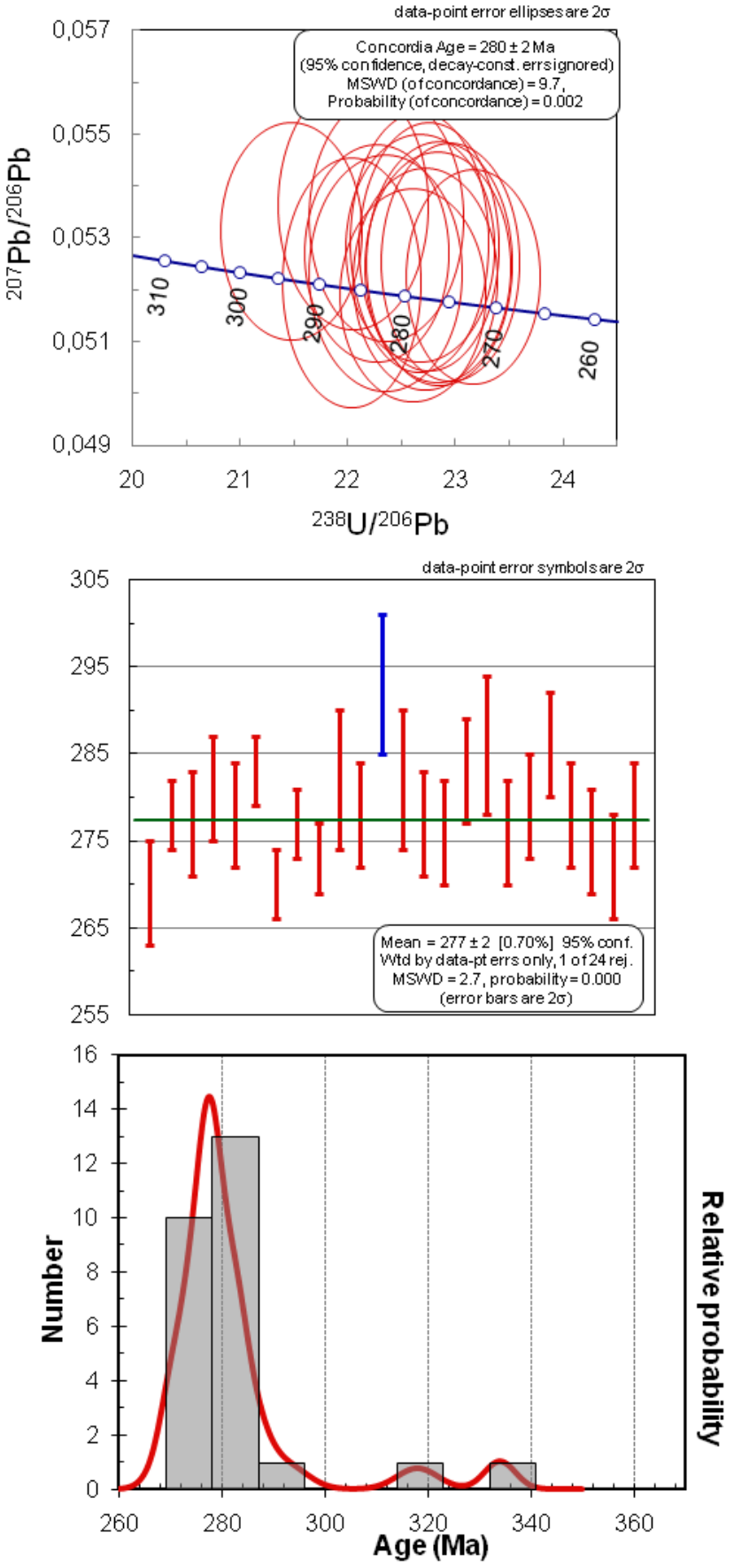

Figure 31. Concordia diagram, weighted average plot and relative probability chart for sample GB-E

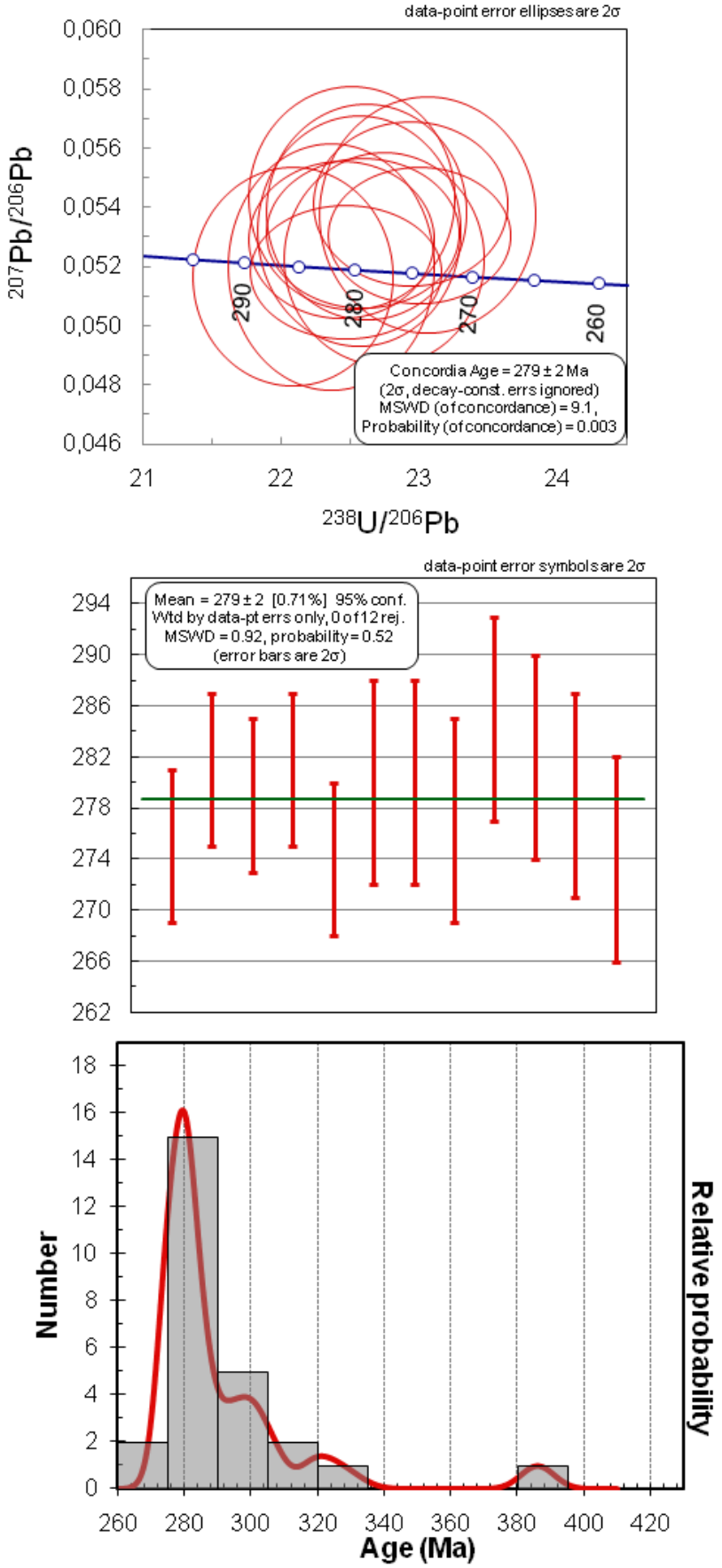

Figure 32. Concordia diagram, weighted average plot and relative probability chart for sample GB-F

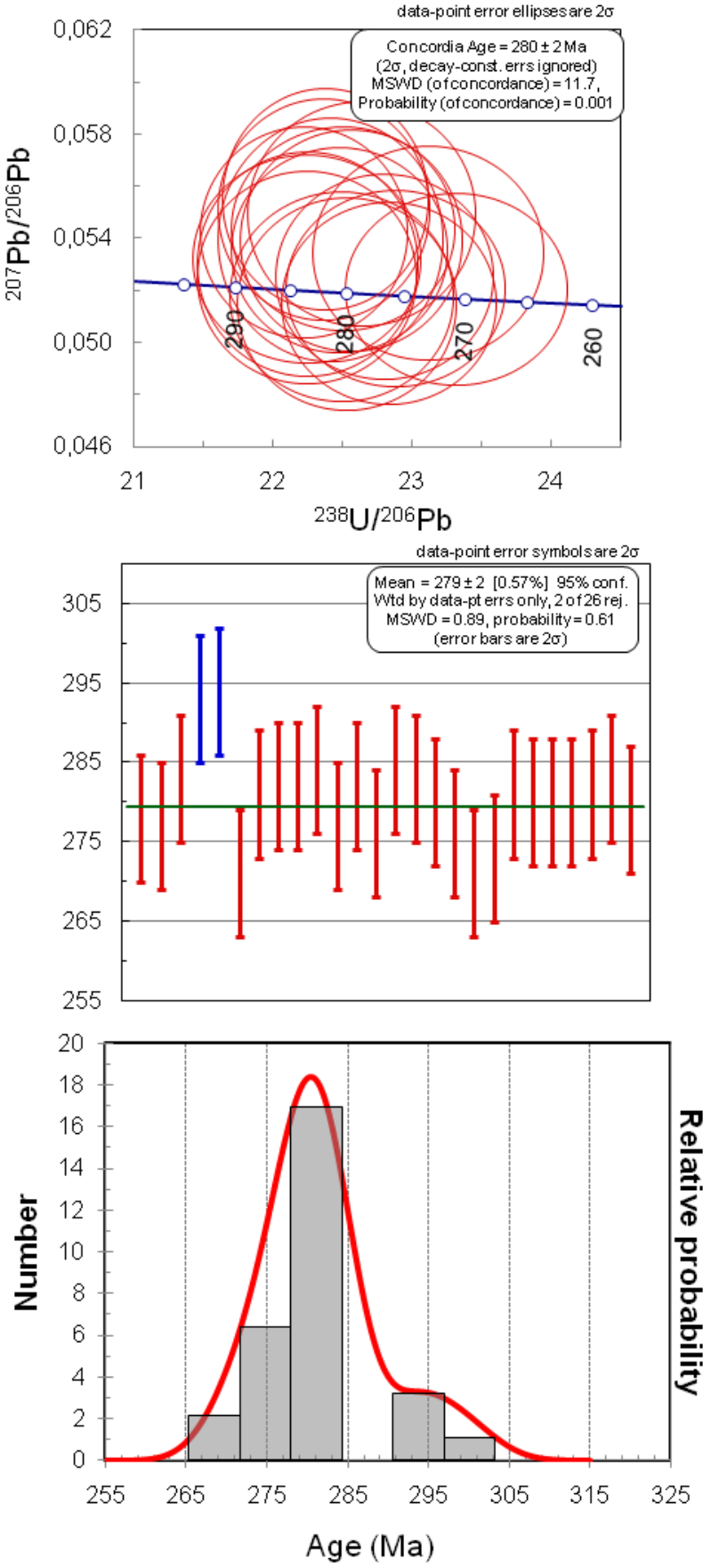

Figure 33. Concordia diagram, weighted average plot and relative probability chart for sample GB-G

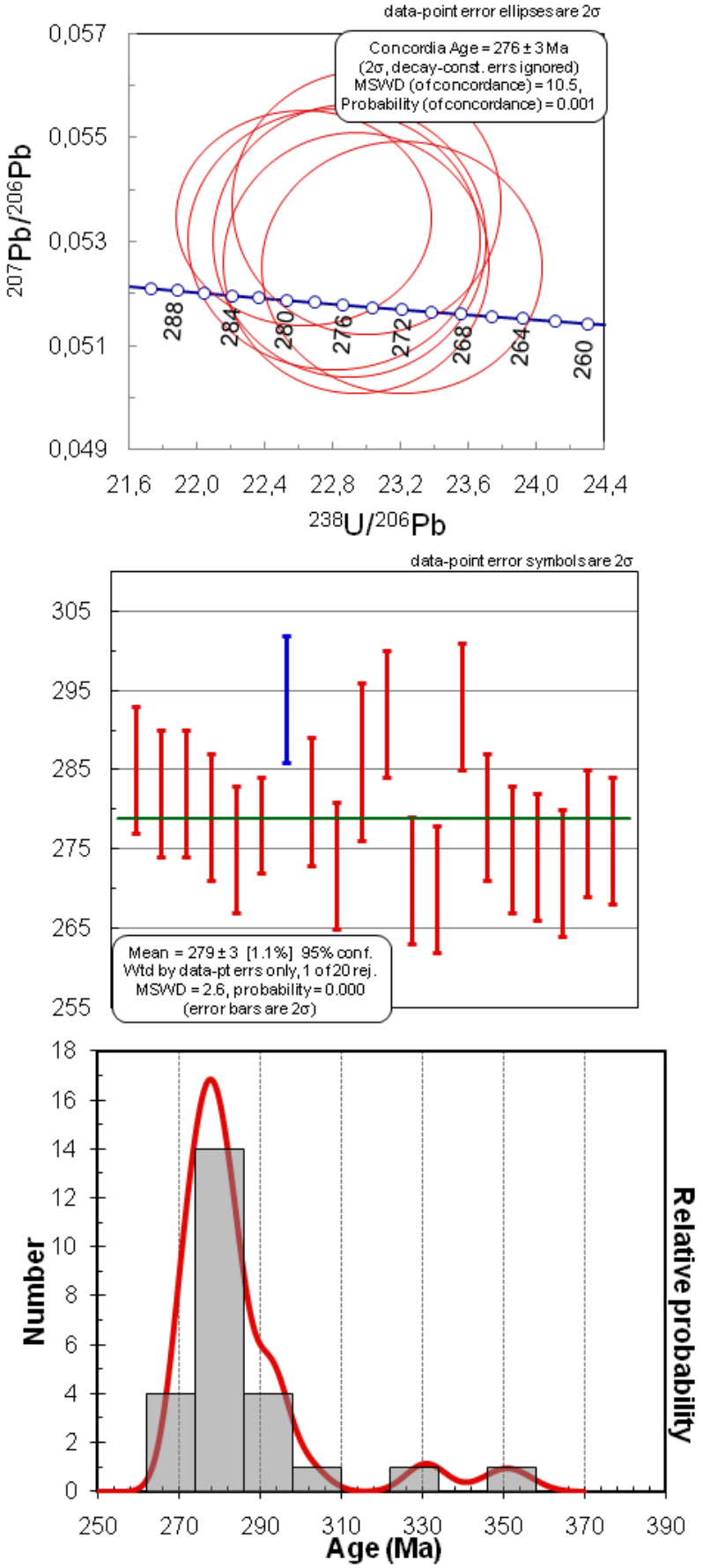

Figure 34. Concordia diagram, weighted average plot and relative probability chart for sample GB-H

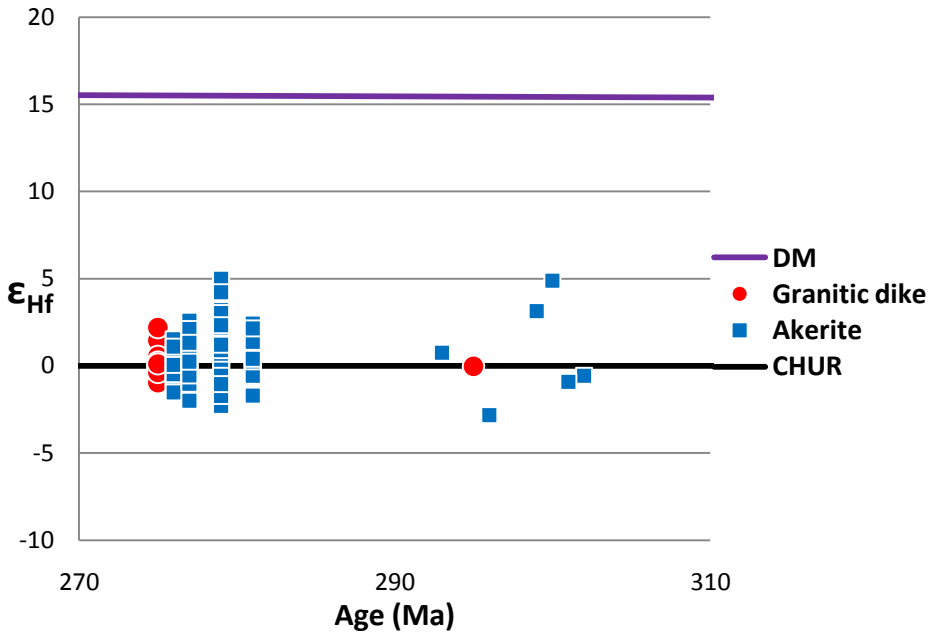

Figure 35. ε_{Hf} plot of akerite (blue squares) and granite (red circles). Solid lines are drawn for DM and CHUR. Akerite show ε_{Hf} values of -3 to +5, granite -1 to +2. Data from Bouvier et al. (2008) and Griffin et al. (2000)

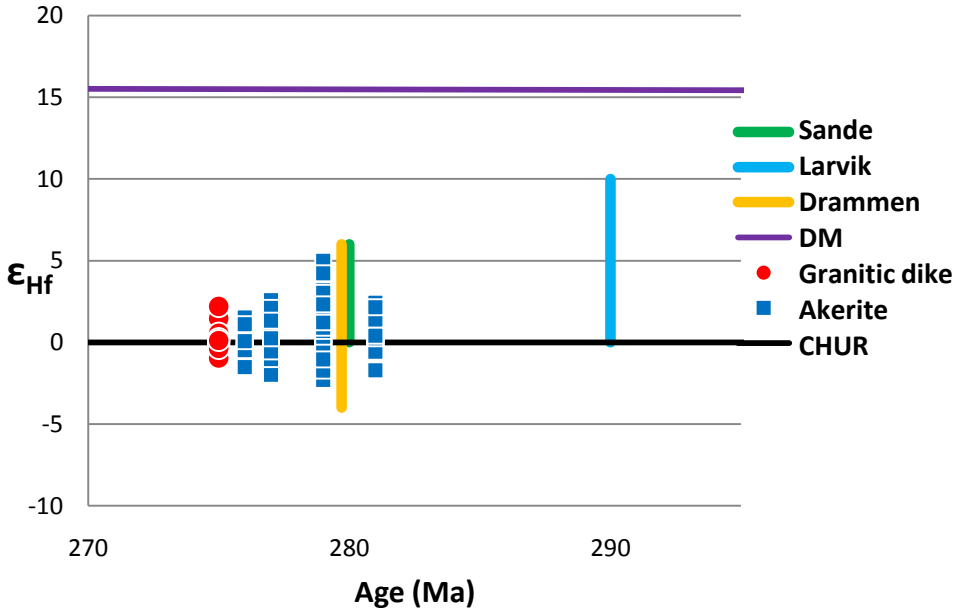

Figure 36. ε_{Hf} plot of the analyzed akerite and granite with solid lines showing ε_{Hf} values for Drammen granite (yellow), Sande larvikite (green) and Larvik larvikite (blue). All rock suites largely overlap, although a somewhat higher average value is found for the Larvik complex, and to a degree also for Sande. The Drammen granite covers a larger span of ε_{Hf} values than found in the akerite. Data from Haug (2007), Andersen et al. (2009b), Bouvier et al. (2008) and Griffin et al. (2000).

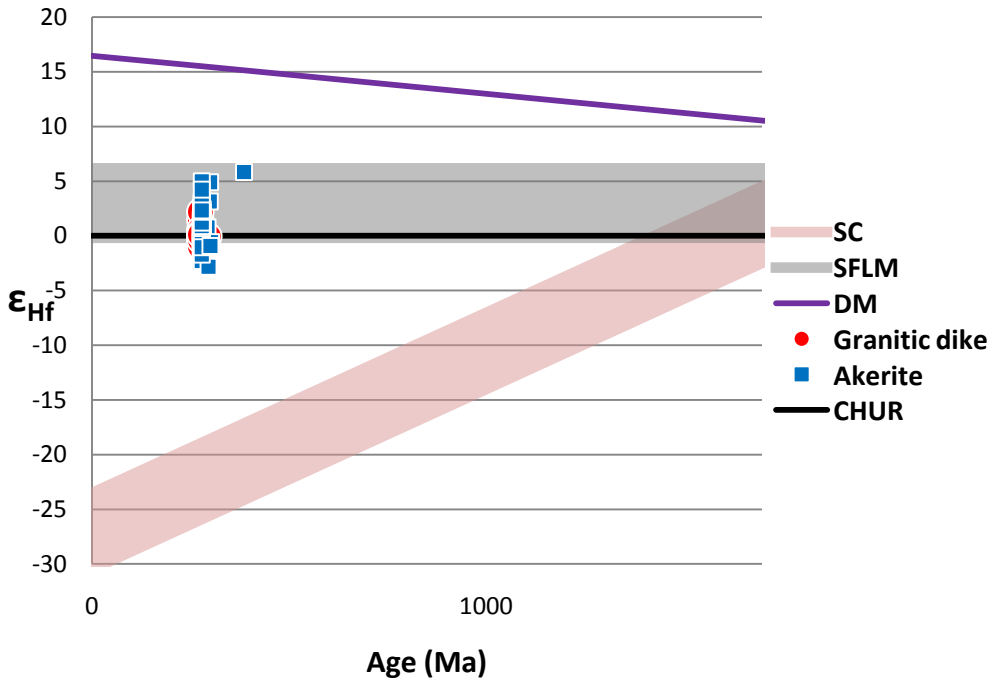

Figure 37. ε_{Hf} values of all analyzed samples plotted with average values of Svecofennian crust (SF) and sub-Fennoscandian lithospheric mantle (SFLM). Mean akerite values plot in the lower range of the SFLM field, and significantly higher than SC values. Data from Griffin et al. (2000), Söderlund (2005), Bouvier et al. (2008) and Andersen et al. (2009a).

4.7 Fractional crystallization modeling

The computer program MELTS (Ghiorso and Sack 1995) are used for modeling of fractional crystallization and equilibrium crystallization of magmas, based on thermodynamic properties of minerals and silicate melts. In the modeling performed, fractional crystallization was simulated, because this is the most reasonable mechanism for the evolution of a mafic magma into a magma of intermediate or felsic composition in this setting (Neumann 1980).

MELTS modeling was done using high-Ti and low-Ti B_1 basalts from Holmestrand, Vestfold (Neumann et al. 2002) as representatives of possible parent magmas (Table 5). According to Neumann et al. (2002), the Vestfold B_1 basalts are the most primitive of the Oslo Rift igneous rocks, and are thus considered suitable representatives of uncontaminated mantle melts. Based on this conclusion, the B_1 basalt has been chosen as input data for the fractional crystallization modeling.

The temperature interval (1400-900°C), pressure range of (3-10kb) and oxygen fugacity (QFM-QFM+2) applied were chosen to cover the ranges claimed by previous workers to be realistic for fractionation of similar rocks in the Oslo Rift (Neumann 1976, Neumann 1980,

Neumann et al. 1985, Neumann et al. 1988a, Andersen and Seiersten 1994). The aim of the modeling is to test if a magma with the major element composition of the akerite can be generated through fractional crystallization of a primary basaltic magma like the B_1 basalt, and to quantify at what pressure, temperature and degree of fractionation the remaining liquid corresponds to the akerite bulk composition.

Resulting liquid compositions of the two B_1 suites calculated for fractionation temperatures of 1040°C, 1060°C, 1080°C and 1100°C and pressures of 4, 5, 6 and 7 kb are plotted against average akerite values (Fig. 38). Fe_2O_3, FeO and MnO are plotted as one component, named FeO++. All plots are based on a FMQ buffer log fO_2 value. Values of FMQ+1 and FMQ+2 were tested for different pressures, giving exactly the same output data. The low-Ti basalt generally gives the best reproduction of the akerite composition, with the closest fit at a pressure of 5kb and temperatures between 1050°C and 1090°C. This gives 75-85% fractionation. The best-fitting plots show some deviation on TiO_2, MgO, K_2O and P_2O_5, but has good correlation on the most abundant oxides SiO_2, Al_2O_3, FeO++, CaO and to a degree Na_2O. The temperatures of best correlation at 5kb pressure are listed (Table 6). Although some discrepancies are found between the resulting liquid composition and akerite, the major elements SiO_2, Al_2O_3, FeO++, CaO, constituting 87% of the bulk composition, are all in agreement with akerite values within the 40°C temperature interval of 1050°C-1090°C. The minor elements show somewhat more deviations.

Sample set	SiO_2	TiO_2	Al_2O_3	FeO++	MgO	CaO	Na_2O	K_2O	P_2O_5
High-Ti B_1	44.77	4.80	9.09	15.27	10.56	12.19	1.62	1.15	0.55
Low-Ti B_1	47.94	2.94	12.68	13.97	7.90	10.15	2.56	1.67	0.42
Akerite	58.52	1.48	16.42	7.37	2.09	4.57	4.65	3.30	0.50

Table 5. Major element oxide values (average wt % values) for the two input data sets used in the fractional crystallization modeling (low-Ti and High-Ti B1 basalt from Holmestrand (Neumann et al. 2002)), plus corresponding values for akerite.

T (°C)	SiO_2	TiO_2	Al_2O_3	FeO++	MgO	CaO	Na_2O	K_2O	P_2O_5
1240	48.11	3.09	13.22	12.99	7.33	10.16	2.69	1.76	**0.44**
1230	47.94	3.22	13.70	13.20	6.77	9.82	2.82	1.85	0.47
1220	47.79	3.34	14.15	13.39	6.25	9.47	2.95	1.95	0.49
1210	47.66	3.46	14.58	13.58	5.76	9.10	3.07	2.04	**0.51**
1200	47.56	3.57	14.99	13.74	5.30	8.73	3.19	2.13	0.54
1190	47.48	3.67	15.37	13.89	4.87	8.36	3.31	2.22	0.56
1180	47.43	3.76	15.74	14.03	4.46	7.99	3.43	2.31	0.58
1170	47.41	3.84	16.08	14.14	4.09	7.61	3.54	2.40	0.60
1160	47.41	3.90	16.41	14.24	3.73	7.25	3.66	2.49	0.63
1150	48.96	3.46	17.19	12.83	3.09	6.80	3.96	2.71	0.68
1140	50.57	3.06	**17.36**	11.58	2.65	6.34	4.21	3.07	0.78
1130	52.12	2.77	17.30	10.50	2.27	5.87	4.42	**3.51**	0.79
1120	53.44	2.54	17.19	9.59	**1.98**	5.46	4.57	3.93	0.80
1110	54.57	2.35	17.04	8.80	1.74	5.12	**4.68**	**4.33**	0.81
1100	55.55	2.19	16.87	8.11	1.55	4.82	4.75	4.71	0.82
1090	56.41	2.06	16.69	**7.50**	1.39	**4.56**	4.80	5.07	0.84
1080	57.17	1.95	**16.50**	6.96	**1.25**	4.34	4.82	5.41	0.85
1070	57.82	1.85	16.30	6.50	1.14	4.15	4.82	5.73	0.88
1060	58.32	1.78	16.08	6.15	1.06	4.02	4.83	5.93	0.91
1050	**58.61**	1.75	15.85	5.99	0.99	4.00	4.94	5.85	0.94
1040	59.01	1.73	15.64	5.88	0.94	3.89	5.06	5.74	0.90
1030	59.39	1.70	15.43	**5.79**	0.88	3.77	5.19	5.61	0.84
1020	59.77	1.69	15.21	5.67	0.80	**3.69**	**5.31**	5.48	0.80
1010	60.12	1.67	14.98	5.60	0.74	3.60	5.44	5.34	0.76
1000	60.47	**1.51**	14.74	5.66	0.66	3.53	5.58	5.18	0.72
990	60.82	1.37	14.48	5.71	0.58	3.47	5.73	5.00	0.69
980	61.19	**1.24**	14.18	5.73	0.52	3.41	5.87	4.83	0.66
970	61.56	1.12	13.87	5.75	0.45	3.36	6.01	4.67	0.64
960	61.91	1.01	13.54	5.75	0.40	3.31	6.15	4.50	0.62
950	62.26	0.91	13.20	5.74	0.34	3.27	6.29	4.34	0.61
940	62.60	0.82	12.85	5.73	0.30	3.24	6.42	4.19	0.60
930	62.93	0.75	12.48	5.71	0.25	3.21	6.55	4.03	0.59
920	63.26	0.67	12.11	5.68	0.21	3.18	6.68	3.88	0.59
910	63.58	0.61	11.72	5.65	0.18	3.16	6.81	3.72	0.59
Akerite	**58.52**	**1.48**	**16.42**	**7.37**	**2.09**	**4.57**	**4.65**	**3.30**	**0.50**
Larvikite	**58.72**	**1.20**	**17.95**	**5.82**	**1.23**	**3.71**	**5.36**	**4.29**	**0.45**

Table 6. Major element oxide values (wt%) attained from modeled fractionation of low-Ti B_1 basalt from Holmestrand. Pressure is 5kb, f_{O_2} is at QFM buffer level. FeO++ is $FeO+Fe_2O_3+MnO$. Red numbers mark the values of best correlation between the resulting liquid composition and measured akerite values. The grey area shows the temperature interval of 1050-1090°C, where the major oxides SiO_2, Al_2O_3, FeO++ and CaO show values corresponding to akerite. These four oxides make up 87% of the akerite bulk composition. B_1 values are taken from Neumann et al. (2002). Average values for Larvik larvikite, ring section 2 (Neumann 1980) are added for comparison. Blue numbers mark the values of best correlation between the resulting liquid composition and larvikite values. Note that the larvikite deviates significantly more from the resulting liquid composition than does the akerite.

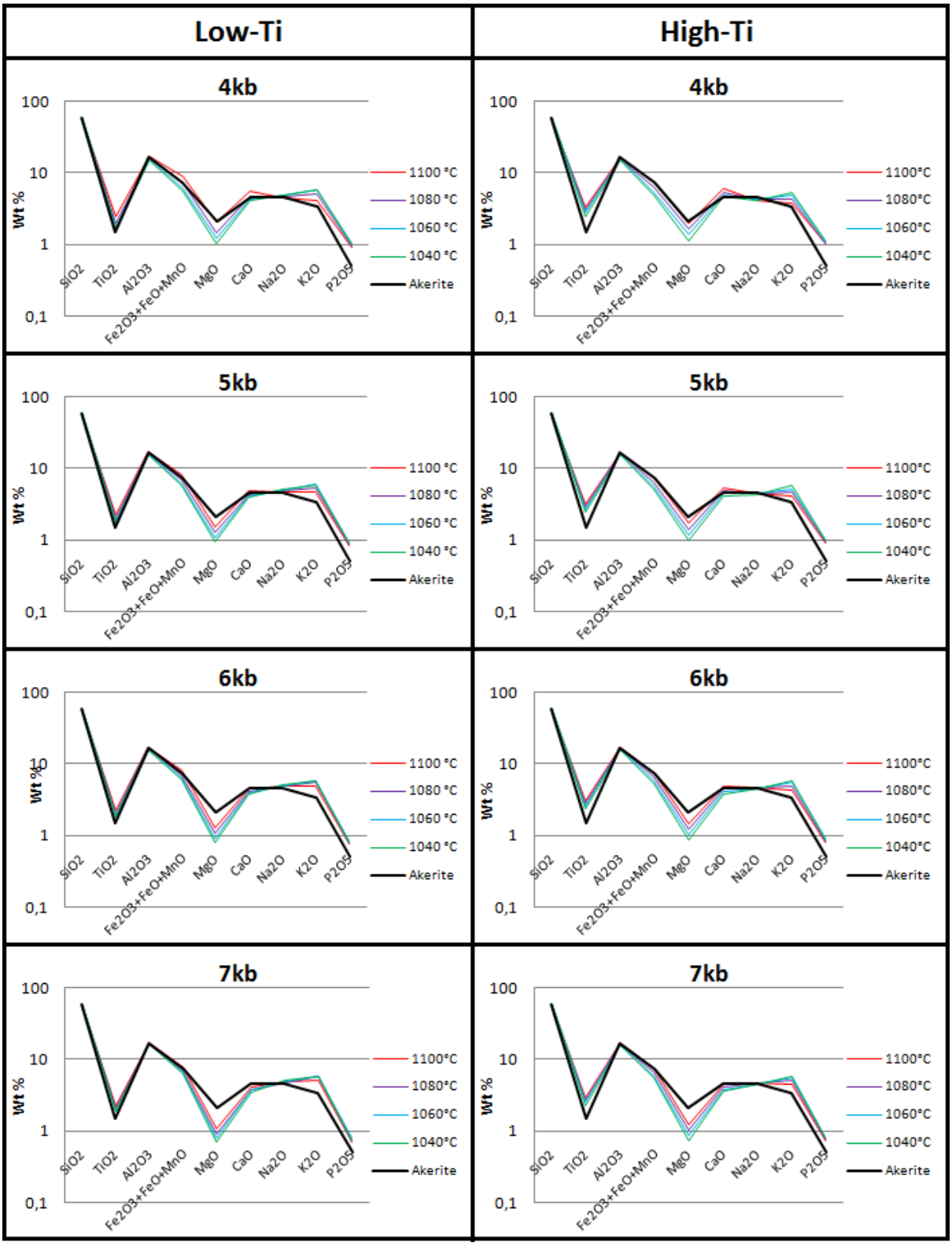

Figure 38. Plots of modeled fractionation of B_1 basalt from Holmestrand. B_1 values are taken from Neumann et al. (2002). All plots are with f_{O_2} at QFM buffer level. Higher f_{O_2} were tested (QFM+1 and QFM+2), giving identical results. The best correlation is found at 5kb pressure, with temperatures in the range of 1050-1090°C (Table 6). Low-Ti B_1 generally show bether fit than high-Ti B_1.

5 Discussion

5.1 Field observations

Oftedahl (1946) and Neumann (1980), among others, claimed that akerite is a border-facies of the nordmarkite, highly contaminated by the near-lying Cambro-Silurian metasediments. A series of field observations point to the conclusion that the Sognsvann-Holmenkollen akerite is a separate plutonic body emplaced later than the neighboring RP 5, and earlier than the nordmarkite and grefsen syenite. The contact between akerite and nordmarkite is generally sharp, with abundant apophyses cutting into the akerite (Figs. 8), and akeritic xenoliths found in the nordmarkite (Fig. 7). The akerite shows clear signs of hydrothermal alteration near the contact with the nordmarkite and with the numerous dikes cutting the akerite body. This alteration decreases away from the contact zones. Along the contact with the Cambro-Silurian metasediments, the akerite shows signs of contamination from the wall-rock (Fig. 9). This is, however, restricted to a narrow zone, and is not found more than a few meters away from the contact. At the contact to the RP body to the north, apophyses of akerite cut the RP.

These field observations, however, do not rule out the possibility that a volume of nordmarkitic magma was separated out at a deeper level, and then subjected to extensive contamination from the Cambro-Silurian wall-rocks, before solidifying and later being intruded by more or less uncontaminated nordmarkitic magma.

5.2 Major and trace element chemistry

The akerite has a SiO_2 content similar to the silica-saturated larvikites of the Larvik complex (Neumann 1980) (Table 6). It is, however, lower in Na_2O, K_2O and Al, and higher in Fe_{tot}, MgO and CaO than the larvikites (Fig. 13, Table 6). It has a less evolved character than the larvikites, (Figs. 13-14, Table 6), but follows the same line of evolution (Figs. 13-14).

Previous studies have shown that the B_1 basalts show a gradual increase in silica saturation with time, from the oldest undersaturated basalts of the southern Vestfold Graben to the youngest tholeiitic basalt at Krokskogen north of Oslo (Neumann et al. 2002, Larsen et al. 2006). Tholeiites are normally generated through higher levels of partial melting than undersaturated basalts, corresponding to a later stage of progressive partial melting (Winter 2001). The ten ring sections of the Larvik complex show an increase in alkalinity with time, a development believed to be due to increased fractionation in the underlying magma chamber.

Thus, the combination of low alkalinity, high silica content, and a less evolved nature (lower D.I, higher Mg, Fe and Ca) of the akerite relative to the Larvik plutonic complex (Figs.13-14, Table 6), may indicate generation through a lower degree of fractional crystallization of a similar source, at a later stage of progressive partial melting.

The alkalinity of a rock could be changed through mobilization of Na and K during hydrothermal events (Deer et al. 1992). It does, however, seem unlikely that this has been an important process in the akerite. Except for the anomalous sample GB-D, all samples show very uniform values of both Na and K (and other elements) despite large variations in the extent of hydrothermal alteration of minerals such as pyroxenes, amphibole and biotite.

The increased ratio of incompatible to compatible trace elements in akerite relative to B_1, is consistent with further fractionation and/or crustal contamination of the same magma (Figs. 17-18). Neumann et al (2002) reported a negative Sr anomaly indicating plagioclase fractionation. This trend is also found in the akerite, which shows a moderately negative anomaly relative to B_1. The suggested plagioclase fractionation corresponds well with data from the fractional crystallization modeling, where plagioclase is a fractionating phase below 1140°C (for low-Ti B_1 at 5kb).

5.3 Mineral chemistry

Neumann (1976) presented chemical data on amphiboles and pyroxenes of intermediate plutonic rocks from a number of locations in the Oslo Rift. Amphiboles and pyroxenes of the akerite show mean oxide values near the average for Oslo Rift monzonites. This is supported by the close correlation in the Na+K/Fe+Mn/Mg plot (Fig. 22) where the analyzed amphiboles are plotted against data for amphiboles from the Sande cauldron (Andersen 1984a)

The exsolution lamellae of orthopyroxene seen in the clinopyroxene grains of the akerite are consistent with the calculated composition of Wo_{40}-Wo_{46}. Due to the miscibility gap between orthopyroxene and augite series (Klein and Dutrow 2008), augite, and diopside below ~Wo_{46} will contain lamellas of orthopyroxene, in an amount increasing with decreasing Wo content.

The nordmarkite amphiboles are significantly less homogeneous in composition than amphiboles of the akerite and granite (Fig. 21). The zonal variations of Na, Fe, Mg and Ca

displayed in the EMP element maps (Fig. 20), are reflected in the more pronounced within-grain than between-grain chemical variations found in the structural formula (Table 4)

The biotites analyzed, all from the akerite, differs somewhat from analyses done on biotite from the Drammen granite by Trønnes and Brandon (1992). These differences largely reflect the differences in bulk chemistry between akerite and the highly silicic Drammen granite. As expected, FeO and TiO_2 are higher in the akerite. SiO_2, Al_2O_3 are slightly lower compared to the Drammen granite. Although MgO shows trace element values in bulk rock analyses of the Drammen granite, the MgO content in biotites is higher here than in the akerite, reflecting the lack of other Mg-bearing minerals.

Neumann (1976) suggests that the monzonites and associated rocks of the Oslo Rift crystallized from magmas with oxygen fugacities (f_{O_2}) close to the QFM buffer. The clinopyroxenes of the akerite show an average $Fe^{3+}/(Fe^{3+}+Fe^{2+})$ ratio somewhat lower (0.09) (Appendix, Table 47) than the mean value for Oslo Rift monzonites (0.17) (Neumann 1976) indicating low f_{O_2} at the time of crystallization of clinopyroxenes. Neumann et al. (1985) reports $Fe^{3+}/(Fe^{3+}+Fe^{2+})$ ratios of ~0.05 for clinopyroxenes in a series of Oslo Rift gabbroic intrusions, suggesting a f_{O_2} level near the QFM buffer during crystallization of these rocks.

5.4 Alteration

Sample GB-D differs somewhat from the other akerite samples in terms of bulk chemistry and normative minerals. The high modal albite and low modal anorthite and orthoclase combined with low Ba are consistent with albitization. The cause for the lack of quartz, in a rock where all other samples show 6.5 – 7.8 % modal quartz, remains an enigma. Due to the high chemical resistancy of quartz (Deer et al. 1992), post-magmatic removal is unlikely, and the lack of quartz must thus be explained by magmatic processes.

Signs of alteration are found in most samples. The amphiboles of the akerite are generally seen as overgrowths on ortho- and clinopyroxene, indicating alteration of these to amphibole at some stage after crystallization of the pyroxenes. This is supported by the low $Fe^{3+}/(Fe^{3+}+Fe^{2+})$ ratio of the clinopyroxenes, indicating low f_{O_2} at the time of crystallization, plus the fractionation modelling, where pyroxenes (and no amphiboles) are crystallized at all temperatures from initial crystallization to final consumption of melt. Extensive hydrothermal

activity in this area have been reported by several workers (Nilsen 1992, Corfu and Dahlgren 2008b). This points to the conclusion that the akerite, at a late-magmatic or early post-magmatic stage have been infiltrated by fluids, causing hydration of the pyroxenes, generating the abundant edenite amphiboles. This event may also have caused the biotite overgrowths on magnetite. Other signs of hydrothermal alteration found in the akerite are hematite overgrowth on pyrite, sericitization/saussuritization of feldspars and serpentinization of orthopyroxene (Fig. 26, Appendix, Tables 7-22). Some samples show extensive chloritization of pyroxenes, amphibole and biotite. Chlorite are commonly formed by alteration of ferromagnesian minerals at temperatures below ~400°C, and pressures up to a few kilobars (Deer et al. 1992), indicating that the chloritization of the akerite have occurred at a late stage of cooling, possible in connection with intrusion of the neighboring nordmarkite, and adjacent dikes. This is consistent with field observations, where the highest levels of chloritization are found near contacts with later intrusions. Due to the large differences in stability temperatures of these different alteration products, several events of hydrothermal alteration must have occurred in the akerite.

5.5 U-Pb dating

Sample GB-B (granite) showed the highest U levels (mean 71 ppm) and the highest degree of discordance. The zircons of this sample were found to differ greatly in texture from the akerite samples, showing a pronounced pattern of concentric zoning. Zoning in zircons reflects compositional variations in Zr, Si, Hf, P, Y, REE, U and Th (Corfu et al. 2003). This is consistent with this sample showing the largest scatter in U values. The seven analyzed akerite samples show mean U values of 33-61ppm. When dating zircons with low U contents, taken from rocks of lower Paleozoic, or younger, age, the most precise dates are generally obtained using the $^{206}Pb/^{238}U$ weighted average age (Bowring and Schmitz 2003). In such rocks, ^{235}U and radiogenic ^{207}Pb are low, and thus, the uncertainties of the $^{207}Pb/^{235}U$ and $^{207}Pb/^{206}Pb$ ratio correspondingly high (Mundil et al. 2001). It may be argued that applying this procedure is a way of neglecting the full potential of the U-Pb system, where the superiority relative to other methods lies in the possibility of comparing the two independent decay series. However, in the case of low-U zircons of relatively young ages, the $^{206}Pb/^{238}U$ weighted average age have proven to be the most robust, and is thus the most commonly used procedure of calculating U-Pb ages (Bowring and Schmitz 2003). The U levels are low for all

analyzed samples and, being of Permian age, the $^{206}Pb/^{238}U$ weighted average ages are therefore considered the most reliable. This gives the Sognsvann-Holmenkollen akerite an emplacement age of 279Ma, while the granitic dike cutting the akerite was emplaced at 275Ma.

5.6 Lu-Hf isotope geochemistry

The ε_{Hf} values of the akerite (-3 to +5), plotting in the lower half of the SFLM (Soderlund et al. 2005, Andersen et al. 2009a) (Fig. 37), is indicative of a lithospheric mantle magma source, and only minor crustal contamination, or alternatively, a more depleted asthenospheric magma source, subjected to a higher degree of crustal contamination. Assuming an increasing degree of depletion with time for the B_1 magma source, as indicated by Neumann et al (2002) and (2004), the assumed increase in ε_{Hf} would have to be compensated for by a higher degree of crustal contamination to reach the measured levels of the akerite. However, accepting the conclusion of Neumann (1980), Neumann et al. (1988b) and Rasmussen et al. (1988) that the Larvik larvikites are more or less uncontaminated B_1 derivates, the akerite, showing similar ε_{Hf} values as the larvikite, could be of the same origin without having suffered extensive crustal contamination. The slightly lower values of the akerite compared to larvikites of the Larvik plutonic complex may indicate that the former are somewhat more contaminated, but could also be explained by heterogeneities of the magma source, as described by Neumann et al. (1988b), (1990), (1992), (2002) and (2004).

5.7 Fractional crystallization modeling

In the modeling of fractional crystallization, more than one combination of P and T give close fit on most oxides. Some discrepancies are, however, found with any combination. At any P and T, the low-Ti B_1 gave the best fit. For a pressure of 5 kb, which appears to give the closest-fitting curves, the SiO_2 value equals the measured mean of akerite at ~1050°C. Al_2O_3 comes somewhat higher at ~1080°C, while the FeO++ and CaO values both equal akerite at ~1090°C. Na_2O, MgO and K_2O places somewhat higher at ~1110°C, ~1120°C and ~1130°C respectively. TiO_2 needs fractionation to ~1000°C to find the best fit, while the P_2O_5 value equals akerite at a temperature as high as ~1210°C.

Although some of these oxide values differs considerably from the measured values of akerite at any given temperature, the simulations shows good fit when the major constituents,

SiO_2, Al_2O_3, FeO++ and to a lesser degree, Na_2O and CaO, are weighted more than the minor constituents TiO_2, MgO, K_2O and P_2O_5. The oxides SiO_2, Al_2O_3, FeO++ and CaO, which make up 87% of the rock mass, are all corresponding with akerite values within the 40°C temperature interval of 1050°C to 1090°C (Table 6). Na_2O and K_2O are somewhat lower in the akerite at these temperatures. Although extensive hydrothermal removal of alkalis seems unlikely in the akerite, parts of the discrepancies concerning these two elements may possibly be explained by their high mobility during hydrothermal alteration. TiO_2 and P_2O_5 makes up respectively 1.48 and 0.50 wt % of the akerite, and thus, the large discrepancies of these oxides constitutes a very little bulk compositional difference between the modeled values and the akerite. Based on these results, it seems likely that the akerite were generated by fractional crystallization of a magma similar to the magma that crystallized to form the B_1 basalts some 20 million years earlier.

Neumann et al (1988a) examined fluid- and glass inclusions in clinopyroxene from an olivine pyroxenite xenolith found in a basalt flow at Krokskogen near Oslo. The xenolith is believed to represent cumulates after fractional crystallization of a lithospheric magma (ε_{Nd} of xenolith was +1.9 to +2.6), leading to the generation of the host basalt. P-T analyses of the fluid inclusions indicated a minimum pressure of 5.5-6kb and a maximum temperature of 1100-1200°C for crystallization of the pyroxenite. Ultra-low density bobbles trapped in the glass inclusions were found to represent pressures lower than the fluid inclusions. These values are near the temperature and pressure found from modeling to give the best bulk chemical correlation between a fractionated B_1 basaltic magma and the akerite (Fig.38, Table 6).

Andersen and Seiersten (1994) analyzed fluid inclusions in apatite from magnetite pyroxenite cumulates found within the Larvik plutonic complex. Solid inclusions of calcic amphibole, phlogopite, titanite, calcite and REE carbonate were found in the apatite. They concluded that the apatite and the minerals of the inclusions had crystallized at a pressure of 5-8kb. Although situated within the larvikite complex, these pyroxenites are believed to be cumulates after an earlier phase, brought up by ascending larvikite magmas. The pressure of crystallization indicated from these studies are thus not necessarily representative for the Larvik larvikites, but may give an indication of at which pressure range the earliest melts of the Oslo Rift was subjected to fractional crystallization. The pressures indicated by the modeled fractionation of B_1 basalt to akerite (~5kb) are somewhat low compared to the pressures favored by Andersen

and Seiersten (1994) for the pyroxenite cumulates (close to 8kb), but still within the range considered possible.

Based on stability field calculations of the observed mineral assemblage, Neumann (1980) suggests a pressure of crystallization of 7-10kb for the larvikites.

5.8 Magma source

Pascal et al (2004) postulated the Lithosphere-Asthenosphere boundary as the depth of melt initiation in the early phase of rifting. Neumann et al. (1988b) reports ε_{Nd} values of +3.3 to +4.2 for the early basalts, larvikites and RP lavas, and conclude that the Oslo Rift magmatic rocks are derived from a heterogeneous, mildly depleted source within the lithospheric mantle. Anthony et al. (1989) and Neumann et al (1990), (2002) and (2004) suggests that the earliest B_1 lavas are derived from an enriched HIMU-type lithospheric magma source, while later suites contain a gradually increasing component of a more depleted PREMA-type source, which finally became dominating when the HIMU-type source were exhausted. Although normally taken to indicate an asthenospheric source, the PREMA mantle reservoir of the Olso Rift is believed to be located at the base of the lithosphere (Neumann et al. 1990, Neumann et al. 2002, Neumann et al. 2004). The unusual isotopic affinity has been explained by interaction with asthenospheric material, possibly associated with a mantle plume (Neumann et al. 2002, Neumann et al. 2004). The later B1 basalt, including the low-Ti B_1 suites of the central Vestfold Graben represent the mixing phase, while the Larvik pluton and later units are believed to be dominated by the PREMA-type source (Neumann et al. 2004). It must be noted, that in terms of ε_{Nd} values, the PREMA-type affinity reported by Neumann et al (2004) to be indicative of interaction with asthenospheric material, are well within the SFLM field.

Based on Sr, Nd and Pb isotopic signatures, several authors have concluded that the larvikites and RP lavas are generated through fractional crystallization of a mantle magma of the same source as the B_1 basalts, with only minor crustal contamination (Neumann. 1980, Neumann et al. 1988b, Rasmussen et al. 1988). The similarities in ε_{Hf} values (Fig. 36), geochemical development (Figs. 13-14), and trace element affinity (Fig. 19) between the larvikites/RP-lavas and the akerite, strongly indicate a common source of these rocks. The close correlation in bulk chemistry between the akerite and a B_1 basaltic magma fractionated to ~1070°C at

~5kb (Fig. 38, Table 9), combined with the reported Sr, Nd and Pb isotope similarities between B_1 basalts and larvikite, indicate that both larvikite and akerite were generated through fractional crystallization of a B_1-type basaltic magma.

6 Conclusions

The Sognsvann-Holmenkollen akerite makes up a relatively small plutonic body of porphyric quartz monzonite emplaced at 279Ma. Based on field relations it is found to be older than the neighboring nordmarkite to the north, and younger than the RP lavas to the west. The akerite body is cut by several veins including a 275Ma granite.

In terms of bulk composition, the metaluminous, alkali-calcic akerite places amongst the least alkaline intermediate rocks of the Oslo Rift. The abundant quartz observed through petrographic examination reflects the calculated silica saturation, which, except for one strongly deviating sample, gave values for normative quartz of 6.5 to 7.8%. The closest similarities within the available bulk chemical data of Oslo-rift intermediate rocks, are found with the earliest, silica saturated Larvik larvikites. The akerite does, however, have a somewhat lower alkalinity, and a less evolved composition, without being lower in silica than the early larvikites. It is significantly more silica saturated and less alkaline than the later Larvik ring sections. This is taken to indicate magma derivation at a later stage of progressive partial melting, and a lower degree of fractionation for the akerite relative to the Larvik larvikites. This is supported by the lower age and more northerly location of the akerite, combined with the fact that the B_1 basalts, taken to be representative of the magma source, by earlier studies have been found to be progressively younger and less alkaline to the north. The postulate that akerite has evolved from a magma source similar to B_1 basalt has been proven possible by several findings: It is compatible with the trace element affinity, the Hf isotopic data, and the close compositional similarities found through modeled fractionation of B_1 magmas. Based on these findings, it is considered likely that the Sognsvann-Holmenkollen akerite evolved through fractional crystallization of a magma similar to B_1 basalt. Fractionation modeling and calculated FeO/Fe_2O_3 ratios of clinopyroxene indicate that the fractional crystallization occurred at mid-crustal levels and at relatively dry conditions.

The calculated ε_{Hf} values of -3 to +5, strongly indicate a magma source within the lithospheric mantle. The slightly lower average value of akerite relative to larvikite and the assumed sub-fennoscandian lithospheric mantle levels are explained either by inhomogeneities of the mantle source, or minor crustal contamination.

After emplacement, the akerite has been subject to several events of hydrothermal alteration.

7 References

Andersen, T. 1984a. Crystallization history of a Permian composite monzonite-alkali syenite pluton in the Sande cauldron, Oslo rift, southern Norway. *Lithos* 17, 153-170.

Andersen, T. 1984b. Crystallization History of a Permian Composite Monzonite Alkali Syenite Pluton in the Sande Cauldron, Oslo Rift, Southern Norway. *Lithos* 17, 153-170.

Andersen, T., Andersson, U.B., Graham, S., Aberg, G. and Simonsen, S.L. 2009a. Granitic magmatism by melting of juvenile continental crust: new constraints on the source of Palaeoproterozoic granitoids in Fennoscandia from Hf isotopes in zircon. *Journal of the Geological Society* 166, 233-247.

Andersen, T., Erambert, M., Larsen, A.O. and Selbekk, R.S. 2010. Petrology of Nepheline Syenite Pegmatites in the Oslo Rift, Norway: Zirconium Silicate Mineral Assemblages as Indicators of Alkalinity and Volatile Fugacity in Mildly Agpaitic Magma. *Journal of Petrology* 51, 2303-2325.

Andersen, T., Graham, S. and Sylvester, A., G. 2007. Timing and tectonic significance of Sveconorwegian A-type granitic magmatism in Telemark, southern Norway: New results from laser-ablation ICPMS U-Pb dating of zircon. *NGU Bulletin* 447, 17-31.

Andersen, T. and Knudsen, T.L. 2000. Crustal contaminants in the Permian Oslo Rift, South Norway: constraints from Precambrian geochemistry. *Lithos* 53, 247-264.

Andersen, T. and Seiersten, M. 1994. Deep cumulates in a shallow intrusion: Origin and crystallization history of a pyroxenite (jacupirangite sl) body in the Larvik Pluton, Oslo Region, South Norway. *NEUES JAHRBUCH FUR MINERALOGIE MONATSHEFTE*, 255-255.

Andersen, T., Simonsen, S., L. and Haug, L., E. 2009b. LAM-ICPMS Lu-Hf isotope data on magmatic zircons from felsic and intermediate intrusions in the Oslo Rift: Constraints on the mantle source. *NGF Winter Conference*, January 13-15, Bergen.

Andresen, P. 1985. *En geokjemisk undersøkelse med henblikk på kjemisk-stratigrafisk identifikasjon av de lavere rombeporfyrer i den sentrale Oslograben*. Hovedoppgave, Museum of Natural History, University of Oslo. 109.

Anthony, E.Y., Segalstad, T.V. and Neumann, E.R. 1989. An Unusual Mantle Source Region for Nepelinithes from the Oslo Rift, Norway. *Geochimica Et Cosmochimica Acta* 53, 1067-1076.

Antoshechkina, P. and Asimow, P. *Adiabat_1ph download and information page* 2008 [Accsessed: 2011.06.02. Available at http://magmasource.caltech.edu/adiabat_1ph/.

Barth, T.F.W. 1945. *Studies on the Igneous Rock Complex of the Oslo Region: Systematic Petrography of the Plutonic Rocks*: J. Dybwad.

Black, L., P. and Gulson, B., L. 1978. The age of the Mud Tank carbonatite, Strangways Range, Northern Territory. *BMR Journal of Australian Geology and Geophysics* 3, 227-232.

Bouvier, A., Vervoort, J.D. and Patchett, P.J. 2008. The Lu-Hf and Sm-Nd isotopic composition of CHUR: Constraints from unequilibrated chondrites and implications for the bulk composition of terrestrial planets. *Earth and Planetary Science Letters* 273, 48-57.

Bowring, S.A. and Schmitz, M.D. 2003. High-precision U-Pb zircon geochronology and the stratigraphic record. *In* Hanchar, J.M. and Hoskin, P.W.O. (eds). *Zircon*. Reviews in Mineralogy & Geochemistry, 53, 305-326.

Brøgger, W., C. 1890. *Die Mineralien der Syenitpegmatitgänge der Südnorwegischen Augit- und Nephelinsyenite*, Leipzig: Verlag von Wihelm Engelmann.

Bylund, G. and Patchett, P.J. 1977. Paleomagnetic and Rb-Sr Isotopic Evidence for Age of Särna Alkaline Complex, Western Central Sweden. *Lithos* 10, 73-79.

Calcagnile, G. 1982. The Lithosphere Asthenosphere System in Fennoscandia. *Tectonophysics* 90, 19-35.

Cassell, B.R., Mykkeltveit, S., Kanestrom, R. and Husebye, E.S. 1983. A North-Sea - Southern-Norway Seismic Crustal Profile. *Geophysical Journal of the Royal Astronomical Society* 72, 733-753.

Corfu, F. and Dahlgren, S. 2008a. Cronology of the Oslo Rift: further U-Pb results. Paper read at Nordic Geological Winter Meeting, 2008. 01. 07-10, at Ålborg, Denmark.

Corfu, F. and Dahlgren, S. 2008b. Perovskite U-Pb ages and the Pb isotopic composition of alkaline volcanism initiating the Penno-Carboniferous Oslo Rift. *Earth and Planetary Science Letters* 265, 256-269.

Corfu, F., Hanchar, J.M., Hoskin, P.W.O. and Kinny, P. 2003. Atlas of zircon textures. *In* Hanchar, J.M. and Hoskin, P.W.O. (eds). *Zircon*. Reviews in Mineralogy & Geochemistry, 53, 469-500.

Dahlgren, S. and Corfu, F. 2001. Northward sediment transport from the late Carboniferous Variscan Mountains: zircon evidence from the Oslo Rift, Norway. *Journal of the Geological Society* 158, 29-36.

Deer, W., A., Howie, R., A and Zussman, J. 1992. *The Rock Forming Minerals*. 2 ed: Pearson Prentice Hall.

Ebbing, J., Afework, Y., Olesen, O. and Nordgulen, O. 2005. Is there evidence for magmatic underplating beneath the Oslo Rift? *Terra Nova* 17, 129-134.

Ebbing, J., Skilbrei, J.R. and Olesen, O. 2007. Insights into the magmatic architecture of the Oslo Graben by petrophysically constrained analysis of the gravity and magnetic field. *Journal of Geophysical Research-Solid Earth* 112.

Eliasson, T. and Schöberg, H. 1991. U-Pb dating of the post-kinematic Sveconorwegian (Grenvillian) Bohus granite, SW Sweden: evidence of restitic zircon. *Precambrian Research* 51, 337-350.

Faure, G. and Mensing, T., M. 2005. *Isotopes; principles and applications*. 3 ed: John Wiley and Sons, inc.

Finch, R.J. and Hanchar, J.M. 2003. Structure and chemistry of zircon and zircon-group minerals. *In* Hanchar, J.M. and Hoskin, P.W.O. (eds). *Zircon*. Reviews in Mineralogy & Geochemistry, 53, 1-25.

Frost, B.R., Barnes, C.G., Collins, W.J., Arculus, R.J., Ellis, D.J. and Frost, C.D. 2001. A geochemical classification for granitic rocks. *Journal of Petrology* 42, 2033-2048.

Geological Survey of Japan. 2011 [Accsessed: 2011.02.14. Available at http://www.aist.go.jp/GSJ/.

Ghiorso, M.S. and Sack, R.O. 1995. Chemical Mass-Transfer in Magmatic Processes 4. A Revised and Iinternally Consistent Thermodynamic Model for the Interpolation and Extrapolation of Liquid-solid Equilibria in Magmatic Systams at Elevated-Temperatures and Pressures. *Contributions to Mineralogy and Petrology* 119, 197-212.

Gjelle, S. and Sigmond, E., M., O. 1994. *Bergartsklassifikasjon og kartsammenstilling*. Skrifter. 113: NGU. 77 pp.

Griffin, W.L., Pearson, N.J., Belousova, E., Jackson, S.E., van Achterbergh, E., O'Reilly, S.Y. and Shee, S.R. 2000. The Hf isotope composition of cratonic mantle: LAM-MC-ICPMS analysis of zircon megacrysts in kimberlites. *Geochimica Et Cosmochimica Acta* 64, 133-147.

Guggisberg, B., Kaminski, W. and Prodehl, C. 1991. Crustal Structure of the Fennoscandian Shield - a Traveltime Interpretation of the Long-Range Fennolora Seismic Refraction Profile. *Tectonophysics* 195, 105-&.

Haug, L., E. 2007. *Mantel- og skorpekomponenter i Drammensgranitten. En LAM-ICPMS Lu-Hf isotopstudie av zirkon*. Ms. Thesis, Institute of Geosciences, University of Oslo.

Heeremans, M. 2011. *A plume beneath the Oslo Graben?* www.MantlePlumes.org, 2005.06.30 2011 [Accsessed: 02.03 2011]. Available at http://www.mantleplumes.org/Norway.html.

Heeremans, M., Larsen, B.T. and Stel, H. 1996. Paleostress reconstruction from kinematic indicators in the Oslo Graben, southern Norway. New constraints on the mode of rifting. *Tectonophysics* 266, 55-79.

Heinonen, A.P., Andersen, T. and Ramo, O.T. 2010. Re-evaluation of Rapakivi Petrogenesis: Source Constraints from the Hf Isotope Composition of Zircon in the Rapakivi Granites and Associated Mafic Rocks of Southern Finland. *Journal of Petrology* 51, 1687-1709.

Holtedahl, O. and Dons, J.A. 1966. *supplement to Geological Guide to Oslo And District*. Universitetsforlaget

Hoskin, P.W.O. and Schaltegger, U. 2003. The composition of zircon and igneous and metamorphic petrogenesis. *In* Hanchar, J.M. and Hoskin, P.W.O. (eds). *Zircon*. Reviews in Mineralogy & Geochemistry, 53, 27-62.

Ireland, T.R. and Williams, I.S. 2003. Considerations in zircon geochronology by SIMS. *In* Hanchar, J.M. and Hoskin, P.W.O. (eds). *Zircon*. Reviews in Mineralogy & Geochemistry, 53, 215-241.

Jacobsen, S. and Wasserburg, G. 1978. Nd and sr isotopic study of the permian oslo rift. *In* Zartmann, R., E. (ed). *Short papers of the Fourth International Conference on Geochronology, Cosmochronology and Isotope Geology*: US Geological Survey Open File Rep. 78-701, 194-196.

Janousek, V., Farrow, C. and Erban, V. 2008. GCDkit for Windows.

Kanestrøm, R. 1971. Seismic investigations of the crust and upper mantle in Norway, 17–27.

Kinck, J.J., Husebye, E.S. and Larsson, F.R. 1993. The Moho Depth Distribution in Fennoscandia and the Regional Tectonic Evolution from Archean to Permian Times. *Precambrian Research* 64, 23-51.

Kinck, J.J., Husebye, E.S. and Lund, C.E. 1991. The South Scandinavian Crust - Structural Complexities from Seismic-Reflection and Refraction Profiling. *Tectonophysics* 189, 117-133.

Kirstein, L.A., Davies, G.R. and Heeremans, M. 2006. The petrogenesis of Carboniferous-Permian dyke and sill intrusions across northern Europe. *Contributions to Mineralogy and Petrology* 152, 721-742.

Klein, C. and Dutrow, B. 2008. *Manual of mineral science*. 23 ed: John Wiley & Sons, Inc. 675 pp.

Kristoffersen, M. 2011. *Provenance of the Asker Group, Oslo Rift. A detrital zircon U-Pb - Lu-Hf study.*, Intitute of Geosciences, Department of Mathematics and Natural Sciences Master Thesis, University of Oslo.

Larsen, B., T., Olaussen, S., Sundvoll, B. and Heeremans, M. 2006. Vulkaner, forkastninger og ørkenklima. Osloriften og Nordsjøen i Karbon og Perm, 359-251 millioner år. *In* Ramberg, I., B., Bryhni, I. and Nøttvedt, A. (eds). *Landet blir til, Norges geologi*: Norsk Geologisk Forening, 284-327.

Larsen, B.T., Olaussen, S., Sundvoll, B. and Heeremans, M. 2008. The permo-Carboniferous Olso Rift through six stages and 65 million years. *Episodes* 31, 52-58.

Le Maitre, R.W., Streckeisen, A., Zanettin, B., Le Bas, M.J., B., B., Bateman, P., Bellieni, G., Dudek, A., Efremova, S., Keller, J., Lameyre, J., Sabine, P.A., Schmid, R., Sørensen, H. and Woolley, A.R. 2004. *Igneous Rocks: A classification and glossary of terms. Recommendations of the International Union of Geological Sciences Subcommission on the Systematics of Igneous Rocks*. *I* Le Maitre, R.W. (red): Cambridge University press.

Leake, B.E., Woolley, A.R., Arps, C.E.S., Birch, W.D., Gilbert, M.C., Grice, J.D., Hawthorne, F.C., Kato, A., Kisch, H.J., Krivovichev, V.G., Linthout, K., Laird, J., Mandarino, J.A., Maresch, W.V., Nickel, E.H., Rock, N.M.S., Schumacher, J.C., Smith, D.C., Stephenson, N.C.N., Ungaretti, L., Whittaker, E.J.W. and Guo, Y.Z. 1997. Nomenclature of amphiboles: Report of the subcommittee on amphiboles of the International Mineralogical Association, commission on new minerals and mineral names. *American Mineralogist* 82, 1019-1037.

Lie, J.E., Pedersen, T. and Husebye, E.S. 1990. Observations of Seismic Reflectors in the Lower Lithosphere Beneath the Skagerrak. *Nature* 346, 165-168.

Ludwig K., R. 2008. *User's manual for Isoplot 3.7; A Geochronological Toolkit for Microsoft Excel*. Special Publication. 4: Berkeley Geochronology Center.

Meert, J.G., Torsvik, T.H., Eide, E.A. and Dahlgren, S. 1998. Tectonic significance of the Fen Province, S. Norway: constraints from geochronology and paleomagnetism. *The Journal of geology* 106, 553-564.

Middlemost, E.A.K. 1989. Iron oxidation ratios, norms and the classification of volcanic rocks. *Chemical Geology* 77, 19-26.

Middlemost, E.A.K. 1994. Naming Materials in the Magma Igneous Rock Systam. *Earth-Science Reviews* 37, 215-224.

Morimoto, N. 1989. Nomenclature of Pyroxenes. *Canadian Mineralogist* 27, 143-156.

Mundil, R., Metcalfe, I., Ludwig, K.R., Renne, P.R., Oberli, F. and Nicoll, R.S. 2001. Timing of the Permian-Triassic biotic crisis: implications from new zircon U/Pb age data (and their limitations). *Earth and Planetary Science Letters* 187, 131-145.

Nakrem, H., A and Worsley, D. 2006. Jordens elste oldtid. Kambrium, ordovisium og silur - et yrende liv i havet; 542-416 millioner år. *In* Ramberg, I., B., Bryhni, I. and Nøttvedt, A. (eds). *Landet blir til Norges geologi*: Norsk Geologisk Forening, 148-177.

Neumann, E., R. 1976. Compositional relations among pyroxenes, amphiboles and other mafic phases in the Oslo Region plutonic rocks. *Lithos* 9, 85-109.

Neumann, E., R. 1978. Petrology of the Plutonic Rocks. *In* Dons, J.A. and Larsen, B.T. (eds). *The Oslo Paleorift A Review and Guide to Excursions*. NGU Bulletin: Universitetsforlaget, 45, 25-34.

Neumann, E., R. 1980. Petrogenesis of the Oslo Region Larvikites and Associated Rocks. *Journal of Petrology* 21, 499-531.

Neumann, E., R., Wilson, M., Heeremans, M., Spencer, E., A., Obst, K., Timmermann, M., J. and Kirstein, L. 2004. Carboniferous-Permian rifting and magmatism in southern Scandinavia, the North Sea and northern Germany: a review. *In* Wilson, M., Neumann, E., R., Davies, G., R., Timmermann, M., J., Heeremans, M. and Larsen, B., T. (eds). *Permo-Carboniferous magmatism and rifting in Europe*. Special Publication Geological Society, 223.

Neumann, E.R. 1994. The Oslo Rift - P-T Relations and Lithospheric Structure. *Tectonophysics* 240, 159-172.

Neumann, E.R., Andersen, T. and Mearns, E.W. 1988a. Olivine Clinopyroxenite Xenoliths in the Oslo Rift, SE Norway. *Contributions to Mineralogy and Petrology* 98, 184-193.

Neumann, E.R., Brunfelt, A.O. and Finstad, K.G. 1977. Rare-Earth Elements in some Igneous Rocks in Oslo Rift, Norway. *Lithos* 10, 311-319.

Neumann, E.R., Dunworth, E.A., Sundvoll, B.A. and Tollefsrud, J.I. 2002. B-1 basaltic lavas in Vestfold-Jeloya area, central Oslo rift: derivation from initial melts formed by progressive partial melting of an enriched mantle source. *Lithos* 61, 21-53.

Neumann, E.R., Larsen, B.T. and Sundvoll, B. 1985. Compositional Variations Among Gabbroic Intrusions in the Oslo Rift. *Lithos* 18, 35-59.

Neumann, E.R., Olsen, K.H., Baldridge, W.S. and Sundvoll, B. 1992. The Oslo Rift - A Review. *Tectonophysics* 208, 1-18.

Neumann, E.R., Pallesen, S. and Andresen, P. 1986. Mass Estimates of Cumulates and Residues after Anatexis in the Oslo Graben. *Journal of Geophysical Research-Solid Earth and Planets* 91, 1629-1640.

Neumann, E.R., Sundvoll, B. and Overli, P.E. 1990. A Mildly Depleted Upper Mantle Beneath Southeast Norway - Evidence from Basalts in the Permo-Carboniferous Oslo Rift. *Tectonophysics* 178, 89-107.

Neumann, E.R., Tilton, G.R. and Tuen, E. 1988b. Sr, Nd and Pb Isotope Geochemistry of the Oslo Rift Igneous Province, Southeast Norway. *Geochimica Et Cosmochimica Acta* 52, 1997-2007.

Nilsen, O. 1992. Petrology and metallogeny associated with the Tryvann Granite Complex, Oslo region. *NGU Bulletin* 423, 1-18.

Nordgulen, Ø. 1999. Geologisk kart over Norge, berggrunnskart Hamar, M 1: 250 000. *Norges geologiske undersøkelse*.

Nordgulen, Ø. and Andresen, A. 2006. Jordas urtid. De elste bergarter dannes;4600-850 millioner år. *In* Ramberg, I., B., Bryhni, I. and Nøttvedt, A. (eds). *Landet blir til Norges geologi*: Norsk Geologisk Forening, 62-119.

Oftedahl, C. 1946. Studies on the Igneous Rock Complex of the Oslo Region VI. On Akerites, Felsites and Romb Phorphyry: Det Norske Vitenskapsakademi, Oslo. Skrifter 1946.

Oftedahl, C. 1948. Studies on the Igneous Rock Complex of the Oslo Region: The Feldspars. *Skrifter*: Det Norske Vitenskapsakedemi i Oslo.

Olaussen, S., Larsen, B.T. and Steel, R. 1994. The upper carboniferous-permian Oslo Rift; basin fill in relation to tectonic development. *In* Embry, A., F., Beauchamp, B. and Glass, D., J. (eds). *Pangaea: Global Environments and Resources*. Memoir. 17: Canadian Society of Petroleum Geologists, 175-197.

Parrish, R.R. and Noble, S.R. 2003. Zircon U-Th-Pb geochronology by isotope dilution - Thermal Ionization Mass Spectrometry (ID-TIMS). *In* Hanchar, J.M. and Hoskin, P.W.O. (eds). *Zircon*. Reviews in Mineralogy & Geochemistry, 53, 183-213.

Pascal, C., Cloetingh, S., A., P., L. and Davies, G., R. 2004. Asymmetric lithosphere as the cause of rifting and magmatism in the Permo-Carboniferous Oslo Graben. *In* Wilson, M., Neumann, E., R., Davies, G., R., Timmermann, M., J., Heeremans, M. and Larsen, B.T. (eds). *Permo-Carboniferous Magmatism and Rifting in Europe*. Special Publication: Geological Society, 223, 139-156.

Pedersen, L.E., Heaman, L.M. and Holm, P.M. 1995. Further Constraints on the Temporal Evolution of the Oslo Rift from Precise U-Pb Zircon Dating in the Siljan-Skrim Area. *Lithos* 34, 301-315.

Petersen, J.S. 1978. Structure of the larvikite-lardalite complex, Oslo-region, Norway, and its evolution. *Geologische Rundschau* 67, 330-342.

Plomerova, J., Arvidsson, R., Babuska, V., Granet, M., Kulhanek, O., Poupinet, G. and Sileny, J. 2001. An array study of lithospheric structure across the Protogine zone, Varmland, south-central Sweden - signs of a paleocontinental collision. *Tectonophysics* 332, 1-21.

Pouchou, J.L. and Pichoir, F. 1984. A new model for quantitative X-ray microanalysis. I. Application to the analysis of homogeneous samples. *La Recherche Aérospatiale*, 13-38.

Ramberg, I.B. 1976. *Gravity Interpretation of the Oslo graben and Associated Igneous Rocks*. Edited by Roberts, D. NGU Bulletin. 38. 194 pp.

Ramberg, I.B. and Larsen, B.T. 1978. Tectonomagmatic evolution. *In* Dons, J.A. and Larsen, B.T. (eds). *The Oslo Paleorift A Review and Guide to Excursions*. NGU Bulletin. 45: Universitetsforlaget, 55-73.

Ramberg, I.B. and Smithson, S.B. 1971. Gravity Interpretation of Southern Oslo Graben Area, Norway. *Transactions-American Geophysical Union* 52, 921-&.

Rasmussen, E., Neumann, E.R., Andersen, T., Sundvoll, B., Fjerdingstad, V. and Stabel, A. 1988. Petrogenetic Processes associated with Intermediate and Silicic Magmatism in the Oslo Rift, Southeast Norway. *Mineralogical Magazine* 52, 293-307.

Rosa, D.R.N., Finch, A.A., Andersen, T. and Inverno, C.M.C. 2009. U-Pb geochronology and Hf isotope ratios of magmatic zircons from the Iberian Pyrite Belt. *Mineralogy and Petrology* 95, 47-69.

Segalstad, T.V. 1979. Petrology of the Skien Basaltic Rocks, Southwestern Oslo Region, Norway. *Lithos* 12, 221-239.

Sippel, J., Saintot, A., Heeremans, M. and Scheck-Wenderoth, M. 2010. Paleostress field reconstruction in the Oslo region. *Marine and Petroleum Geology* 27, 682-708.

Slagstad, T. 2006. Did hot, high heat-producing granites determine the location of the Oslo Rift? *Tectonophysics* 412, 105-119.

Soderlund, U., Isachsen, C.E., Bylund, G., Heaman, L.M., Jonathan Patchett, P.J., Vervoort, J.D. and Andersson, U.B. 2005. U-Pb baddeleyite ages and Hf, Nd isotope chemistry constraining repeated mafic magmatism in the Fennoscandian Shield from 1.6 to 0.9 Ga. *Contributions to Mineralogy and Petrology* 150, 174-194.

Soderlund, U., Patchett, J.P., Vervoort, J.D. and Isachsen, C.E. 2004. The Lu-176 decay constant determined by Lu-Hf and U-Pb isotope systematics of Precambrian mafic intrusions. *Earth and Planetary Science Letters* 219, 311-324.

Steiger, R.H. and Jager, E. 1977. Subcommission on Geochronology - Convention on Use of Decay Constants in Geochronology and Cosmochronology. *Earth and Planetary Science Letters* 36, 359-362.

Stein, M. and Hofmann, A.W. 1994. Mantle Plumes and Episodic Crustal Growth. *Nature* 372, 63-68.

Stratford, W. and Thybo, H. 2011. Crustal structure and composition of the Oslo Graben, Norway. *Earth and Planetary Science Letters* 304, 431-442.

Sun, S.S. and McDonough, W. 1989. Chemical and isotopic systematics of oceanic basalts: implications for mantle composition and processes. *Geological Society, London, Special Publications* 42, 313.

Sundvoll, B. and Larsen, B.T. 1990. Rb-Sr isotope systematics in the magmatic rocks of the Oslo Rift. *NGU Bulletin* 418, 27-46.

Sundvoll, B. and Larsen, B.T. 1994. Architecture and Early Evolution of the Oslo Rift. *Tectonophysics* 240, 173-189.

Sundvoll, B., Larsen, B.T. and Wandaas, B. 1992. EARLY MAGMATIC PHASE IN THE OSLO RIFT AND ITS RELATED STRESS REGIME. *Tectonophysics* 208, 37-54.

Sundvoll, B., Neumann, E.R., Larsen, B.T. and Tuen, E. 1990. Age Relations Among Oslo Rift Magmatic Rocks - Implications for Tectonic and Magmatic Modeling. *Tectonophysics* 178, 67-87.

Sundvoll, B.A. 1978. Isotope- and Trace-Element Chemistry, Geochronology. *In* Dons, J.A. and Larsen, B.T. (eds). *The Oslo Paleorift A Review and Guide to Excursions*. NGU Bulletin: Universitetsforlaget, 45, 35-40.

Sæther, E. 1962. Studies on the igneous rock complex of the Oslo region. XVIII. General investigation of the igneous rocks in the area north of Oslo. *Skr Nor Vid-Akad Oslo, I Mat-Naturv Kl, Sy Serie* 1, 1-184.

Tera, F. and Wasserburg, G., J. 1972. U-Th-Pb Systamatics in 3 Apollo 14 Basalts and Problem of Initial Pb in Lunar Rocks. *Earth and Planetary Science Letters* 14, 281-304.

Timmerman, M.J., Heeremans, M., Kirstein, L.A., Larsen, B.T., Spencer-Dunworth, E.A. and Sundvoll, B. 2009. Linking changes in tectonic style with magmatism in northern Europe during the late Carboniferous to latest Permian. *Tectonophysics* 473, 375-390.

Torsvik, T.H., Eide, E.A., Meert, J.G., Smethurst, M.A. and Walderhaug, H.J. 1998. The Oslo Rift: new palaeomagnetic and Ar-40/Ar-39 age constraints. *Geophysical Journal International* 135, 1045-1059.

Torsvik, T.H., Smethurst, M.A., Burke, K. and Steinberger, B. 2008. Long term stability in deep mantle structure: Evidence from the similar to 300 Ma Skagerrak-Centered Large Igneous Province (the SCLIP). *Earth and Planetary Science Letters* 267, 444-452.

Tryti, J. and Sellevoll, M.A. 1977. Seismic Crustal Study of Oslo Rift. *Pure and Applied Geophysics* 115, 1061-1085.

Trønnes, R.G. and Brandon, A.D. 1992. Mildly Peraluminous High-Silica Granites in a Continental Rift - the Drammen and Finnemarka Batholiths, Oslo Rift, Norway. *Contributions to Mineralogy and Petrology* 109, 275-294.

U.S. Geological Survey. 2011 [Accsessed: 2011.02.14. Available at http://www.usgs.gov/.

Watson, E.B., Cherniak, D.J., Hanchar, J.M., Harrison, T.M. and Wark, D.A. 1997. The incorporation of Pb into zircon. *Chemical Geology* 141, 19-31.

Wessel, P. and Husebye, E.S. 1987. The Oslo Graben Gravity High and Taphrogenesis. *Tectonophysics* 142, 15-26.

Wetherill, G., W. 1956. Discordant uranium-lead ages.

Wiedenbeck, M., Alle, P., Corfu, F., Griffin, W.L., Meier, M., Oberli, F., Vonquadt, A., Roddick, J.C. and Speigel, W. 1995. 3 Natural Zircon Standards for U-Th-Pb, Lu-Hf, Trace-Eelement and REE Analyses. *Geostandards Newsletter* 19, 1-23.

Winter, J., D. 2001. *An introduction to Igneous and Metamorphic Petrology*. 1 ed: Prentice Hall. 697 pp.

Woodhead, J.D. and Hergt, J.M. 2005. A preliminary appraisal of seven natural zircon reference materials for in situ Hf isotope determination. *Geostandards and Geoanalytical Research* 29, 183-195.

Ziegler, P., A. 1982. *Geological Atlas of Western and Central Europe*: Elsevier. 130 pp.

Zindler, A. and Hart, S. 1986. Chemical geodynamics. *Annual Review of Earth and Planetary Sciences* 14, 493-571.

8 Appendix

8.1 Petrographic microscopy

Sample GB-A	
	
Sample spot	In the akerite body. Close to the contact between and Cambro-Silurian limestone.
Hand sample	Porphyritic. Black phenocrysts in a grey matrix with abundant dark minerals. Two distinct white zones cut the sample.
Thin section	<4 mm plagioclase phenocrysts. Fine grained inequigranular matrix.
Minerals	
Plagioclase	<4 mm size. Hypidiomorphic. Intermediately saussuritized in the white zones. Except from this, generally unaltered.
Alkali feldspar	<2 mm size. Allotriomorphic. Some grains show zoning.
Amphibole	<1.5 mm size. Allotriomorphic. Often found around a core of pyroxene. Z^C: 20°. X: light yellow, Y: dark olive green, Z: light green.
Clinopyroxene	<1.5 mm size. Allotriomorphic. Shows linear exsolution lamellae of orthopyroxene. Commonly rimmed by amphibole.
Orthopyroxene	<1.5 mm size. Allotriomorphic. Commonly rimmed by amphibole. Cross-cut by alteration veins.
Biotite	<1 mm size. Allotriomorphic. Often found as rims around magnetite. Some chloritic alteration.
Quartz	<0.5 mm size. Allotriomorphic. Interstitial.
Apatite	<0.2 mm size. Panidiomorphic. Randomly distributed.
Zircon	<0.2 mm size. Hypidiomorphic. Randomly distributed.
Opaques	<0.6 mm size. Allotriomorphic. Mainly magnetite with exsolution lamellae of ilmenite. Commonly rimmed by biotite.
Calcite	<0.4 mm size. Hypidiomorphic. Found only in the two white, highly altered zones cutting the thin section.
Chlorite	Allotriomorphic. Secondary from biotite, amphibole and pyroxene. Found in the white zones.
Hematite	<0.1 mm size. Allotriomorphic.

Table 7. Field of view of photo is ~30mm (horizontally).

Sample GB-B	
	
Sample spot	From a dike in the interior of the body.
Hand sample	Aphyric. Light red with some dark minerals.
Thin section	Medium grained. More quartz and less dark minerals than in the samples.
Minerals	
Alkali feldspar	<3 mm size. Hypidiomorphic. Strongly sericitized.
Amphibole	<1.5 mm size. Allotriomorphic. Z^C: 16°. X: greenish yellow, Y: bluish green, Z: light green.
Biotite	<2.5 mm size. Allotriomorphic. Highly chloritized.
Quartz	<2.5 mm size. Allotriomorphic.
Zircon	<0.2 mm size. Hypidiomorphic. Randomly distributed.
Opaques	<0.4 mm size. Allotriomorphic. Mainly magnetite with exsolution lamellae of ilmenite.
Calcite	<0.4 mm size. Allotriomorphic.
Chlorite	Allotriomorphic. Secondary from biotite and amphibole.
Hematite	<0.4 mm size. Allotriomorphic.
Epidote	<0.1 mm size. Allotriomorphic.

Table 8. Field of view of photo is ~30mm (horizontally).

Sample GB-C

Sample spot	In the interior of the body.
Hand sample	Porphyritic. Dark grey phenocrysts in a light grey matrix with abundant dark minerals.
Thin section	<7 mm plagioclase phenocrysts. Fine grained inequigranular matrix.
Minerals	
Plagioclase	<7 mm size. Hypidiomorphic. Weakly saussuritized. Maximum extinction angle (two measurements): 9°→An_{25}/An_{13}, 11°→An_{26}/An_{11}.
Alkali feldspar	<2.5 mm size. Allotriomorphic. Intermediately sericitized. Some grains show zoning.
Amphibole	<1 mm size. Allotriomorphic. Often found around a core of pyroxene. Z^C: 28°. X: light yellow, Y: dark olive green, Z: light green.
Clinopyroxene	<1 mm size. Allotriomorphic. Shows linear exsolution lamellae of orthopyroxene. Commonly rimmed by amphibole. Some grains show chloritic alteration.
Orthopyroxene	<1 mm size. Allotriomorphic. Commonly rimmed by amphibole. Cross-cut by alteration veins.
Biotite	<0.5 mm size. Allotriomorphic. Often found as rims around magnetite. Some chloritic alteration.
Quartz	<0.7 mm size. Allotriomorphic. Interstitial.
Apatite	<0.4 mm size. Panidiomorphic. Randomly distributed.
Zircon	<0.1 mm size. Hypidiomorphic. Randomly distributed.
Opaques	<1 mm size. Allotriomorphic. Mainly magnetite with exsolution lamellae of ilmenite. Commonly rimmed by biotite.
Chlorite	Allotriomorphic. Secondary from biotite, amphibole and pyroxene.

Table 9. Field of view of photo is ~30mm (horizontally).

Sample GB-D

Sample spot	In the interior of the body.
Hand sample	Porphyritic. Light grey phenocrysts in a light red matrix with abundant dark minerals.
Thin section	<10 mm plagioclase phenocrysts. Fine grained inequigranular matrix.
Minerals	
Plagioclase	<10 mm size. Hypidiomorphic. Strongly saussuritized. Maximum extinction angle (two measurements): 12°→An_{27}/An_{10}, 35°→An_{61}.
Alkali feldspar	<5 mm size. Allotriomorphic. Strongly sericitized.
Amphibole	<1 mm size. Allotriomorphic. Found in association with chlorite and possibly relict pyroxenes. Z^C: 10°. X: light yellow, Y: dark olive green, Z: light green.
Pyroxene	Some highly altered grains found. Associated with amphibole and chlorite.
Apatite	<0.5 mm size. Panidiomorphic. Randomly distributed.
Zircon	<0.3 mm size. Hypidiomorphic. Randomly distributed.
Opaques	<1 mm size. Allotriomorphic. Mainly magnetite with exsolution lamellae of ilmenite.
Calcite	<0.2 mm size. Allotriomorphic.
Chlorite	Allotriomorphic. Secondary from pyroxene and amphibole.
Epidote	<0.2 mm size. Allotriomorphic. Mainly found in thin veins cutting the sample.

Table 10. Field of view of photo is ~30mm (horizontally).

Sample GB-E

Sample spot	In the interior of the body.
Hand sample	Porphyritic. Grey phenocrysts in a pale reddish grey matrix with abundant dark minerals.
Thin section	<10 mm plagioclase phenocrysts. Fine grained inequigranular matrix. Several thin fractures cut the sample. Feldspar grains cut by these fractures are generally more altered than in other areas of the sample.
Minerals	
Plagioclase	<10 mm size. Hypidiomorphic. Weakly saussuritized, mainly around the fractures. Maximum extinction angle (two measurements): 14°→An_6/An_{29}, 24°→An_{44}.
Alkali feldspar	<3.5 mm size. Allotriomorphic. Some grains show zoning. Weakly sericitized
Amphibole	<1.5 mm size. Allotriomorphic. Often found around a core of altered pyroxene. Z^C: 5°. X: light yellow, Y: dark olive green, Z: light green.
Clinopyroxene	<1mm size. Allotriomorphic. Shows linear exsolution lamellae of orthopyroxene. Commonly rimmed by amphibole. Abundant chloritic alteration.
Biotite	<1 mm size. Allotriomorphic. Often found as rims around magnetite. Some chloritic alteration.
Quartz	<1 mm size. Allotriomorphic. Interstitial.
Apatite	<0.8 mm size. Panidiomorphic. Randomly distributed.
Zircon	<0.3 mm size. Hypidiomorphic. Randomly distributed.
Opaques	<1.5 mm size. Allotriomorphic. Mainly magnetite with exsolution lamellae of ilmenite. Some grains are rimmed by biotite. Some pyrite, rimmed by hematite.
Chlorite	Allotriomorphic. Secondary from biotite, amphibole and pyroxene.
Hematite	<0.2 mm size. Allotriomorphic.

Table 11. Field of view of photo is ~30mm (horizontally).

Sample GB-F	
	
Sample spot	In the interior of the body.
Hand sample	Porphyritic. Grey phenocrysts in a pale reddish grey matrix with abundant dark minerals.
Thin section	<5.5 mm plagioclase phenocrysts. Fine grained inequigranular matrix.
Minerals	
Plagioclase	<5.5 mm size. Hypidiomorphic. Weakly saussuritized, mainly around fractures. Maximum extinction angle (two measurements): 18°→An_{35}, 30°→An_{54}. Some grains show zoning.
Alkali feldspar	<3 mm size. Allotriomorphic. Some grains show zoning. Weakly sericitized.
Amphibole	<1.5 mm size. Allotriomorphic. Often found around a core of altered pyroxene. Z^C: 20°. X: light yellow, Y: dark olive green, Z: light green.
Clinopyroxene	<1mm size. Allotriomorphic. Shows linear exsolution lamellae of orthopyroxene. Commonly rimmed by amphibole. Abundant chloritic alteration.
Orthopyroxene	
Biotite	<1 mm size. Allotriomorphic. Often found as rims around magnetite. Minor chloritic alteration.
Quartz	<0.8 mm size. Allotriomorphic. Interstitial.
Apatite	<0.5 mm size. Panidiomorphic. Randomly distributed.
Zircon	<0.8 mm size. Hypidiomorphic. Randomly distributed.
Opaques	<1 mm size. Allotriomorphic. Mainly magnetite with exsolution lamellae of ilmenite. Some grains are rimmed by biotite. Some pyrite found, rimmed by hematite.
Chlorite	Allotriomorphic. Secondary from biotite, amphibole and pyroxene.
Hematite	<0.1 mm size. Allotriomorphic.

Table 12. Field of view of photo is ~30mm (horizontally).

Sample GB-G

Sample spot	In the interior of the body.
Hand sample	Porphyritic. White phenocrysts in a light red matrix with abundant dark minerals.
Thin section	<6 mm plagioclase phenocrysts. Fine grained inequigranular matrix.
Minerals	
Plagioclase	<6 mm size. Hypidiomorphic. Strongly saussuritized. Maximum extinction angle (two measurements): 20°→An_{37}, 11°→An_{12}/An_{27}. Some grains show a less altered rim.
Alkali feldspar	<3 mm size. Allotriomorphic. Intermediately sericitized. Some grains show zoning.
Amphibole	<2 mm size. Allotriomorphic. Some grains have a core of relict pyroxene. Z^C: 17°. X: light yellow, Y: dark olive green, Z: light green.
Pyroxene	<1mm size. Allotriomorphic. Commonly rimmed by amphibole. Highly altered.
Biotite	<1 mm size. Allotriomorphic. Highly altered to chlorite.
Quartz	<0.7 mm size. Allotriomorphic. Interstitial.
Apatite	<0.5 mm size. Panidiomorphic. Randomly distributed.
Zircon	<0.1 mm size. Hypidiomorphic. Randomly distributed.
Opaques	<0.8 mm size. Allotriomorphic. Mainly magnetite with exsolution lamellae of ilmenite. Rarely rimmed by biotite.
Chlorite	Allotriomorphic. Secondary from biotite, amphibole and pyroxene.
Hematite	Found in thin veins cutting the sample. Allotriomorphic.
Epidote	Found in thin veins cutting the sample. Allotriomorphic.

Table 13. Field of view of photo is ~30mm (horizontally).

Sample GB-H

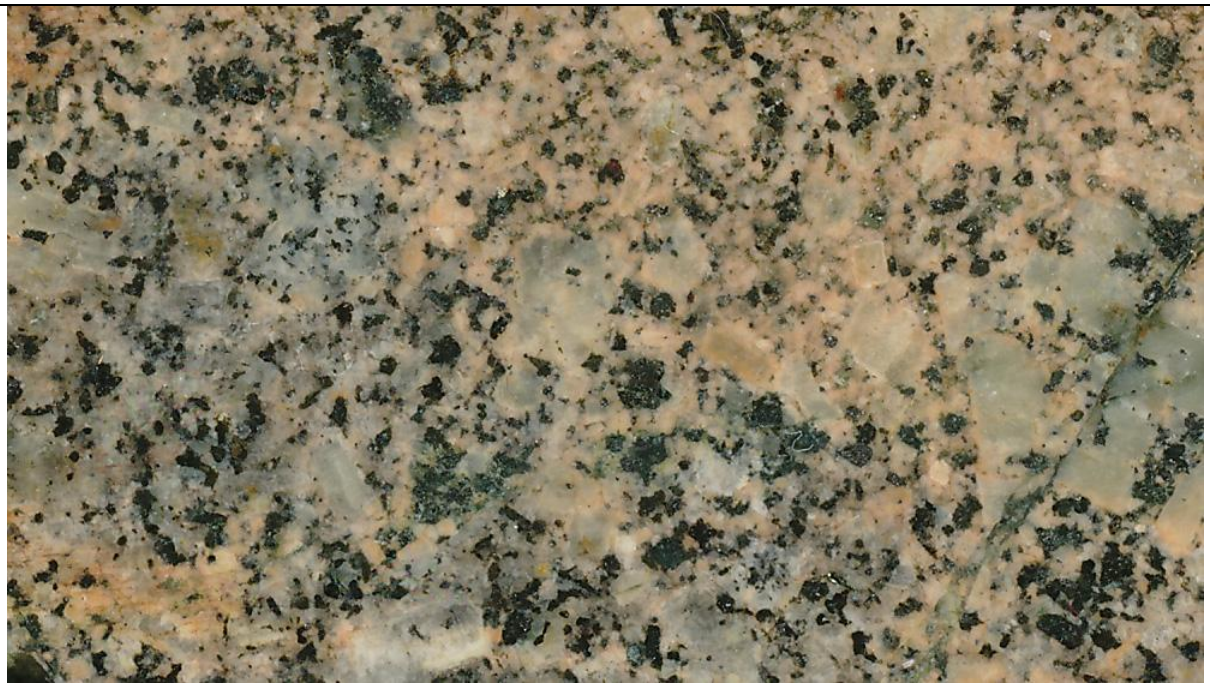

Sample spot	In the body close to the contact between and RP2.
Hand sample	Porphyritic. Grayish white phenocrysts in a light red matrix with abundant dark minerals.
Thin section	<10 mm plagioclase phenocrysts. Fine grained inequigranular matrix. Some thin fractures cut the sample.
Minerals	
Plagioclase	<10 mm size. Hypidiomorphic. Strongly saussuritized. Maximum extinction angle (two measurements): 17°→An_3/An_{32}, 33°→An_{59}.
Alkali feldspar	<3 mm size. Allotriomorphic. Strongly sericitized. Some grains show zoning.
Amphibole	<1.5 mm size. Allotriomorphic. Some grains found around a core of altered pyroxene. Z^C: 18°. X: light yellow, Y: dark olive green, Z: light green.
Clinopyroxene	<0.5mm size. Allotriomorphic. Highly altered. Commonly rimmed by amphibole.
Biotite	<1 mm size. Allotriomorphic. Highly altered to chlorite.
Quartz	<0.8 mm size. Allotriomorphic. Interstitial.
Apatite	<0.7 mm size. Panidiomorphic. Randomly distributed.
Zircon	<0.2 mm size. Hypidiomorphic. Randomly distributed.
Opaques	<0.8 mm size. Allotriomorphic. Mainly magnetite with exsolution lamellae of ilmenite. Few grains are rimmed by biotite.
Chlorite	Allotriomorphic. Secondary from biotite, amphibole and pyroxene.
Hematite	<0.3 mm size. Allotriomorphic.
Epidote	<0.3 mm size. Allotriomorphic. Mainly in veins.

Table 14. Field of view of photo is ~30mm (horizontally).

Sample GB-18	
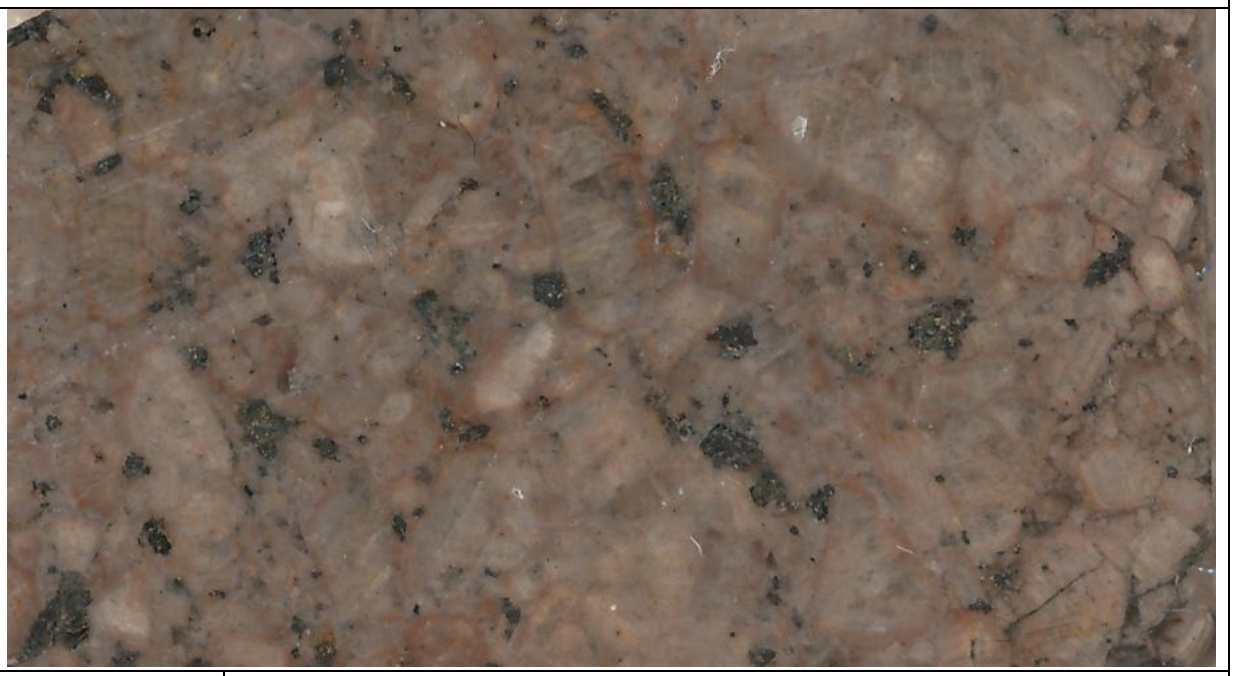	
Sample spot	Within the nordmarkite body. 0.5m from the contact between nordmarkite and.
Hand sample	Brownish red.
Thin section	Aphyric. Inequigranular. Medium grained. Low abundance of dark minerals. ~98% strongly sericitized alkali feldspar + quartz. No plagioclase found.
Minerals	
Alkali feldspar	<6 mm size. Hypidiomorphic. Strongly sericitized.
Amphibole	<1.5 mm size. Allotriomorphic. Altered. Z^C: 7°. X: olive green, Y: dark bluish green, Z: dark blue-grayish green. Shows irregular alteration zones.
Quartz	<2 mm size. Allotriomorphic. Interstitial.
Zircon	<0.2 mm size. Hypidiomorphic. Randomly distributed.
Opaques	<1.5 mm size. Allotriomorphic. Mainly magnetite with exsolution lamellae of ilmenite.
Hematite	<0.2 mm size. Allotriomorphic.

Table 15. Field of view of photo is ~30mm (horizontally).

Sample GB-19

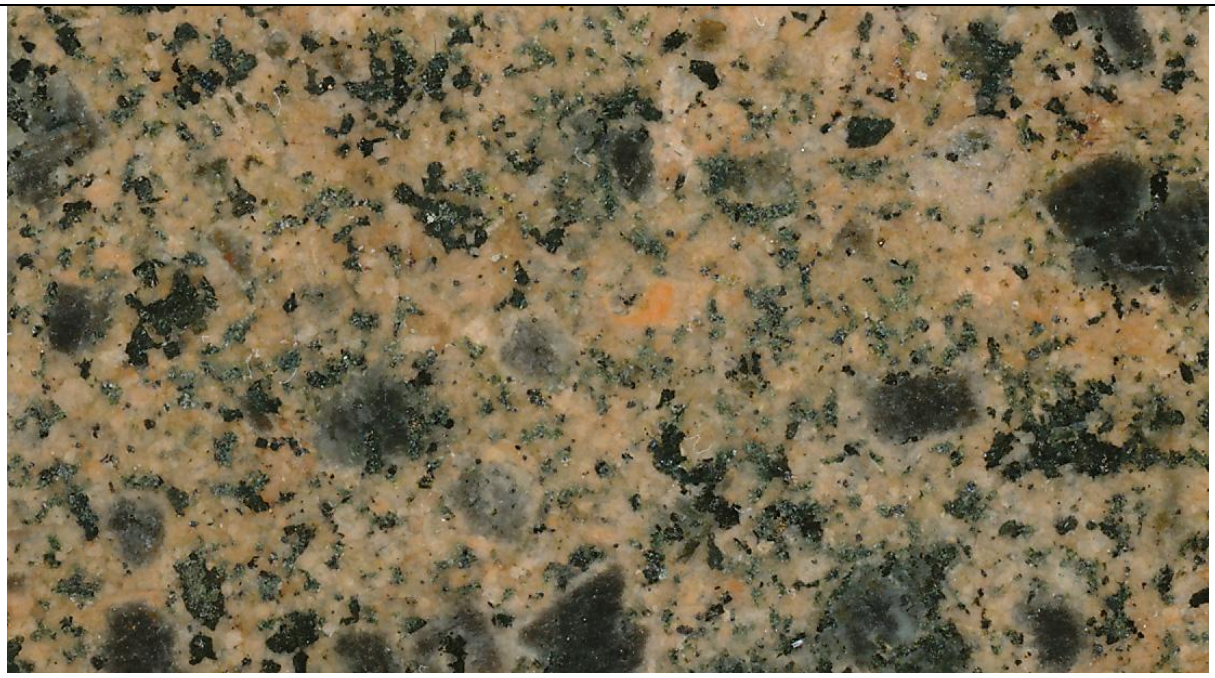

Sample spot	In the body. 0.6m south of sample GB-18.
Hand sample	Porphyritic. Dark grey-black phenocrysts in a red matrix.
Thin section	<5 mm feldspar phenocrysts. Fine grained inequigranular matrix.
Minerals	
Plagioclase	<5 mm size. Hypidiomorphic. Intermediately saussuritized. Maximum extinction angle: 25°→An_{46}. Phenocrysts less altered than matrix grains.
Alkali feldspar	<5 mm size. Allotriomorphic. Strongly sericitized. Some grains show zoning.
Amphibole	<1.5 mm size. Allotriomorphic. Often found around a core of highly altered pyroxene. Z^C: 29°. X: light yellow, Y: dark olive green, Z: green.
Pyroxene	<1mm size. Allotriomorphic. Commonly rimmed by amphibole. Highly altered.
Biotite	<0.7 mm size. Allotriomorphic. Rarely found as rims around magnetite. Some chloritic alteration.
Quartz	<1 mm size. Allotriomorphic. Interstitial.
Apatite	<0.4 mm size. Panidiomorphic. Randomly distributed.
Zircon	<0.1 mm size. Hypidiomorphic. Randomly distributed.
Opaques	<0.6 mm size. Allotriomorphic. Mainly magnetite with exsolution lamellae of ilmenite. Few grains are rimmed by biotite.
Calcite	<1 mm size. Hypidiomorphic.
Chlorite	Allotriomorphic. Secondary from biotite, amphibole and pyroxene.
Epidote	<0.4 mm size. Hypidiomorphic.
Fluorite	<0.3 mm size. Two anhedral grains found.

Table 16. Field of view of photo is ~30mm (horizontally).

Sample GB-20

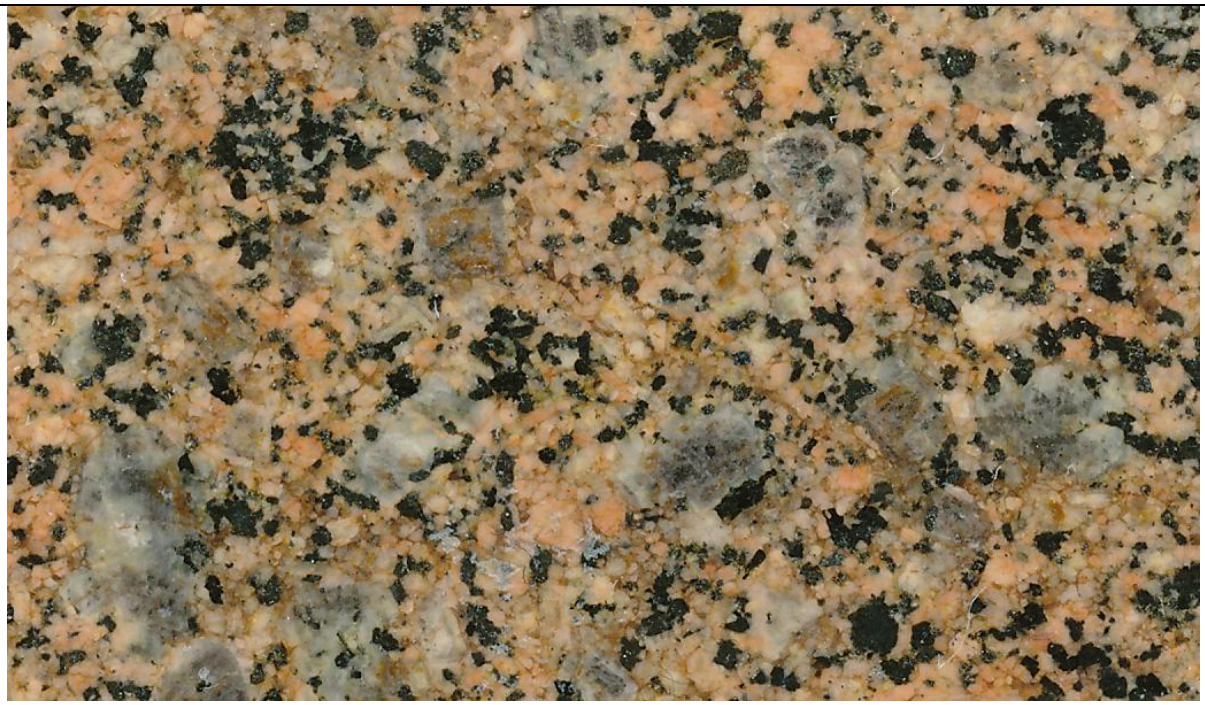

Sample spot	In the body. 1.3m south of sample GB-18.
Hand sample	Porphyritic. Grey phenocrysts in a red matrix with abundant dark minerals.
Thin section	<5 mm plagioclase phenocrysts. Fine grained inequigranular matrix. Highly altered.
Minerals	
Plagioclase	<5 mm size. Hypidiomorphic. Strongly saussuritized. Maximum extinction angle (two measurements): 21°→An_{38}, 25°→An_{46}. Some grains show a less altered rim.
Alkali feldspar	<3mm size. Allotriomorphic. Strongly sericitized.
Amphibole	<1.5 mm size. Allotriomorphic. Altered. Few grains show a core of relict pyroxene. Z^C: 19°. X: light yellow, Y: dark olive green, Z: light green.
Pyroxene	Some relict pyroxenes found as cores of amphibole grains.
Biotite	<1 mm size. Allotriomorphic. Highly altered to chlorite.
Quartz	<1 mm size. Hypidiomorphic. Interstitial mosaic of mainly 0.1-0.4 mm sized grains.
Apatite	<0.8 mm size. Panidiomorphic. Randomly distributed.
Zircon	<0.2mm size. Hypidiomorphic. Randomly distributed.
Opaques	<1mm size. Allotriomorphic. Mainly magnetite with exsolution lamellae of ilmenite. Some grains are rimmed by biotite. Some pyrite found, with rims of hematite.
Calcite	<0.3 mm size. Hypidiomorphic.
Chlorite	Allotriomorphic. Secondary from biotite, amphibole and pyroxene.
Hematite	<0.7 mm size. Allotriomorphic.
Epidote	<0.5 mm size. Hypidiomorphic.

Table 17. Field of view of photo is ~30mm (horizontally).

Sample GB-21

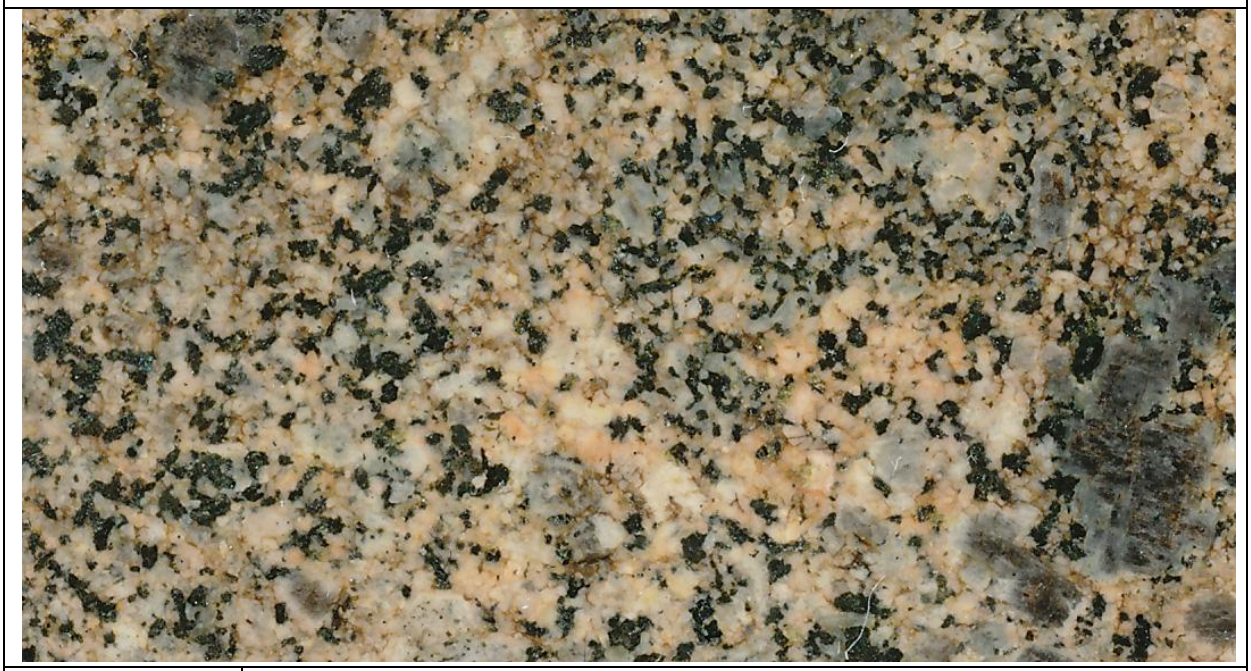

Sample spot	In the body. 6.7m south of sample GB-18.
Hand sample	Porphyritic. Grey-black phenocrysts in a light red matrix with abundant dark minerals.
Thin section	<6 mm plagioclase phenocrysts. Fine grained inequigranular matrix.
Minerals	
Plagioclase	<6 mm size. Hypidiomorphic. Intermediately saussuritized. Maximum extinction angle (two measurements): 20°→An_{37}, 19°→An_{36}.
Alkali feldspar	<3 mm size. Allotriomorphic. Some grains show zoning. Intermediately sericitized.
Amphibole	<1.5 mm size. Allotriomorphic. Intermediately altered. Z^C: 26°. X: light yellow, Y: dark olive green, Z: light green.
Pyroxene	Few relicts can be found.
Biotite	<0.4 mm size. Allotriomorphic. Most grains are strongly chloritized. Few grains are found as rims around opaques.
Quartz	<1 mm size. Allotriomorphic. Interstitial.
Apatite	<0.4 mm size. Panidiomorphic. Randomly distributed.
Zircon	<0.1 mm size. Hypidiomorphic. Randomly distributed.
Opaques	<1.5 mm size. Allotriomorphic. Mainly magnetite with exsolution lamellae of ilmenite. Few grains are rimmed by biotite.
Calcite	<0.7 mm size. Hypidiomorphic.
Chlorite	Allotriomorphic. Secondary from biotite, amphibole and pyroxene.
Hematite	<0.5 mm size. Allotriomorphic.
Epidote	<0.5 mm size. Allotriomorphic.

Table 18. Field of view of photo is ~30mm (horizontally).

Sample GB-22

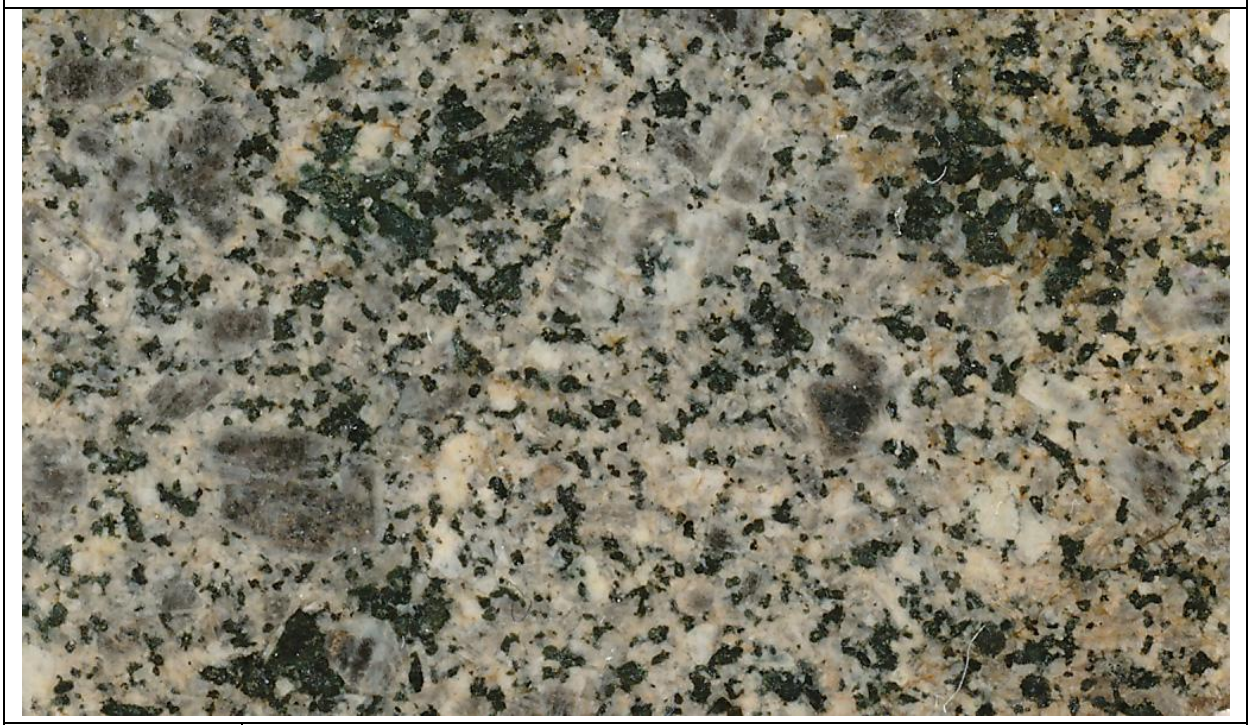

Sample spot	In the body. 8.8m south of sample GB-18.
Hand sample	Porphyritic. Dark grey-black phenocrysts in a light grey matrix with abundant dark minerals.
Thin section	<4 mm plagioclase phenocrysts. Fine grained inequigranular matrix.
Minerals	
Plagioclase	<4 mm size. Hypidiomorphic. Intermediately saussuritized. Maximum extinction angle (two measurements): 10°→An_{12}/An_{26}, 20°→An_{37}.
Alkali feldspar	<2.5 mm size. Allotriomorphic. Some grains show zoning. Weakly sericitized.
Amphibole	<2 mm size. Allotriomorphic. Often found around a core of strongly altered pyroxene. Z^C: 7°. X: light yellow, Y: dark olive green, Z: light green.
Pyroxene	<1mm size. Allotriomorphic. Strongly altered. Often rimmed by amphibole.
Biotite	<0.7 mm size. Allotriomorphic. Some grains found as rims around opaques. Most grains strongly chloritized.
Quartz	<1 mm size. Allotriomorphic. Interstitial.
Apatite	<0.7 mm size. Panidiomorphic. Randomly distributed.
Zircon	<0.3 mm size. Hypidiomorphic. Randomly distributed.
Opaques	<0.5 mm size. Allotriomorphic. Mainly magnetite with exsolution lamellae of ilmenite. Some grains are rimmed by biotite. Some pyrite found, with rims of hematite.
Chlorite	Allotriomorphic. Secondary from biotite, amphibole and pyroxene.
Hematite	Allotriomorphic. Found as rims on opaques.
Epidote	<0.1 mm size. Allotriomorphic.

Table 19. Field of view of photo is ~30mm (horizontally).

Sample GB-23

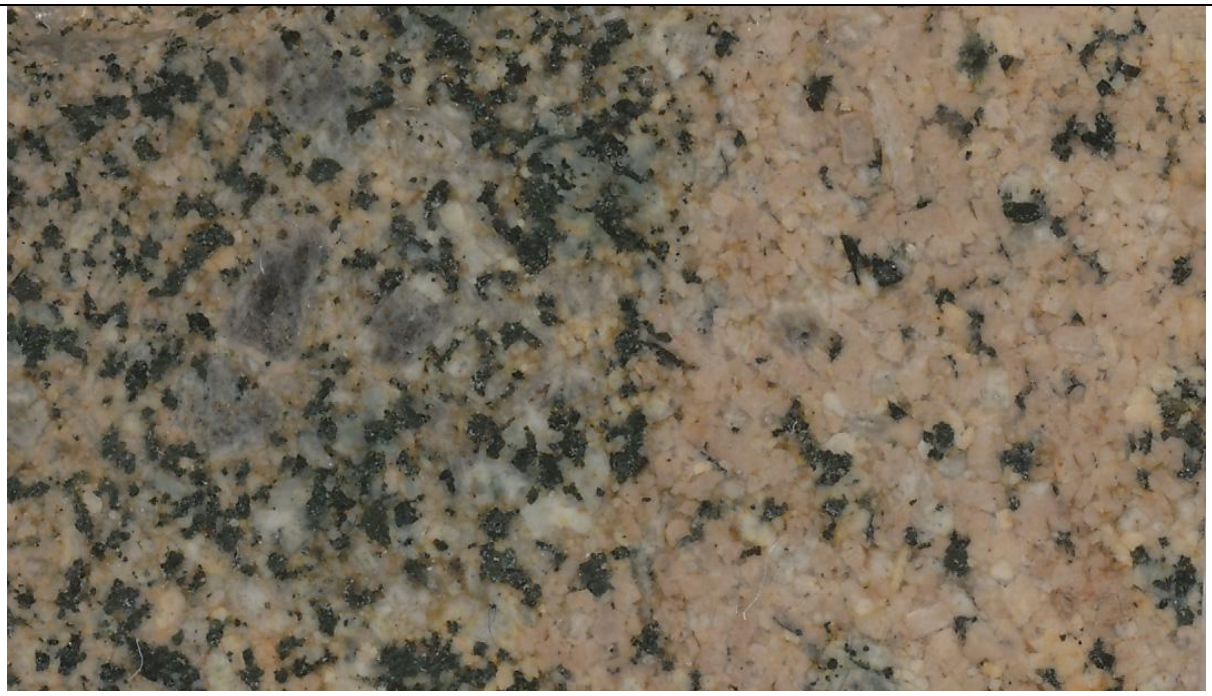

Sample spot	In the body. 12.1m south of sample GB-18. In an area cut by several dikes.
Hand sample	Divided into two parts. Part 1 is to the right in the photo, part 2 to the left. **1:** An aphyric red part with minor dark minerals. This is a dike cutting the. **2:** A porphyritic part with grey phenocrysts in a light red matrix with abundant dark minerals.
Thin section	*Dike*: Mainly strongly sericitized alkali feldspar and interstitial quartz. Some amphiboles and opaques. : <4 mm plagioclase phenocrysts. Fine grained inequigranular matrix. Strongly altered.
Minerals	
Plagioclase	<4 mm size. Hypidiomorphic. Intermediately saussuritized. Maximum extinction angle (two measurements): 14°→An_6/An_{29}, 24°→An_{44}.
Alkali feldspar	<3 mm size. Strongly sericitized. Allotriomorphic in. Hypidiomorphic in dike.
Amphibole	<2.5 mm size. Allotriomorphic. Z^C: 27°. X: light yellow, Y: dark olive green, Z: light green. Most abundant in.
Biotite	: <1 mm size. Allotriomorphic. Strongly chloritized. *Vein:* <2 mm size. Hypidiomorphic. Weakly chloritized.
Quartz	<1 mm size. Allotriomorphic. Interstitial. Most abundant in vein.
Apatite	<0.3 mm size. Panidiomorphic. Randomly distributed. Not found in dike.
Zircon	<0.2 mm size. Hypidiomorphic. Randomly distributed.
Opaques	<0.5 mm size. Allotriomorphic. Contains exsolution lamellae of ilmenite. Most abundant in.
Calcite	<0.3 mm size. Hypidiomorphic.
Chlorite	Allotriomorphic. Secondary from biotite and amphibole.
Hematite	<0.5 mm size. Allotriomorphic. Most abundant in dike.
Epidote	<0.3 mm size. Allotriomorphic.

Table 20. Field of view of photo is ~30mm (horizontally).

Sample GB-24

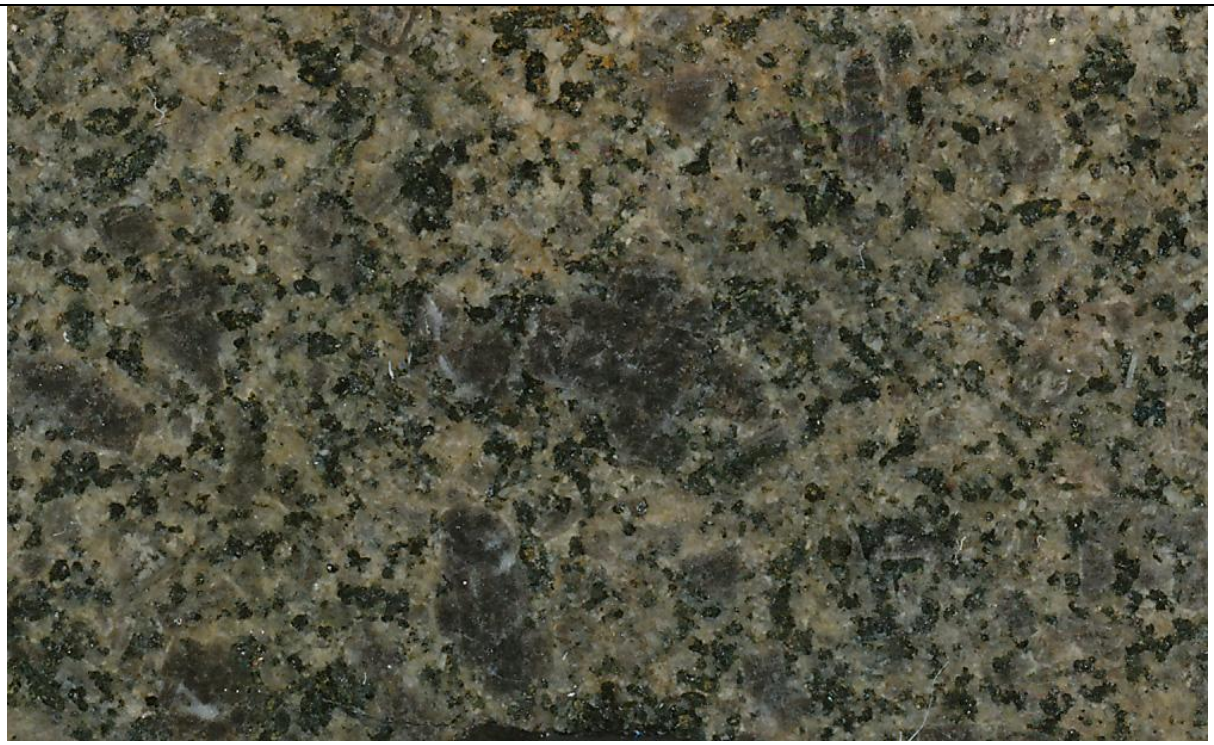

Sample spot	In the body. 17.6m south of sample GB-18.
Hand sample	Porphyritic. Dark grey-black phenocrysts in a light grey matrix with abundant dark minerals.
Thin section	<10 mm plagioclase phenocrysts. Fine grained inequigranular matrix.
Minerals	
Plagioclase	<10 mm size. Hypidiomorphic. Some grains are weakly saussuritized. Maximum extinction angle (two measurements): 12°→An_{10}/An_{27}, 23°→An_{42}.
Alkali feldspar	<3 mm size. Allotriomorphic. Some grains are weakly sericitized.
Amphibole	<2 mm size. Allotriomorphic. Often found around a core of altered pyroxene. Z^C: 31°. X: light yellow, Y: dark olive green, Z: light green.
Pyroxene	<1mm size. Allotriomorphic. Strongly altered. Commonly rimmed by amphibole.
Biotite	<1 mm size. Allotriomorphic. Some grains found as rims around opaques. Weakly chloritized.
Quartz	<0.5 mm size. Allotriomorphic. Interstitial.
Apatite	<0.6 mm size. Panidiomorphic. Randomly distributed.
Zircon	<0.2 mm size. Hypidiomorphic. Randomly distributed.
Opaques	<0.5 mm size. Allotriomorphic. Contains exsolution lamellae of ilmenite. Some grains are rimmed by biotite.
Chlorite	Allotriomorphic. Secondary from biotite, amphibole and pyroxene.

Table 21. Field of view of photo is ~30mm (horizontally).

Sample GB-25

Sample spot	In the body. 30.3m south of sample GB-18.
Hand sample	Porphyritic. Dark grey phenocrysts in a light grey matrix with abundant dark minerals.
Thin section	<5 mm plagioclase phenocrysts. Fine grained inequigranular matrix.
Minerals	
Plagioclase	<5 mm size. Hypidiomorphic. Some grains are weakly saussuritized. Maximum extinction angle: No suitable grains found.
Alkali feldspar	<3 mm size. Allotriomorphic. Some grains are weakly sericitized.
Amphibole	<2 mm size. Allotriomorphic. Often found around a core of pyroxene. Z^C: 18°. X: light yellow, Y: dark olive green, Z: light green. Generally unaltered.
Clinopyroxene	<1mm size. Allotriomorphic. Shows linear exsolution lamellas of orthopyroxene. Commonly rimmed by amphibole.
Orthopyroxene	<0.7 mm size. Allotriomorphic. Cross-cut by alteration veins. Commonly rimmed by amphibole.
Biotite	<0.5 mm size. Allotriomorphic. Often found as rims around magnetite. Generally unaltered.
Quartz	<0.5 mm size. Allotriomorphic. Interstitial.
Apatite	<0.6 mm size. Panidiomorphic. Randomly distributed.
Zircon	<0.2 mm size. Hypidiomorphic. Randomly distributed.
Opaques	<0.8 mm size. Allotriomorphic. Contains exsolution lamellae of ilmenite. Some grains are rimmed by biotite.

Table 22. Field of view of photo is ~30mm (horizontally).

8.2 ICP-OES bulk chemical analysis

Major elements

Sample	SiO_2	TiO_2	Al_2O_3	Fe_2O_3	MnO	MgO	CaO	Na_2O	K_2O	P_2O_5	LOI (%)	Total
BCR-2(1)	53.572	2.253	13.317	13.637	0.196	3.517	6.970	3.111	1.795	0.348		98.716
BCR-2(2)	53.965	2.274	13.364	13.672	0.198	3.548	6.964	3.138	1.818	0.352		99.295
BCR2-LITERATURE	54.100	2.260	13.500	13.800	0.200	3.590	7.120	3.160	1.790	0.350		
JB2(1)	53.889	1.190	14.743	14.302	0.219	4.619	9.853	2.054	0.419	0.097		101.386
JB-2 LITERATURE	53.500	1.190	14.700	14.250	0.218	4.620	9.820	2.040	0.420	0.101		
GB-A	59.074	1.452	16.435	7.066	0.158	2.018	4.800	4.334	3.335	0.508	0.093	99.179
GB-B	68.926	0.486	15.252	2.637	0.101	0.401	0.903	5.008	4.979	0.073	0.293	98.767
GB-C	58.645	1.520	16.281	7.331	0.158	2.138	4.787	4.235	3.436	0.520	0.111	99.050
GB-D	57.151	1.475	16.786	7.585	0.151	2.029	3.994	6.530	2.533	0.469	0.633	98.702
GB-E	58.118	1.548	16.242	7.479	0.158	2.246	4.943	4.259	3.280	0.500	0.234	98.773
GB-F	58.227	1.523	16.479	7.255	0.161	2.157	4.954	4.336	3.221	0.521	0.120	98.834
GB-G	58.911	1.452	16.346	7.045	0.154	2.087	4.321	4.277	3.543	0.502	0.775	98.638
GB-H	59.514	1.383	16.389	6.702	0.160	1.942	4.202	4.615	3.744	0.504	0.563	99.154

Table 23. Major element analyses. Standards are in gray.

Trace elements

Sample	Cr	Ni	Zn	V	Sc	Co	Ba	Sr	Zr	Hf	La	Ce	Nd	Dy	Yb	Y	Th	Be
BCR-2(1)	15	13	132	409	33	36	669	338	187	0.0	23	47	28	5.8	3.1	37	10	2.1
BCR-2(2)	15	13	133	412	33	36	671	340	189	-0.5	24	50	31	6.4	3.2	36	4	1.6
BCR2-LITERATURE	*18*	*18*	*127*	*416*	*33*	*37*	*677*	*340*	*184*	*4.9*	*25*	*53*	*28*	*6.4*	*3.5*	*37*	*6*	*2.3*
JB2(1)	25	16	112	558	53	26	221	179	54	0.0	3	6	5	4.3	3.2	24	0	0.0
JB-2 LITERATURE	*28*	*17*	*110*	*575*	*54*	*38*	*222*	*178*	*51*	*1.5*	*2*	*7*	*7*	*3.7*	*2.6*	*25*	*0*	*0.3*
GB-A	123	7	124	87	15	13	1958	523	811	16.2	78	203	89	9.2	3.2	60	11	3.2
GB-B	165	4	66	12	7	4	1195	153	671	16.7	129	269	114	9.7	3.8	83	19	2.7
GB-C	150	8	110	98	16	14	1891	523	782	16.2	75	190	85	8.7	3.2	59	10	3.2
GB-D	79	6	68	92	15	12	1570	559	852	16.1	81	201	85	9.1	3.2	61	14	3.2
GB-E	170	8	87	100	16	14	1810	515	801	16.4	73	186	80	8.5	3.2	58	12	3.2
GB-F	129	8	109	96	16	13	1938	528	765	15.6	75	184	81	8.6	3.2	58	12	3.2
GB-G	172	7	78	89	15	12	2022	531	872	17.9	79	195	84	9.2	3.3	60	11	3.3
GB-H	179	6	110	76	15	11	2262	541	880	18.9	75	203	82	8.6	3.2	59	13	3.8

Table 24. Trace element analyses. Standards are in gray.

8.3 U-Pb isotope analysis

Sample GB-A

	ppm				*Ratios*							*Discordance*			*Ages*				
Name	U	^{206}Pb	$^{206}Pb_c$(%)	206/204	$^{207}Pb/^{206}Pb$	1SE	$^{207}Pb/^{235}U$	1SE	$^{206}Pb/^{238}U$	1SE	Rho	Central (%)	Min rim (%)	207/206	1s	207/235	1s	206/238	1s
GB-A01	20	0.8	0.00E+00	486	0.04948	0.00135	0.30124	0.00889	0.04415	0.00050	0.381	64.4	28.2	459	34	286	4	265	2
GB-A02	54	2.3	0.00E+00	633	0.05383	0.00090	0.32847	0.00609	0.04426	0.00035	0.426	-23.8		377	22	284	3	273	2
GB-A04	16	0.8	0.00E+00	332	0.05406	0.00076	0.32705	0.00532	0.04388	0.00036	0.504	-26.4	-8.2	641	26	319	4	276	2
GB-A06	15	0.8	0.00E+00	315	0.05242	0.00071	0.32014	0.00523	0.04429	0.00040	0.551	-8.2		883	25	351	4	276	2
GB-A07	10	0.5	0.00E+00	397	0.05564	0.00096	0.34023	0.00665	0.04435	0.00040	0.464	-36.9	-20.2	330	22	288	3	283	2
GB-A08	14	0.7	0.00E+00	258	0.05880	0.00110	0.34978	0.00736	0.04314	0.00042	0.464	-52.4	-42.4	438	38	297	5	280	2
GB-A09	37	1.9	0.00E+00	753	0.05959	0.00070	0.35916	0.00518	0.04371	0.00036	0.575	-54.3	-49.3	304	31	282	4	279	2
GB-A10	9	0.4	0.00E+00	242	0.05586	0.00110	0.33649	0.00753	0.04369	0.00047	0.479	-39.1	-20.6	406	35	294	5	280	3
GB-A11	89	4.5	0.00E+00	1579	0.05643	0.00058	0.34661	0.00472	0.04455	0.00040	0.663	-41	-34.3	560	38	305	6	272	3
GB-A12	13	0.6	0.00E+00	221	0.05484	0.00087	0.33521	0.00622	0.04433	0.00043	0.524	-31.8	-14.4	374	29	292	4	282	3
GB-A13	38	1.9	0.00E+00	925	0.05303	0.00053	0.32765	0.00421	0.04481	0.00036	0.623	-14.8		421	25	313	4	299	2
GB-A15	47	2.4	0.00E+00	1371	0.05303	0.00060	0.32870	0.00455	0.04495	0.00036	0.573	-14.5		1119	68	394	12	282	2
GB-A16	16	0.8	0.00E+00	375	0.05593	0.00079	0.33696	0.00558	0.04370	0.00038	0.522	-39.5	-27.7	469	22	302	4	281	2
GB-A18	48	2.5	0.00E+00	1540	0.05441	0.00050	0.33966	0.00418	0.04527	0.00038	0.673	-27	-17.9	449	31	295	4	276	2
GB-A19	19	1	0.00E+00	342	0.05408	0.00072	0.33299	0.00538	0.04466	0.00041	0.57	-25.3	-8.8	468	29	309	5	288	3
GB-A20	17	0.9	0.00E+00	842	0.05639	0.00079	0.35523	0.00605	0.04569	0.00044	0.567	-39.3	-28.4	447	43	295	6	276	3
GB-A22	60	3	0.00E+00	18102	0.06106	0.00077	0.36882	0.00558	0.04381	0.00037	0.554	-58.1	-53.6	373	31	287	4	277	2
GB-A23	25	1.1	0.00E+00	474	0.05616	0.00088	0.32495	0.00584	0.04196	0.00037	0.486	-43.1	-30.7	589	25	312	4	276	2
GB-A24	87	4.1	0.00E+00	1741	0.05413	0.00053	0.32279	0.00392	0.04325	0.00032	0.600	-28.1	-17.5	388	19	297	3	285	2
GB-A25	29	1.4	0.00E+00	483	0.06847	0.00084	0.41266	0.00607	0.04371	0.00036	0.556	-70.2	-68.1	364	37	288	5	279	2
GB-A26	52	2.6	0.00E+00	2171	0.05521	0.00063	0.36082	0.00496	0.04740	0.00037	0.560	-29.7	-18.5	330	25	289	3	283	2
GB-A27	20	1	0.00E+00	173	0.07693	0.00262	0.47431	0.01671	0.04472	0.00039	0.249	-76.4	-72	171	60	267	7	279	3

Table 25

Sample GB-B

	ppm				*Ratios*							*Discordance*				*Ages*			
Name	U	^{206}Pb	$^{206}Pb_c$(%)	206/204	$^{207}Pb/^{206}Pb$	1SE	$^{207}Pb/^{235}U$	1SE	$^{206}Pb/^{238}U$	1SE	Rho	Central (%)	Min rim (%)	207/206	1s	207/235	1s	206/238	1s
GB-B01	43	2.1	0.00E+00	306	0.10276	0.003	0.66081	0.02057	0.04664	0.00051	0.351	-84.3	-82.8	1675	53	515	13	294	3
GB-B02	129	6.5	0.00E+00	2083	0.05337	0.00042	0.32821	0.01033	0.04461	0.00136	0.968	-18.7	-8.2	344	18	288	8	281	8
GB-B03	97	4.8	0.00E+00	1147	0.05476	0.00046	0.32965	0.0109	0.04366	0.0014	0.967	-32.2	-24.2	402	18	289	8	275	9
GB-B04	214	10.8	0.00E+00	5414	0.05382	0.00038	0.33103	0.01126	0.04461	0.00148	0.978	-23.1	-14.6	363	15	290	9	281	9
GB-B05	45	2.7	0.00E+00	296	0.10241	0.00358	0.78672	0.02994	0.05571	0.00084	0.397	-81.1	-79	1668	62	589	17	350	5
GB-B07	58	2.8	0.00E+00	327	0.08319	0.00148	0.52662	0.01069	0.04591	0.00045	0.481	-79	-77.5	1274	34	430	7	289	3
GB-B08	54	2.7	0.00E+00	441	0.07911	0.00172	0.51022	0.01225	0.04678	0.00047	0.42	-76.6	-74.2	1175	41	419	8	295	3
GB-B09	20	1	0.00E+00	582	0.05381	0.00055	0.33435	0.01373	0.04506	0.00179	0.969	-22.3	-9.5	363	22	293	10	284	11
GB-B10	67	3.1	0.00E+00	874	0.05795	0.00058	0.35411	0.00502	0.04432	0.00045	0.714	-48.1	-43	528	21	308	4	280	3
GB-B13	47	2.4	0.00E+00	832	0.06019	0.00112	0.3933	0.00855	0.04739	0.00054	0.522	-52.3	-43.6	610	39	337	6	298	3
GB-B14	72	3.3	0.00E+00	1183	0.05334	0.00041	0.31568	0.00421	0.04293	0.00047	0.818	-21.5	-12.1	343	17	279	3	271	3
GB-B15	134	6.8	0.00E+00	2904	0.06028	0.00083	0.39559	0.00636	0.04759	0.0004	0.518	-52.3	-46.3	614	29	338	5	300	2
GB-B17	88	4.1	0.00E+00	956	0.05877	0.00085	0.35263	0.00579	0.04352	0.00034	0.469	-51.9	-44.4	559	31	307	4	275	2
GB-B18	69	3.4	0.00E+00	748	0.06132	0.00076	0.38916	0.00657	0.04603	0.00053	0.679	-56.6	-52.4	650	26	334	5	290	3
GB-B20	58	2.7	0.00E+00	1075	0.05511	0.00056	0.33624	0.00509	0.04425	0.00049	0.737	-33.7	-25.1	417	22	294	4	279	3
GB-B21	85	3.9	0.00E+00	2960	0.05167	0.00042	0.30712	0.0043	0.04311	0.00049	0.809	0.4		271	18	272	3	272	3
GB-B22	35	1.6	0.00E+00	580	0.05354	0.00064	0.31962	0.00534	0.0433	0.0005	0.694	-22.8	-8	352	26	282	4	273	3
GB-B23	56	2.6	0.00E+00	5221	0.05451	0.00046	0.32818	0.00474	0.04366	0.00051	0.814	-30.4	-22.6	392	18	288	4	275	3
GB-B25	38	1.7	0.00E+00	847	0.06346	0.00241	0.38153	0.01504	0.0436	0.00045	0.263	-63.3	-48.9	724	77	328	11	275	3
GB-B26	34	1.6	0.00E+00	632	0.05386	0.00062	0.32589	0.00538	0.04388	0.00052	0.722	-24.8	-11.7	365	23	286	4	277	3
GB-B27	43	2	0.00E+00	1233	0.05728	0.00077	0.34523	0.0063	0.04371	0.00054	0.673	-46.1	-38.3	502	29	301	5	276	3

Table 26

Sample GB-C

	ppm				*Ratios*							*Discordance*			*Ages*				
Name	U	^{206}Pb	$^{206}Pb_c$(%)	206/204	$^{207}Pb/^{206}Pb$	1SE	$^{207}Pb/^{235}U$	1SE	$^{206}Pb/^{238}U$	1SE	Rho	Central (%)	Min rim (%)	207/206	1s	207/235	1s	206/238	1s
GB-C01	26	1.3	0.00E+00	310	0.06754	0.00083	0.42565	0.00714	0.04571	0.00052	0.682	-67.7	-65.4	854	24	360	5	288	3
GB-C02	27	1.1	0.00E+00	336	0.05383	0.00085	0.31711	0.00576	0.04273	0.00038	0.487	-26.4	-4.2	364	34	280	4	270	2
GB-C03	66	2.7	0.00E+00	1240	0.05052	0.00077	0.30411	0.00491	0.04366	0.00024	0.337	26.4	14.2	219	34	270	4	275	1
GB-C05	62	2.7	0.00E+00	1199	0.05344	0.0006	0.33636	0.00475	0.04565	0.00039	0.607	-17.6	-1.6	347	25	294	4	288	2
GB-C06	50	2.1	0.00E+00	1224	0.05255	0.00061	0.31485	0.00412	0.04346	0.00026	0.457	-11.6		309	26	278	3	274	2
GB-C07	55	2.4	0.00E+00	706	0.05919	0.00116	0.36027	0.00733	0.04415	0.00024	0.267	-52.6	-42	574	41	312	5	278	1
GB-C08	37	1.5	0.00E+00	700	0.05608	0.00072	0.33731	0.00477	0.04362	0.00026	0.423	-40.4	-30	456	28	295	4	275	2
GB-C09	36	1.6	0.00E+00	391	0.06372	0.00103	0.39496	0.00706	0.04495	0.00035	0.430	-62.6	-57.9	732	33	338	5	283	2
GB-C10	69	2.8	0.00E+00	5483	0.05166	0.00054	0.30734	0.00376	0.04315	0.00028	0.528	0.7		270	23	272	3	272	2
GB-C11	32	1.4	0.00E+00	1374	0.05249	0.00074	0.32687	0.0052	0.04517	0.00033	0.461	-7.3		307	31	287	4	285	2
GB-C12	49	2	0.00E+00	831	0.07121	0.0013	0.42161	0.00826	0.04294	0.00031	0.37	-73.4	-70.5	963	36	357	6	271	2
GB-C13	50	2.2	0.00E+00	1253	0.05716	0.0006	0.34712	0.00413	0.04404	0.00024	0.465	-45.1	-38.3	498	22	303	3	278	2
GB-C14	46	1.9	0.00E+00	4955	0.05207	0.0006	0.31039	0.00435	0.04324	0.00035	0.575	-5.5		288	26	274	3	273	2
GB-C15	54	2.4	0.00E+00	543	0.08722	0.00116	0.55912	0.00837	0.04649	0.00032	0.453	-80.3	-79.3	1365	24	451	5	293	2
GB-C16	33	1.4	0.00E+00	661	0.05824	0.00072	0.36222	0.00511	0.04511	0.0003	0.475	-48.3	-41.2	539	27	314	4	284	2
GB-C17	36	1.5	0.00E+00	935	0.05292	0.00085	0.3056	0.01556	0.04188	0.00202	0.949	-19.1		325	34	271	12	264	13
GB-C18	33	1.4	0.00E+00	483	0.06531	0.00087	0.40312	0.02096	0.04477	0.00225	0.967	-65.4	-61.9	784	27	344	15	282	14
GB-C19	51	2.2	0.00E+00	787	0.0536	0.00068	0.3254	0.00516	0.04403	0.00042	0.606	-22.1	-5	354	28	286	4	278	3
GB-C20	40	1.8	0.00E+00	498	0.06868	0.00095	0.43162	0.00659	0.04558	0.00029	0.419	-69.2	-66.5	889	27	364	5	287	2
GB-C21	45	2	0.00E+00	926	0.05459	0.00067	0.34735	0.00488	0.04615	0.00031	0.483	-27.1	-12.8	396	26	303	4	291	2
GB-C22	77	3.1	0.00E+00	889	0.05151	0.00062	0.29969	0.00475	0.0422	0.00044	0.652	1		264	26	266	4	266	3
GB-C23	45	1.9	0.00E+00	895	0.05155	0.0006	0.31249	0.00526	0.04396	0.00053	0.721	4.5		266	26	276	4	277	3
GB-C24	39	1.7	0.00E+00	755	0.06487	0.00135	0.39668	0.0089	0.04435	0.00037	0.373	-65	-59.3	770	44	339	6	280	2
GB-C25	47	2	0.00E+00	1586	0.0497	0.00062	0.30636	0.0053	0.04471	0.00054	0.696	56.9	26.7	181	27	271	4	282	3
GB-C26	38	1.6	0.00E+00	613	0.05319	0.00075	0.32915	0.00632	0.04488	0.00059	0.681	-16.3		337	30	289	5	283	4
GB-C27	48	2.2	0.00E+00	568	0.07505	0.00096	0.48245	0.00711	0.04662	0.00034	0.502	-74.2	-72.6	1070	25	400	5	294	2
GB-C28	38	1.6	0.00E+00	987	0.07051	0.00111	0.42726	0.00745	0.04395	0.00033	0.434	-72.1	-69.6	943	32	361	5	277	2
GB-C29	66	2.8	0.00E+00	1230	0.05221	0.00047	0.31535	0.00501	0.04381	0.00057	0.825	-6.3		295	20	278	4	276	4

Table 27

Sample GB-D

	ppm						*Ratios*					*Discordance*			*Ages*				
Name	U	^{206}Pb	$^{206}Pb_c$(%)	206/204	$^{207}Pb/^{206}Pb^*$	1SE	$^{207}Pb/^{235}U$	1SE	$^{206}Pb/^{238}U$	1SE	Rho	Central (%)	Min rim (%)	207/206	1s	207/235	1s	206/238	1s
GB-D01	41	1.8	0.00E+00	744	0.05229	0.00063	0.32146	0.00609	0.04459	0.00065	0.771	-5.8		298	27	283	5	281	4
GB-D02	72	3	0.00E+00	8746	0.05295	0.00054	0.31331	0.00556	0.04291	0.00063	0.822	-17.5	-3.3	327	22	277	4	271	4
GB-D03	47	2.2	0.00E+00	688	0.06155	0.00091	0.39909	0.00818	0.04702	0.00067	0.695	-56.3	-51.2	659	32	341	6	296	4
GB-D04	56	2.4	0.00E+00	1845	0.05177	0.00063	0.31482	0.0063	0.0441	0.0007	0.797	1.1		275	27	278	5	278	4
GB-D05	41	1.8	0.00E+00	536	0.0542	0.0007	0.33645	0.00738	0.04502	0.0008	0.81	-25.8	-11.5	379	28	294	6	284	5
GB-D06	61	2.6	0.00E+00	1577	0.0523	0.00053	0.31769	0.00489	0.04405	0.00051	0.755	-7.1		299	23	280	4	278	3
GB-D07	58	2.5	0.00E+00	797	0.05401	0.00095	0.32724	0.00807	0.04394	0.00076	0.703	-25.9	-4.6	372	39	287	6	277	5
GB-D08	33	1.4	0.00E+00	356	0.05234	0.00061	0.31618	0.00733	0.04381	0.00088	0.867	-8.1		300	25	279	6	276	5
GB-D10	40	1.8	0.00E+00	621	0.06315	0.00092	0.40187	0.00885	0.04616	0.00076	0.748	-60.6	-56.3	713	29	343	6	291	5
GB-D11	55	2.3	0.00E+00	724	0.05315	0.00059	0.32029	0.00553	0.04371	0.00058	0.764	-18.1	-2.8	335	25	282	4	276	4
GB-D13	112	4.7	0.00E+00	20975	0.05131	0.00038	0.30226	0.00455	0.04272	0.00056	0.870	6		255	16	268	4	270	3
GB-D14	72	3	0.00E+00	1531	0.05106	0.00053	0.30612	0.00528	0.04348	0.0006	0.800	12.9		244	23	271	4	274	4
GB-D15	42	1.8	0.00E+00	606	0.05989	0.00099	0.36322	0.0071	0.04399	0.00045	0.529	-54.9	-47.5	600	35	315	5	278	3
GB-D17	45	1.9	0.00E+00	659	0.06307	0.00092	0.38158	0.00695	0.04388	0.00048	0.597	-62.4	-58.3	711	30	328	5	277	3
GB-D18	40	1.8	0.00E+00	4124	0.05275	0.00068	0.32552	0.00563	0.04476	0.00051	0.662	-11.5		318	29	286	4	282	3
GB-D19	58	2.6	0.00E+00	986	0.0522	0.00064	0.33082	0.00515	0.04597	0.00044	0.621	-1.5		294	27	290	4	290	3
GB-D20	49	2.1	0.00E+00	792	0.05127	0.00057	0.31081	0.00558	0.04396	0.00062	0.785	9.8		253	24	275	4	277	4
GB-D21	39	1.8	0.00E+00	1315	0.05347	0.00034	0.33167	0.00243	0.044988	0.00016	0.477	-19.1	-10.4	349	15	291	2	284	1
GB-D22	41	2.1	0.00E+00	183	0.11308	0.0017	0.78264	0.01192	0.050195	0.00011	0.146	-84.9	-84.3	1850	26	587	7	316	1
GB-D24	43	2.1	0.00E+00	376	0.06886	0.0009	0.46	0.0061	0.04845	0.00013	0.195	-67.4	-64.8	895	27	384	4	305	1
GB-D25	38	1.8	0.00E+00	730	0.04957	0.00049	0.31053	0.00331	0.045434	0.00019	0.388	65.2	50.3	175	22	275	3	286	1
GB-D26	36	1.6	0.00E+00	442	0.05247	0.00046	0.31854	0.00437	0.044028	0.00047	0.773	-9.5		306	19	281	3	278	3
GB-D27	26	1.4	1.20E+01	81	0.11068	0.00818	0.6905	0.05192	0.045246	0.00063	0.184	-86	-82.3	1811	130	533	31	285	4

Table 28

Sample GB-E

	ppm						*Ratios*					*Discordance*			*Ages*				
Name	U	^{206}Pb	$^{206}Pb_c$(%)	206/204	$^{207}Pb/^{206}Pb$	1SE	$^{207}Pb/^{235}U$	1SE	$^{206}Pb/^{238}U$	1SE	Rho	Central (%)	Min rim (%)	207/206	1s	207/235	1s	206/238	1s
GB-E02	60	3.2	0.00E+00	2709	0.05479	0.00131	0.32666	0.00829	0.043244	0.00037	0.337	-33.1	-1.2	404	52	287	6	273	2
GB-E03	48	2.6	0.00E+00	620	0.05498	0.00132	0.32396	0.00813	0.042736	0.00031	0.293	-35.1	-5	411	52	285	6	270	2
GB-E04	16	0.9	0.00E+00	1519	0.06019	0.00212	0.36629	0.01338	0.04414	0.00043	0.264	-55.5	-35.4	610	72	317	10	278	3
GB-E05	34	1.9	0.00E+00	476	0.05527	0.00139	0.33479	0.00889	0.043933	0.00037	0.319	-35.2	-4.2	423	54	293	7	277	2
GB-E06	15	0.8	0.00E+00	321	0.06091	0.00194	0.36839	0.01239	0.043869	0.00047	0.317	-57.7	-42	636	66	318	9	277	3
GB-E07	30	2	0.00E+00	981	0.06201	0.0018	0.5	0.01395	0.053145	0.00052	0.319	-51.8	-37.4	674	58	380	10	334	3
GB-E08	15	0.9	0.00E+00	444	0.06359	0.00219	0.4	0.01371	0.044039	0.00038	0.245	-63.2	-50.7	728	71	332	10	278	2
GB-E09	14	0.8	0.00E+00	233	0.05955	0.00195	0.36825	0.01253	0.044852	0.0004	0.264	-53	-32.6	587	70	318	9	283	2
GB-E10	22	1.2	0.00E+00	1007	0.05232	0.00093	0.32274	0.0071	0.044737	0.00058	0.588	-5.9		300	41	284	5	282	4
GB-E11	28	1.4	0.00E+00	1098	0.05281	0.0009	0.3211	0.00678	0.044101	0.00055	0.591	-13.5		320	36	283	5	278	3
GB-E12	30	1.5	0.00E+00	886	0.05908	0.00112	0.36265	0.0082	0.044517	0.00054	0.540	-51.9	-42	570	40	314	6	281	3
GB-E13	56	3	0.00E+00	1202	0.05313	0.00086	0.34111	0.00695	0.046565	0.00058	0.611	-12.5		334	36	298	5	293	4
GB-E14	15	0.7	0.00E+00	337	0.06536	0.00158	0.3842	0.01047	0.042634	0.00054	0.464	-67.1	-61	786	47	330	8	269	3
GB-E15	19	1	0.00E+00	728	0.05339	0.00097	0.32928	0.00737	0.044735	0.00059	0.585	-18.7		345	39	289	6	282	4
GB-E16	22	1.1	0.00E+00	723	0.05283	0.00098	0.32013	0.007	0.04395	0.00051	0.534	-14		321	37	282	5	277	3
GB-E17	15	0.9	0.00E+00	1504	0.05651	0.0012	0.4	0.00984	0.050486	0.00067	0.533	-33.6	-13.4	472	45	337	7	318	4
GB-E18	20	1	0.00E+00	433	0.05251	0.00096	0.3	0.00695	0.043759	0.00053	0.551	-10.5		308	41	279	5	276	3
GB-E19	51	2.7	0.00E+00	1196	0.05269	0.00086	0.32618	0.00664	0.044896	0.00055	0.603	-10.5		316	36	287	5	283	3
GB-E20	18	0.9	0.00E+00	2037	0.05361	0.00098	0.33526	0.00748	0.045355	0.00058	0.575	-19.8		355	39	294	6	286	4
GB-E21	30	1.6	0.00E+00	1053	0.05243	0.00091	0.31658	0.00669	0.043789	0.00053	0.568	-9.4		304	39	279	5	276	3
GB-E22	64	3.3	0.00E+00	3175	0.05189	0.00084	0.31657	0.00644	0.044244	0.00054	0.602	-0.6		281	36	279	5	279	3
GB-E23	25	1.3	0.00E+00	763	0.05212	0.00098	0.32612	0.00726	0.04538	0.00054	0.531	-1.6		291	41	287	6	286	3
GB-E24	21	1.1	0.00E+00	338	0.05292	0.00103	0.32183	0.00727	0.04411	0.00051	0.513	-14.7		325	42	283	6	278	3
GB-E25	33	1.7	0.00E+00	877	0.05253	0.00093	0.3155	0.00668	0.043561	0.0005	0.542	-11.1		309	38	278	5	275	3
GB-E26	151	7.8	0.00E+00	3583	0.05225	0.00085	0.3	0.00609	0.043176	0.00047	0.558	-8.2		296	36	275	5	272	3
GB-E27	77	4	0.00E+00	1575	0.0522	0.00087	0.31688	0.00653	0.044026	0.00053	0.585	-5.7		294	35	280	5	278	3

Table 29

Sample GB-F

	ppm						*Ratios*					*Discordance*				*Ages*			
Name	U	^{206}Pb	$^{206}Pb_c$(%)	206/204	$^{207}Pb/^{206}Pb$	1SE	$^{207}Pb/^{235}U$	1SE	$^{206}Pb/^{238}U$	1SE	Rho	Central (%)	Min rim (%)	207/206	1s	207/235	1s	206/238	1s
GB-F02	15	0.8	0.00E+00	291	0.05412	0.00113	0.32537	0.00794	0.043607	0.00055	0.514	-27.4		376	46	286	6	275	3
GB-F03	22	1.1	0.00E+00	554	0.05973	0.00161	0.36417	0.01082	0.04422	0.00055	0.422	-54.2	-39.6	594	55	315	8	279	3
GB-F04	38	2	0.00E+00	888	0.05857	0.00114	0.35255	0.00798	0.04366	0.0005	0.508	-51.1	-40.1	551	41	307	6	275	3
GB-F05	19	1	0.00E+00	359	0.05288	0.00108	0.32497	0.00776	0.044573	0.00055	0.512	-13.4		324	43	286	6	281	3
GB-F06	20	1.1	0.00E+00	310	0.0938	0.00302	0.6099	0.02102	0.047159	0.00057	0.353	-82.1	-79.9	1504	59	483	13	297	4
GB-F07	42	2.2	0.00E+00	963	0.05524	0.00107	0.33879	0.00792	0.044478	0.00058	0.555	-34.3	-13.7	422	42	296	6	281	4
GB-F08	17	0.9	0.00E+00	1249	0.05859	0.00116	0.36684	0.00854	0.045408	0.00055	0.524	-49.2	-37.7	552	41	317	6	286	3
GB-F11	26	1.9	0.00E+00	53	0.27497	0.01556	2.33963	0.13661	0.061711	0.00089	0.247	-90.9	-90	3335	84	1224	42	386	5
GB-F12	23	1.2	0.00E+00	596	0.05311	0.00103	0.32421	0.00749	0.044273	0.00056	0.544	-16.6		334	46	285	6	279	3
GB-F13	21	1.2	0.00E+00	662	0.06511	0.00129	0.41748	0.00983	0.046507	0.00059	0.543	-63.7	-58.6	778	41	354	7	293	4
GB-F14	31	1.7	0.00E+00	1088	0.05539	0.00102	0.34311	0.00773	0.044927	0.00059	0.578	-34.5	-16.2	428	38	300	6	283	4
GB-F15	22	1.2	0.00E+00	734	0.05181	0.00092	0.31801	0.00692	0.044513	0.00056	0.58	1.3		277	41	280	5	281	3
GB-F16	35	2	0.00E+00	859	0.05259	0.00111	0.34569	0.00899	0.047673	0.00072	0.58	-3.6		311	47	301	7	300	4
GB-F17	37	2.1	0.00E+00	835	0.05482	0.00102	0.36256	0.00812	0.04797	0.0006	0.557	-26	-2.9	405	40	314	6	302	4
GB-F18	28	1.7	0.00E+00	2720	0.05377	0.001	0.38596	0.0102	0.052064	0.00098	0.713	-9.7		361	40	331	7	327	6
GB-F19	35	1.8	0.00E+00	768	0.05306	0.00094	0.31811	0.00678	0.04348	0.00051	0.550	-17.6		331	41	280	5	274	3
GB-F21	30	1.1	0.00E+00	424	0.05318	0.00159	0.32499	0.01064	0.044319	0.00059	0.405	-17.3		337	64	286	8	280	4
GB-F22	58	2.1	0.00E+00	1330	0.05429	0.00154	0.33255	0.01044	0.044425	0.0006	0.428	-27.4		383	60	292	8	280	4
GB-F23	46	1.9	0.00E+00	117	0.13506	0.00719	0.94564	0.05225	0.050782	0.00075	0.266	-87.3	-85.5	2165	90	676	27	319	5
GB-F24	100	3.7	0.00E+00	3746	0.05227	0.00147	0.31686	0.00983	0.04397	0.00057	0.420	-6.8		297	62	279	8	277	4
GB-F25	51	1.9	0.00E+00	703	0.05166	0.00151	0.32252	0.01035	0.045276	0.00061	0.416	5.6		271	68	284	8	285	4
GB-F26	45	1.7	0.00E+00	387	0.05834	0.00186	0.37129	0.01289	0.046159	0.00064	0.397	-47.4	-22.9	543	67	321	10	291	4
GB-F27	24	0.9	0.00E+00	373	0.05196	0.0017	0.32043	0.01136	0.044722	0.00061	0.386	-0.7		284	73	282	9	282	4
GB-F28	65	2.6	0.00E+00	477	0.07728	0.0024	0.5	0.01767	0.048742	0.00067	0.404	-74.5	-70.4	1128	59	425	12	307	4
GB-F29	716	26.2	0.00E+00	4416	0.05384	0.00149	0.3	0.01008	0.044211	0.00058	0.427	-24		364	59	288	8	279	4
GB-F30	32	1.2	0.00E+00	566	0.05373	0.00163	0.32129	0.01073	0.04337	0.0006	0.417	-24.4		360	65	283	8	274	4

Table 30

Sample GB-G

	ppm						*Ratios*					*Discordance*				*Ages*			
Name	U	^{206}Pb	$^{206}Pb_c$(%)	206/204	$^{207}Pb/^{206}Pb$	1SE	$^{207}Pb/^{235}U$	1SE	$^{206}Pb/^{238}U$	1SE	Rho	Central (%)	Min rim (%)	207/206	1s	207/235	1s	206/238	1s
GB-G01	35	1.3	0.00E+00	454	0.05509	0.00174	0.33958	0.0117	0.044705	0.00062	0.403	-32.9		416	68	297	9	282	4
GB-G02	38	1.4	0.00E+00	4574	0.05252	0.00167	0.32557	0.01136	0.044963	0.00065	0.414	-8.1		308	71	286	9	284	4
GB-G03	30	1.1	0.00E+00	2558	0.05253	0.00161	0.31756	0.01072	0.043848	0.00061	0.414	-10.5		308	68	280	8	277	4
GB-G04	34	1.3	0.00E+00	397	0.05991	0.00199	0.37123	0.01348	0.044944	0.00066	0.405	-53.9	-34.4	600	68	321	10	283	4
GB-G05	36	1.4	0.00E+00	220	0.10815	0.0067	0.70187	0.04489	0.047068	0.00075	0.25	-85.1	-81.8	1769	107	540	27	296	5
GB-G06	45	1.7	0.00E+00	1083	0.06047	0.00198	0.36625	0.01297	0.043928	0.0006	0.383	-56.5	-39.3	620	70	317	10	277	4
GB-G07	61	2.3	0.00E+00	5769	0.05548	0.00174	0.3	0.01167	0.044696	0.0006	0.396	-35.5		432	69	299	9	282	4
GB-G08	51	1.8	0.00E+00	1823	0.0515	0.00158	0.31099	0.01047	0.043799	0.0006	0.409	5.1		263	70	275	8	276	4
GB-G09	47	1.8	0.00E+00	627	0.05723	0.00215	0.35307	0.0142	0.044747	0.00065	0.361	-44.5	-5.8	500	83	307	11	282	4
GB-G10	76	2.8	0.00E+00	995	0.05424	0.00166	0.3365	0.01127	0.044999	0.00061	0.407	-26.1		381	68	295	9	284	4
GB-G11	47	1.8	0.00E+00	765	0.05999	0.002	0.38411	0.01396	0.046438	0.00068	0.402	-52.7	-32.7	603	71	330	10	293	4
GB-G12	29	1.1	0.00E+00	365	0.05302	0.00176	0.32856	0.01187	0.044945	0.00065	0.401	-14.3		330	72	288	9	283	4
GB-G13	47	1.8	0.00E+00	838	0.05632	0.00171	0.34617	0.01163	0.044576	0.00064	0.426	-40.4	-7.7	465	67	302	9	281	4
GB-G14	48	1.8	0.00E+00	728	0.05149	0.00166	0.31509	0.01111	0.044384	0.00063	0.403	6.7		263	71	278	9	280	4
GB-G15	44	1.7	0.00E+00	941	0.0584	0.00187	0.37591	0.01324	0.046684	0.00068	0.413	-47.1	-22.4	545	69	324	10	294	4
GB-G16	110	4	0.00E+00	2549	0.05207	0.00154	0.31372	0.01026	0.043694	0.00061	0.430	-4.6		289	65	277	8	276	4
GB-G17	279	9.9	0.00E+00	2528	0.05205	0.00151	0.30777	0.0099	0.042886	0.0006	0.434	-6		288	66	272	8	271	4
GB-G18	51	1.8	0.00E+00	564	0.05342	0.00167	0.31866	0.011	0.043261	0.00064	0.425	-21.7		347	72	281	8	273	4
GB-G19	56	2	0.00E+00	1191	0.05644	0.00173	0.33457	0.01131	0.042997	0.00061	0.419	-43.1	-11.8	470	69	293	9	271	4
GB-G20	48	1.8	0.00E+00	540	0.05394	0.00192	0.33177	0.01276	0.044612	0.00066	0.382	-24.1		368	76	291	10	281	4
GB-G21	36	1.3	0.00E+00	517	0.05175	0.00164	0.3172	0.0111	0.044456	0.00065	0.419	2.3		274	72	280	9	280	4
GB-G22	50	1.9	0.00E+00	669	0.05435	0.0016	0.33301	0.01096	0.044435	0.00065	0.443	-27.9		386	62	292	8	280	4
GB-G23	32	1.2	0.00E+00	360	0.05391	0.00174	0.32938	0.01163	0.044314	0.00064	0.409	-24.4		367	71	289	9	280	4
GB-G24	49	1.8	0.00E+00	1472	0.05352	0.00161	0.32829	0.01092	0.044484	0.00063	0.426	-20.5		351	66	288	8	281	4
GB-G25	64	2.4	0.00E+00	1590	0.0532	0.00164	0.32978	0.0113	0.044957	0.00068	0.438	-16.3		337	72	289	9	283	4
GB-G26	82	3.2	0.00E+00	1429	0.0532	0.00153	0.34988	0.0113	0.047698	0.0007	0.455	-11.2		337	64	305	9	300	4
GB-G27	49	1.8	0.00E+00	683	0.06168	0.00192	0.3754	0.0129	0.044141	0.00065	0.428	-59.3	-45.8	663	65	324	10	278	4
GB-G28	59	2.2	0.00E+00	1087	0.05494	0.00175	0.33461	0.01177	0.044173	0.00065	0.420	-32.7		410	70	293	9	279	4

Table 31

Sample GB-H

	ppm						*Ratios*					*Discordance*				*Ages*			
Name	U	^{206}Pb	$^{206}Pb_c$(%)	206/204	$^{207}Pb/^{206}Pb$	1SE	$^{207}Pb/^{235}U$	1SE	$^{206}Pb/^{238}U$	1SE	Rho	Central (%)	Min rim (%)	207/206	1s	207/235	1s	206/238	1s
GB-H01	69	3.5	0.00E+00	1082	0.05444	0.00085	0.34887	0.00731	0.04648	0.00065	0.664	-25.3	-7.2	389	33	304	6	293	4
GB-H02	28	1.3	0.00E+00	521	0.05945	0.00121	0.36236	0.00886	0.044208	0.0006	0.559	-53.3	-43.5	584	42	314	7	279	4
GB-H03	53	2.5	0.00E+00	970	0.05346	0.00084	0.32569	0.00678	0.044189	0.0006	0.654	-20.4		348	35	286	5	279	4
GB-H04	34	1.6	0.00E+00	490	0.05725	0.00099	0.34768	0.0075	0.044047	0.00057	0.595	-45.5	-34.2	501	37	303	6	278	3
GB-H05	33	1.6	0.00E+00	557	0.05709	0.00108	0.35101	0.00829	0.044592	0.00063	0.595	-44.1	-30.9	495	40	305	6	281	4
GB-H06	33	1.7	0.00E+00	397	0.05845	0.00137	0.37639	0.01016	0.046703	0.00063	0.501	-47.2	-32.1	547	50	324	7	294	4
GB-H07	35	2.2	0.00E+00	96	0.19572	0.01107	1.50977	0.08955	0.055947	0.001	0.301	-89.7	-88.5	2791	88	934	36	351	6
GB-H08	19	0.9	0.00E+00	503	0.05259	0.00103	0.3	0.00757	0.043594	0.00061	0.581	-11.9		311	42	279	6	275	4
GB-H09	26	1.2	0.00E+00	493	0.05375	0.00103	0.3	0.00768	0.043479	0.00061	0.591	-24.4		361	41	284	6	274	4
GB-H10	22	1.1	0.00E+00	313	0.06664	0.00209	0.41089	0.01408	0.044718	0.00061	0.401	-67.3	-59.2	827	61	350	10	282	4
GB-H11	36	2.1	0.00E+00	78	0.19193	0.00768	1.39332	0.06026	0.052652	0.00086	0.378	-90.1	-89.4	2759	63	886	26	331	5
GB-H12	22	1	0.00E+00	467	0.0525	0.00099	0.31195	0.00744	0.043091	0.00063	0.609	-11.8		307	43	276	6	272	4
GB-H13	28	1.4	0.00E+00	269	0.09882	0.00268	0.61013	0.01861	0.04478	0.00063	0.459	-84.1	-82.7	1602	49	484	12	282	4
GB-H14	32	1.6	0.00E+00	501	0.05589	0.00097	0.34949	0.00855	0.045355	0.00079	0.708	-37	-22.9	448	36	304	6	286	5
GB-H15	20	1	0.00E+00	294	0.05305	0.00103	0.32072	0.00792	0.043848	0.00067	0.623	-16.7		331	45	282	6	277	4
GB-H16	16	0.8	0.00E+00	203	0.05303	0.00107	0.31932	0.0079	0.043674	0.00062	0.577	-16.8		330	44	281	6	276	4
GB-H17	70	3.5	0.00E+00	1033	0.05545	0.00084	0.4	0.00726	0.046322	0.00064	0.674	-32.9	-19.4	430	32	308	5	292	4
GB-H18	35	1.8	0.00E+00	118	0.13617	0.0059	0.89828	0.04173	0.047844	0.0008	0.36	-88.1	-86.8	2179	70	651	22	301	5
GB-H19	59	2.9	0.00E+00	483	0.06861	0.0015	0.42814	0.01132	0.045257	0.00067	0.559	-69.3	-65.2	887	45	362	8	285	4
GB-H20	29	1.4	0.00E+00	375	0.05793	0.00116	0.34759	0.00836	0.043518	0.00059	0.559	-48.9	-36.8	527	43	303	6	275	4
GB-H21	27	1.3	0.00E+00	433	0.07408	0.00167	0.4602	0.01257	0.045055	0.0007	0.566	-74.4	-71.5	1044	44	384	9	284	4
GB-H22	24	1.2	0.00E+00	386	0.05546	0.0011	0.32879	0.00815	0.042998	0.00064	0.599	-37.8	-18.8	431	44	289	6	271	4
GB-H25	30	1.5	0.00E+00	1268	0.0623	0.00131	0.38412	0.01013	0.044721	0.00071	0.601	-60.1	-53.1	684	43	330	7	282	4
GB-H26	19	1.2	0.00E+00	1591	0.0723	0.00616	0.58539	0.05109	0.05872	0.00111	0.217	-64.8	-33	995	172	468	33	368	7
GB-H28	39	1.9	0.00E+00	516	0.05562	0.00099	0.33185	0.00782	0.043273	0.00067	0.654	-38.3	-23.1	437	39	291	6	273	4
GB-H29	41	1.9	0.00E+00	406	0.05523	0.00111	0.32574	0.00817	0.042772	0.00064	0.598	-36.7	-16.5	422	44	286	6	270	4

Table 32

Mud Tank (run as unknown)

	ppm						*Ratios*						*Discordance*		*Ages*				
Name	U	^{206}Pb	$^{206}Pb_c$(%)	206/204	$^{207}Pb/^{206}Pb$	1SE	$^{207}Pb/^{235}U$	1SE	$^{206}Pb/^{238}U$	1SE	Rho	Central (%)	Min rim (%)	207/206	1s	207/235	1s	206/238	1s
MT-01	16	1.6	0.00E+00	1165	0.06282	0.00195	1.04574	0.03669	0.120735	0.00199	0.470	4.9		702	62	727	18	735	11
MT-02	16	1.6	0.00E+00	1134	0.06374	0.00198	1.05294	0.03751	0.119819	0.00209	0.490	-0.5		733	62	730	19	730	12
MT-03	12	1.2	0.00E+00	1433	0.0635	0.00212	1.0307	0.03898	0.117727	0.00208	0.467	-1.1		725	70	719	19	717	12
MT-04	13	1.3	0.00E+00	483	0.06395	0.0021	1.0376	0.03899	0.11767	0.00215	0.486	-3.3		740	67	723	19	717	12
MT-05	14	1.3	0.00E+00	480	0.06579	0.00214	1.06311	0.03927	0.117196	0.00205	0.473	-11.3		800	65	735	19	714	12
MT-06	14	1.4	0.00E+00	602	0.06447	0.00212	1.03444	0.03853	0.116364	0.00204	0.471	-6.6		757	67	721	19	710	12
MT-101	9	1.2	0.00E+00	550	0.06494	0.00118	1.06136	0.02618	0.11853	0.00198	0.677	-6.9		772	37	734	13	722	11
MT-102	10	1.3	0.00E+00	494	0.06309	0.00115	1.02079	0.02485	0.117348	0.00188	0.659	0.6		711	37	714	12	715	11
MT-103	10	1.2	0.00E+00	503	0.06336	0.00106	1.03395	0.02494	0.118358	0.00206	0.72	0.1		720	34	721	12	721	12
MT-104	10	1.3	0.00E+00	656	0.06497	0.00112	1.04414	0.02527	0.116561	0.00197	0.699	-8.5		773	34	726	13	711	11
MT-105	10	1.3	0.00E+00	703	0.06492	0.00112	1.0416	0.02609	0.116363	0.0021	0.722	-8.5		772	35	725	13	710	12
MT-106	11	1.4	0.00E+00	1229	0.06465	0.00115	1.03142	0.02663	0.115716	0.00217	0.727	-7.9		763	36	720	13	706	13
MT-107	10	1.3	0.00E+00	601	0.06544	0.00115	1.04958	0.02641	0.116321	0.0021	0.718	-10.6	-0.1	789	36	729	13	709	12
MT-01	12	1.3	0.00E+00	774	0.06409	0.00079	1.03368	0.01653	0.11698	0.00119	0.635	-4.5		745	26	721	8	713	7
MT-02	11	1.3	0.00E+00	470	0.06384	0.00087	1.04246	0.01787	0.11844	0.00124	0.609	-2.1		736	29	725	9	722	7
MT-03	12	1.4	0.00E+00	484	0.06581	0.00074	1.07586	0.01882	0.11858	0.0016	0.769	-10.3	-3.8	800	22	742	9	722	9
MT-04	13	1.5	0.00E+00	491	0.06341	0.00058	1.03231	0.01679	0.11807	0.00159	0.827	-0.4		722	19	720	8	719	9
MT-05	13	1.5	0.00E+00	5974	0.06352	0.00078	1.0296	0.019	0.11755	0.00162	0.746	-1.4		726	25	719	10	716	9
MT-06	13	1.5	0.00E+00	411	0.06459	0.00081	1.03579	0.01822	0.11631	0.00143	0.699	-7.2		761	25	722	9	709	8
MT-01	15	2.1	0.00E+00	1057	0.06404	0.00068	1.03957	0.01536	0.11774	0.00121	0.694	-3.6		743	22	724	8	718	7
MT-02	15	2	0.00E+00	11203	0.06349	0.0007	1.04682	0.01541	0.11958	0.00116	0.661	0.5		725	23	727	8	728	7

Table 33

Mud Tank (run as unknown) continued

	ppm				*Ratios*									*Discordance*				*Ages*			
Name	U	^{206}Pb	$^{206}Pb_c$(%)	206/204	$^{207}Pb/^{206}Pb$	1SE	$^{207}Pb/^{235}U$	1SE	$^{206}Pb/^{238}U$	1SE	Rho	Central (%)	Min rim (%)	207/206	1s	207/235	1s	206/238	1s
MT-03	14	1.9	0.00E+00	1869	0.06349	0.00075	1.05112	0.0164	0.12008	0.00122	0.651	0.9		725	24	729	8	731	7
MT-04	15	2	0.00E+00	1747	0.06334	0.0007	1.04326	0.01555	0.11945	0.0012	0.675	1.1		720	22	726	8	727	7
MT-101	19	2.5	0.00E+00	1874	0.0636	0.00061	1.03294	0.02438	0.11778	0.00254	0.915	-1.6		729	19	720	12	718	15
MT-103	16	2	0.00E+00	700	0.06447	0.00097	1.05365	0.02041	0.11854	0.00144	0.625	-4.9		757	31	731	10	722	8
MT-105	14	1.7	0.00E+00	1072	0.06506	0.00092	1.06417	0.0202	0.11864	0.0015	0.668	-7.3		776	29	736	10	723	9
MT-106	15	1.9	0.00E+00	968	0.06413	0.00085	1.059	0.01871	0.11976	0.0014	0.662	-2.4		746	27	733	9	729	8
MT-101	20	2.5	0.00E+00	1907	0.0636	0.0007	1.03162	0.01667	0.11764	0.00138	0.728	-1.7		728	23	720	8	717	8
MT-106	15	1.9	0.00E+00	1134	0.06377	0.00068	1.05622	0.01757	0.12013	0.00154	0.768	-0.4		734	22	732	9	731	9
MT-105	14	1.8	0.00E+00	1125	0.06461	0.00074	1.05976	0.01869	0.11896	0.0016	0.761	-5.2		762	23	734	9	725	9
MT-103	16	2	0.00E+00	728	0.06421	0.00079	1.0478	0.01863	0.11835	0.00152	0.722	-3.9		749	25	728	9	721	9
MT-107	18	2.2	0.00E+00	2170	0.06431	0.0007	1.05337	0.01587	0.1188	0.00123	0.686	-4		752	23	731	8	724	7
MT-107	18	2.2	0.00E+00	1924	0.06408	0.00069	1.05023	0.01557	0.118861	0.00122	0.69	-2.9		744	23	729	8	724	7
MT-101	20	2.6	0.00E+00	1982	0.0637	0.00068	1.03226	0.01469	0.117537	0.00111	0.665	-2.2		732	23	720	7	716	6
MT-103	16	2	0.00E+00	691	0.06449	0.00077	1.05102	0.01622	0.118206	0.00116	0.635	-5.2		758	23	729	8	720	7
MT-105	14	1.8	0.00E+00	1137	0.0651	0.00073	1.06618	0.01624	0.118774	0.00123	0.682	-7.4	-0.7	778	22	737	8	724	7
MT-106	15	2	0.00E+00	919	0.06419	0.00066	1.05926	0.01477	0.119676	0.00113	0.679	-2.7		748	20	733	7	729	7
MT-101	12	1.4	0.00E+00	627	0.06369	0.00075	1.04424	0.0214	0.118914	0.002	0.820	-1		731	24	726	11	724	12
MT-102	12	1.4	0.00E+00	447	0.06267	0.00081	1.04988	0.02443	0.121497	0.00235	0.833	6.4		697	26	729	12	739	14
MT-103	6	0.9	0.00E+00	599	0.06288	0.00621	1.01822	0.10289	0.117448	0.00251	0.211	1.8		704	205	713	52	716	14
MT-104	6	0.9	0.00E+00	629	0.06101	0.00604	0.9743	0.09854	0.115816	0.00239	0.204	11		640	209	691	51	706	14
MT-105	6	0.9	0.00E+00	524	0.06468	0.00162	1.02103	0.0293	0.114482	0.00162	0.492	-9		764	49	714	15	699	9
MT-201	7	0.9	0.00E+00	902	0.06597	0.00127	1.08779	0.02685	0.119597	0.00184	0.623	-10.1		805	39	747	13	728	11
MT-202	7	1	0.00E+00	1364	0.06453	0.00124	1.06865	0.0275	0.120108	0.00205	0.663	-3.9		759	38	738	13	731	12
MT-203	8	1.2	0.00E+00	2312	0.06448	0.00126	1.05568	0.02552	0.118741	0.0017	0.592	-4.8		757	39	732	13	723	10
MT-204	8	1.1	0.00E+00	968	0.06573	0.00137	1.0693	0.02773	0.117992	0.00181	0.591	-10.4		798	43	738	14	719	10
MT-01	11	1.4	0.00E+00	426	0.06334	0.00035	1.06146	0.0087	0.121535	0.00074	0.746	2.9		720	11	735	4	739	4
MT-02	11	1.4	0.00E+00	426	0.06334	0.00035	1.06146	0.0087	0.121535	0.00074	0.746	2.9		720	11	735	4	739	4
MT-03	7	1.2	0.00E+00	569	0.06409	0.00056	1.06637	0.03969	0.120682	0.00437	0.972	-1.4		744	19	737	20	734	25
MT-04	7	1.2	0.00E+00	380	0.06423	0.00055	1.1	0.04094	0.121635	0.0045	0.974	-1.3		749	18	742	20	740	26

Table 34

8.4 Lu-Hf isotope analysis

Name	$^{176}Hf/^{177}Hf$	1SE	$^{178}Hf/^{177}Hf$	1SE	Fract	1SE	$^{176}Yb/^{177}Hf$	1SE	$^{176}Lu/^{177}Hf$	1SE	Hf	1SE	Yb	1SE	Lu	1SE	Yb Fract	1SE
A04	0.282689	0.000014	1.46730	0.00005	-1.24	0.01	0.0308	0.0014	0.0007	0.0000	1.28	0.03	0.055	0.003	0.006	0.000	-1.36	0.08
A05	0.282637	0.000016	1.46720	0.00004	-1.24	0.01	0.0376	0.0021	0.0007	0.0000	1.36	0.04	0.075	0.006	0.007	0.000	-1.34	0.06
A06	0.282645	0.000019	1.46727	0.00005	-1.23	0.00	0.0501	0.0013	0.0010	0.0000	1.20	0.02	0.085	0.003	0.009	0.000	-1.33	0.04
A07	0.282707	0.000018	1.46733	0.00004	-1.24	0.00	0.0345	0.0008	0.0008	0.0000	1.22	0.01	0.059	0.001	0.007	0.000	-1.49	0.06
A08	0.282680	0.000014	1.46724	0.00004	-1.23	0.00	0.0506	0.0007	0.0011	0.0000	1.22	0.01	0.086	0.001	0.009	0.000	-1.45	0.04
A09	0.282647	0.000015	1.46733	0.00004	-1.24	0.00	0.0328	0.0006	0.0007	0.0000	1.38	0.02	0.061	0.001	0.007	0.000	-1.35	0.07
A10	0.282614	0.000018	1.46723	0.00004	-1.23	0.00	0.0526	0.0004	0.0011	0.0000	1.21	0.01	0.089	0.001	0.010	0.000	-1.27	0.05
A11	0.282712	0.000017	1.46727	0.00003	-1.25	0.01	0.0410	0.0013	0.0009	0.0000	1.30	0.02	0.074	0.002	0.008	0.000	-1.27	0.06
A12	0.282687	0.000014	1.46726	0.00005	-1.23	0.00	0.0335	0.0001	0.0007	0.0000	1.42	0.01	0.067	0.000	0.007	0.000	-1.50	0.06
A13	0.282690	0.000016	1.46726	0.00004	-1.24	0.00	0.0382	0.0016	0.0008	0.0000	1.61	0.02	0.081	0.004	0.009	0.000	-1.44	0.05
A15	0.282651	0.000020	1.46720	0.00004	-1.44	0.01	0.0293	0.0008	0.0009	0.0000	1.40	0.11	0.056	0.004	0.008	0.000	-1.41	0.07
A16	0.282621	0.000012	1.46720	0.00003	-1.43	0.00	0.0332	0.0007	0.0008	0.0000	1.64	0.02	0.075	0.002	0.009	0.000	-1.38	0.08
A17	0.282614	0.000023	1.46731	0.00005	-1.43	0.00	0.0279	0.0005	0.0007	0.0000	1.66	0.06	0.064	0.001	0.008	0.000	-1.30	0.10
A19	0.282628	0.000020	1.46730	0.00003	-1.41	0.00	0.0326	0.0010	0.0010	0.0001	1.69	0.12	0.073	0.003	0.011	0.000	-1.59	0.06
A22	0.282626	0.000013	1.46727	0.00004	-1.43	0.00	0.0287	0.0007	0.0007	0.0000	1.80	0.04	0.072	0.003	0.009	0.000	-1.66	0.07
A23	0.282681	0.000013	1.46722	0.00003	-1.44	0.00	0.0252	0.0003	0.0006	0.0000	1.85	0.02	0.063	0.001	0.008	0.000	-1.52	0.05
A24	0.282620	0.000010	1.46732	0.00004	-1.44	0.00	0.0276	0.0007	0.0007	0.0000	1.74	0.05	0.066	0.001	0.009	0.000	-1.40	0.06
A25	0.282617	0.000021	1.46732	0.00009	-1.44	0.01	0.0359	0.0009	0.0011	0.0001	1.35	0.11	0.066	0.004	0.010	0.001	-1.40	0.12
A26	0.282635	0.000018	1.46724	0.00003	-1.46	0.01	0.0375	0.0014	0.0011	0.0001	1.50	0.11	0.075	0.005	0.010	0.001	-1.24	0.07
A27	0.282644	0.000010	1.46730	0.00003	-1.44	0.00	0.0281	0.0006	0.0007	0.0000	1.83	0.03	0.071	0.002	0.009	0.000	-1.56	0.05
B01	0.282636	0.000052	1.46726	0.00008	-1.37	0.02	0.0557	0.0009	0.0020	0.0000	0.97	0.03	0.074	0.003	0.014	0.001	-1.25	0.14
B02	0.282659	0.000014	1.46723	0.00003	-1.43	0.00	0.0426	0.0008	0.0011	0.0000	2.32	0.05	0.136	0.002	0.018	0.001	-1.55	0.03
B03	0.282651	0.000019	1.46710	0.00006	-1.44	0.01	0.0739	0.0013	0.0023	0.0001	1.23	0.12	0.125	0.012	0.019	0.001	-1.49	0.04
B04	0.282606	0.000028	1.46710	0.00007	-1.44	0.01	0.0738	0.0010	0.0025	0.0001	1.83	0.09	0.185	0.009	0.031	0.002	-1.55	0.06
B08	0.282608	0.000010	1.46722	0.00003	-1.44	0.00	0.0598	0.0020	0.0017	0.0001	1.90	0.06	0.154	0.002	0.021	0.000	-1.57	0.02
B09	0.282617	0.000015	1.46723	0.00004	-1.45	0.00	0.0215	0.0007	0.0006	0.0000	1.96	0.01	0.058	0.002	0.008	0.000	-1.24	0.06
B10	0.282683	0.000015	1.46716	0.00006	-1.43	0.00	0.0641	0.0024	0.0017	0.0001	1.61	0.10	0.140	0.005	0.018	0.001	-1.62	0.04

Table 35

Name	176Hf/177Hf	1SE	178Hf/177Hf	1SE	Fract	1SE	176Yb/177Hf	1SE	176Lu/177Hf	1SE	Hf	1SE	Yb	1SE	Lu	1SE	Yb Fract	1SE
B17	0.282598	0.000019	1.46721	0.00005	-1.43	0.00	0.0748	0.0036	0.0026	0.0001	1.88	0.10	0.190	0.007	0.033	0.001	-1.48	0.03
B20	0.282577	0.000010	1.46713	0.00003	-1.44	0.00	0.0681	0.0034	0.0020	0.0002	1.84	0.05	0.166	0.004	0.023	0.001	-1.48	0.02
B21	0.282613	0.000014	1.46731	0.00005	-1.45	0.00	0.0417	0.0025	0.0010	0.0000	1.75	0.07	0.100	0.009	0.013	0.001	-1.71	0.04
B22	0.282633	0.000013	1.46722	0.00003	-1.44	0.00	0.0410	0.0006	0.0011	0.0000	1.81	0.02	0.101	0.001	0.014	0.000	-1.49	0.04
B23	0.282625	0.000011	1.46724	0.00003	-1.45	0.00	0.0516	0.0007	0.0013	0.0000	1.79	0.01	0.128	0.002	0.016	0.000	-1.48	0.03
B25	0.282612	0.000013	1.46727	0.00003	-1.45	0.00	0.0838	0.0067	0.0020	0.0002	1.87	0.03	0.210	0.014	0.026	0.002	-1.55	0.03
B26	0.282607	0.000016	1.46712	0.00005	-1.44	0.00	0.0568	0.0016	0.0017	0.0001	1.76	0.07	0.133	0.003	0.020	0.000	-1.41	0.03
B27	0.282621	0.000013	1.46724	0.00003	-1.44	0.00	0.0442	0.0005	0.0011	0.0000	2.12	0.02	0.129	0.002	0.017	0.000	-1.57	0.04
C02	0.282693	0.000033	1.46725	0.00007	-1.35	0.01	0.0432	0.0018	0.0014	0.0001	0.94	0.10	0.050	0.003	0.008	0.001	-1.37	0.05
C03	0.282602	0.000013	1.46725	0.00003	-1.35	0.00	0.0475	0.0007	0.0011	0.0000	1.77	0.01	0.117	0.002	0.014	0.000	-1.46	0.03
C04	0.282598	0.000014	1.46722	0.00005	-1.33	0.00	0.0378	0.0011	0.0011	0.0001	2.07	0.10	0.103	0.004	0.014	0.001	-1.38	0.05
C06	0.282635	0.000013	1.46720	0.00005	-1.33	0.00	0.0458	0.0011	0.0013	0.0001	1.55	0.10	0.097	0.004	0.013	0.001	-1.35	0.04
C07	0.282589	0.000010	1.46726	0.00003	-1.35	0.01	0.0484	0.0008	0.0017	0.0000	1.45	0.05	0.099	0.004	0.017	0.001	-1.48	0.04
C08	0.282589	0.000022	1.46722	0.00005	-1.33	0.00	0.0317	0.0007	0.0009	0.0000	2.04	0.07	0.090	0.001	0.013	0.000	-1.34	0.05
C09	0.282604	0.000014	1.46720	0.00006	-1.32	0.00	0.0447	0.0013	0.0012	0.0001	1.69	0.11	0.103	0.005	0.014	0.001	-1.59	0.05
C10	0.282622	0.000010	1.46731	0.00003	-1.35	0.00	0.0315	0.0011	0.0008	0.0000	2.16	0.03	0.093	0.004	0.012	0.000	-1.54	0.05
C11	0.282657	0.000016	1.46719	0.00004	-1.35	0.01	0.0297	0.0011	0.0007	0.0000	2.00	0.05	0.079	0.003	0.010	0.000	-1.50	0.05
C12	0.282629	0.000012	1.46732	0.00003	-1.34	0.00	0.0342	0.0009	0.0010	0.0000	2.03	0.03	0.095	0.002	0.013	0.000	-1.56	0.05
C13	0.282660	0.000032	1.46725	0.00009	-1.32	0.01	0.0485	0.0012	0.0011	0.0000	1.68	0.09	0.115	0.005	0.013	0.001	-1.41	0.06
C14	0.282613	0.000016	1.46724	0.00005	-1.33	0.01	0.0445	0.0012	0.0011	0.0001	1.65	0.07	0.098	0.003	0.012	0.000	-1.36	0.04
C15	0.282627	0.000015	1.46737	0.00003	-1.34	0.00	0.0365	0.0004	0.0009	0.0000	1.53	0.01	0.076	0.001	0.009	0.000	-1.25	0.04
C16	0.282727	0.000019	1.46740	0.00006	-1.32	0.01	0.0471	0.0021	0.0015	0.0001	1.22	0.12	0.072	0.004	0.011	0.000	-1.40	0.05
C17	0.282602	0.000019	1.46717	0.00005	-1.34	0.01	0.0283	0.0016	0.0008	0.0000	1.55	0.08	0.059	0.004	0.008	0.000	-1.62	0.07
C18	0.282572	0.000028	1.46718	0.00004	-1.33	0.01	0.0390	0.0011	0.0014	0.0000	1.16	0.07	0.060	0.003	0.011	0.001	-1.60	0.06
C20	0.282545	0.000021	1.46732	0.00006	-1.34	0.00	0.0550	0.0007	0.0019	0.0000	1.13	0.01	0.087	0.001	0.015	0.000	-1.39	0.08
C22	0.282639	0.000016	1.46726	0.00004	-1.32	0.00	0.0437	0.0007	0.0012	0.0000	2.13	0.05	0.128	0.003	0.018	0.000	-1.44	0.04
C23	0.282651	0.000016	1.46722	0.00004	-1.31	0.00	0.0412	0.0010	0.0013	0.0001	1.35	0.09	0.076	0.003	0.013	0.000	-1.34	0.04
C25	0.282620	0.000014	1.46728	0.00003	-1.36	0.00	0.0394	0.0005	0.0013	0.0000	1.43	0.06	0.076	0.002	0.013	0.000	-1.57	0.05
C26	0.282574	0.000039	1.46720	0.00008	-1.32	0.01	0.0368	0.0008	0.0011	0.0000	1.72	0.08	0.085	0.003	0.012	0.001	-1.20	0.11

Table 36

Name	176Hf/177Hf	1SE	178Hf/177Hf	1SE	Fract	1SE	176Yb/177Hf	1SE	176Lu/177Hf	1SE	Hf	1SE	Yb	1SE	Lu	1SE	Yb Fract	1SE
C28	0.282649	0.000013	1.46726	0.00004	-1.34	0.00	0.0448	0.0013	0.0012	0.0001	1.42	0.10	0.088	0.003	0.011	0.000	-1.31	0.04
D01	0.282632	0.000024	1.46711	0.00005	-1.32	0.01	0.0491	0.0009	0.0011	0.0000	1.66	0.05	0.112	0.002	0.013	0.000	-1.38	0.06
D02	0.282628	0.000015	1.46723	0.00003	-1.33	0.00	0.0346	0.0008	0.0010	0.0000	2.05	0.08	0.097	0.002	0.014	0.000	-1.49	0.04
D03	0.282623	0.000041	1.46735	0.00008	-1.32	0.01	0.0429	0.0020	0.0014	0.0001	1.52	0.10	0.091	0.004	0.015	0.001	-1.37	0.07
D04	0.282615	0.000013	1.46722	0.00005	-1.32	0.00	0.0308	0.0015	0.0010	0.0001	1.88	0.08	0.077	0.001	0.012	0.001	-1.35	0.05
D05	0.282632	0.000014	1.46722	0.00005	-1.32	0.00	0.0325	0.0019	0.0008	0.0000	1.93	0.08	0.084	0.006	0.011	0.000	-1.33	0.05
D06	0.282675	0.000010	1.46713	0.00005	-1.32	0.00	0.0320	0.0015	0.0008	0.0000	1.89	0.06	0.079	0.005	0.010	0.000	-1.63	0.06
D07	0.282624	0.000018	1.46725	0.00008	-1.35	0.00	0.0313	0.0012	0.0008	0.0001	1.92	0.10	0.082	0.003	0.011	0.001	-1.34	0.06
D08	0.282659	0.000015	1.46719	0.00003	-1.35	0.00	0.0320	0.0003	0.0009	0.0000	2.24	0.05	0.099	0.003	0.014	0.000	-1.46	0.04
D10	0.282619	0.000012	1.46730	0.00006	-1.35	0.00	0.0343	0.0009	0.0010	0.0001	1.73	0.11	0.083	0.003	0.011	0.000	-1.49	0.05
D11	0.282624	0.000020	1.46728	0.00007	-1.34	0.01	0.0377	0.0007	0.0013	0.0000	2.09	0.12	0.109	0.004	0.018	0.001	-1.32	0.08
D13	0.282597	0.000018	1.46730	0.00004	-1.34	0.00	0.0400	0.0016	0.0013	0.0001	2.10	0.14	0.112	0.004	0.018	0.001	-1.35	0.05
D14	0.282685	0.000014	1.46721	0.00004	-1.35	0.00	0.0472	0.0017	0.0015	0.0001	1.84	0.12	0.117	0.006	0.019	0.001	-1.59	0.04
D15	0.282596	0.000012	1.46716	0.00004	-1.36	0.00	0.0274	0.0009	0.0007	0.0000	1.81	0.05	0.068	0.003	0.009	0.000	-1.32	0.05
D17	0.282663	0.000023	1.46723	0.00007	-1.35	0.00	0.0306	0.0003	0.0011	0.0000	1.62	0.11	0.068	0.004	0.012	0.001	-1.65	0.07
D18	0.282631	0.000019	1.46718	0.00005	-1.33	0.00	0.0351	0.0005	0.0012	0.0000	1.54	0.08	0.075	0.005	0.013	0.001	-1.57	0.07
D20	0.282620	0.000016	1.46728	0.00003	-1.34	0.00	0.0361	0.0010	0.0009	0.0000	1.92	0.07	0.094	0.002	0.012	0.000	-1.34	0.05
D21	0.282653	0.000015	1.46714	0.00005	-1.33	0.00	0.0421	0.0007	0.0011	0.0000	2.15	0.07	0.123	0.003	0.016	0.000	-1.42	0.05
D23	0.282706	0.000042	1.46697	0.00019	-1.32	0.01	0.0472	0.0001	0.0010	0.0000	0.99	0.12	0.064	0.008	0.007	0.001	-1.22	0.16
D25	0.282674	0.000013	1.46723	0.00004	-1.35	0.00	0.0307	0.0009	0.0009	0.0000	2.29	0.06	0.094	0.002	0.015	0.000	-1.34	0.03
D26	0.282623	0.000013	1.46721	0.00003	-1.33	0.00	0.0272	0.0005	0.0007	0.0000	2.17	0.03	0.081	0.002	0.010	0.000	-1.40	0.05
D28	0.282564	0.000015	1.46721	0.00005	-1.33	0.00	0.0289	0.0005	0.0008	0.0000	1.90	0.05	0.074	0.002	0.010	0.000	-1.19	0.06
E01	0.282559	0.000009	1.46726	0.00004	-1.34	0.00	0.0390	0.0007	0.0009	0.0000	1.70	0.02	0.092	0.002	0.011	0.001	-1.25	0.04
E02	0.282625	0.000016	1.46725	0.00005	-1.32	0.00	0.0529	0.0015	0.0013	0.0001	1.68	0.05	0.119	0.003	0.014	0.001	-1.36	0.04
E03	0.282592	0.000012	1.46721	0.00005	-1.35	0.00	0.0368	0.0009	0.0008	0.0000	1.62	0.01	0.084	0.002	0.009	0.000	-1.48	0.03
E04	0.282690	0.000035	1.46720	0.00005	-1.35	0.01	0.0364	0.0009	0.0008	0.0000	1.47	0.02	0.074	0.002	0.008	0.000	-1.51	0.06
E05	0.282646	0.000017	1.46711	0.00004	-1.36	0.00	0.0410	0.0008	0.0009	0.0000	1.39	0.03	0.080	0.003	0.009	0.000	-1.43	0.04
E06	0.282626	0.000010	1.46721	0.00004	-1.34	0.00	0.0310	0.0004	0.0007	0.0000	1.54	0.01	0.066	0.001	0.008	0.000	-1.50	0.05
E08	0.282664	0.000013	1.46723	0.00004	-1.31	0.00	0.0327	0.0008	0.0010	0.0001	1.64	0.08	0.072	0.002	0.011	0.000	-1.77	0.06

Table 37

Name	176Hf/177Hf	1SE	178Hf/177Hf	1SE	Fract	1SE	176Yb/177Hf	1SE	176Lu/177Hf	1SE	Hf	1SE	Yb	1SE	Lu	1SE	Yb Fract	1SE
E09	0.282635	0.000015	1.46727	0.00003	-1.33	0.00	0.0385	0.0003	0.0009	0.0000	1.75	0.02	0.092	0.001	0.010	0.000	-1.37	0.04
E10	0.282689	0.000016	1.46722	0.00004	-1.33	0.01	0.0451	0.0010	0.0010	0.0000	1.81	0.03	0.114	0.003	0.013	0.000	-1.34	0.06
E11	0.282607	0.000010	1.46710	0.00002	-1.34	0.00	0.0352	0.0012	0.0008	0.0000	1.67	0.03	0.082	0.004	0.009	0.000	-1.45	0.06
E12	0.282639	0.000016	1.46735	0.00002	-1.31	0.01	0.0443	0.0008	0.0015	0.0001	1.32	0.08	0.082	0.005	0.013	0.001	-1.44	0.06
E14	0.282653	0.000019	1.46720	0.00005	-1.35	0.00	0.0327	0.0005	0.0008	0.0000	1.70	0.03	0.078	0.001	0.009	0.000	-1.30	0.05
E15	0.282585	0.000015	1.46717	0.00004	-1.33	0.00	0.0242	0.0005	0.0007	0.0000	1.87	0.04	0.061	0.001	0.009	0.000	-1.46	0.06
E16	0.282693	0.000011	1.46711	0.00003	-1.34	0.01	0.0386	0.0010	0.0012	0.0001	1.91	0.08	0.100	0.003	0.015	0.000	-1.52	0.04
E18	0.282611	0.000017	1.46719	0.00004	-1.33	0.00	0.0322	0.0004	0.0008	0.0000	1.71	0.03	0.076	0.001	0.009	0.000	-1.32	0.05
E19	0.282608	0.000031	1.46717	0.00006	-1.31	0.00	0.0404	0.0021	0.0013	0.0001	1.54	0.07	0.081	0.002	0.013	0.001	-1.44	0.07
E20	0.282635	0.000018	1.46723	0.00005	-1.34	0.00	0.0363	0.0008	0.0008	0.0000	1.60	0.02	0.082	0.001	0.009	0.000	-1.62	0.06
E21	0.282599	0.000014	1.46719	0.00003	-1.33	0.00	0.0322	0.0007	0.0008	0.0000	1.74	0.02	0.077	0.002	0.009	0.000	-1.43	0.04
E22	0.282675	0.000011	1.46721	0.00002	-1.33	0.00	0.0382	0.0007	0.0009	0.0000	1.95	0.04	0.104	0.003	0.013	0.000	-1.43	0.04
E23	0.282623	0.000012	1.46719	0.00005	-1.31	0.00	0.0325	0.0004	0.0010	0.0000	1.61	0.09	0.074	0.004	0.012	0.001	-1.26	0.07
E25	0.282654	0.000016	1.46718	0.00004	-1.31	0.00	0.0350	0.0010	0.0011	0.0001	1.79	0.07	0.085	0.001	0.013	0.000	-1.39	0.06
E27	0.282623	0.000018	1.46704	0.00004	-1.32	0.00	0.0516	0.0015	0.0017	0.0001	1.77	0.10	0.125	0.004	0.021	0.001	-1.45	0.04
F01	0.282693	0.000012	1.46731	0.00004	-1.35	0.00	0.0534	0.0011	0.0008	0.0000	1.40	0.01	0.103	0.003	0.008	0.000	-1.56	0.03
F02	0.282664	0.000014	1.46733	0.00003	-1.33	0.00	0.0502	0.0010	0.0008	0.0000	1.61	0.04	0.111	0.002	0.010	0.000	-1.56	0.03
F03	0.282704	0.000021	1.46732	0.00007	-1.35	0.01	0.0530	0.0013	0.0008	0.0001	1.40	0.07	0.103	0.003	0.008	0.000	-1.39	0.05
F04	0.282575	0.000025	1.46722	0.00005	-1.35	0.01	0.0642	0.0014	0.0010	0.0001	1.31	0.07	0.111	0.005	0.009	0.001	-1.26	0.07
F05	0.282669	0.000019	1.46745	0.00004	-1.35	0.00	0.0482	0.0005	0.0007	0.0000	1.43	0.05	0.096	0.003	0.007	0.000	-1.43	0.05
F06	0.282690	0.000015	1.46732	0.00004	-1.35	0.00	0.0682	0.0014	0.0010	0.0000	1.37	0.03	0.132	0.003	0.010	0.000	-1.55	0.03
F07	0.282675	0.000015	1.46723	0.00004	-1.34	0.00	0.0454	0.0007	0.0007	0.0000	1.38	0.02	0.087	0.002	0.007	0.000	-1.39	0.05
F08	0.282608	0.000014	1.46737	0.00005	-1.32	0.00	0.0457	0.0002	0.0007	0.0000	1.60	0.06	0.102	0.003	0.008	0.000	-1.38	0.05
F11	0.282712	0.000015	1.46731	0.00004	-1.35	0.00	0.0492	0.0004	0.0007	0.0000	1.43	0.02	0.097	0.002	0.007	0.000	-1.45	0.04
F12	0.282687	0.000014	1.46719	0.00004	-1.35	0.00	0.0549	0.0013	0.0008	0.0000	1.36	0.02	0.102	0.002	0.008	0.000	-1.51	0.03
F13	0.282609	0.000075	1.46729	0.00030	-1.33	0.01	0.0675	0.0021	0.0013	0.0001	0.86	0.09	0.082	0.010	0.009	0.001	-1.92	0.13
F14	0.282605	0.000016	1.46727	0.00004	-1.33	0.00	0.0454	0.0009	0.0007	0.0000	1.49	0.03	0.093	0.003	0.007	0.000	-1.50	0.05
F15	0.282652	0.000018	1.46737	0.00004	-1.33	0.01	0.0511	0.0003	0.0007	0.0000	1.55	0.07	0.110	0.004	0.007	0.000	-1.66	0.06
F16	0.282739	0.000017	1.46737	0.00004	-1.34	0.00	0.0544	0.0017	0.0008	0.0000	1.44	0.02	0.110	0.004	0.008	0.000	-1.66	0.02

Table 38

Name	176Hf/177Hf	1SE	178Hf/177Hf	1SE	Fract	1SE	176Yb/177Hf	1SE	176Lu/177Hf	1SE	Hf	1SE	Yb	1SE	Lu	1SE	Yb Fract	1SE
F17	0.282590	0.000019	1.46730	0.00005	-1.39	0.01	0.0719	0.0011	0.0020	0.0001	1.65	0.04	0.163	0.004	0.023	0.001	-1.56	0.04
F18	0.282667	0.000019	1.46728	0.00005	-1.33	0.00	0.0476	0.0005	0.0007	0.0000	1.36	0.04	0.091	0.002	0.007	0.000	-1.38	0.06
F19	0.282754	0.000018	1.46732	0.00004	-1.35	0.00	0.0429	0.0009	0.0006	0.0000	1.43	0.04	0.084	0.003	0.007	0.000	-1.51	0.05
F21	0.282642	0.000020	1.46724	0.00004	-1.39	0.01	0.0567	0.0030	0.0015	0.0001	1.47	0.09	0.110	0.003	0.014	0.001	-1.52	0.04
F23	0.282629	0.000018	1.46733	0.00004	-1.37	0.01	0.0527	0.0010	0.0008	0.0000	1.22	0.02	0.091	0.002	0.007	0.000	-1.48	0.04
F25	0.282601	0.000020	1.46721	0.00004	-1.35	0.00	0.0438	0.0004	0.0007	0.0000	1.42	0.04	0.088	0.003	0.006	0.000	-1.39	0.05
F26	0.282722	0.000022	1.46731	0.00006	-1.36	0.01	0.0607	0.0015	0.0010	0.0001	1.38	0.08	0.119	0.008	0.010	0.001	-1.62	0.07
F27	0.282692	0.000019	1.46737	0.00004	-1.35	0.01	0.0595	0.0011	0.0009	0.0000	1.21	0.02	0.099	0.003	0.008	0.000	-1.46	0.03
F29	0.282558	0.000029	1.46726	0.00004	-1.39	0.01	0.1187	0.0060	0.0026	0.0003	1.65	0.10	0.258	0.007	0.027	0.002	-1.46	0.02
F30	0.282650	0.000020	1.46726	0.00003	-1.35	0.00	0.0486	0.0008	0.0007	0.0000	1.40	0.03	0.096	0.002	0.007	0.000	-1.54	0.06
G01	0.282677	0.000027	1.46717	0.00006	-1.35	0.01	0.0633	0.0017	0.0013	0.0001	1.71	0.06	0.158	0.003	0.016	0.001	-1.48	0.04
G02	0.282671	0.000012	1.46731	0.00004	-1.35	0.00	0.0539	0.0004	0.0009	0.0000	1.54	0.02	0.116	0.002	0.010	0.000	-1.55	0.03
G03	0.282626	0.000012	1.46741	0.00003	-1.35	0.00	0.0451	0.0004	0.0007	0.0000	1.59	0.02	0.098	0.002	0.008	0.000	-1.67	0.04
G05	0.282528	0.000026	1.46727	0.00004	-1.40	0.01	0.0672	0.0030	0.0016	0.0001	1.41	0.07	0.123	0.002	0.015	0.001	-1.56	0.03
G08	0.282672	0.000012	1.46720	0.00004	-1.34	0.00	0.0556	0.0010	0.0009	0.0000	1.53	0.02	0.114	0.002	0.009	0.000	-1.66	0.04
G09	0.282595	0.000021	1.46720	0.00004	-1.35	0.01	0.0662	0.0027	0.0015	0.0001	1.51	0.08	0.130	0.003	0.015	0.001	-1.33	0.04
G10	0.282696	0.000017	1.46723	0.00004	-1.33	0.01	0.0462	0.0003	0.0007	0.0000	1.98	0.03	0.127	0.002	0.010	0.000	-1.43	0.04
G11	0.282630	0.000013	1.46724	0.00004	-1.35	0.00	0.0444	0.0006	0.0007	0.0000	1.73	0.03	0.106	0.001	0.008	0.000	-1.60	0.04
G12	0.282678	0.000019	1.46727	0.00006	-1.35	0.01	0.0463	0.0015	0.0009	0.0001	1.76	0.10	0.113	0.007	0.010	0.001	-1.55	0.06
G13	0.282633	0.000017	1.46747	0.00006	-1.35	0.01	0.0624	0.0027	0.0011	0.0001	1.67	0.06	0.153	0.008	0.013	0.001	-1.43	0.04
G14	0.282669	0.000013	1.46728	0.00003	-1.36	0.00	0.0578	0.0009	0.0009	0.0000	1.65	0.02	0.131	0.002	0.011	0.000	-1.60	0.03
G15	0.282701	0.000023	1.46722	0.00005	-1.33	0.01	0.0619	0.0017	0.0014	0.0001	1.82	0.07	0.160	0.006	0.018	0.001	-1.47	0.05
G16	0.282688	0.000018	1.46727	0.00005	-1.34	0.01	0.0671	0.0019	0.0014	0.0001	2.41	0.11	0.215	0.005	0.025	0.001	-1.50	0.03
G18	0.282600	0.000021	1.46740	0.00005	-1.34	0.00	0.0551	0.0005	0.0009	0.0000	2.03	0.07	0.154	0.004	0.013	0.001	-1.49	0.06
G19	0.282700	0.000018	1.46728	0.00004	-1.35	0.00	0.0572	0.0007	0.0009	0.0000	1.58	0.01	0.123	0.002	0.010	0.000	-1.48	0.03
G20	0.282647	0.000016	1.46720	0.00004	-1.37	0.00	0.0496	0.0019	0.0008	0.0000	1.50	0.04	0.102	0.003	0.009	0.000	-1.51	0.04
G21	0.282597	0.000024	1.46742	0.00007	-1.35	0.01	0.0435	0.0002	0.0007	0.0000	1.56	0.02	0.094	0.002	0.007	0.000	-1.29	0.07
G22	0.282679	0.000017	1.46731	0.00004	-1.34	0.01	0.0691	0.0015	0.0013	0.0001	1.91	0.04	0.184	0.005	0.018	0.001	-1.49	0.02
G23	0.282733	0.000012	1.46730	0.00004	-1.36	0.00	0.0475	0.0010	0.0007	0.0000	1.80	0.01	0.117	0.003	0.009	0.000	-1.50	0.04

Table 39

Name	176Hf/177Hf	1SE	178Hf/177Hf	1SE	Fract	1SE	176Yb/177Hf	1SE	176Lu/177Hf	1SE	Hf	1SE	Yb	1SE	Lu	1SE	Yb Fract	1SE
G24	0.282656	0.000015	1.46719	0.00005	-1.37	0.01	0.0503	0.0018	0.0008	0.0000	1.64	0.06	0.112	0.005	0.009	0.000	-1.46	0.05
G25	0.282605	0.000014	1.46719	0.00005	-1.37	0.00	0.0511	0.0004	0.0009	0.0000	1.67	0.02	0.119	0.002	0.010	0.000	-1.46	0.05
G26	0.282445	0.000028	1.46722	0.00004	-1.41	0.01	0.1293	0.0026	0.0034	0.0001	1.18	0.02	0.208	0.003	0.028	0.000	-1.43	0.02
G27	0.282667	0.000020	1.46733	0.00005	-1.39	0.01	0.0827	0.0009	0.0018	0.0001	1.61	0.07	0.184	0.007	0.020	0.001	-1.57	0.03
G28	0.282734	0.000052	1.46727	0.00009	-1.41	0.01	0.1395	0.0082	0.0034	0.0003	0.92	0.06	0.168	0.004	0.020	0.001	-1.58	0.06
H03	0.282625	0.000015	1.46721	0.00003	-1.30	0.00	0.0455	0.0035	0.0011	0.0000	2.03	0.07	0.124	0.009	0.015	0.001	-1.42	0.03
H04	0.282634	0.000017	1.46733	0.00004	-1.28	0.00	0.0312	0.0003	0.0009	0.0000	2.60	0.05	0.115	0.002	0.016	0.001	-1.31	0.06
H05	0.282571	0.000019	1.46727	0.00006	-1.32	0.00	0.0609	0.0022	0.0019	0.0001	1.84	0.09	0.153	0.008	0.025	0.001	-1.45	0.03
H06	0.282561	0.000018	1.46727	0.00005	-1.37	0.01	0.0596	0.0012	0.0021	0.0000	1.38	0.03	0.113	0.001	0.020	0.000	-1.50	0.04
H07	0.282522	0.000032	1.46730	0.00008	-1.32	0.01	0.0867	0.0088	0.0030	0.0004	1.27	0.05	0.149	0.012	0.026	0.003	-1.40	0.04
H08	0.282652	0.000020	1.46721	0.00007	-1.29	0.01	0.0353	0.0002	0.0009	0.0000	2.14	0.11	0.104	0.005	0.013	0.001	-1.49	0.08
H09	0.282584	0.000013	1.46734	0.00005	-1.30	0.00	0.0359	0.0003	0.0007	0.0000	1.87	0.01	0.094	0.001	0.010	0.000	-1.27	0.06
H10	0.282639	0.000031	1.46725	0.00006	-1.30	0.01	0.0402	0.0006	0.0008	0.0000	1.87	0.06	0.103	0.003	0.011	0.000	-1.26	0.08
H11	0.282625	0.000140	1.46704	0.00031	-1.38	0.02	0.0444	0.0006	0.0013	0.0000	0.50	0.04	0.031	0.002	0.005	0.000	-2.35	0.41
H13	0.282667	0.000012	1.46717	0.00003	-1.32	0.01	0.0428	0.0015	0.0011	0.0000	2.30	0.06	0.135	0.008	0.017	0.001	-1.52	0.03
H14	0.282665	0.000020	1.46719	0.00004	-1.31	0.00	0.0371	0.0004	0.0008	0.0000	1.94	0.05	0.100	0.003	0.011	0.000	-1.38	0.05
H15	0.282674	0.000015	1.46713	0.00006	-1.34	0.01	0.0441	0.0011	0.0013	0.0001	1.63	0.09	0.097	0.004	0.015	0.001	-1.57	0.05
H16	0.282654	0.000018	1.46710	0.00004	-1.33	0.01	0.0433	0.0009	0.0010	0.0000	1.88	0.04	0.110	0.004	0.013	0.000	-1.36	0.04
H18	0.282579	0.000017	1.46733	0.00006	-1.36	0.01	0.0543	0.0017	0.0017	0.0001	1.51	0.09	0.115	0.004	0.018	0.001	-1.35	0.04
H19	0.282546	0.000031	1.46721	0.00006	-1.36	0.01	0.0648	0.0006	0.0022	0.0000	1.24	0.05	0.111	0.005	0.019	0.001	-1.37	0.07
H20	0.282660	0.000018	1.46717	0.00004	-1.34	0.00	0.0435	0.0007	0.0009	0.0000	1.98	0.05	0.120	0.003	0.013	0.000	-1.42	0.04
H22	0.282660	0.000021	1.46737	0.00009	-1.32	0.01	0.0453	0.0019	0.0014	0.0001	1.74	0.13	0.108	0.004	0.017	0.001	-1.42	0.07
H24	0.282650	0.000016	1.46719	0.00004	-1.35	0.01	0.0497	0.0014	0.0011	0.0001	1.41	0.07	0.096	0.005	0.011	0.000	-1.47	0.05
H25	0.282873	0.000079	1.46782	0.00014	-1.29	0.02	0.0575	0.0004	0.0020	0.0000	0.49	0.02	0.039	0.001	0.007	0.000	-1.81	0.27
H28	0.282676	0.000011	1.46732	0.00003	-1.33	0.00	0.0374	0.0003	0.0008	0.0000	1.98	0.03	0.102	0.002	0.012	0.000	-1.37	0.04
H29	0.282680	0.000013	1.46724	0.00003	-1.33	0.00	0.0386	0.0007	0.0009	0.0000	2.40	0.07	0.126	0.002	0.016	0.001	-1.54	0.04

Table 40

Mud Tank (standard)

Name	$^{176}Hf/^{177}Hf$	1SE	$^{178}Hf/^{177}Hf$	1SE	Fract	1SE	$^{176}Yb/^{177}Hf$	1SE	$^{176}Lu/^{177}Hf$	1SE	Hf	1SE	Yb	1SE	Lu	1SE	Yb Fract	1SE
MT-101210-TA-01	0.282497	0.000014	1.46733	0.00003	-1.27	0.00	0.0017	0.0000	0.0000	0.0000	2.14	0.03	0.005	0.000	0.001	0.000	-1.33	0.61
MT-101210-GB-02	0.282529	0.000012	1.46724	0.00003	-1.28	0.00	0.0020	0.0000	0.0000	0.0000	2.14	0.03	0.006	0.000	0.001	0.000	-3.27	0.56
MT-101210-TA-03	0.282471	0.000012	1.46719	0.00003	-1.26	0.00	0.0016	0.0000	0.0000	0.0000	2.05	0.02	0.005	0.000	0.001	0.000	1.27	0.87
MT-101210-GB-04	0.282553	0.000014	1.46739	0.00003	-1.26	0.00	0.0019	0.0000	0.0000	0.0000	1.98	0.02	0.005	0.000	0.001	0.000	-0.86	0.61
MT-101210-GB-05	0.282529	0.000014	1.46730	0.00003	-1.25	0.00	0.0021	0.0000	0.0000	0.0000	1.98	0.02	0.006	0.000	0.001	0.000	-3.70	0.64
MT-101210-GB-06	0.282505	0.000010	1.46733	0.00003	-1.25	0.00	0.0017	0.0000	0.0000	0.0000	2.06	0.02	0.005	0.000	0.001	0.000	1.20	0.75
MT-101210-GB-07	0.282476	0.000014	1.46728	0.00002	-1.46	0.00	0.0017	0.0000	0.0000	0.0000	2.48	0.03	0.006	0.000	0.001	0.000	-0.96	0.57
MT-101210-GB-08	0.282522	0.000011	1.46728	0.00003	-1.46	0.00	0.0016	0.0000	0.0000	0.0000	2.59	0.03	0.006	0.000	0.001	0.000	-1.85	0.49
MT-101210-GB-09	0.282491	0.000010	1.46728	0.00003	-1.45	0.00	0.0015	0.0000	0.0000	0.0000	2.63	0.02	0.006	0.000	0.001	0.000	-1.18	0.66
MT-101210-GB-10	0.282463	0.000009	1.46720	0.00003	-1.46	0.00	0.0019	0.0000	0.0000	0.0000	2.62	0.03	0.007	0.000	0.001	0.000	-3.59	0.55
MT-101210-GB-11	0.282462	0.000010	1.46727	0.00004	-1.46	0.00	0.0013	0.0000	0.0000	0.0000	2.68	0.03	0.005	0.000	0.001	0.000	0.64	0.69
MT-101210-GB-12	0.282497	0.000010	1.46727	0.00002	-1.46	0.00	0.0015	0.0000	0.0000	0.0000	2.56	0.02	0.005	0.000	0.001	0.000	-3.64	0.70
MT-101210-GB-12	0.282493	0.000007	1.46718	0.00004	-1.46	0.00	0.0016	0.0000	0.0000	0.0000	2.48	0.03	0.005	0.000	0.001	0.000	-1.62	0.68
MT-101210-GB-13	0.282501	0.000010	1.46724	0.00004	-1.46	0.00	0.0018	0.0000	0.0000	0.0000	2.46	0.03	0.006	0.000	0.001	0.000	-1.57	0.52
MT-101213-MK-01	0.282500	0.000010	1.46724	0.00003	-1.37	0.00	0.0015	0.0000	0.0000	0.0000	2.72	0.03	0.006	0.000	0.001	0.000	-3.12	0.43
MT-101213-MK-02	0.282526	0.000011	1.46726	0.00002	-1.38	0.00	0.0019	0.0000	0.0000	0.0000	2.84	0.04	0.008	0.000	0.001	0.000	-3.46	0.47
MT-101213-GB-03	0.282516	0.000008	1.46727	0.00003	-1.36	0.00	0.0017	0.0000	0.0000	0.0000	2.46	0.03	0.006	0.000	0.001	0.000	-2.46	0.63
MT-101213-GB-04	0.282470	0.000011	1.46729	0.00002	-1.37	0.00	0.0016	0.0000	0.0000	0.0000	2.63	0.03	0.006	0.000	0.001	0.000	0.83	0.59
MT-101213-SLS-05	0.282494	0.000008	1.46723	0.00003	-1.37	0.00	0.0016	0.0000	0.0000	0.0000	2.61	0.03	0.006	0.000	0.001	0.000	-2.22	0.47
MT-101213-GB-06	0.282517	0.000010	1.46723	0.00002	-1.38	0.00	0.0018	0.0000	0.0000	0.0000	2.54	0.02	0.006	0.000	0.001	0.000	-1.89	0.54
MT-101213-GB-07	0.282523	0.000011	1.46728	0.00003	-1.37	0.00	0.0014	0.0000	0.0000	0.0000	2.75	0.05	0.005	0.000	0.001	0.000	1.90	0.65

Table 41.

Mud Tank (continued)

MT-101213-GB-08	0.282456	0.000012	1.46723	0.00003	-1.36	0.00	0.0019	0.0000	0.0000	0.0000	2.68	0.04	0.007	0.000	0.001	0.000	-1.54	0.46
MT-101213-GB-09	0.282528	0.000010	1.46728	0.00003	-1.36	0.00	0.0013	0.0000	0.0000	0.0000	2.77	0.05	0.005	0.000	0.001	0.000	-0.94	0.69
MT-101213-GB-10	0.282521	0.000011	1.46708	0.00003	-1.34	0.00	0.0012	0.0000	0.0000	0.0000	2.75	0.05	0.005	0.000	0.001	0.000	-6.29	0.79
MT-101213-GB-11	0.282521	0.000010	1.46705	0.00003	-1.35	0.00	0.0014	0.0000	0.0000	0.0000	2.81	0.05	0.005	0.000	0.001	0.000	1.58	0.58
MT-101213-GB-12	0.282474	0.000008	1.46706	0.00003	-1.34	0.00	0.0013	0.0000	0.0000	0.0000	2.80	0.05	0.005	0.000	0.001	0.000	-2.14	0.82
MT-101213-GB-13	0.282506	0.000010	1.46694	0.00002	-1.35	0.00	0.0014	0.0000	0.0000	0.0000	2.81	0.04	0.006	0.000	0.001	0.000	-0.32	0.53
MT-110113-SLS-01	0.282501	0.000012	1.46736	0.00002	-1.37	0.00	0.0010	0.0000	0.0000	0.0000	2.34	0.01	0.003	0.000	0.000	0.000	6.25	0.99
MT-110113-SLS-02	0.282535	0.000010	1.46724	0.00004	-1.39	0.00	0.0010	0.0000	0.0000	0.0000	2.19	0.03	0.003	0.000	0.000	0.000	-8.54	0.83
MT-110113-GB-03	0.282512	0.000008	1.46731	0.00002	-1.39	0.00	0.0026	0.0001	0.0000	0.0000	2.74	0.02	0.010	0.000	0.001	0.000	0.43	0.43
MT-110113-GB-04	0.282539	0.000010	1.46731	0.00003	-1.40	0.00	0.0023	0.0001	0.0000	0.0000	2.71	0.04	0.009	0.000	0.001	0.000	-3.65	0.40
MT-110113-SLS-05	0.282548	0.000015	1.46729	0.00003	-1.40	0.00	0.0016	0.0000	0.0000	0.0000	2.74	0.02	0.006	0.000	0.001	0.000	-3.68	0.68
MT-110113-SLS-06	0.282519	0.000012	1.46731	0.00002	-1.40	0.00	0.0015	0.0000	0.0000	0.0000	2.96	0.03	0.006	0.000	0.001	0.000	-1.69	0.62
MT-110113-GB-07	0.282468	0.000011	1.46728	0.00003	-1.40	0.00	0.0015	0.0000	0.0000	0.0000	2.95	0.02	0.006	0.000	0.001	0.000	-1.02	0.53
MT-110113-GB-08	0.282481	0.000012	1.46730	0.00003	-1.41	0.00	0.0015	0.0000	0.0000	0.0000	2.99	0.04	0.006	0.000	0.001	0.000	-2.27	0.67
MT-110120-SLS-01	0.282509	0.000010	1.46728	0.00002	-1.30	0.00	0.0016	0.0000	0.0000	0.0000	3.47	0.04	0.007	0.000	0.001	0.000	-0.97	0.45
MT-110120-SLS-02	0.282496	0.000009	1.46728	0.00003	-1.31	0.00	0.0013	0.0000	0.0000	0.0000	2.96	0.04	0.005	0.000	0.001	0.000	0.06	0.54
MT-110120-GB-03	0.282504	0.000012	1.46728	0.00002	-1.34	0.00	0.0023	0.0000	0.0000	0.0000	2.66	0.03	0.008	0.000	0.001	0.000	-2.71	0.46
MT-110120-GB-04	0.282515	0.000010	1.46725	0.00003	-1.32	0.00	0.0027	0.0000	0.0001	0.0000	2.72	0.02	0.010	0.000	0.001	0.000	-1.58	0.31
MT-110120-SLS-05	0.282479	0.000012	1.46727	0.00002	-1.34	0.00	0.0020	0.0000	0.0000	0.0000	2.83	0.03	0.008	0.000	0.001	0.000	-0.68	0.50
MT-110120-SLS-06	0.282510	0.000013	1.46728	0.00003	-1.34	0.00	0.0013	0.0000	0.0000	0.0000	2.82	0.02	0.005	0.000	0.001	0.000	-2.08	0.75
MT-110120-GB-07	0.282506	0.000010	1.46722	0.00003	-1.35	0.00	0.0014	0.0000	0.0000	0.0000	2.78	0.02	0.005	0.000	0.001	0.000	-2.49	0.82
MT-110120-GB-08	0.282525	0.000011	1.46725	0.00003	-1.36	0.00	0.0015	0.0000	0.0000	0.0000	2.83	0.03	0.006	0.000	0.001	0.000	-1.72	0.76
MT-110120-SLS-09	0.282498	0.000013	1.46727	0.00002	-1.36	0.00	0.0003	0.0000	0.0000	0.0000	2.97	0.03	0.001	0.000	0.000	0.000	4.26	2.50

Table 42

Temora (standard)

Name	$^{176}Hf/^{177}Hf$	1SE	$^{178}Hf/^{177}Hf$	1SE	Fract	1SE	$^{176}Yb/^{177}Hf$	1SE	$^{176}Lu/^{177}Hf$	1SE	Hf	1SE	Yb	1SE	Lu	1SE	Yb Fract	1SE
TEM-101210-GB-01	0.282590	0.000013	1.46715	0.00004	-1.26	0.00	0.0412	0.0003	0.0012	0.0000	1.80	0.02	0.101	0.002	0.015	0.000	-1.11	0.05
TEM-101210-GB-02	0.282697	0.000016	1.46727	0.00003	-1.28	0.00	0.0385	0.0007	0.0011	0.0000	2.02	0.04	0.106	0.004	0.015	0.000	-1.42	0.04
TEM-101210-GB-03	0.282692	0.000013	1.46728	0.00004	-1.27	0.00	0.0360	0.0008	0.0011	0.0000	2.02	0.01	0.101	0.002	0.015	0.001	-1.40	0.04
TEM-101210-GB-04	0.282643	0.000009	1.46721	0.00003	-1.45	0.00	0.0469	0.0003	0.0014	0.0000	2.39	0.03	0.153	0.003	0.023	0.000	-1.54	0.02
TEM-101210-GB-05	0.282685	0.000021	1.46719	0.00006	-1.45	0.01	0.0523	0.0009	0.0018	0.0001	1.65	0.14	0.116	0.009	0.019	0.001	-1.37	0.04
TEM-101210-GB-06	0.282623	0.000010	1.46724	0.00003	-1.47	0.00	0.0433	0.0005	0.0013	0.0000	2.39	0.03	0.141	0.003	0.022	0.000	-1.64	0.02
TEM-101210-GB-07	0.282653	0.000009	1.46733	0.00002	-1.46	0.00	0.0152	0.0000	0.0005	0.0000	2.51	0.03	0.053	0.001	0.008	0.000	-1.51	0.07
TEM-101210-GB-08	0.282685	0.000008	1.46723	0.00003	-1.47	0.00	0.0371	0.0005	0.0011	0.0000	2.43	0.03	0.124	0.003	0.019	0.000	-1.55	0.03
TEM-101210-GB-09	0.282648	0.000010	1.46722	0.00002	-1.47	0.00	0.0441	0.0005	0.0013	0.0000	2.23	0.02	0.136	0.002	0.020	0.000	-1.52	0.03
TEM-101210-GB-10	0.282683	0.000013	1.46724	0.00004	-1.47	0.00	0.0366	0.0007	0.0011	0.0000	2.23	0.03	0.112	0.003	0.017	0.000	-1.45	0.04
TEM-101213-GB-01	0.282668	0.000011	1.46722	0.00004	-1.36	0.00	0.0184	0.0003	0.0006	0.0000	2.43	0.09	0.061	0.002	0.010	0.000	-1.39	0.09
TEM-101213-GB-02	0.282644	0.000010	1.46729	0.00003	-1.39	0.00	0.0346	0.0004	0.0010	0.0000	2.55	0.04	0.122	0.003	0.018	0.000	-1.38	0.04
TEM-101213-GB-03	0.282613	0.000009	1.46719	0.00003	-1.36	0.00	0.0322	0.0002	0.0010	0.0000	2.16	0.03	0.097	0.001	0.014	0.000	-1.53	0.05
TEM-101213-GB-04	0.282663	0.000009	1.46718	0.00004	-1.36	0.00	0.0239	0.0004	0.0008	0.0000	2.37	0.03	0.078	0.002	0.013	0.000	-1.53	0.05
TEM-101213-GB-05	0.282684	0.000010	1.46718	0.00003	-1.36	0.00	0.0674	0.0031	0.0019	0.0001	2.17	0.05	0.201	0.006	0.028	0.001	-1.43	0.02
TEM-101213-GB-06	0.282674	0.000007	1.46724	0.00003	-1.37	0.00	0.0577	0.0016	0.0017	0.0001	2.45	0.07	0.195	0.004	0.030	0.001	-1.60	0.03
TEM-101213-GB-07	0.282665	0.000011	1.46716	0.00005	-1.36	0.00	0.0431	0.0006	0.0013	0.0000	2.46	0.03	0.145	0.003	0.022	0.000	-1.47	0.02
TEM-101213-GB-08	0.282669	0.000010	1.46719	0.00003	-1.36	0.00	0.0247	0.0004	0.0007	0.0000	2.59	0.02	0.086	0.002	0.013	0.000	-1.59	0.03
TEM-101213-GB-09	0.282667	0.000010	1.46710	0.00004	-1.34	0.00	0.0300	0.0010	0.0010	0.0000	2.16	0.00	0.089	0.003	0.014	0.000	-1.53	0.04
TEM-101213-GB-10	0.282723	0.000013	1.46709	0.00006	-1.35	0.00	0.0285	0.0003	0.0009	0.0000	2.06	0.06	0.081	0.002	0.013	0.000	-1.56	0.05
TEM-101213-GB-11	0.282680	0.000010	1.46691	0.00002	-1.36	0.00	0.0302	0.0006	0.0009	0.0000	2.31	0.03	0.097	0.003	0.015	0.000	-1.36	0.05
TEM-101213-GB-12	0.282693	0.000011	1.46724	0.00003	-1.37	0.00	0.0368	0.0012	0.0011	0.0000	2.34	0.01	0.119	0.004	0.018	0.000	-1.44	0.03

Table 43

Temora (continued)

TEM-101213-GB-13	0.282652	0.000011	1.46722	0.00003	-1.37	0.00	0.0438	0.0005	0.0014	0.0000	2.41	0.02	0.146	0.002	0.023	0.000	-1.43	0.03
TEM-110113-GB-01	0.282702	0.000012	1.46728	0.00003	-1.37	0.00	0.1080	0.0029	0.0020	0.0001	1.70	0.03	0.256	0.008	0.025	0.001	-1.46	0.01
TEM-110113-GB-02	0.282696	0.000012	1.46733	0.00004	-1.39	0.00	0.0481	0.0003	0.0009	0.0000	2.24	0.03	0.149	0.003	0.015	0.000	-1.35	0.03
TEM-110113-GB-03	0.282712	0.000012	1.46722	0.00002	-1.38	0.00	0.0632	0.0010	0.0013	0.0000	2.31	0.03	0.207	0.006	0.022	0.001	-1.50	0.02
TEM-110113-GB-04	0.282618	0.000013	1.46724	0.00002	-1.38	0.00	0.0728	0.0009	0.0014	0.0001	2.08	0.03	0.208	0.002	0.021	0.001	-1.49	0.03
TEM-110113-GB-05	0.282660	0.000012	1.46730	0.00002	-1.39	0.00	0.0275	0.0009	0.0005	0.0000	2.19	0.01	0.083	0.003	0.008	0.000	-1.39	0.05
TEM-110113-GB-06	0.282673	0.000010	1.46725	0.00002	-1.38	0.00	0.0704	0.0002	0.0014	0.0000	2.20	0.01	0.215	0.001	0.022	0.000	-1.40	0.02
TEM-110113-GB-07	0.282658	0.000008	1.46728	0.00003	-1.37	0.00	0.0371	0.0015	0.0008	0.0000	2.27	0.03	0.112	0.004	0.012	0.000	-1.34	0.03
TEM-110113-GB-08	0.282668	0.000012	1.46738	0.00004	-1.35	0.00	0.0265	0.0004	0.0005	0.0000	2.04	0.03	0.074	0.001	0.008	0.000	-1.49	0.05
TEM-110113-GB-09	0.282670	0.000017	1.46723	0.00005	-1.38	0.00	0.0496	0.0006	0.0010	0.0000	2.26	0.04	0.156	0.001	0.016	0.001	-1.49	0.04
TEM-110113-GB-10	0.282687	0.000017	1.46727	0.00003	-1.40	0.00	0.0535	0.0013	0.0012	0.0001	2.16	0.08	0.161	0.005	0.019	0.001	-1.58	0.03
TEM-110113-GB-11	0.282649	0.000013	1.46723	0.00006	-1.43	0.01	0.0382	0.0010	0.0010	0.0001	1.79	0.11	0.092	0.004	0.011	0.000	-1.68	0.05
TEM-110120-SLS-01	0.282673	0.000011	1.46727	0.00003	-1.32	0.00	0.0337	0.0008	0.0010	0.0000	2.87	0.05	0.131	0.003	0.020	0.000	-1.43	0.03
TEM-110120-SLS-02	0.282661	0.000010	1.46726	0.00003	-1.32	0.00	0.0465	0.0004	0.0013	0.0000	2.84	0.06	0.185	0.002	0.026	0.001	-1.53	0.03
TEM-110120-GB-03	0.282677	0.000007	1.46729	0.00003	-1.33	0.00	0.0423	0.0013	0.0011	0.0000	2.72	0.05	0.160	0.006	0.022	0.001	-1.28	0.03
TEM-110120-GB-04	0.282650	0.000013	1.46725	0.00003	-1.34	0.00	0.0346	0.0013	0.0009	0.0000	2.71	0.07	0.134	0.003	0.017	0.001	-1.45	0.03
TEM-110120-GB-05	0.282642	0.000012	1.46707	0.00003	-1.34	0.00	0.0465	0.0012	0.0013	0.0000	2.66	0.05	0.168	0.007	0.023	0.001	-1.34	0.02
TEM-110120-GB-06	0.282658	0.000011	1.46700	0.00003	-1.33	0.00	0.0421	0.0004	0.0011	0.0000	2.46	0.03	0.145	0.001	0.019	0.000	-1.28	0.03
TEM-110120-SLS-07	0.282660	0.000010	1.46722	0.00002	-1.35	0.00	0.0462	0.0006	0.0012	0.0000	2.74	0.04	0.175	0.005	0.023	0.000	-1.45	0.03
TEM-110120-GB-08	0.282672	0.000012	1.46723	0.00002	-1.36	0.00	0.0338	0.0005	0.0008	0.0000	2.57	0.02	0.118	0.003	0.015	0.000	-1.50	0.04
TEM-110120-GB-09	0.282645	0.000012	1.46727	0.00003	-1.36	0.00	0.0557	0.0004	0.0014	0.0000	2.56	0.02	0.197	0.003	0.026	0.000	-1.44	0.02

Table 44

8.5 Mineral analyses

AMPHIBOLES

Measured values

	Analysis													
Oxide	**[1.1**	**2.1]**	**4.1**	**13.1**	**16.1**	**18.1**	**10.2**	**[17.2**	**18.2]**	**26.2**	**29.2**	**31.2**	**27.1**	**28.1**	**29.1**
SiO_2	46.169	46.022	45.994	45.870	45.886	46.668	46.308	45.870	46.311	45.813	45.962	46.002	46.359	46.072	46.200
TiO_2	1.622	1.704	1.770	1.743	1.801	1.618	1.798	1.774	1.686	1.820	1.795	1.863	1.238	1.279	1.237
Al_2O_3	6.600	6.546	6.543	6.535	6.763	6.271	6.543	6.644	6.488	6.559	6.572	6.625	5.706	5.712	5.552
Cr_2O_3	0.000	0.002	0.000	0.034	0.000	0.021	0.000	0.015	0.000	0.000	0.029	0.000	0.000	0.000	0.000
FeO	16.705	16.586	16.614	16.275	15.713	16.371	14.880	17.242	16.136	15.704	17.162	16.113	17.350	17.700	17.651
MnO	0.476	0.512	0.370	0.445	0.496	0.459	0.443	0.487	0.449	0.395	0.518	0.467	1.795	1.777	2.014
MgO	12.232	12.379	12.286	12.610	12.978	12.718	13.367	11.775	12.543	12.860	11.909	12.750	11.319	11.170	10.829
CaO	11.277	11.023	11.247	11.060	11.044	11.234	11.109	10.890	11.114	10.884	11.172	11.101	10.659	10.543	10.588
Na_2O	1.600	1.742	1.702	1.780	1.759	1.727	1.763	1.611	1.674	1.765	1.621	1.703	2.237	2.272	2.268
K_2O	0.977	1.017	1.083	1.079	1.097	1.020	1.106	0.974	0.900	1.094	0.987	1.025	0.761	0.812	0.789
Total	97.647	97.534	97.550	97.431	97.521	98.106	97.302	97.279	97.281	96.877	97.728	97.600	97.408	97.333	97.096

	Analysis													
Oxide	**30.1**	**31.1**	**32.1**	**[33.1**	**34.1**	**35.1**	**36.1]**	**[1.2**	**2.2**	**3.2]**	**[4.2**	**5.2**	**6.2]**	**[7.2**	**8.2]**
SiO_2	46.221	46.452	50.644	51.416	51.783	51.322	51.396	52.559	52.383	51.278	50.639	52.647	50.512	51.031	51.378
TiO_2	1.296	1.255	0.814	0.509	0.728	0.774	0.680	0.620	0.592	0.659	1.335	0.769	0.254	1.137	0.720
Al_2O_3	5.663	5.917	2.351	1.937	1.104	1.106	1.162	1.557	1.173	1.085	3.637	1.123	1.265	3.156	1.055
Cr_2O_3	0.000	0.000	0.000	0.000	0.000	0.011	0.002	0.000	0.000	0.000	0.000	0.000	0.013	0.000	0.000
FeO	18.509	18.100	18.680	16.385	21.796	22.835	22.084	12.735	18.799	23.041	11.213	23.548	23.914	11.090	23.157
MnO	1.948	1.853	2.807	2.613	2.689	2.912	3.017	2.728	2.653	2.896	1.821	2.632	2.303	1.978	2.846
MgO	10.314	10.988	10.071	11.743	7.758	7.033	7.706	13.823	9.798	7.090	15.313	7.293	7.139	15.249	6.707
CaO	10.634	10.669	4.840	4.269	2.046	3.057	3.869	7.038	2.675	3.433	8.957	2.438	10.933	8.618	1.972
Na_2O	2.128	2.212	6.056	6.102	6.764	6.803	6.346	5.439	7.284	5.803	4.659	6.544	0.989	4.663	7.005
K_2O	0.800	0.827	1.305	0.783	1.211	1.198	1.141	0.915	1.237	1.178	1.022	1.284	0.325	0.937	1.188
Total	97.481	98.221	97.550	95.738	95.844	97.052	97.401	97.399	96.583	96.442	98.558	98.233	97.646	97.825	96.013

Table 45. Numbers in brackets denote analyses done at the same grain. Black: akerite. red: granite. blue: nordmarkite.

AMPHIBOLES

Structural formula based on 23.000 oxygens

	Analysis													
Ion	**[1.1**	**2.1]**	**4.1**	**13.1**	**16.1**	**18.1**	**10.2**	**[17.2**	**18.2]**	**26.2**	**29.2**	**31.2**	**27.1**	**28.1**	**29.1**
Si^{4+}	6.926	6.904	6.908	6.895	6.872	6.957	6.918	6.922	6.948	6.902	6.910	6.889	7.031	7.011	7.050
Ti^{4+}	0.183	0.192	0.200	0.197	0.203	0.181	0.202	0.201	0.190	0.206	0.203	0.210	0.141	0.146	0.142
Al^{3+}	1.167	1.157	1.158	1.158	1.194	1.102	1.152	1.182	1.147	1.165	1.164	1.169	1.020	1.024	0.999
Cr^{3+}	0.000	0.000	0.000	0.004	0.000	0.002	0.000	0.002	0.000	0.000	0.003	0.000	0.000	0.000	0.000
Fe^{2+}	2.096	2.081	2.087	2.046	1.968	2.041	1.859	2.176	2.025	1.979	2.158	2.018	2.201	2.253	2.252
Mn^{2+}	0.060	0.065	0.047	0.057	0.063	0.058	0.056	0.062	0.057	0.050	0.066	0.059	0.231	0.229	0.260
Mg^{2+}	2.736	2.768	2.751	2.826	2.897	2.826	2.977	2.649	2.805	2.888	2.669	2.846	2.559	2.534	2.463
Ca^{2+}	1.813	1.805	1.810	1.781	1.772	1.794	1.778	1.761	1.786	1.757	1.799	1.781	1.732	1.719	1.731
Na^{+}	0.465	0.507	0.496	0.519	0.511	0.499	0.511	0.471	0.487	0.515	0.473	0.494	0.658	0.670	0.671
K^{+}	0.187	0.195	0.208	0.207	0.210	0.194	0.211	0.187	0.172	0.210	0.189	0.196	0.147	0.158	0.154
Total	15.633	15.675	15.664	15.690	15.689	15.656	15.664	15.614	15.618	15.672	15.634	15.662	15.720	15.744	15.722

	Analysis														
Ion	**30.1**	**31.1**	**32.1**	**[33.1**	**34.1**	**35.1**	**36.1]**	**[1.2**	**2.2**	**3.2]**	**[4.2**	**5.2**	**6.2]**	**[7.2**	**8.2]**
Si^{4+}	7.046	7.009	7.685	7.809	8.036	7.951	7.912	7.761	7.978	7.979	7.361	8.019	7.790	7.458	8.031
Ti^{4+}	0.149	0.142	0.093	0.058	0.085	0.090	0.079	0.069	0.068	0.077	0.146	0.088	0.029	0.125	0.085
Al^{3+}	1.017	1.052	0.421	0.347	0.202	0.202	0.211	0.271	0.210	0.199	0.623	0.202	0.230	0.544	0.194
Cr^{3+}	0.000	0.000	0.000	0.000	0.000	0.001	0.000	0.000	0.000	0.000	0.000	0.000	0.002	0.000	0.000
Fe^{2+}	2.360	2.284	2.370	2.081	2.829	2.959	2.843	1.573	2.394	2.998	1.363	3.000	3.084	1.355	3.027
Mn^{2+}	0.252	0.237	0.361	0.336	0.353	0.382	0.393	0.341	0.342	0.382	0.224	0.340	0.301	0.245	0.377
Mg^{2+}	2.344	2.471	2.278	2.659	1.795	1.624	1.768	3.043	2.224	1.645	3.318	1.656	1.641	3.322	1.563
Ca^{2+}	1.737	1.725	0.787	0.695	0.340	0.507	0.638	1.113	0.436	0.572	1.395	0.398	1.807	1.349	0.330
Na^{+}	0.629	0.647	1.782	1.797	2.035	2.043	1.894	1.557	2.151	1.751	1.313	1.932	0.296	1.321	2.123
K^{+}	0.156	0.159	0.253	0.152	0.240	0.237	0.224	0.172	0.240	0.234	0.190	0.249	0.064	0.175	0.237
Total	15.689	15.726	16.029	15.934	15.915	15.997	15.963	15.900	16.045	15.837	15.933	15.883	15.244	15.894	15.967

Table 46. Numbers in brackets denote analyses done at the same grain. Black: akerite. red: granite. blue: nordmarkite.

CLINOPYROXENE

Measured values

	Analysis													
Oxide	**8.1**	**[9.1**	**10.1**	**11.1**	**12.1]**	**17.1**	**19.1**	**9.2**	**11.2**	**13.2**	**[15.2**	**16.2]**	**28.2**	**30.2**
SiO_2	52.52	51.73	52.18	52.28	52.36	52.37	51.93	52.20	52.42	52.15	51.75	51.47	51.44	52.15
TiO_2	0.45	0.52	0.22	0.22	0.34	0.52	0.58	0.34	0.82	0.76	0.86	0.82	1.11	0.86
Al_2O_3	1.03	1.25	0.68	0.63	0.95	1.38	1.52	0.90	2.00	1.82	2.24	2.16	2.73	2.06
Cr_2O_3	0.02	0.00	0.01	0.02	0.00	0.00	0.00	0.04	0.04	0.01	0.04	0.00	0.03	0.02
FeO	12.09	11.90	13.02	12.62	13.89	11.08	9.89	12.45	10.06	11.27	12.09	11.22	10.49	9.85
MnO	0.63	0.66	0.78	0.70	0.84	0.78	0.66	0.65	0.56	0.54	0.53	0.70	0.56	0.49
MgO	12.74	12.16	12.12	12.28	13.44	14.31	13.77	12.80	14.95	15.04	13.80	13.46	15.24	15.53
CaO	20.83	21.71	20.53	20.93	19.07	20.19	21.79	20.28	20.18	19.23	18.90	20.04	18.65	19.14
Na_2O	0.45	0.40	0.38	0.37	0.33	0.33	0.39	0.37	0.32	0.23	0.44	0.44	0.49	0.30
K_2O	0.00	0.01	0.00	0.01	0.00	0.00	0.00	-0.01	0.00	0.02	0.01	0.02	0.00	0.00
Total	100.76	100.30	99.92	100.07	101.19	100.95	100.49	100.01	101.33	101.07	100.65	100.27	100.73	100.40

Structural formulas based on 6.000 oxygens and 4.000 cations

	Analysis													
Ion	**8.1**	**[9.1**	**10.1**	**11.1**	**12.1]**	**17.1**	**19.1**	**9.2**	**11.2**	**13.2**	**[15.2**	**16.2]**	**28.2**	**30.2**
Si^{4+}	1.965	1.947	1.978	1.976	1.954	1.941	1.930	1.970	1.927	1.927	1.929	1.924	1.898	1.929
Ti^{4+}	0.013	0.015	0.006	0.006	0.009	0.014	0.016	0.010	0.023	0.021	0.024	0.023	0.031	0.024
Al^{3+}	0.045	0.055	0.031	0.028	0.042	0.060	0.067	0.040	0.086	0.079	0.098	0.095	0.119	0.090
Cr^{3+}	0.001	0.000	0.000	0.001	0.000	0.000	0.000	0.001	0.001	0.000	0.001	0.000	0.001	0.001
Fe^{3+}	0.024	0.038	0.021	0.025	0.041	0.040	0.051	0.020	0.027	0.031	0.020	0.033	0.043	0.019
Fe^{2+}	0.355	0.336	0.392	0.374	0.393	0.304	0.256	0.373	0.282	0.317	0.357	0.318	0.281	0.285
Mn^{2+}	0.020	0.021	0.025	0.023	0.026	0.025	0.021	0.021	0.017	0.017	0.017	0.022	0.017	0.015
Mg^{2+}	0.711	0.682	0.685	0.692	0.748	0.791	0.763	0.720	0.819	0.829	0.767	0.750	0.838	0.856
Ca^{2+}	0.835	0.875	0.834	0.848	0.762	0.802	0.868	0.820	0.795	0.761	0.755	0.802	0.737	0.758
Na^{+}	0.033	0.030	0.028	0.027	0.024	0.024	0.028	0.027	0.023	0.016	0.032	0.032	0.035	0.022
K^{+}	0.000	0.000	0.000	0.000	0.000	0.000	0.000	-0.001	0.000	0.001	0.001	0.001	0.000	0.000
Total	4.000	4.000	4.000	4.000	4.000	4.000	4.000	4.000	4.000	4.000	4.000	4.000	4.000	4.000

Table 47. Numbers in brackets denote analyses done at the same grain.

ORTHOPYROXENE

Measured values

	Analysis																
Oxide	**3.1**	**[6.1**	**7.1]**	**15.1**	**[20.1**	**21.1**	**22.1**	**23.1]**	**[24.1**	**25.1]**	**[19.2**	**20.2]**	**[22.2**	**23.2]**	**[24.2**	**25.2]**	**33.2**
SiO_2	51.955	51.215	51.429	51.420	53.009	50.670	51.948	51.683	51.898	50.670	52.239	52.390	51.681	52.079	52.870	52.857	52.014
TiO_2	0.389	0.318	0.316	0.334	0.355	0.422	0.450	0.402	0.533	0.399	0.334	0.389	0.372	0.276	0.311	0.251	0.441
Al_2O_3	0.798	0.520	0.412	0.612	1.097	1.656	1.635	1.268	1.469	1.079	0.707	0.912	0.639	0.557	0.617	0.498	1.053
Cr_2O_3	0.000	0.018	0.000	0.000	0.000	0.000	0.000	0.020	0.000	0.005	0.000	0.010	0.013	0.023	0.000	0.000	0.013
FeO	24.663	27.803	28.542	26.872	21.209	25.241	24.544	22.869	21.333	26.971	21.783	22.591	25.840	26.298	22.718	25.380	23.894
MnO	1.051	1.291	1.567	1.250	0.734	1.050	1.039	0.597	0.601	1.290	0.980	1.093	1.188	1.230	1.305	1.166	0.964
MgO	19.186	17.148	16.507	17.879	22.197	18.985	19.183	20.282	21.830	17.121	21.159	20.883	18.753	18.807	21.306	19.509	19.940
CaO	1.463	1.656	1.469	1.601	1.737	1.049	1.546	1.833	1.533	1.250	1.566	1.567	1.569	1.509	1.590	1.589	1.433
Na_2O	0.027	0.039	0.016	0.013	0.007	0.026	0.033	0.040	0.024	0.017	0.027	0.020	0.028	0.019	0.016	0.022	0.043
K_2O	0.000	0.010	0.000	0.013	0.003	0.000	0.012	0.005	0.004	0.000	0.005	0.007	0.004	0.000	0.005	0.003	0.002
Total	99.505	100.02	100.25	99.982	100.32	99.060	100.37	98.998	99.205	98.799	98.785	99.861	100.09	100.79	100.71	101.27	99.796

Structural formula based on 3.000 oxygens

	Analysis																
Ion	**3.1**	**[6.1**	**7.1]**	**15.1**	**[20.1**	**21.1**	**22.1**	**23.1]**	**[24.1**	**25.1]**	**[19.2**	**20.2]**	**[22.2**	**23.2]**	**[24.2**	**25.2]**	**33.2**
Si^{4+}	0.989	0.988	0.992	0.987	0.983	0.972	0.979	0.981	0.975	0.985	0.989	0.985	0.985	0.987	0.986	0.991	0.983
Ti^{4+}	0.006	0.005	0.005	0.005	0.005	0.006	0.006	0.006	0.008	0.006	0.005	0.006	0.005	0.004	0.004	0.004	0.006
Al^{3+}	0.018	0.012	0.009	0.014	0.024	0.037	0.036	0.028	0.033	0.025	0.016	0.020	0.014	0.012	0.014	0.011	0.023
Cr^{3+}	0.000	0.000	0.000	0.000	0.000	0.000	0.000	0.000	0.000	0.000	0.000	0.000	0.000	0.000	0.000	0.000	0.000
Fe^{2+}	0.393	0.448	0.461	0.431	0.329	0.405	0.387	0.363	0.335	0.438	0.345	0.355	0.412	0.417	0.354	0.398	0.378
Mn^{2+}	0.017	0.021	0.026	0.020	0.012	0.017	0.017	0.010	0.010	0.021	0.016	0.017	0.019	0.020	0.021	0.019	0.015
Mg^{2+}	0.544	0.493	0.475	0.511	0.614	0.543	0.539	0.574	0.611	0.496	0.597	0.585	0.533	0.531	0.592	0.545	0.562
Ca^{2+}	0.030	0.034	0.030	0.033	0.035	0.022	0.031	0.037	0.031	0.026	0.032	0.032	0.032	0.031	0.032	0.032	0.029
Na^{+}	0.001	0.001	0.001	0.000	0.000	0.001	0.001	0.001	0.001	0.001	0.001	0.001	0.001	0.001	0.001	0.001	0.002
K^{+}	0.000	0.000	0.000	0.000	0.000	0.000	0.000	0.000	0.000	0.000	0.000	0.000	0.000	0.000	0.000	0.000	0.000
Total	1.997	2.003	1.999	2.002	2.000	2.003	1.997	2.000	2.002	1.997	1.999	2.000	2.003	2.003	2.003	2.000	1.999

Table 48. Numbers in brackets denote analyses done at the same grain.

BIOTITE

Measured values

	Analysis							
Oxide	**5.1**	**14.1**	**26.1**	**12.2**	**14.2**	**21.2**	**27.2**	**32.2**
SiO_2	37.252	37.724	36.811	37.637	37.009	37.651	37.116	36.356
TiO_2	3.737	3.733	4.260	4.197	4.064	3.731	3.247	3.897
Al_2O_3	11.777	12.182	11.230	11.998	11.769	11.922	11.964	11.550
Cr_2O_3	0.014	0.000	0.002	0.000	0.023	0.000	0.027	0.002
FeO	18.479	18.897	20.931	19.479	20.541	20.334	21.225	21.035
MnO	0.242	0.200	0.233	0.228	0.243	0.256	0.271	0.155
MgO	12.885	13.008	11.331	11.855	11.430	11.969	11.806	10.847
CaO	0.000	0.000	0.000	0.034	0.000	0.013	0.205	0.032
Na_2O	0.129	0.088	0.097	0.163	0.143	0.157	0.268	0.211
K_2O	9.714	9.597	9.618	9.444	9.372	9.165	8.675	9.136
Total	94.187	95.399	94.511	95.020	94.567	95.179	94.804	93.220

Structural formula based on 22.000 oxygens

	Analysis							
Ion	**5.1**	**14.1**	**26.1**	**12.2**	**14.2**	**21.2**	**27.2**	**32.2**
Si^{4+}	5.765	5.757	5.756	5.783	5.754	5.790	5.755	5.756
Ti^{4+}	0.435	0.428	0.501	0.485	0.475	0.432	0.379	0.464
Al^{3+}	2.148	2.191	2.069	2.173	2.156	2.161	2.186	2.155
Cr^{3+}	0.002	0.000	0.000	0.000	0.003	0.000	0.003	0.000
Fe^{2+}	2.392	2.411	2.737	2.503	2.671	2.615	2.752	2.785
Mn^{2+}	0.032	0.026	0.031	0.030	0.032	0.033	0.036	0.021
Mg^{2+}	2.973	2.959	2.641	2.716	2.649	2.744	2.729	2.560
Ca^{2+}	0.000	0.000	0.000	0.006	0.000	0.002	0.034	0.005
Na^{+}	0.039	0.026	0.029	0.049	0.043	0.047	0.081	0.065
K^{+}	1.918	1.868	1.918	1.851	1.859	1.798	1.716	1.845
Total	15.703	15.667	15.682	15.595	15.642	15.621	15.670	15.657

Table 49.